Intervention Methods Against Mosquito-borne Diseases

Thesis submitted for the degree of Doctor of Philosophy

Trinity Term 2017

Joshua Blight

St Cross College

0 Preface

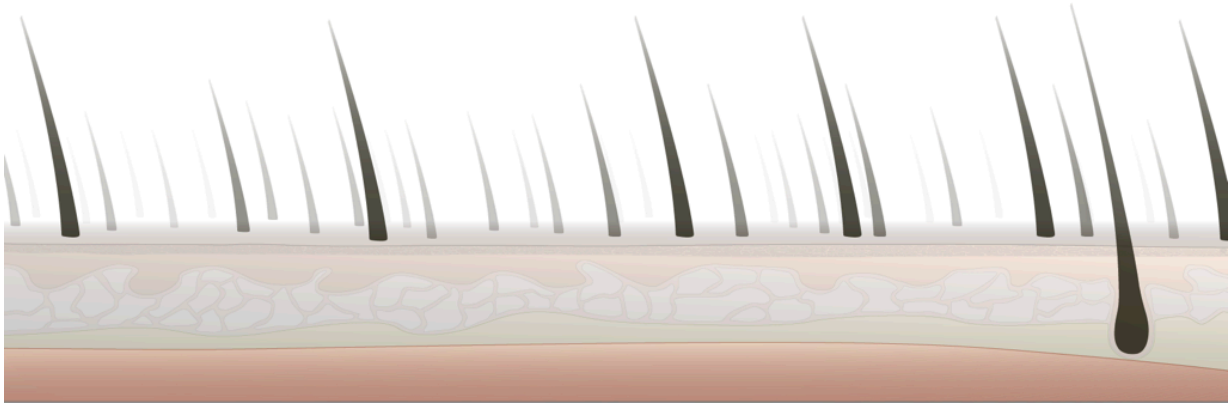

0.1 Abstract

Mosquito-borne diseases account for hundreds of thousands of deaths each year, highlighting the need for successful intervention methods, which can be targeted at either the pathogen, mosquito vector, or human host. This thesis aims to contribute to better intervention methods focused against malaria and dengue by either (i) improving available research tools, (ii) enhancing the understanding of a promising intervention method or (iii) designing new intervention candidates. Firstly, a superior method for studying *in vitro* malaria infection of the liver is shown, with implications for vaccine and drug interventions. Secondly, the biology of *Wolbachia* infection in *Anopheles gambiae* mosquitoes in the context of the target of rapamycin signalling cascade is investigated in an attempt to improve our understanding of its malaria inhibitory phenotype and inability to stably infect *An. gambiae* mosquitoes. Finally, an algorithm is developed for the design of a hypothesis driven conservation-based vaccine against viral mosquito diseases with a particular focus on dengue.

0.2 Acknowledgments

I wish to acknowledge the following for their continued support, professional guidance and invaluable contribution throughout this thesis. Foremost my two supervisors, Prof. Arturo Reyes-Sandoval and Prof. Steven Sinkins for their support and guidance throughout my DPhil. I would also like to thank Prof. Adrian Hill for helping to support my DPhil.

In addition, but by no means less important I would like to thank the following for their support; everyone in the Jenner Institute, Wellcome Trust Centre for Human Genetics, Functional Genomics Facility and the Nuffield Department of Medicine (NDM). In particular, I wish to thank Mark Shipman for his fantastic help with all my microscopy work. Andrew Worth for his amazing cell sorting. David Ferguson for his brilliant electron microscopy techniques providing beautiful *Wolbachia* images. Paul Pattinson from the physics department for his amazing generosity in creating my photolithography moulds. Paulo Bettencourt and Emma Dickinson for helping with the massive *in vitro* hepatocyte infections early in the mornings. Also, to Paulo for letting me work together to use my new technique with his MHC peptidomics work. Alex Fyfe and Sumi Biswas for providing an excellent mosquito facility, an indispensable tool for my work. Chris Preece for his guidance and help with cryopreservation techniques. Jose Lourenco, Annette Boehmer and Ellie Barnes for their early help with vaccine design. James Larkin for taking the time to train me in a regulated rat procedure in the final stages of my DPhil. Ahmed Salman and Leiden, Netherlands for providing the transgenic parasites. Viv Clark and Heather Gray for their exceptionally run FGF facility. Alex Spencer for her help and guidance. I would also like to thank the NDM for their DPhil Studentship and support throughout my DPhil, especially Prof. Robert Gilbert and Zoe Stockdale. Also, everyone from St Cross College for their fantastic support, facilities and wonderfully kind environment.

I would also like to particularly thank Phillip Kemlo for his fantastic and indispensable help with the computer programming side of the vaccine design algorithm. I would also like to say how immensely grateful I am to Dr Holger Kramer and Dame Frances Ashcroft for allowing me to use their Free-Flow Electrophoresis (FFE) machine and especially to Holger who has given me so much support throughout my thesis with the FFE machine. I would also like to thank everyone from the FFE company for their incredible help, guidance and generosity.

Furthermore, I wish to thank fellow DPhil student Erwan Atcheson for taking the time to help with mosquito mashing and the endless cycles up and down the hill with samples. Also, Dr Cesar Lopez for his support around the lab and Dr Aadil El- Turabi for his continual and unerring help with problems I encountered in the lab and the help with all the rat liver extractions. Dr Kirsty Stainton and Dr Vincent Georghegan for their amazing *Wolbachia* help and friendship. Dr Sofia Pinto for her early help in my DPhil.

I would like to give an enormous thanks to Dr Eduardo Alves. Without this person behind me throughout the DPhil and in the final write-up stages I would not be at this stage,

and without this DPhil I would never had made such an amazing friend for life. Dr Janet Midega for her fantastic mentoring since my BSc, without this person I would not have even applied for Oxford. Finally, I would like to thank my family for their emotional support throughout my DPhil and sister Ashleigh for her proofreading.

Finally, as with any work based on published literature it is impossible to cover all fields of research within a limited space, I therefore apologise to any groups within the field that I have not been able to represent.

0.3 Figure and Table Inventory

Figures

Tables

0.4 List of Abbreviations

Abbreviations used in this thesis are listed below.

+RNA	positive strand RNA
3-MA	3-methyladenine
4E-BP	eIF4-E binding protein
5'-TOP	5'-terminal oligopyrimidine tract
aa	amino acids
ADE	antibody dependent enhancement
AF	autophagic flux
agSesn	*Anopheles gambiae* sestrin
AICAR	5-aminoimidazole-4-carboxamide 1-β-D-ribofuranoside, acadesine, N^1-(β-D-Ribofuranosyl)-5-aminoimidazole-4-carboxamide
AKT/PKB	protein kinase B
AL	a-loop
AMP	5'-adenosine monophosphate
AMPK	5'-adenosine monophosphate-activated protein kinase
APTES	(3-aminopropyl)triethoxysilane
BCA	bicinchoninic acid
BLAST	basic local alignment search tool
C	capsid
CE	cloning enhancer
CelTOS	cell-traversal protein for ookinetes and sporozoites
CHIKV	chikungunya virus
CSP	circumsporozoite protein
cZE	continuous zone electrophoresis
DA	dissected-accudenz
DAF	dissected-accudenz-FFE
DENV	dengue virus

Deptor	DEP domain-containing mTOR-interacting protein
DF	dissected-FFE
dH_2O	deionised water
DMEM	Dulbecco's modified Eagles medium
DMSO	dimethyl sulphoxide
dsRNA	double stranded RNA
E	envelope
EBA	erythrocyte binding protein
EDA	exploratory data analysis
EEF	exoerythrocytic form
ER	endoplasmic reticulum
FACS	fluorescence-activated cell sorting
FcR	fragment, crystallisable receptor
FFE	free-flow electrophoresis
FKBP12	FK506-binding protein 12
FOXO	forkhead box
FSC	forward scatter
GEST	gamete egress and sporozoite traversal
GM	genetic modification
GPTES	(3-glycidyloxypropyl)triethoxysilane
GTP	guanosine triphosphate
HM	hydrophobic motif
HPV	human papilloma virus
HSP	heat shock protein
HSPG	heparan sulfate proteoglycans
i.m.	intramuscular
i.p.	intraperitoneal
i.v.	intravenous
IEDB	immune epitope database and analysis resource
IF4E	initiation factor 4E
ILP	insulin-like peptides
InR	insulin receptor
IQR	inter-quartile range
iZE	interval zone electrophoresis
JNK	c-jun n-terminal kinase
LAP	LC3-associated phagocytosis
LB	luria broth
LC-MS/MS	liquid chromatography-tandem mass spectrometry
LIC	ligation-independent cloning
LLINs	long lasting insecticidal bednets
LN2	liquid nitrogen
M	matrix
MA	mash-accudenz
MAF	mash-accudenz-FFE
MAPK	mitogen-activated protein kinase
MCS	multiple cloning site

MF	mash-FFE
mH_2O	molecular grade water
mLST8	mammalian lethal with SEC18 protein 8
mq	mosquito
mq/mL	mosquitoes per mL (referred to as ‘originating mosquito dose’)
mRNA	messenger ribonucleic acid
MSP1	merozoite surface protein 1
mTOR	mammalian target of rapamycin
NPC	non-parenchymal cells
NS	non-structural
OEH-I	ovarian ecdysteroidogenic hormone I
P/S	penicillin/streptomycin
PAGE	polyacrylamide
PAMP	pathogen-associated molecular patterns
PBS	phosphate buffered saline
PC	parenchymal cells
PCR	polymerase chain reaction
Perm	permiabilisation buffer
PKC	protein kinase c
PL	phospholipase
PLP1	perforin-like protein 1
PRR	pathogen recognition receptor
PRR5	proline-rich protein 5
prM	pre-membrane
PVDF	polyvinylidene difluoride
pI	isoelectric point
PV	*Plasmodium vivax*
PVM	parasitophorous vacuole
qPCR	quantitative polymerase chain reaction
RAPA	rapamycin
RAPTOR	regulatory-associated protein of mTOR
RBC	red blood cell
RdRp	RNA dependent RNA polymerase
RH	reticulocyte binding homologs
RiBi	bibosome biogenesis
RICTOR	rapamycin-insensitive companion of mTOR
RIDL	release of insects carrying a dominant lethal
RON	rhoptry neck protein
RPM	revolutions per minute
RT	room temperature
RT-PCR	real-time polymerase chain reaction
RTK	receptor tyrosine kinase
S17	40s ribosomal protein S17
S6K	P70-S6 kinase
S6p	serine 235/235 phosphorylated S6 protein of 40s subunit
SDS	sodium dodecyl sulfate

SEM	standard error of the mean
SFC	spot-forming cells
SIN1	stress-activated map kinase-interacting protein 1
SIP	sterile isotonic percoll
SLR	sequestosome 1-like Receptors
SOC	super optimal broth
SPADNS	sulfanilic acid azochromotrop
SPECT	sporozoite microneme protein essential for cell traversal
spz	sporozoite
spz/mL	sporozoites per mL
spz/mq	sporozoites per mosquito
TAE	tris-acetate-EDTA
TC	tissue culture
TCTP	translationally controlled tumour protein
TEA	triethanolamine
TLP	TRAP-like protein
TLR	toll-like receptor
TM	turn motif
TOR	target of rapamycin
TRAP	thrombospondin-related adhesive protein
TRS	indoor residual spraying
TSC	tuberous sclerosis complex
UI	user-interface
UIS3	up-regulated in infective sporozoites gene 3
UIS4	up-regulated in infective sporozoites gene 4
URI	unconventional prefoldin RPB5
VLP	virus like particle
WT	wild type
xg	geforce

0.5 Patents

Patents achieved for work in this thesis.

- **Dengue T-Cell Vaccine** – Granted. Available at: http://www.ndm.ox.ac.uk/mexico/_asset/file/multivalent-Dengue-vaccine.pdf
- **Chikungunya Vaccine** – Patent Pending
- **HPV Vaccine** – Patent Pending

0.6 Table of Contents

1 Introduction

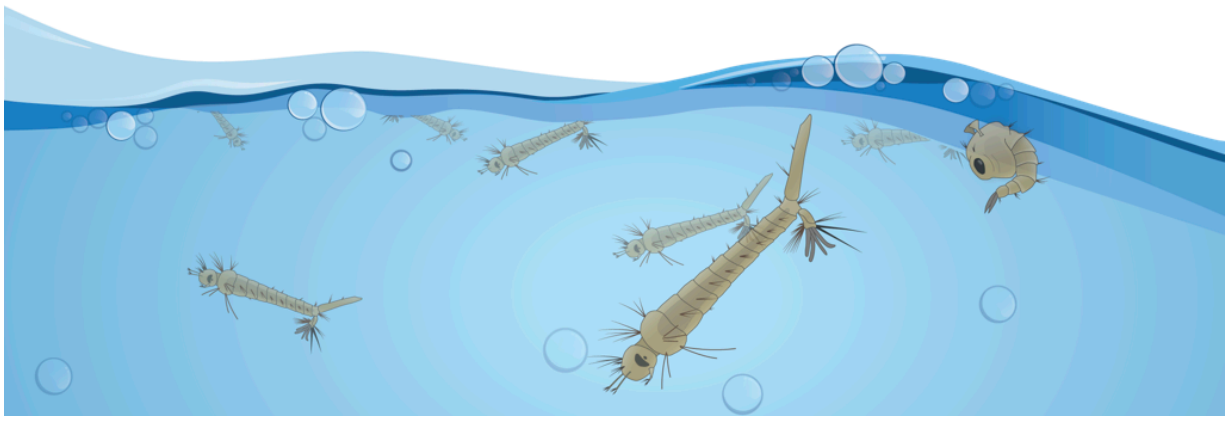

This chapter aims to briefly cover the most relevant mosquito-borne diseases and provides an overview of the interventions currently in use or in development, laying the foundation for a more detailed review of specific pathogens and the different interventions in subsequent chapters.

1.1 Mosquito-borne Diseases

Mosquitoes are small flying insects within the order *Diptera*, family *Culicidae*, consisting of over 3500 individual species[1]. They are typified by a segmented abdomen, one pair of wings and three pairs of legs attached to a thorax and a head bearing two antennae, compound eyes and feeding apparatus consisting of a tubular structure named a proboscis[1]. Adequate circulation of nutrients and hormones is achieved via an open circulatory network system within a liquid medium (haemolymph) and exchange of gases is achieved via a complex network of tubes (tracheoles) starting at holes (spiracles) found along the insect's body[1]. Carbohydrate sources such as nectar are used by both males and females for flight[1].

Additionally most mosquito species have evolved to obtain blood-derived proteins from vertebrates due to the nutrient requirements of egg development in females[2], a process known as vitellogenesis[3,4]. Blood feeding from a host is therefore an absolute requirement for the survival of these mosquito species, which has enabled other organisms requiring vertebrates for their replication to exploit this requirement, 'piggybacking' on the mosquito, some of which are pathogenic to the vertebrate[2,5]. Mosquito-borne protozoa[6], viruses[7-9] and nematodes[10] all exploit the requirement of saliva injection into the vertebrate during blood feeding to enable effective pathogen transfer[11]. Some of the major human pathogens transmitted by mosquitoes include the malaria parasite, dengue virus, chikungunya virus, West Nile virus, filarial nematodes, Japanese encephalitis virus, yellow fever virus[5], rift valley fever virus[12] and zika virus[13], which are transmitted by either *Culex, Aedes* or *Anopheles* mosquitoes[5]. Consequently,

this means that the prevalence of these diseases is tightly dependent on mosquito behaviour, lifespan and prevalence[14] (Figure 1-1).

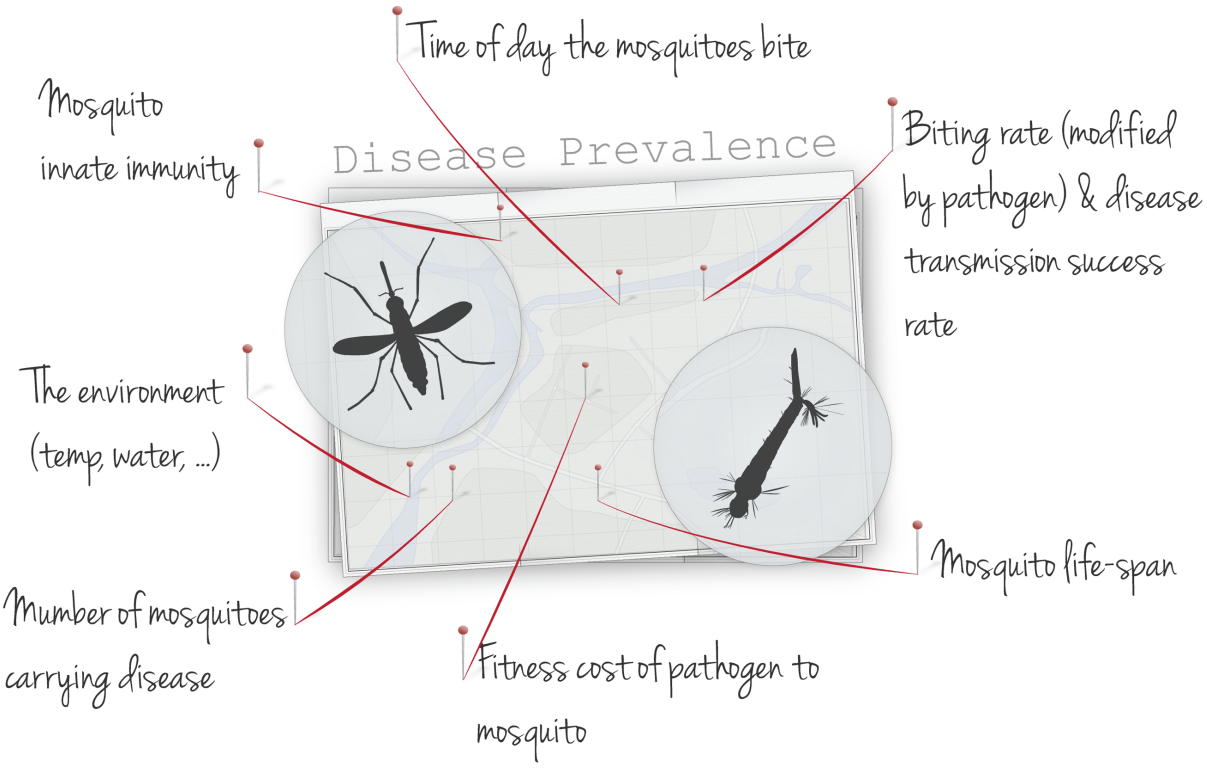

Figure 1-1 I Mosquito-related variables affecting disease prevalence. Prevalence of mosquito-borne diseases depends on many mosquito variables including (but not exhaustive), the time of day of peak biting activity which affects the availability of human hosts, whether the environment is suitable for mosquito survival, the number of mosquitoes infected with the disease, how pathogenic the pathogen is to the mosquito (affecting mosquito survival), the effectiveness of the mosquito innate immune response, the rate that mosquitoes bite which determines the chances of successful pathogen transmission to the human host, how effective the bite is at transferring the pathogen and the mosquito lifespan which can be modified by many of the other variables, such as biting rate (affects chances of being killed by human host), environmental, and pathogen fitness cost. Based on information from[14-19]. Human-related variables not discussed here.

1.1.1 Mosquito-borne Disease Prevalence

Environmental conditions are critical to mosquito prevalence, partly due to constraints of their lifecycle. Mosquito eggs hatch into larvae which are dependent on standing water, before eclosing into adults[20,21] (Figure 1-2). Therefore, mosquito population abundance correlates with wet seasons when larval habitats are plentiful[22]. Furthermore, being cold-blooded, mosquitoes are restricted to a specific range of environmental temperatures[14,23] and are susceptible to desiccation in low humidity[19]. These factors will have a considerable effect on the number of mosquitoes available to transmit diseases[14,24]. Furthermore, temperature also has consequences for pathogen development within the mosquito host[14], for example increased temperature reduces the incubation time for dengue viruses in *Aedes aegypti*[25].

Climate change is predicted to expand the global distribution of mosquitoes, making new areas habitable and current ones more habitable, with an associated increase in the prevalence of mosquito-borne diseases[2,14,26]; mediated by predicted increases in global temperatures and rising sea levels[26]. El Niño, which is associated with warmer temperatures, high rainfall and droughts[27] has been linked to malaria epidemics[28] and may increase with global warming[29].

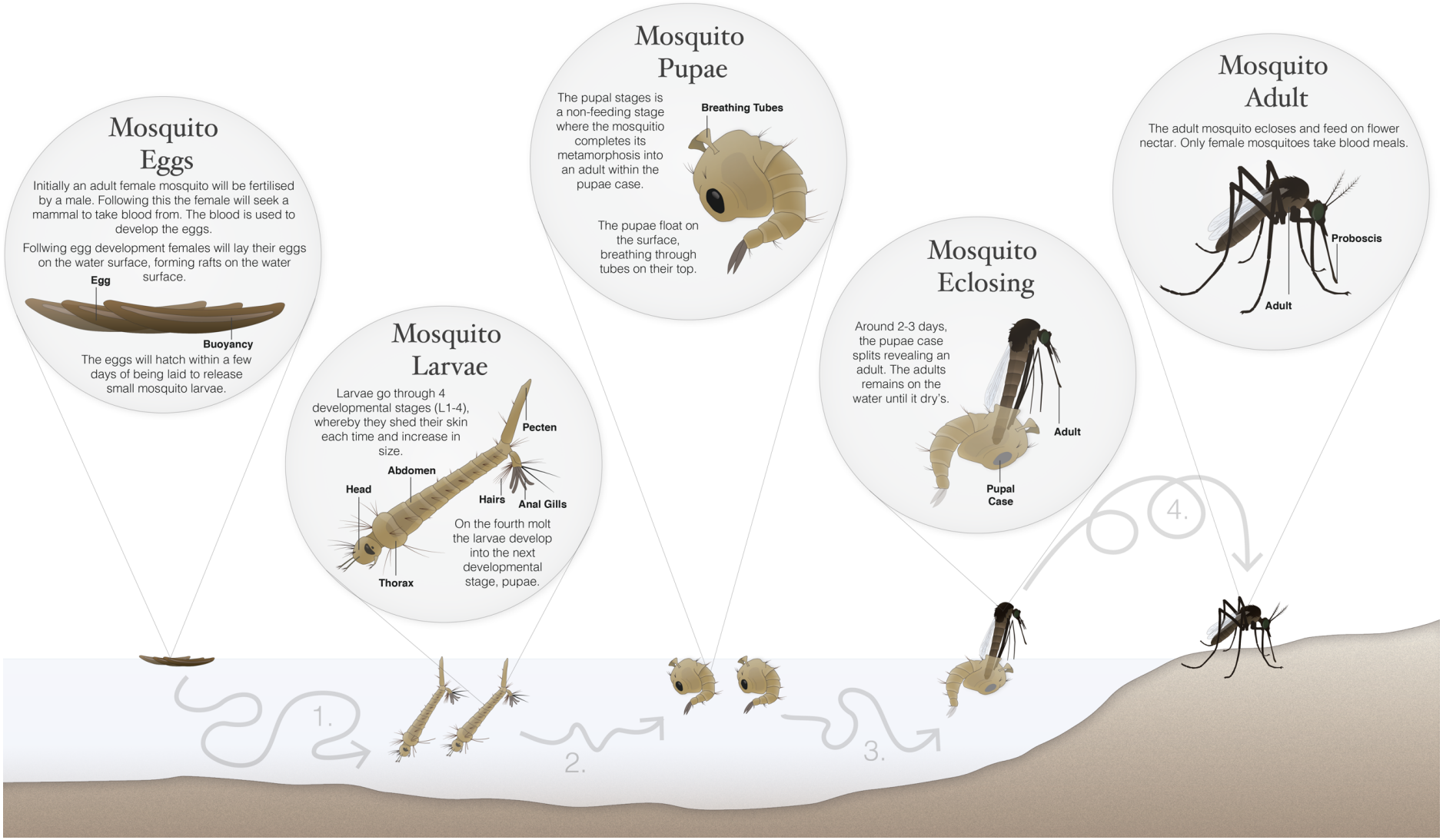
Mosquito Eggs
Initially an adult female mosquito will be fertilised by a male. Following this the female will seek a mammal to take blood from. The blood is used to develop the eggs.
Follwing egg development females will lay their eggs on the water surface, forming rafts on the water surface.
Egg
Buoyancy
The eggs will hatch within a few days of being laid to release small mosquito larvae.
Mosquito Larvae
Larvae go through 4 developmental stages (L1-4), whereby they shed their skin each time and increase in size.
Pecten
Abdomen
Head
Hairs
Anal Gills
Thorax
On the fourth molt the larvae develop into the next developmental stage, pupae.
Mosquito Pupae
The pupal stages is a non-feeding stage where the mosquitio completes its metamorphosis into an adult within the pupae case.
Breathing Tubes
The pupae float on the surface, breathing through tubes on their top.
Mosquito Eclosing
Around 2-3 days, the pupae case splits revealing an adult. The adults remains on the water until it dry's.
Adult
Pupal Case
Mosquito Adult
The adult mosquito ecloses and feed on flower nectar. Only female mosquitoes take blood meals.
Proboscis
Adult
1.
2.
3.
4.

Figure 1-2 | The generic mosquito life-cycle. Female mosquitoes take a blood meal with subsequent vitellogenesis and development of fertilised eggs[4]. The female then lays her eggs on standing water, each mosquito species has different water preferences such as fresh and salt water. Larvae hatch from the eggs and within a week pupate for a few days before eclosing as adults. Some species of eggs can overwinter, remaining desiccated for many months[21].

However, until the mid 20th century malaria was found far further north than it is now, suggesting global warming may not be as critical as once thought and can be counteracted by human interventions such as removal of mosquito larval habitats, an increase in alternative blood meals from more farm animals, improved housing and concerted efforts to eradicate mosquitoes by use of insecticides[30]. This highlights the implications of human activity on mosquito prevalence and the effect of unequal distribution of health intervention methods in endemic areas[14]. For example, the increase in urban environments with the associated increase of standing water in containers has provided a perfect habitat for *Aedes* mosquitoes[31]. Furthermore, an increase in commerce was responsible for the introduction of *Aedes albopictus* in Italy in 1990 and France in 1999 through used tires from the United States and Japan[32-34].

Mosquito behaviour is also critical to disease prevalence. For example, *Anopheles gambiae* s.s. is generally known to enter houses and feed during the evening[15,16]. Therefore, modifying human behaviour by sleeping under long-lasting insecticidal bednets (LLINs) prevents biting[35,36]. However, recent evidence suggest that their use is selecting for mosquitoes with an outdoor feeding habit[35,36]. Furthermore, malaria infected *Anopheles* mosquitoes have been shown to increase biting, spend more time feeding and are more likely to return to feeding when interrupted[37-39]. Temperature has also been show to modulate feeding intensity[14]. Malaria infection has even been shown to make infected humans more attractive to mosquitoes[40].

Finally, lifespan is a critical determinant of disease prevalence by affecting the chances of disease transmission. For successful transmission, a mosquito during its lifespan must feed on an infective individual, survive long enough for the pathogen to develop (the extrinsic incubation period), and transfer the parasite via another blood feed[18]. Therefore, anything which reduces lifespan would reduce disease prevalence[18]. Interestingly, a comprehensive meta-analysis[17] suggested that malaria infection is associated with a reduction in mosquito lifespan, likely due to a combination of parasite-mediated factors, including resource competition[41,42], elevated immune activation[43] and increased biting behaviour[37-39], indicating the likely trade-off between lifespan and increased transmission[17].

1.1.2 Malaria, Dengue and Chikungunya

Human malaria is caused by the protist *Plasmodium*, of which *P. falciparum* and *P. vivax* cause the majority of cases and are transmitted by *Anopheles* mosquitoes[44]. In 2015 alone there were an estimated 212 million clinical cases of malaria and 429,000 deaths, with a disproportionate 90% of cases and 92% of deaths mainly in children in sub-Saharan African[45]. Most deaths are caused by *P. falciparum*[44], due to its virulent

phenotype including cerebral malaria[5]. However, global transmission has fallen thanks to an intensification of control methods, so that it is estimated that 32 out of the 99 countries with reported cases could eliminate malaria within the next decade[44,46]. Unfortunately, drug and insecticide resistance is becoming a major concern[46-49]. In addition to this, most current intervention methods have been targeted at *P. falciparum* and not *P. vivax* which can remain dormant as hypnozoites before recrudescing[46].

Malaria transmission occurs in Central & South America, Africa and Asia[44] (Figure 1-3). In Africa, the *An. gambiae* complex is the important malaria vector[44]. The clinical symptoms of malaria are due to the repeated infection and bursting of red blood cells (RBCs) by the malaria parasite causing the characteristic cyclical pyrexia and associated emesis and acute hypertension[44]. In severe cases high haemolytic anaemia, ketoacidosis, hypoglycaemia and coma can occur with a high risk of death[44].

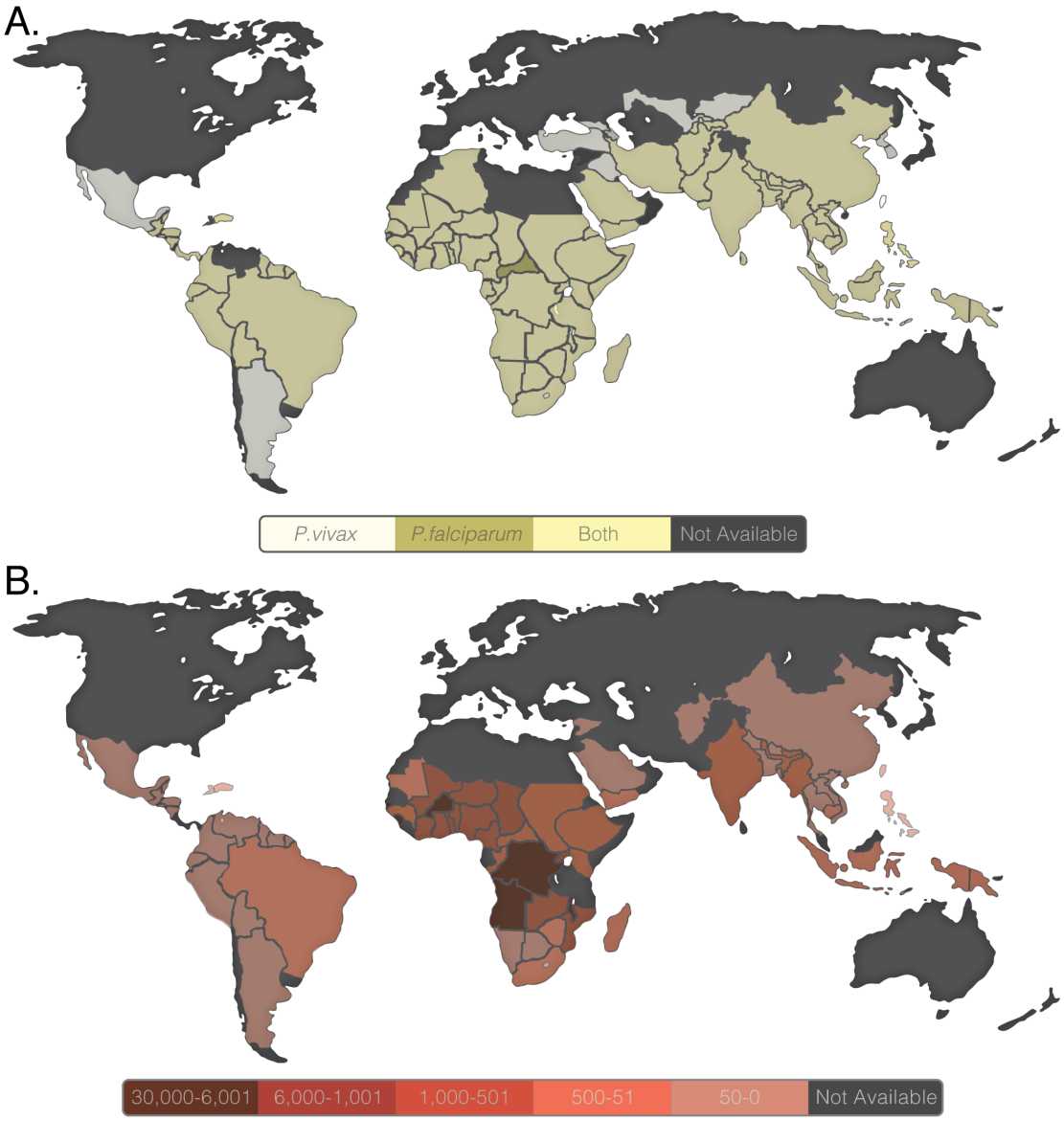

Figure 1-3 I Worldwide epidemiology choropleths. A) Worldwide distribution of *P. falciparum* and *P. vivax,* 2015. B) Inpatients deaths due to malaria in 2015. Data from world malaria report 2015[50] using information from Global Malaria Mapper (www.worldMalariareport.org).

Dengue and chikungunya are human viruses transmitted mainly by *Aedes aegypti* and *Aedes albopictus*[7,8]. Dengue is a positive sense RNA flavivirus (DENV) which exists as four circulating serotypes[7], found worldwide in either epidemic or endemic occurrence focused in tropical regions with a steady geographical expansion[51]. Infections are estimated at 390 million a year with 96 million symptomatic cases[51]. Chikungunya is a positive sense RNA alphavirus (CHIKV) originating from Africa as an enzootic spillover into humans and currently exists as four lineages[8,52,53]. The two African enzootic lineages are the West African (WA) lineage and East Central South Africa (ECSA) lineage[8,52,53]. The other two lineages originated from the ECSA lineage and are called the Asian and recently emerged Indian Ocean (EIO) lineage[8,52,53]. These linages have spread considerably since their original discovery as a consequence of travel and commerce, and now exist as urban infections maintained between humans and mosquitoes across all three continents[8,52,53].

It is thought that historically many DENV infections were actually CHIKV infections as infected individuals exhibit similar symptoms[8,53]. Dengue infection is asymptomatic in up to 75% of cases, however it can present as a spectrum from limited dengue fever (DF) to more severe haemorrhagic and capillary leak syndrome[54-56]. A key risk factor for severe haemorrhagic disease is a second infection with a different serotype[54-56]. Milder symptoms include fever, vomiting and joint pain, which can progress to more severe and potentially fatal vascular leakage and haemorrhaging[7]. CHIKV infection is also associated with a fever and joint pain however, the joint pain is considerable and unlike DENV symptoms, occurs in most infections. In rare cases hosts with underlying conditions can suffer fatalities[8].

1.2 Intervention Methods

Intervention methods against mosquito-borne diseases can be broadly classified into two groups; those that target the mosquito and those targeting the human host (Figure 1-4).

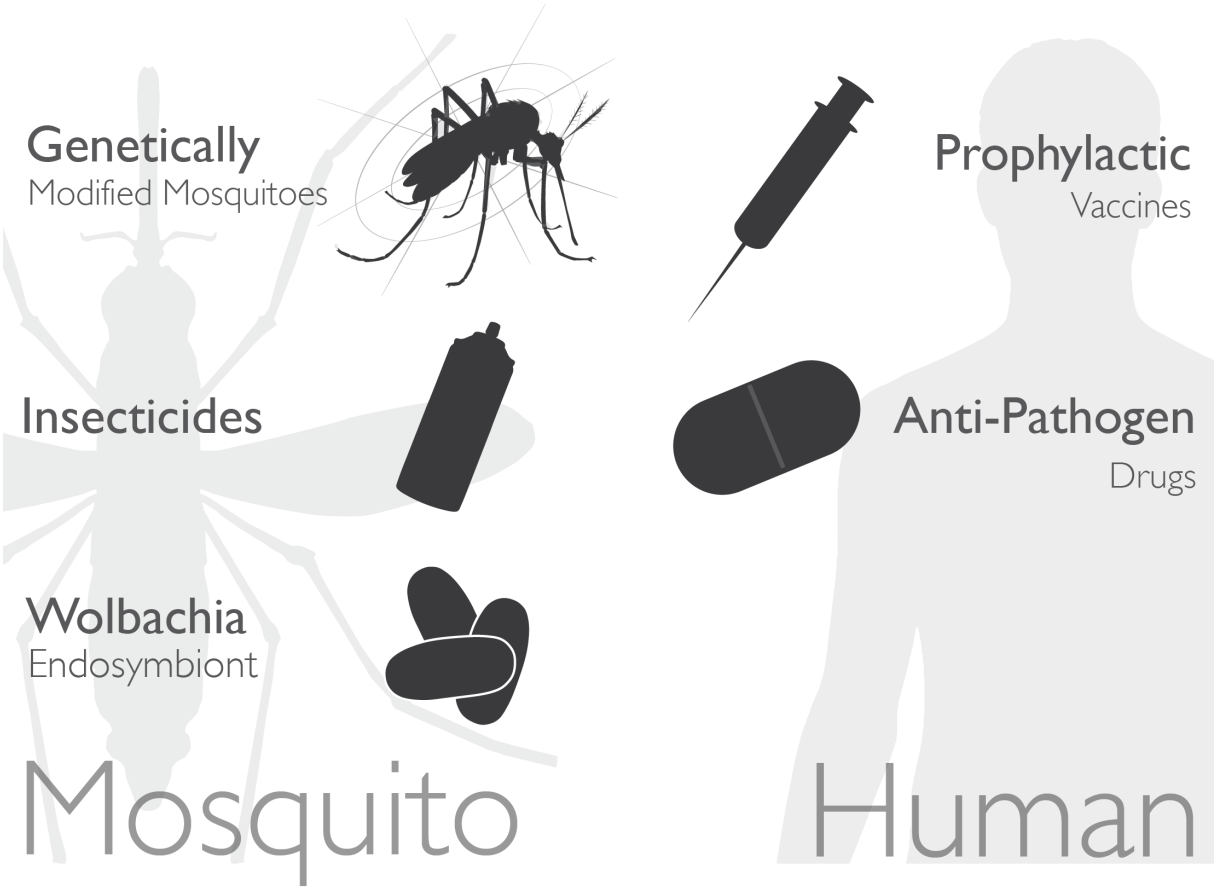

Figure 1-4 I Intervention methods. Common intervention methods for mosquito-borne diseases. Left, vector-based. Right, host-based.

1.2.1 Vector-based Intervention Methods

One of the most widely used vector-based intervention methods for malaria are LLINs and indoor residual spraying (IRS), which have been a major contributor to the recent reduction in malaria deaths and infections, especially in Africa[45,57,58]. Both methods utilise insecticides to kill mosquitoes, whilst LLINs also aim to reduce mosquito host feeding[45,57,58]. However, their effectiveness is now under threat due to increased development of insecticide resistance[45,57,58]. For example, pyrethroid resistance in 2015 was found in three quarters of monitored countries in *Anopheles* mosquitoes[45]. In addition to the many known mechanisms of pyrethroid resistance[59], mosquitoes have been reported to change their behaviour shifting to become more exophillic[60] and biting earlier before people sleep under LLINs[61,62].

Approximately 25% of all insecticides sold worldwide are pyrethroids[59] which are the only insecticides suitable for LLINs[47] and the major insecticide used for IRS due to its

fast activity and its acceptable human safety profile[63,64]. Furthermore, resistance to any pyrethroid gives resistance to all pyrethroids[59]. Therefore, the effectiveness of LLIN's and IRS is under threat. Resistance against other insecticides include organophosphates, organochlorides and carbamates has also been detected[63].

Unfortunately, history is but repeating itself. Use of DDT for IRS was pioneered in 1955 by the World Health Organisation (WHO) to eradicate malaria[63]. However, the major development of DDT resistance contributed to a reduction in effectiveness in some areas[63]. In 2012 WHO released a plan to tackle insecticide resistance and maintain its effectiveness, which included increased monitoring and the development of new control methods[64,65]. Nonetheless, we need novel mosquito-based intervention methods which are as effective as LLINs to continue the downward trend in malaria prevalence.

One of the most interesting novel mosquito-based intervention methods is the use of the mosquito endosymbiont *Wolbachia*, a Gram-negative genus of intracellular bacteria within the *Rickettsiale* order[66]. *Wolbachia* infections are restricted to invertebrate hosts[67] and are estimated to naturally infect over 50% of the worlds arthropod species[68,69]. Interestingly, in specific mosquito infections *Wolbachia* is able to reduce or prevent the mosquito transmission of many human mosquito-borne diseases including dengue, chikungunya[70], zika[71] and malaria[72,73]. The endosymbiont is theorised to achieve this in a combination of ways such as reducing the mosquito lifespan, competing with the pathogen for resources and priming the mosquito innate immune system[67]. Pathogen inhibition in mosquitoes is however generally only associated with non-native strain infections[67]. The commonly used strains for pathogen inhibition are *w*Mel and *w*MelPop[74,75].

*w*MelPop is associated with a higher fitness cost due to its strong life-shortening phenotype[75]. However, what allows this intervention method to outdo others is that *Wolbachia* infection is associated with a reproductive advantage to the female mosquito[66,67,76]. The bacteria manipulate host reproduction to achieve this, and the strains used for these intervention methods are associated with a form know as cytoplasmic incompatibility (CI; Figure 1-5)[66,67,76]. In CI, *Wolbachia* infected males only produce viable offspring when mating with females also infected with the same *Wolbachia* strain[66,67,76]. However, infected females can successfully mate with both infected and uninfected males[66,67,76]. Therefore, it is a selective advantage for females to have the infection and since it is transferred maternally to offspring this leads to highly effective invasion of the population by the *Wolbachia*.[66,67,76]

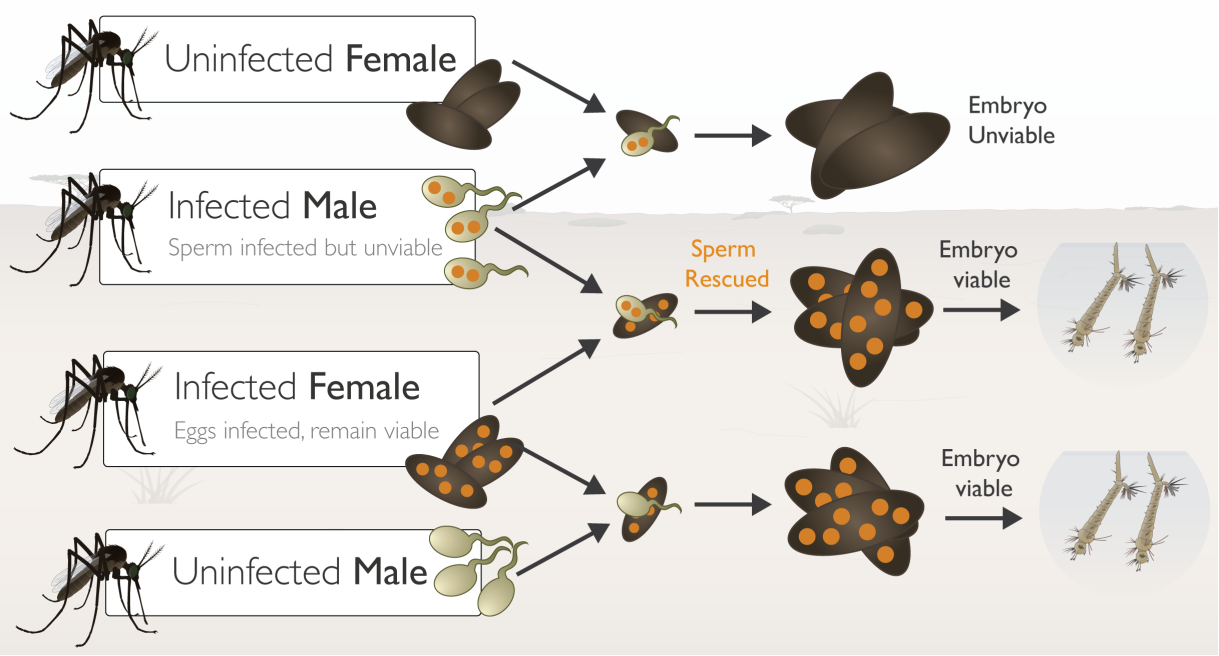

Figure 1-5 I *Wolbachia* cytoplasmic incompatibility. *Wolbachia* infected females produce viable offspring from any mating situation. *Wolbachia* infected males only produced viable offspring when mating with infected females[67].

Wolbachia-based interventions against DENV have shown highly promising results in field trials in Australia with *w*Mel in *Aedes aegypti*[77] with trials in Colombia, Vietnam, Brazil and Indonesia are currently ongoing[66,78] (see www.eliminateDengue.com for updates). Unfortunately, this promising field work cannot be replicated in the major malaria vector *An. gambiae* due to the current inability to create a stable vertically transmitted infection[72,73]. Therefore, work has currently only been done on somatic infections[72,73]. However, in 2013 a promising report showed the establishment of a stable *An. stephensi* infection with an anti-malarial phenotype; reducing *Plasmodium* infection load in mosquitoes[79].

Another attractive intervention method currently in field trials are genetically modified (GM) mosquitoes. Similar to *Wolbachia* the transmission of the genetic modification requires mating and acts either to (i) reduce population numbers[80]; commonly by inducing sterility[81-83], or (ii) replacing a population with another less amenable to pathogen infection[84,85]. Both techniques have their own associated problems, for example the reduction of population size using the sterile male technique requires expensive large scale releases over long periods of time and there may be a risk of population replacement with another disease vector[80,81]. Conversely the population replacement technique in some cases requires the maintenance of a deleterious trait within the population which can be difficult to achieve[80,86,87].

Oxitec (www.oxitec.com) have pioneered the OX513A genetically modified *Aedes aegypti* mosquito, which uses the Release of Insects carrying a Dominant Lethal (RIDL) system to reduce the population size using a dominant lethal gene that prevents

development of male and female offspring with heterozygous expression of the lethal gene[80,88]. These offspring originate from the mating of a wildtype (WT) female with a GM homozygous lethal gene carrying male[80,88]. The gene is repressible with tetracycline to allow rearing of homozygous stock and males are subsequently released to mate with WT females (Figure 1-6)[80,88]. Trials using male OX513A have shown that the GM mosquitoes were able to compete with WT males[88] and reduce the population effectively[89]. However, large quantities (approximately 3500 males per week per hectare) were needed to achieve this[89]. In 2014 results were published of a successful field trial in Brazil which reduced the population by approximately 81-95%, however this work did not look at transmission of circulating pathogens[90]. A similar effect was seen in Panama trials and promisingly they also showed no species replacement with *Aedes albopitus*[91]. Oxitec have ongoing trials in Brazil and is progressing to trials in India and Florida, United States (www.oxitec.com).

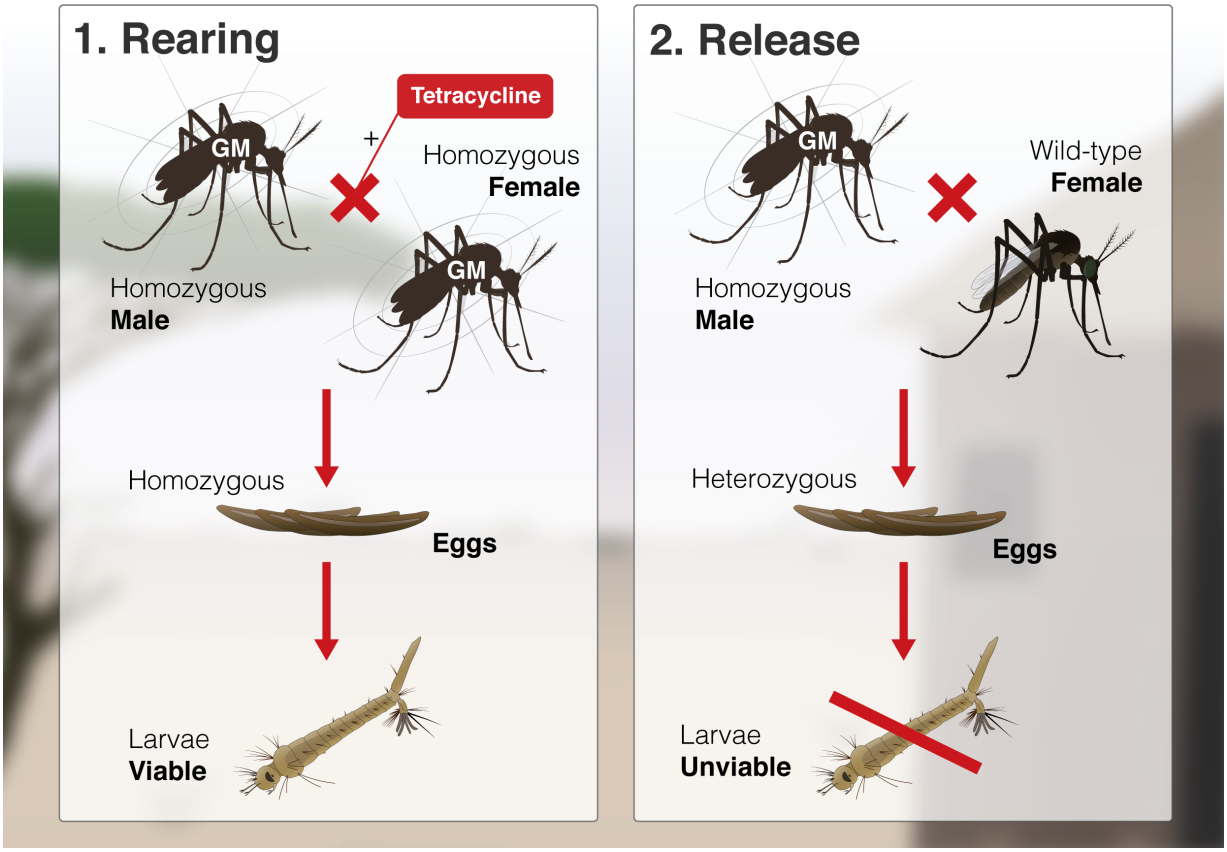

Figure 1-6 I OX513A RIDL mosquitoes. 1) The homozygous colony is maintained on tetracycline to repress the lethal gene. 2) Homozygous males are sorted and released into the environment to compete for wildtype females. The resultant heterozygous progeny are unviable and do not develop into adults[80,88].

1.2.2 Host-based Intervention Methods

Two major human-based intervention methods include vaccines and pharmacological treatments targeted against the pathogen. History has shown that vaccines are an effective method of eradicating diseases, however some of the worlds current major diseases are proving difficult to develop vaccines for[92]. Greater understanding of these

pathogens and their host interactions will likely be critical to designing effective vaccines. Malaria is a perfect example of this (Figure 1-7). The RTS,S-AS01 (GlaxoSmithKline) vaccine is the most developed[93,94], however, its phase III efficacy and safety trial showed that protection dropped quickly[95] and therefore the vaccine was not endorsed by WHO[96]. RTS,S-AS01 consists of a truncated form of the *P. falciparum* circumsporozoite protein (CSP), an abundant malaria parasite surface protein, which is fused to the hepatitis B surface antigen and combined with a liposome adjuvant[93]. Many alterations of the RTS,S-AS01 vaccination regime are now being tested with hopes of improving protection[97,98].

An alternative vaccine approach is the use of attenuated sporozoites. The most developed of these is the irradiated PfSPZ vaccine (Sanaria), which in a recent American study showed 92.3% and 80% protection three weeks post vaccination with homologous and heterologous parasite strains respectively[99]. However, by six months only 7 out of 10 and 1 out of 10 were protected from homologous and heterologous challenge respectively[99]. A recent phase I study in Mali involving 46 volunteers was used to explore efficacy against natural infections, which showed a reasonable 48.3% efficacy during a malaria season[100]. However, the required intravenous vaccination route, the five dose regime and the requirement of liquid nitrogen for vaccine transport[99-101] currently make this vaccination approach impracticable for use in sub-Saharan African.

These vaccines are pre-erythrocytic targeting the liver-stage. However, vaccines targeting mosquito transmission and the erythrocytic stage of malaria are also in development[102].

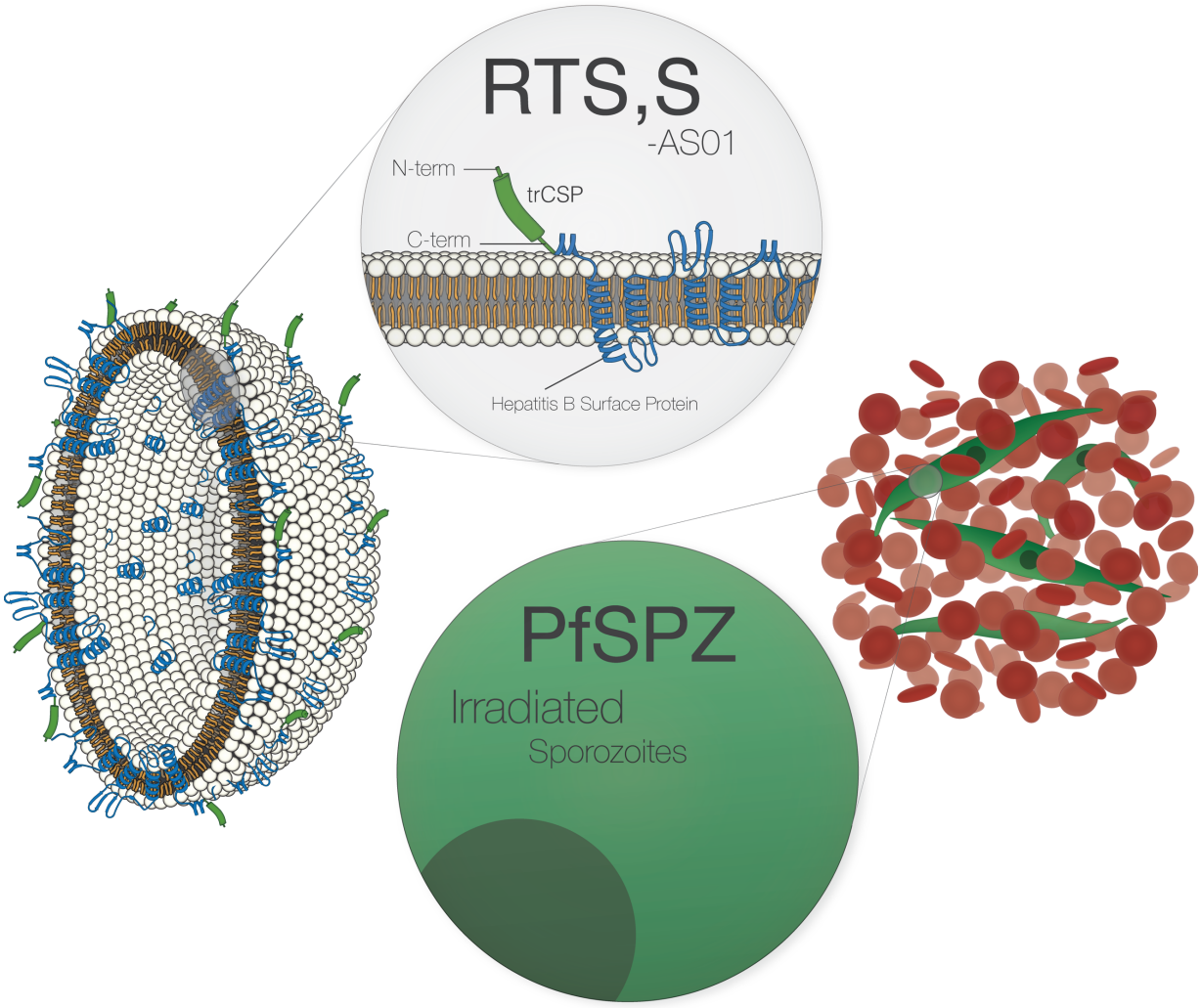

Figure 1-7 I Malaria vaccines. Top; RTS,S-AS01 vaccine consists a truncated from of the *P. falciparum* CSP fused to the hepatitis B surface antigen which forms a lipid-based VLP[93]. Bottom; PfSPZ irradiated sporozoites.

In contrast to malaria, vaccinating against dengue has an added difficulty due to the risk of disease enhancement which is observed in natural infections, where pre-existing antibodies from an earlier serotype cross-react with poor neutralising ability against different serotypes in a subsequent infection[103]. Therefore, vaccines should be effective against all four serotypes. The recently and only approved live attenuated chimeric dengue vaccine (CYD-TDV) by Sanofi Pasteur[104] is believed to suffer from the enhancement phenomenon as it showed an increase in the risk of severe dengue in infants below five years[105-109]. This is a major concern to the many other tetravalent vaccines also in development, all of which contain regions of the DENV proteome known to elicit robust antibody responses[110,111]. Two of these recently entered phase III trials; the attenuated DENVax (Takeda) containing four chimeric constructs based on a DENV2 backbone, and the TV003/TV005 (NIAID) based on four attenuated serotypes[104]. A CD8 T-cell specific vaccine would avoid antibody mediated disease

enhancement, however there are currently none published, even though recent evidence suggests they could be highly protective[112,113].

Over 15 vaccines are currently in development against CHIKV, the most developed being the VRC-CHKVLP059-00-VP (NIAID) a virus-like particle (VLP) created using CHIKV structural proteins[114] and TSI-GSD-218 (Salk Institute) a live attenuated virus, which are undergoing Phase II trials[115]. Most of the vaccines in development aim to induce a protective humoral response[115].

The second host-based intervention method is pharmacological treatments which target the pathogen. For dengue[103] and chikungunya[116] there are currently no antiviral drugs available. However there is considerable research being undertaken into their development[116-120]. For *P. falciparum* malaria, the front-line anti-malarial drug choice is artemisinin combination therapy (ACT), which involves combining a highly effective but short half-life artemisinin derivative with another longer half-life anti-malarial such as mefloquine or lumefantrine. Unfortunately, like previous anti-malarials such as chloroquine, sulphadoxine-pyrimethamine and mefloquine, the effectiveness of artemisinin has been found to be declining in Asia, typified by increased parasite clearance times. This resistance was originally identified in western Cambodia[49,121] and is now found in Thailand, Vietnam, Laos and Myanmar[48,122-125]. A mutation in the kelch13 gene has been associated with resistance[126]. Complete resistance to this front-line drug is a major concern for the eradication of malaria and highlights the need for new anti-malarials. Concerted screening programs[127-132] are attempting to identify new effective drug candidates, such as the recent discovery of E209, a promising tetraoxane analogue which is effective independent of the kelch13 mutation[127] and NITD609 a spiroindolone[132].

High-throughput assays for screening new drugs are based on either looking at phenotypic changes to the pathogen following drug treatment or investigating the effect of a drug on purified proteins at a biochemical level[133,134]. Phenotypic studies are commonly preferred as prior knowledge of the candidate drug targets is not required[133,134]. In the case of the malaria, studies look at the effect of *Plasmodium* development in *in vitro* blood[135] or hepatocyte cultures[136]. However, hepatocyte based cultures are a more difficult technique than blood stage culturing and there are still multiple roadblocks that need to be overcome to before hepatocyte cultures can be used effectively for high-throughput screening[133] (discussed more in Chapter 3). Alternatively, studies look at the effect of drug treatment on *Plasmodium* infected animals models by measuring blood parasitaemia[127] or transmission blocking in mosquitoes[137]. Similarly, vaccine candidates can be identified by studying and manipulating the development of parasites in *in vitro* cultures[138-140] and testing their efficacy with *in vivo* animal challenges[141].

1.3 Final Comment

The steady decline in malaria cases demonstrates how effective some of the current vector intervention methods can be, in particular, the introduction of LLINs across Africa[45]. However, many of these intervention methods are losing their efficacy due to insecticide resistance in the mosquito or drug resistance in the parasite[45]. Other mosquito borne-diseases with more limited intervention methods such as dengue are continuing to rise[51], highlighting the need for new intervention methods. However, some of the interventions in development are impractical for real world use, such as irradiated sporozoites, and a more precise method is needed to identify vaccine and drug candidates. Others need a better understanding of the underlying physiology such as *Wolbachia* in *An. gambiae* or a more novel approach such as dengue vaccines. This thesis attempts to address some of these issues in malaria and dengue by trying to improve methods for identifying new vaccine and drug candidates, improving the understanding of *Wolbachia* infection in *An. gambiae,* and developing a novel CD8 T-cell based dengue vaccine.

1.4 Thesis Aims

The aim of this thesis is to attempt to improve intervention methods against two key mosquito borne-diseases, dengue and malaria, which are highly debilitating[103] or associated with high mortality[45] respectively, through either improved understanding of mechanisms of intervention, development of better research tools to identify new pathogen targets, or by creation of novel intervention methods.

Firstly, this study attempts to improve the current *in vitro* system used to study liver stage malaria which in its current form is considerably hindering the discovery of new drug and vaccine candidates[142-144]. Next, it attempts to investigate *Wolbachia's* molecular interactions with *Anopheles* mosquito cells and its inability to establish stable infections within the *An. gambiae* host. Finally, a sequence conservation and hypothesis directed approach is used to design one of the first T-cell only based dengue vaccines which will soon enter phase I trials.

1.5 Thesis Outline

Malaria

To develop an *in vitro* hepatocyte system which provides high quantities of malaria infected hepatocytes far superior to current methods to aid identification of new drug and vaccine candidates by investigating sporozoite purification and hepatocyte culture methods.

⇒ Develop a superior method of purifying malaria sporozoites from mosquitoes which allows processing of large quantities of mosquitoes in a short period with a high level of sporozoite purity from the mosquito host.

⇒ Characterise the purification process and assess its effects on *in vitro* hepatocyte culture infections.

⇒ Develop an optimal hepatocyte culture system with the greatest permissibility to malaria infection.

To investigate the effect of *Wolbachia* on the mosquito target of rapamycin (TOR) signalling network with special interest on the consequences for malaria infection.

⇒ Characterise the impact of *Wolbachia* infection on the mosquito TOR axis.

⇒ Attempt to elucidate any molecular intervention methods that *Wolbachia* uses to modulate the TOR axis.

⇒ Investigate physiological host consequences of *Wolbachia*-mediated TOR modulation, with a special interest in the implications for developing stable *Anopheles gambiae* infections and the anti-malaria phenotype.

Dengue

To develop an effective conservation-based tetravalent human vaccine against dengue.

⇒ Develop a computational platform to assess protein conservation within dengue and other viruses such as chikungunya using readily available public sequences.

⇒ Assess conservation and combine with structural and functional features and published immunological data to develop a T-cell based dengue vaccine.

⇒ Assess the effectiveness of the vaccine in a preclinical setup.

2 Materials and Methods

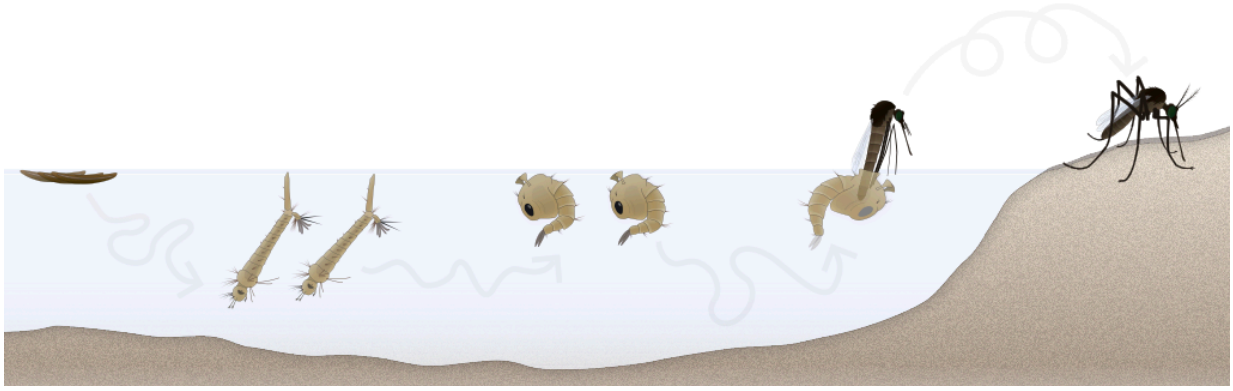

This chapter provides a list of all the materials used in this thesis and a detailed description of all methods.

2.1 Materials

2.1.1 Reagents

Commercially available reagents used in this thesis are listed in Table 2-1.

Table 2-1 I Commercially available reagents used throughout this thesis.

Reagent	Supplier	Cat. Number
Tissue Culture		
Schneider's *Drosophila* Medium	Pan-Biotech	P04-90500
SPODOPAN Protein-Free Medium	Pan-Biotech	P04-851000
Hepatocyte Growth Medium *(consists growth media C-25010B and supplement mix C-39642)*	Promocell	C-25010
Hepatocyte Basal Medium *(phenol red free)*	Promocell	C-25215
Dulbecco's Modified Eagle's Medium	Sigma-Aldrich	D6546
RPMI-1640 Medium	Sigma-Aldrich	R0883
Falcon Non-Vented TC Flasks (25, 75, 150cm^2)	BD Falcon	353082, 353135, 355000
Falcon 175cm^2 Vented TC Flasks	BD Falcon	353112
1-50mL Individually Wrapped (paper/plastic) Serological Pipettes	Corning	4485-90
Foetal Bovine Serum (heat inactivated)	Sigma-Aldrich	F9665

Penicillin-Streptomycin	Sigma-Aldrich	P4333
L-Glutamine	Sigma-Aldrich	G7513
TrypLE Express Trypsin	Thermo Sci	12605-010
96, 48, 24, 12, 6- Well Tissue-Culture Treated Plates	BD Falcon	353077, 230, 47, 43, 224
24-Well Glass Bottom TC Plates	MatTek Corp	P24G-1.5-13-F
35mm Glass Bottom Dishes	MatTek	P35G-0.170-14-C
Water (sterile)	Sigma-Aldrich	W3500
Phosphate Buffered Saline (with $MgCl_2$ $CaCl_2$; sterile)	Sigma-Aldrich	D8662
0.2µM Syringe Filters	VWR	S14-0061
Trypan Blue	Sigma-Aldrich	T8154
HepG2 [HEPG2] Hepatoma Line	ATCC	ATCC HB-8062
4a3b Cell Line	N/A	N/A
Nunc 1.0mL Cryovials	Thermo Sci	374081
Amaxa Nucleofector Kit V	Lonza	VCA-1003
Tocopherol	Sigma-Aldrich	T3251
Bortezimib	Cell Signal	2206s
PP242	Sigma-Aldrich	P0037
Pepstatin A	Sigma-Aldrich	P5318
Bafilomycin A1	Sigma-Aldrich	B1793
E64D	Enzolifesciences	BML-PI107-000
3-Methyladenine	Sigma-Aldrich	M9281
AICAR	Sigma-Aldrich	A9978
Rapamycin	Sigma-Aldrich	R0395
Collagen I Rat Protein, Tail	Thermo Sci	A1048301
Collagen IV From Human Cell Culture	Sigma-Aldrich	C6745
Fibronectin From Bovine Plasma	Sigma-Aldrich	F1141
Laminin from Engelbreth-Holm-Swarm Murine Sarcoma Basement Membrane	Sigma-Aldrich	L2020
Lipofectamine 3000 Reagent	Thermo Sci	L3000001
Promofectin Insect	PromoKine	PK-CT-2000-INC-50

Bambanker Serum-Free Cell Freezing Medium	Wako	302-14681
General Consumables		
50mL PP Centrifuge Tubes	BD Falcon	352070
15mL PP Centrifuge Tubes	BD Falcon	352096
0.1mL 8-tube PCR Tubes (lids attached)	VWR	732-0546
TipOne Filter Tips (10, 20, 200, 1000µL)	Starlab	S1121-3810, S1120-1810, -8810, S1126-7810
TipOne Refill Tips (10, 200, 1000µL)	Starlab	S1111-3700, -0700, -6700
1.5mL Eppendorfs (safelock, PCR clean)	Eppendorf	0030123328
2.0mL Eppendorfs (safelock, PCR clean)	Eppendorf	0030123344
0.5mL Eppendorfs (safelock, PCR clean)	Eppendorf	0030121023
1.5mL Protein Lo-Bind Eppendorfs	Eppendorf	0030108094
2.0mL Protein Lo-Bind Eppendorfs	Eppendorf	0030108132
5.0mL Protein Lo-Bind Eppendorfs	Eppendorf	0030108302
1.5mL DNA Lo-Bind Eppendorfs	Eppendorf	0030108051
2.0mL Deep-Well Plates Protein Lo-Bind	Eppendorf	0030504305
Heamocytometers	Immune Systems	BVS100
Carbonate-Bicarbonate Buffer	Sigma-Aldrich	C3041
100mL Costar Sterile Reservoirs	Corning	4872
Dimethyl Sulphoxide (DMSO)	Sigma-Aldrich	472301
PBS Tablets	Sigma-Aldrich	P4417
Methanol, Reagent Grade	Sigma-Aldrich	32213
Molecular Grade Ethanol	Sigma-Aldrich	E7023
Ethanol, Reagent Grade	Sigma-Aldrich	32221
Isopropanol, Reagent Grade	Sigma-Aldrich	24137
Giemsa Stain	Sigma-Aldrich	32884
Syringe (2, 5, 10mL)	BD	302187, 307727, 307736
Scalpel	Swann Morton	0302
Micro Tissue Grinder	VWR	KART6102

Molecular Biology		
Tris Acetate-EDTA Buffer	Sigma-Aldrich	T8280
Agarose	Sigma-Aldrich	A9539
SYBR Safe DNA Gel Stain	Thermo Sci	S33102
Amphicillin	Sigma-Aldrich	A5354
Kanamycin	Sigma-Aldrich	K0254
pIEX-4 DNA Plasmid	Merck	71235
pIEX-5 DNA Plasmid	Merck	71242
pIB/V5-His Vector Kit	Thermo Sci	V802001
pGEM-T	Promega	A3600
Nunc Petri Dishes	Sigam-Aldrich	Z717223
Restriction Enzymes	NEB	Assorted
LigaFast Ligation Enzyme	Promega	M8221
OneTaq Quick-Load 2x Master Mix With Standard Buffer	NEB	M0486S
AccuPrime *Pfx* DNA Polymerase High Fidelity	Thermo Sci	12344024
TURBO DNA-free Kit	Thermo Sci	AM1907
Superscipt III One-Step RT-PCR Kit	Thermo Sci	12574018
Superscipt III First-Strand Synthesis Kit	Thermo Sci	18080051
MegaScript T7 Transcription Kit	Thermo Sci	AM1333
Phenol-Chloroform Isoamyl (25:24:1)	Sigma-Aldrich	77617
Chloroform-Isoamyl (24:1)	Sigma-Aldrich	25666
Chloroform	Sigma-Aldrich	528730
NEB 5-Alpha Competent *E.coli*	NEB	C2987I
LB-Broth	Fisher Sci	1282-1670
LB-Agar	Sigma-Aldrich	L7025
Molecular Grade Water	AppliChem	A7398,1000
In-Fusion HD Cloning Plus CE	TaKaRa	638916
1Kb Plus DNA Ladder	Thermo Sci	10787018
EndoFree Plasmid Maxi Kit	Qiagen	12362
EndoFree Plasmid Giga Kit	Qiagen	12391

QIAquick PCR Purification Kit	Qiagen	28104
QIAquick Gel Extraction Kit	Qiagen	28706
QIAprep Spin Miniprep Kit	Qiagen	27104
TRIzol Reagent	Thermo Sci	15596026
RNeasy Mini Kit	Qiagen	74104
iScript cDNA Synthesis Kit	Bio-Rad Labs	1708890
SsoAdvanced Universal SYBR Green Supermix	Bio-Rad Labs	1725270
Hard-Shell 96-Well PCR Plates, Low Profile	Bio-Rad Labs	HSP9645
Microseal 'B' Film	Bio-Rad Labs	120709
6x Loading Dye	NEB	B7021S
Xtracta Tool	Sigma-Aldrich	Z722390
Snap Cap Tubes For Bacteria	Sigma-Aldrich	Z617954
Tris-EDTA Buffer (pH8)	Sigma-Aldrich	93283
Protein Biology		
2-β Mercaptoethanol	Fisher Sci	M/P200/05
Skim Milk Powder	Sigma-Aldrich	70166
Tween 20	Fisher Sci	10113103
Mini-PROTEAN TGX Gels	Bio-Rad Labs	Assorted
Criterion TGX Gels	Bio-Rad Labs	Assorted
Precision Plus Protein Unstained Standards	Bio-Rad Labs	161-0363
Precision Plus Protein WesternC Standards	Bio-Rad Labs	161-0385
4x Laemmli Sample Buffer	Bio-Rad Labs	161-0747
10x Tris/Glycine/SDS	Bio-Rad Labs	161-0732
Trans-Blot Turbo Mini PVDF Transfer Packs	Bio-Rad Labs	170-4156
Trans-Blot Turbo Midi PVDF Transfer Packs	Bio-Rad Labs	170-4157
Clarity Western ECL Substrate	Bio-Rad Labs	170-5061
Goat Anti-Rabbit IgG (H+L)-HRP Conjugate	Bio-Rad Labs	170-6515
Goat Anti-Mouse IgG (H+L)-HRP Conjugate	Bio-Rad Labs	170-6516
Pierce Silver Stain Kit	Thermo Sci	24612
Pierce BCA Assay	Thermo Sci	23225
Sodium Azide	Sigma-Aldrich	S2002

RIPA Buffer	Sigma-Aldrich	R0278
Protease Inhibitor Cocktail	Sigma-Aldrich	P8341
Phosphatase Inhibitor Cocktail	Sigma-Aldrich	P0044
Multiscreen-IP Filter Plate, 0.45µM	Millipore	MAIPS4510
Imaging		
VECTASHIELD Antifade Mounting Medium	Vector Labs	H-1000
Immersion Oil	Sigma-Aldrich	10890
Triton X-100	Sigma-Aldrich	X100
Clear Nail Varnish	N/A	N/A
16% Paraformaldehyde *(methanol free)*	Thermi Sci	28906
Round Coverslips 13mm *(No.1,5)*	VWR	631-0150
LIVE/DEAD Fixable Red Dead Cell Stain Kit	Thermo Sci	L23102
Lyso-ID Red Detection Kit	Enzo Lifesciences	ENZ-51005-500
Anti-Rabbit IgG (H+L), CF 488A Antibody	Sigma-Aldrich	SAB4600044
Partec CellTrics Strainers (100, 50µM)	Partec	04-0042-2318, -2317
Fixation and Perm Buffer	EBiosciences	BML-PI107-000
Free-Flow Electrophoresis		
Accudenz	Accurate Chemical	AN-7050
Triethanolamine	Sigma-Aldrich	90278
Sucrose	Sigma-Aldrich	S0389
Glacial Acetic Acid	Sigma-Aldrich	A6283
Bleach (~14%)	Sigma-Aldrich	425044
Petrol ether (40-60^{o}C)	Fisher Sci	P/1760/17
Plate Sealers	4titude	4ti-0500
pluriStrainer Cell Strainer (20, 40µM)	pluriSelect	43-50020-03, 43-50040-01
Falcon Cell Strainer (70, 100µM)	BD Falcon	352350, 352360
Tryptic Soya Broth	Oxoid	BO0509M
Sulfanilic Acid Azochromotrop (SPADNS)	Sigma-Aldrich	S9256
Horse Blood Agar Plates	Oxoid	PB0114A
Animal Research / Liver Perfusion		

Ketaset (Ketamine)	Oxford University Vet Services	N/A
Rompun (Xylazine)	Oxford University Vet Services	N/A
Isoflurane	Oxford University Vet Services	N/A
Pentobarbitone	Oxford University Vet Services	N/A
Insulin Syringes (0.5mL)	BD	324892
Needles (19G x 1/2in.)	BD	305187
Syringes (1, 5, 10, 20mL)	BD	309629, 309646, 301604, 301625
Microscope Slides	Thermi Sci	AAAA000080##32E
3M Vetbond Tissue Adhesive (IMS Vet)	3M	70200742529
Tro-Venocath (22G) - Blue	Trogemedical	TR-1602
Percoll	Sigma-Aldrich	P1644
Liver Digest Medium	Thermo Sci	17703034
Liver Perfusion Medium (x1)	Thermo Sci	17701038
Heparin	AppliChem	A3004,0250
Microfluidic Device Fabrication		
PDMS	VWR	USPH1546300
APTES (3-Aminopropyl)triethoxysilane	Sigma Aldrich	A3648
GPTES (3-Glycidyloxypropyl)triethoxysilane	Sigma Aldrich	50059
Coverslips	Fisher Sci	13236788
Polycarbonate Membranes	Sigma-Aldrich	WHA111115
Lead-Free Solder	Maplin	N29AR
Silicone Tubing (0.31mm)	VWR	228-0654
Epoxy Resin	Maplin	N60BZ
Primary Antibodies (Work in my models) *See supplemental Table 8-1 for antibodies that do not work in the 4a3b model*		
Anti-Actin	Sigma-Aldrich	A2066
Anti-Lamp1	Abcam	Ab30687
Anti-S6Kp	Cell Signal	4858p

Anti-Ubiquitin	Abcam	Ab137031
Anti-agATG8 Polyclonal (made using service from Eurogentec)	Eurogentec	N/A

2.1.2 Equipment and Software

Specialised equipment and software used during this thesis are listed in Table 2-2.

Table 2-2 | Specialised equipment and software used during this thesis

Reagent	Supplier	Cat. Number
Free-Flow Electrophoresis System (BD System)	FFE Service GmbH	N/A
Generator Series VACULAB	Tantec	N/A
Microfluidic Pump System	Ibidi	10902
ImageStream IS100 System	Amnis	IS100
Peristaltic Pump Tubing (2x4mm)	VWR	228-0703
TransBlot Turbo	Bio-Rad Labs	1704155
Photolithography Setup	Physics Department	N/A
Soldering Iron	Fisher Sci	13025943
Amaxa Nucleofector II	Lonza	N/A
Qubit 3.0 Fluoremeter	Thermo Sci	Q33216
Assorted Medical instruments	Fine Scientific Tools	Assorted
CLARIOstar	BMG Labtech	N/A
Geneious (V8)	Biomatters	N/A
R	R Foundation	N/A
Plotly (plot.ly)	Plotly	N/A
Adobe Illustrator	Adobe	N/A
Amnis IDEAS	Amnis	N/A
Jave SE Development Kit 8	Oracle	N/A
Eclipse IDE	Eclipse Foundation	N/A

2.1.3 Hand-made Solutions, Media and Buffers

- **Complete Schneider's medium:** 500mL Schneider's *Drosophila* medium, 50mL FBS (10%), 5mL penicillin/streptomycin (1%)

- **Plain Schneider's medium:** 500mL Schneider's *Drosophila* medium (no supplements)
- **Dissection Schneider's medium:** 500mL Schneider's *Drosophila* medium, FBS (1%)
- **Complete DMEM (Dulbecco's Modified Eagle's medium):** 500mL DMEM, 50mL FBS (10%), 5mL penicillin/streptomycin (1%), 5mL L-glutamine (1%)
- **Complete primary hepatocyte growth medium:** 500mL hepatocyte growth medium (+ 40mL supplement pack), 2.5-5mL penicillin/streptomycin (0.5-1%)
- **17% w/v Accudenz**: 3.4g/100mL dissolved in deionised water
- **FACS buffer**: 500mL 1x PBS, 5mL FBS (1%)
- **Heparin solution:** 100 units/mL dissolved in 1xPBS
- **Blood stage freezing medium:** 11mL FBS (10%), 4.2mL 5% $NaHCO_3$ (0.2%), 5.5mg neomycin (0.00005%), 22mL DMSO (20%), 74mL RPMI-1640
- **DNA extraction buffer:** 5.844g NaCl (0.1M), 68.46g sucrose (0.2M), 15.756g Tris-HCl (0.1M, pH8), 14.612g EDTA (0.05M), 0.5% SDS (5g)
- **0.1M bicarbonate buffer (pH 9.4):** two tablets/100mL sterile tissue culture treated water
- **Ampicillin stock:** 100mg/mL in water
- **Kanamycin stock:** 50mg/mL in water
- **3-Methyl amine stock:** 100M stock in PBS
- **Bafilomycin A1 stock:** 100µM in DMSO (62.283µg/mL)
- **PP242 stock:** 5nM in DMSO (1.5417mg/mL)
- **AICAR stock:** 100mM in H_2O (25.823mg/mL)
- **4x Reducing Laemmli buffer:** 100µL β-mercaptoethanol was added to 900µL 4x Laemmli buffer (Bio-Rad Labs)
- **Percoll solutions:** SIP**:** 90mL percoll (90%), 10mL 10x PBS. 1.066g/mL: 18mL SIP, 14mL 1xPBS. 1.037g/mL: 14mL SIP, 30.2mL 1x PBS
- **Liver perfusion medium:** 500mL liver perfusion medium, 5mL penicillin/streptomycin (1%)
- **SPADNS solution:** 1% solution in deionised water (dH_2O)
- **FFE buffers:** buffer compositions for continuous zone electrophoresis (cZE)-triethanolamine/sucrose run (below)

  <u>Stock solution:</u> 74.65g triethanolamine (500mM), 28.60mL acetic acid (500mM), 850.0mL dH_2O. Adjust to pH 7.4 with KOH, then adjust to a total of 1L with dH_2O. Conductivity ~20000µS/cm, pH 7.4.

Stabilisation buffer (anode & cathode): *95.80g sucrose (250mM), 200.00mL stock solution. Adjust to a total of 1L with dH_2O. Conductivity ~4850µS/cm, pH7.4.*

Electrode buffer (anode and cathode): *200.00mL stock solution. Adjust to a total of 1L with dH_2O. Conductivity ~6000µS/cm.*

Separation buffer: *191.60g sucrose (250mM), 200.00mL electrode buffer. Adjust to a total of 2L with dH_2O. Conductivity ~650µS/cm, pH 7.4.*

2.1.4 Oligonucleotide Primers

All oligonucleotide primers used for polymerase chain reaction (PCR) or real time (RT) PCR are listed in Table 2-3.

Table 2-3 | Oligonucleotide primers used in this thesis.

Name	Sequence	Target
	PCR	
WSPEC	F: CATACCTATTCGAAGGGATAG R: AGCTTCGAGTGAAACCAATTC	*Wolbachia*
*w*AlbB	F: TGGTCCAATAAGTGATGAAGAAAC R: GATCTCTTTAGTAGCTGATACTG	*Wolbachia*
*w*Mel/MelPop	F: TGGTCCAATAAGTGATGAAGAAAC R: CAGCCTGTCCGGTTGAATT	*Wolbachia*
*w*MelVsPop	F: TATTGAGCCTTCCTCGTACC R: TAGCATGCCGTTTTTCTGTA	*Wolbachia*
pIEX_MCS	F: GTTATCGTGTTCGCCATTAGGG R: GCAAAACCCCACACCAACAA	*N/A*
*ag*Sestrin	F2: TATGGCTCAAAGAATTCGCCA R1: TGTCATGTATCGCATAACTTCG	*An. gambiae*
WSP	F: CATTATAAAAAGTTTTTTTCAGCAGC R: CTAGAAATTAAACGCTACTCCA	*Wolbachia*
ATG8	F: ATGAAGTTCCAGTACAAGGAAGA R: TTAGTTGCTGCTGTCAGCG	*An. gambiae*
WIPI2	F: ATGAGCCTTCTGGCGAGAAC R: TTACTGCTTTTGCTGGTCATGTT	*An. gambiae*
	RT-PCR	
qS7	F: TTCAACAACAAGAAGGCGATCA R: CTTGTACACCGACGCAAAAGTG	*An. gambiae*
qHTH	F2: TGGTCCTATATTGGCGGAGCTA R1: TCGTTTTTGCAAGAAGGTCA	*Wolbachia*
qWSP	F: GCATCTTTTATAGCTGGTGG	*An. gambiae*

	R: AAAGTCCTTCAACATCAACCC	
qP62	F: TCGGAAATGTTGTGCCGTTC R: GTTTGGATGTTTCGCCGCAT	*An. gambiae*
qRheb	F1: CACGAAAAAGACCCGCATCC R1: TGTCCAGCAGCTTGTCGTAG	*An. gambiae*
qTOR	F: GGCTACATCTTGGGTCTCGG R: AGACTGTCCTTGTTACGGCG	*Wolbachia*
qATG1	F: TGATGACAGTGTGGCAACGA R: TTCTGAGATCGGTAGCGTGC	*An. gambiae*
qATG5	F: ACTCGTCGGTACTGATGGGA R: TGCATTGCGGAAACCACTTG	*An. gambiae*
qATG8	F: GTGTGCCTGTGATCGTCGA R: CCTCGTGATGCTCGTGGTAC	*An. gambiae*
qSestrin	F: AAGGAACACGTTGAGCGACT R: CGATTTTGTGACTAGCGCCG	*An. gambiae*
qHSP70 (DNA)	F2: AGGAATGCCAGGAGGAATGC R1: AGTTGGTCCACTTCCAGCTG	*P. berghei*
qHSP60H	F1: GACCAAAGACGATGCCATGC R1: GCACAGCCACTCCATCTGAA	Human
qHSP60R	F1: TGGAGAGGTCATCGTCACCA R1: CACAGCTACTCCATCTGAGAGT	Rat
qHSP60M	F1: TCACCAAAGATGATGCCATGC R1: GCAAGTCGCTCGTTCAGC	Mouse
HPRT1	F1: GCTGAAGATTTGGAAAAGGTG R1: AATCCAGCAGGTCAGCAAAG	Rat
qHSP70 (RNA)	F1: AAGCATTAAATAAAGCGAATACATCCTTAC R1: GGAGATTGGTTTTGACGTTTATGT	*P. berghei*
dsRNA Synthesis		
T7_LacZ	F: TAATACGACTCACTATAGGG AGAATCCGACGGGTTGTTACT R: TAATACGACTCACTATAGGG CACCACGCTCATCGATAATTT	*An. gambiae*
T7_p26	F: TAATACGACTCACTATAGGG CTCGCCACAGGATCTGGATG R: TAATACGACTCACTATAGGG GCACGTGAGCAAAGGTTTGT	*An. gambiae*
T7_ATG1	F: TAATACGACTCACTATAGGG	*An. gambiae*

	GCGATCTGGCGGACTATCT R: TAATACGACTCACTATAGGG CAATCCTTTGCCGCAGTTAT	
T7_ATG5	F: TAATACGACTCACTATAGGG GGTAAACAGGCGATTGATGG R: TAATACGACTCACTATAGGG GGTAACGCCATGGGTTCTT	*An. gambiae*
T7_TOR	F: TAATACGACTCACTATAGGG ACCTGTCGCTGTACGTCAAG R: TAATACGACTCACTATAGGG GCGGGAAATCTTGTTGGTCG	*An. gambiae*

2.1.5 Plasmid Constructs

All plasmids created and used in this thesis are listed in Table 2-4.

Table 2-4 | Plasmids used in this thesis

Name	Backbone	Description
pLacZ	pGEM	For making LacZ dsRNA control
qHSP_60-70	pGEM	For *P. berghei* sporozoite absolute RT-PCR standard curve
qHTH_WSP	pGEM	For *Wolbachia* absolute RT-PCR standard curve
pIEX4_shATG5-1/2	pIEX4 (+U6 promoter)	Plasmids for expression of short hairpin RNA's in 4a3b cells under the *An. gambiae* U6 Promoter.
pIEX4_shATG14-1/2	pIEX4 (+U6 promoter)	
pIEX4_shATG8-1/2	pIEX4 (+U6 promoter)	
pIEX4_shScrambled	pIEX4 (+U6 promoter)	
pIEX5_ATG8-His	pIEX5	Production of ATG8 and WSP for monoclonal production
pIEX5_WSP-His	pIEX5	
pIB_GFP-ATG8	pIB	Production of GFP fused ATG8 and GFP
pIB_GFP-WIPI	pIB	
pIEX4_Sestrin-His	pIEX4	For ectopic *An. gambiae* sestrin expression

2.2 Methods

Molecular Biology

2.2.1 DNA Extraction

Cells were washed three times in 1x PBS and re-suspended in DNA extraction buffer (see 2.1.3), followed by heating to 65°C for 30 min then 95°C for 10 min and finally stored on ice for at least 30 min. Debris was removed by centrifugation (15,000 xg, 15 min) and an equal volume of phenol-chloroform-isoamyl was added to the resultant liquid, shaken and centrifuged (12,000 xg, 5 min). Subsequently, the aqueous phase was transferred to a fresh tube, an equal volume of chloroform-isoamyl added, mixed, and centrifuging (12,000 xg, 5 min). The resultant supernatant was mixed with 0.8 volumes isopropanol and DNA precipitated for 10 min at room temperature (RT), then centrifuged (12,000 xg, 30 min, 4°C). Finally, the DNA pellet was washed in 70% ethanol, centrifuged (12,000 xg, 10 min, 4°C) and pellet re-suspended in molecular grade H_2O (mH_2O).

2.2.2 Polymerase Chain Reaction (PCR)

DNA templates were amplified using either OneTaq DNA polymerase (NEB) for diagnostic purposes or high fidelity Platinum *Pfx* DNA polymerase (Thermo Sci) for cloning purposes as per the manufacturer's standard protocol. Primers (Table 2-3) for cloning also contained 5' restriction or recombination sites.

2.2.3 RNA Extraction

Samples (hepatocyte or insect cells) were washed with 1x PBS three times and re-suspended in TRIzol reagent (50-200µL) and centrifuged (10 min, 12,000 xg, 4°C) to remove cellular debris. The resultant liquid was allowed to reach RT and 20µL chloroform per 100µL TRIzol added, mixed and centrifuged (15 min, 12,000 xg, 4°C). The aqueous phase was transferred to a fresh tube and mixed with 50µL isopropanol per 100µL TRIzol, then allowed to precipitate for 10 min at RT and centrifuged (10 min, 12,000 xg, 4°C). Finally, the supernatant was discarded and the RNA pellet washed with 70% ethanol, then allowed to air dry for 5-10 min and re-suspended in mH_2O (30-50µL). Extracted RNA was treated with TURBO DNase (Thermo Sci) as per the manufactures protocol. Briefly, a 50µL reaction containing 30µL RNA was incubated for 20 min at 30°C, then 5µL DNase inactivation agent added and incubated for 5 min. The inactivation agent was removed by centrifugation (10,000 xg, 1.5 min) and the supernatant stored at -80°C.

2.2.4 Gene Specific cDNA Synthesis

Host gene cDNA for expression in plasmids (Table 2-5) was amplified from RNA using the SuperScript III One-Step RT-PCR System (Thermo Sci), as per manufactures protocol, which reverse transcribes cDNA then PCR amplifies gene specific cDNA using specific primer sets. Briefly, a master mix containing 1µg DNAase-treated RNA and gene specific primers totalling 50µL was made and PCR cycled as per below. These

primers either contained 5' restriction sites for cloning or 15bp overhangs for ligation-independent cloning (LIC).

cDNA Synthesis:	55°C	20 min	
	94°C	2 min	
Denature:	94°C	15 sec	x40
Anneal:	55-66°C	30 sec	
Extend:	68°C	1 min/kb	
Final Extension:	68°C	5 min	

Product size was checked by agarose gel electrophoresis (2.2.6).

Table 2-5 l Genes amplified from cDNA

Name	Length (bp)	Database Reference
ATG8	393	VectorBase ID: AGAP002685
WSP	714	NCBI Accession: AF338346.1
WIPI2	1,260	VectorBase ID: AGAP005910
Sestrin	1,272	VectorBase ID: AGAP007169-RA

2.2.5 Custom Gene Synthesis

On some occasions genes were synthesised using GeneArt services (Thermo Sci) instead of being amplified from DNA or cDNA, listed in Table 2-6. Restriction sites or LIC overhangs were added to sequences.

Table 2-6 | Custom synthesised constructs

Name	Length (bp)	Description
shATG5-1	163	shRNA sequence with U6 *An.gambiae* promoter and poly (T) termination signal.
shATG5-2	163	
shATG8-1	174	
shATG8-2	174	
shATG14-1	174	
shATG14-2	174	
shScrambled	163	

2.2.6 Agarose Gels

1-0.5% agarose gels in 1x tris-acetate-EDTA (TAE) were used to separate DNA fragments by electrophoresis (80V, ~40 min) and imaged using SYBR Safe. DNA was loaded using 6x Loading Dye (NEB) and imaged using a blue light transilluminator.

2.2.7 Gel Extraction

For cloning or sequencing purposes DNA fragments were extracted from 0.5% agarose gels using an Xtracta tool (Sigma) and DNA purified using a QIAprep Spin Miniprep Kit (Qiagen) as per manufacturer's instructions. DNA was re-suspended in mH_2O.

2.2.8 Restriction Digest

PCR fragments and plasmids (1µg) were double digested in 50µL volume using 10 units of each restriction enzyme (NEB) with buffer recommended by manufacturer at 37°C for 2-4 hr. Digested products were separated on a 0.5% agarose gel and extracted as per 2.2.7. If the plasmid was to be used for ligation independent cloning (2.2.11) the digested product was instead heated to denature restriction enzymes at a time and temperature recommended by the manufacturer.

2.2.9 Nucleic Acid Quantification

Nucleic acids were quantified using the Qubit fluorometer (Thermo Sci) using the relevant assay kit as per the manufacturer's protocol. Briefly, 1-4µL sample was combined with working solution to a final volume of 200µL, vortexed and allowed to incubate for 2 min before quantification. Standards were created by adding 10µL standard to 190µL working solution.

2.2.10 DNA Ligation

Gel extracted plasmid and insert digestion products were combined in 10µL total volume at a molar ratio of 1:2 (other ratios where attempted if this ratio failed), with provided buffer and three units of ligase for 5 min at room temperature for ligation with

LigaFast Rapid DNA ligation system (Promega) as per manufacturer's protocol. Controls consisted of uncut vector, no insert and no ligase reactions. DNA quantity was determined using the below equation.

$$ng\ of\ insert = \frac{ng\ of\ vector\ \times\ kb\ size\ of\ insert}{kb\ size\ of\ vector}\ \times\ molar\ ratio\ of\ \frac{insert}{vector}$$

2.2.11 Ligation-Independent Cloning (LIC)

As an alternative to restriction-based cloning some constructs were created using LIC (In-Fusion HD Cloning Plus, Takara) as per manufacturer's standard protocol using Cloning Enhancer (CE). Briefly, inserts were amplified using the provided CloneAmp HiFi PCR premix with 5ng template using primers designed with 15bp overhangs that match the recipient plasmid and treated with CE. Recipient plasmid was double digested as per 2.2.8 and LIC carried out using 2µL of CE-treated insert and 50-100ng linearized vector (up to 6µL) in 10µL total volume with stated buffer for 15 min at 50°C. At each step a sample of product was separated on an agarose gel (2.2.6) to assess success.

2.2.12 Bacterial Transformation

Following successful cloning, NEB 5-alpha competent *E. coli* (NEB) were transformed as per the manufacturer's standard protocol using 1-5µL of ligated insert. Transformed bacteria were allowed to recover in 500µL super optimal broth (SOC) shaking at 250 rpm, 37°C for 1 hr. Different volumes (20-200µL) were spread on pre-warmed (37°C) Luria broth (LB; Lennox) agar plates with the relevant selective antibiotic (ampicillin; 100µg/mL, kanamycin; 50µg/mL) and left overnight at 37°C static. Control transformants with no plasmid and plates with a different antibiotic were used as controls. The following morning plates with suitable confluency for selecting individual colonies were used for down-selection.

2.2.13 Transformant Selection

Five to ten colonies were picked for each plasmid and added to 5mL LB with the relevant selective antibiotic (ampicillin; 100µg/mL, kanamycin; 50µg/mL) and left overnight shaking at 250 rpm, 37°C. The following day plasmids were purified from cultures using the QIAprep Spin Miniprep Kit (Qiagen) and screened by PCR using the relevant screening primer set which amplifies the multiple cloning site (MCS) (see 2.1.4 pIEX_MCS). Amplicon size was checked by agarose gel electrophoresis and sequenced to confirm accuracy.

2.2.14 Bacterial Glycerol Stocks

Transformed bacteria in LB were mixed with 25% glycerol total volume with selective antibiotic (ampicillin; 100µg/mL, kanamycin; 50µg/mL) and stored at -80°C.

2.2.15 DNA Plasmid Purification

Transformed bacteria were up-scaled to 0.5-1.0L of LB with selective antibiotic by initial inoculation in 50mL overnight (250 rpm, 37°C) following by subsequent transfer to 0.5-

1.0L LB and another overnight incubation (250 rpm, 37ºC). Plasmid was then extracted with an EndoFree Plasmid Maxi/Giga Kit (Qiagen) using the manufacturer's standard protocol. DNA pellets were re-suspended in 500µL of 60ºC sterile mH_2O or Tris-EDTA buffer (pH 8) and diluted to 1µg/µL.

2.2.16 Absolute gDNA RT-PCR

Wolbachia density was determined by absolute quantitative PCR (qPCR) using DNA template with a plasmid-based standard curve (qHTH_WSP; Table 2-4) containing a 76bp fragment from *An. gambiae* HTH (AGAP002178) housekeeping gene an a 217bp fragment from *Wolbachia* wsp (NCBI AF338346) gene and was developed previously in our laboratory (Sofia Pinto). Plasmid copy numbers for each dilution of the standard curve was calculated (Table 2-7) based on its mass ($3.60694e^{-18}$g).

Table 2-7 I Calculating plasmid copy numbers for qHTH-WSP standard curve.

Dilution	Plasmid Copy Number
1	14,910,161,976.81
2	149,101,619.77
3	3,000,000.00
4	300,000.00
5	30,000.00
6	3,000.00
7	300.00
8	30.00

Number of plasmid copies (and thus wsp and HTH copies) in each dilution of the standard curve. Dilution one and two were not used in the qPCR setup.

DNA from samples extracted per 2.2.1 was quantitated using the Qubit fluorometer (Thermo Sci; 2.2.9) and all samples diluted to 50ng/µL. A master mix using SsoAdvanced Universal SYBR Green Supermix (Bio-Rad Labs) was made using either HTH (qHTH_F2, R) or wsp (qWSP_F1, _R1) primers with DNA samples run in duplicate on a CFX Connect RT-PCR machine (Bio-Rad Labs), cycled as per below:

Activation:	98°C	2 min	
Denature:	98°C	10 sec	} x40
Anneal & Extend:	60°C	20 sec	
Melt-Curve	65-95°C	2 sec/step	

HTH and wsp copy numbers were calculated using linear fit and wsp copies numbers normalised to sample HTH values.

Plasmodium berghei hepatocyte density was determined using the same technique with a standard curved plasmid containing a 271bp fragment from murine heat shock protein (HSP) 60 (Ensembl: ENSMUST00000027123) housekeeping gene and a 176bp fragment from *P. berghei* HSP70 gene (PBANKA_071190). Murine HSP60 was chosen to allow the plasmid to be used to quantitate human, mouse and rat samples using different primer sets. Plasmid copy numbers for each dilution of the standard curve were calculated based on its mass ($3.75161e^{-18}$g; Table 2-8). Multiple primers were tested to identify the best primer efficiency. qPCR reactions were run as above using primers qHSP60R for Rat, qHSP60H for Human and qHSP60M for mouse and analysed as above.

Table 2-8 I Calculating plasmid copy numbers for qHSP60-70 standard curve.

Dilution	Copy Number
1	3,000,000,000.00
2	300,000,000.00
3	30,000,000.00
4	3,000,000.00
5	300,000.00
6	30,000.00
7	3,000.00
8	300.00
9	30.00

Number of plasmid copies (and thus HSP60 and HSP70 copies) in each dilution of the standard curve. Dilution one was not used in the qPCR setup.

2.2.17 Relative cDNA RT-PCR

For cDNA RT-PCR, DNAase treated RNA (2.2.3) was quantified using the Quibit® fluorometer (2.2.9). Total cDNA was synthesised using iScript cDNA Synthesis Kit (Bio-Rad Labs) using 1µg of DNAse treated RNA as per manufacturers standard protocol. 1-2µL of cDNA from each reaction was combined to create a standard curve (1:5, 1:10, 1:50, 1:100, 1:1000). The remainder was diluted 1 in 20 in mH_2O. A master mix using SsoAdvanced Universal SYBR Green Supermix (Bio-Rad Labs) was made using a housekeeping primer set (S7 for *Anopheles gambiae*, or HPRT1 for Rat*)* and gene of interest primer set, with DNA samples run in duplicate on a CFX Connect RT-PCR machine (Bio-Rad Labs), cycled as per below:

Activation:	95°C	30 sec	
Denature:	95°C	10 sec	} x40
Anneal & Extend:	60°C	20 sec	
Melt-Curve	65-95°C	2 sec/step	

Relative gene expression was calculated using the Paffl method[145].

2.2.18 dsRNA Design and Synthesis

Long dsRNA for use in RNAi was designed using E-RNAi (www.e-rnai.org) with default settings (Table 2-9). cDNA was synthesised and amplified with 5' T7-tagged primers

(2.1.4) using the SuperScript III One-Step RT-PCR System (Thermo Sci) (2.2.4). Product was purified using the QIAquick PCR Purification Kit (Qiagen) as per manufacturer's standard protocol and eluted in 30µL mH_2O. A LacZ control was amplified from a plasmid template. The resultant PCR product was used as template for MEGAscript T7 (Thermo Sci) dsRNA transcription using manufacturer's standard protocol with 16µL template in a double reaction incubated at 37°C overnight. Synthesised dsRNA was purified using the RNeasy Mini Kit (Qiagen) as per manufacturer's standard protocol, eluted in 20-30µL mH_2O and adjusted to 1ng/µL.

Table 2-9 | Long dsRNA constructs with VectorBase ID.

dsRNA	Target	Sequence (5'-3')
dsMTOR	AGAP007873	ACCTGTCGCTGTACGTCAAGACGGAGCTGCGCGAAACTCCGGACG ACATGTTTTTCGAAGACTTTAACCACCACATCTTCGAGATGCTCA CCAGCACAGACAATAACGAGAAAAAGGGCGGAATACTGGCCATCG ATTGTCTCATCAACGGCGATGTCGTGAACACGACCAACAAGATTT CCCGC
dsATG1	AGAP011295	GCGATCTGGCGGACTATCTGGCAGTAAAAGGAACCCTCAGCGAAG ACACCATCCGACTGTTCCTCGGTCAACTGGCAAACGCTATGAAGG CCCTGTACCAGGCAGACGTGGTCCATCGGGATCTAAAGCCGCAAA ATATACTCCTATCACATAACTGCGGCAAAGGATTG
dsP62	AGAP007873	CTCGCCACAGGATCTGGATGAAGTGGCACGCGTGCCGAGCAACAA AACTGCTGCATCCGATCGTCGATGCGGCGAAACATCCAAACCGCC CCGTTACAGTAAGTCCAGCGGTGAACGCAAACAAACCTTTGCTCA CGTGC
dsATG5	AGAP010939	GGTAAACAGGCGATTGATGGAACCTATCCCCGACCAGGATGGTTT CAAACACATTCCAGTAAGGTGCTATGCCGAGGACGGTACGTACCA GCAGAAACTAGTCGCACCCAGCACCGCATCCGGTCAGAAGCGTCT GTTGCAGGATTTGTTGGACGATTTCTCAACACCTGTTAGGAAAGC AGTCGAGGCAAGAACCCATGGCGTTACC

2.2.19 siRNA Design

siRNAs were designed using BLOCK-iT RNAi Designer (Thermo Sci; https://rnaidesigner.thermofisher.com/rnaiexpress) with standard settings and a dTdT overhang (Table 2-10). Two siRNAs were created for each target and the most effective used. A scrambled siRNA was created as a control. Sequences were checked for specificity using the basic local alignment search tool (BLAST; NCBI) and synthesised using the Silencer Select siRNA program (Thermo Sci) and re-suspended to 50µM in mH_2O.

Table 2-10 | siRNA sequences and their VectorBase ID.

siRNA	Target	Sequence
siATG8-1	AGAP002685	Sense: GCAUCGAUGACCUGGACAATT Antisense: UUGUCCAGGUCAUCGAUGCTT
siATG8-2		Sense: CCAGUUCUACUUCCUGAUUTT Antisense: AAUCAGGAAGUAGAACUGGTT
siRheb-1	AGAP001902	Sense: GCAUGGAUUUCCACGGCUATT Antisense: UAGCCGUGGAAAUCCAUGCTT
siRheb-2		Sense: GCGAUCGUUCGAGGUGAUATT Antisense: UAUCACCUCGAACGAUCGCTT
siControl	N/A	Sense: GCAUUAGACCUGGCGUCUATT Antisense: UAGACGCCAGGUCUAAUGCTT

2.2.20 shRNA Design & Creation

shRNA sequences were designed as previously described[146] (Table 2-11). Briefly, shRNAs with a 19 nucleotide stem and CCTCAGC loop with 30-50% CG content were designed and specificity assessed by nucleotide BLAST (NCBI). Two constructs were created per target. A scrambled shRNA was designed as a control. A 5' U6 *An. gambiae* polymerase III promoter, 3' poly(T) terminator sequence and LIC overhangs were added for cloning into the pIEX4 plasmid outside of the MCS (See 2.1.5).

Table 2-11 | shRNA constructs and their VectorBase ID.

shRNA	Target	Sequence (5'-3')
shATG5-1	AGAP010939	ACATGTTTAATTAAGTGTGGCTTCTAACGTTATCCATCGCTAGAA GTGAAACGAATGTGCGTAGGTATATATATGAAATGGAGTTGCTCT CTGCTTAACCGATGTAGAGCCGGAA**CCTCAGC**TTCCGGCTCTACA TCGGTTTTTTTTTTGGAAGCGGAAGAGC
shATG5-2		ACATGTTTAATTAAGTGTGGCTTCTAACGTTATCCATCGCTAGAA GTGAAACGAATGTGCGTAGGTATATATATGAAATGGAGTTGCTCT CTGCTTTGATAAGTTCGACCAGTTC**CCTCAGC**GAACTGGTCGAAC TTATCATTTTTTTTTGGAAGCGGAAGAGC
shATG8-1	AGAP002685	TGATCGACATGTTTAATTAAGTGTGGCTTCTAACGTTATCCATCG CTAGAAGTGAAACGAATGTGCGTAGGTATATATATGAAATGGAGT TGCTCTCTGCTTCGTCATTCCGCCGACGTCG**CCTCAGC**CGACGTC GGCGGAATGACGTTTTTTTTTGGAAGCGGAAGAGCGTGAT
shATG8-2		TGATCGACATGTTTAATTAAGTGTGGCTTCTAACGTTATCCATCG CTAGAAGTGAAACGAATGTGCGTAGGTATATATATGAAATGGAGT TGCTCTCTGCTTTATCCAGACCGTGTGCCTG**CCTCAGC**CAGGCAC ACGGTCTGGATATTTTTTTTTGGAAGCGGAAGAGCGTGAT

shATG14-1	AGAP012246	TGATCGACATGTTTAATTAAGTGTGGCTTCTAACGTTATCCATCG CTAGAAGTGAAACGAATGTGCGTAGGTATATATATGAAATGGAGT TGCTCTCTGCTTCGTACACGAGCCAGCTGGT**CCTCAGC**ACCAGCT GGCTCGTGTACGTTTTTTTTTGGAAGCGGAAGAGCGTGAT
shATG14-2		TGATCGACATGTTTAATTAAGTGTGGCTTCTAACGTTATCCATCG CTAGAAGTGAAACGAATGTGCGTAGGTATATATATGAAATGGAGT TGCTCTCTGCTTGCAGCGCTCGGACAAGGCG**CCTCAGC**CGCCTTG TCCGAGCGCTGCTTTTTTTTTGGAAGCGGAAGAGCGTGAT
shScrambled	N/A	ACATGTTTAATTAAGTGTGGCTTCTAACGTTATCCATCGCTAGAA GTGAAACGAATGTGCGTAGGTATATATATGAAATGGAGTTGCTCT CTGCTTGCTAGTTAGTACGTTCACA**CCTCAGC**TGTGAACGTACTA ACTAGCTTTTTTTTTGGAAGCGGAAGAGC

Loop is in **bold**, stem non-bold and promoter/terminator with overhang underlined.

Protein Biology

2.2.21 Protein Extraction

Biological samples were washed three times in 1x PBS and re-suspended in RIPA buffer (Sigma-Aldrich) with 1x protease and 1x phosphates inhibitor cocktails (Sigma-Aldrich) and left for 30 min (4^{o}C, rocking rpm). Subsequently samples were centrifuged (12,000 xg, 15 min, 4^{o}C) and the supernatant taken and storaged at -20^{o}C.

2.2.22 Protein Quantification

Protein in samples was quantified using a Pierce BCA Protein Assay kit (Thermo Sci) as per the manufacturer's protocol. Briefly, 20µL of sample was mixed with 200µL working reagents in a 96-well microplate and incubated at 37^{o}C for 30 min before absorbance of samples was measured at 562nm using a microplate reader (BMG Labtech). Protein concentration was determined by linear fit using a BSA standard curve run with samples (provided with kit).

2.2.23 Reducing SDS Polyacrylamide Gel (PAGE)

Protein samples were normalised to the same concentration using the same buffer, mixed with 4x reducing (β-mercaptoethanol) Laemmli buffer (Bio-Rad Labs) in a 1:3 ratio and heated to 95^{o}C for 4 min. Prepared samples were run on Bio-Rad Stain-Free Mini-PROTEAN or Criterion TGX gels of assorted percentages using 1x tris-glycine-SDS running buffer (200V, 30-40 min). All samples were run with a protein standard.

2.2.24 Western-Blotting

Protein was transferred to a polyvinylidene fluoride (PVDF) membrane with the TransBlot Turbo (Bio-Rad Lab) semi-dry system using Bio-Rad PVDF transfer packs (Bio-Rad Labs) for 7-10 min (1.3 A, 25 V). Transferred blots were blocked in 10% milk solution made in 1x PBS-tween (0.05%) for 1 hr (RT, gyrating 10 rpm). After blocking, blots were incubated with primary antibody in 1% milk solution (in 1x PBS-tween) in a

small heat-sealable bag overnight (4°C, rocking 8 rpm). The following day blots were washing in 1x PBS-tween (0.05%) solution (3x quick washes, 3x 5 min washes) before being incubated with HRP-conjugated secondary antibody (Bio-Rad Labs) in 1% milk solution (in 1x PBS-tween) for 1-2 hr (RT, gyrating 10 rpm). Subsequently blots were washed with a final 1x PBS wash. For imaging, blots were incubated in Clarity ECL reagent (prepared as per manufacturer's instructions; Bio-Rad Labs) for 2-5 min and exposed using a Chemi Doc MP (Bio-Rad Labs). Equal loading was confirmed by either actin housekeeping gene expression or a stain free blot, which measured total protein transferred onto each lane on the PVDF blot.

2.2.25 Silver Stain

Sensitive total protein detection in SDS PAGE gels was carried out using the Pierce silver stain kit (Thermo Sci) as per manufacturer's standard protocol. Clean plasticware was used for all steps.

2.2.26 Coomassie Blue Stain

Total protein detection in SDS PAGE gels was carried about by washing gels in InstantBlue ultrafast protein stain (Sigma Aldrich) for 15-20 min, then rinsed in water before imaging.

2.2.27 Dot Blot

Dot blots were conducted on FFE fractions in a similar fashion to western blotting. 200µL sample was added to wells in a multiscreen-IP filter plate (0.45µM, Millipore) pre-activated with methanol and incubated overnight (4°C) and the following day pulled through the membrane using a vacuum manifold (Qiagen). Wells were blocked using 10% milk solution in 1x PBS-tween (0.05%) for 1 hr (RT, gyrating 10 rpm). After blocking wells where incubated with primary antibody in 1% milk solution (in 1x PBS-tween) overnight (4°C, rocking 8 rpm). The following day wells were washing in 1x PBS-tween (0.05%) solution (3x quick washes, 3x 5 min washes) before being incubated with HRP-conjugated secondary antibody (Bio-Rad Labs) in 1% milk solution (in 1x PBS-tween) for 1-2 hr (RT, gyrating 10 rpm). Subsequently wells were washed with a final 1x PBS wash. For imaging, wells were incubated in 50µL Clarity ECL reagent (prepared as per manufacturer's instructions; Bio-Rad Labs) for 2-5 min and exposed using a Chemi Doc MP (Bio-Rad Labs).

2.2.28 An. gambiae ATG8 Polyclonal

A polyclonal antibody against *An. gambiae* ATG8 was raised in rabbits using the orthologous *An. gambiae* peptide (H_2N-MKFQYKEEHPFEKRK-$CONH_2$) used by Barth and colleagues[147] from *Drosophila melangoster* which differed by two amino acids (87% homology). The keyhole limpet hemocyanin protein was used a carrier with a 28 day vaccination protocol (Eurogentec, Belgium). Collected serum was double affinity purified and specificity confirmed by ELISA.

Mosquito Cell Culture

2.2.29 4a3b Passage

4a3b *An. gambiae* cells[148] were maintained in Schneider's *Drosophila* medium (10% FBS, 5% penicillin/streptomycin; PanBiotech UK) at 28°C with no ambient CO_2 in non-filter capped tissue culture flasks. Maintained lines consisted of stably infected *Wolbachia* lines (*w*MelPop, *w*AlbB)[149] created in our laboratory by Dr Sofia Pinto using *Wolbachia* extracted from *D. melanogaster* and *Aedes albopictus* and an uninfected line. New infections were established before work commenced to ensure genetic homogeneity between lines. Cultures were passaged every three days by mechanical detachment. The same method was used for seeding tissue culture plates for experiments.

2.2.30 Drug-based mTOR-axis Manipulation

Stock solutions of drugs used for mTOR-axis manipulation (AICAR, PP242, rapamycin, 3MA, wortmannin, bafilomycin) were made as described in 2.1.3, and diluted in complete Schneider's medium to achieve the desired working concentration. Control treatments consisted of the solution used to make the stocks. Cells were plated in TC-treated plates at desired confluency determined by experiment length and medium exchanged for drug supplemented media 24 hr post-plating. Treatment time and concentrations are specified in the results section. Bafilomycin treatment was used when ATG8 lipidation was measured and used 2 hr prior to sample collection.

2.2.31 Starvation

Cells were plated in tissue culture (TC)-treated plates at the desired confluency determined by experiment length and medium exchanged for drug supplemented medium 24 hr post-plating. Cells were washed in plain Schneider's *Drosophila* medium (no FBS, no penicillin/streptomycin) and media replaced with starvation medium (Schneider's *Drosophila* medium, 2% FBS, 5% penicillin/streptomycin). Treatment time specified in results section.

2.2.32 Lipid-based Transfection

Cells were plated in TC-treated plates (12 or 24 well) at desired confluency determined by experiment length and medium exchanged for drug supplemented media 24 hr post-plating. 4a3b cells were transfected using either Lipofectamine 3000 (Thermo Sci) or Promofectin insect (Promocell) using manufacturer's standard protocol (Table 2-12). For siRNAs P3000 was excluded from the mixture. For Lipofectamine 3000, diluted lipofectamine was mixed with the DNA/P3000, left for 15 min and added to wells in 0.5-1mL complete Schneider's medium. For Promofectin insect, diluted promofectin was mixed with the DNA, left for 15 min then made up to stated volume with plain Schneider's *Drosophila* medium and added to cells already in plain Schneider's *Drosophila* medium. After 4 hr, medium was exchanged with complete Schneider's medium.

Table 2-12 I Volumes used per well for Lipofectamine or Promofectin insect.

Plate Size	Lipofectamine 3000				
	Mixture A (µL)		Mixture B (µL)		
	Plain Media	LF3000	Plain Media	Plasmid/siRNA	P3000
12 Well	63	3.75	63	Plasmid 1µg siRNA 5 pmol	2
6 Well	126	7.5	126	Plasmid 2µg	4
	PromoFectin Insect				
	Plain Media	PromoFectin	Plain Media	PromoFectin	
12 Well	30	8	30	Plasmid 0.8µg	--
6 Well	75	16	75	Plasmid 2µg	--

LF3000; Lipofectamine 3000

2.2.33 Amaxa Electroporation

4a3b cells were counted using a haemocytometer and $4.0x10^6$ cells were pelleted/reaction (1500 xg, 5 min) in 2mL Protein Lo-Bind Eppendorf's (Eppendorf) and washed once with 2mL 1x PBS. The resultant pellet was gently re-suspended in 100µL RT complete Nucleofector V solution (82µL Nucleofector solution + 18µL supplement; Lonza) and 1µg of DNA plasmid or 5 pmol siRNA in mH_2O was added. The resultant solution was transferred to a cuvette and electroporated using program T-001 on a Nucleofector II machine (Amaxa) and immediately made up to 600µL in complete Schneider's medium and transferred to 12 well plates pre-prepared with 1.5mL 28°C complete Schneider's medium. See supplemental Figure 8-1 for development of protocol specific to 4a3b cells.

2.2.34 Flow Cytometry-based Cell Proliferation Assay

4a3b cells ($1x10^7$ cells) were pelleted (1500 xg, 5 min) and re-suspended in 1mL 1x PBS in a clean 15mL centrifuge tube. With the tube on its side 100µL 1x PBS was pipetted into the tube near the opening and 1.1µL CellTrace Violet stock (Thermo Sci) added to the PBS droplet. Subsequently the lid was replaced and the tube inverted, followed by a brief vortex to mix the diluted dye. Following a 5 min incubation the total volume was make up to 12mL in 1x PBS and cells washed twice (1500 xg, 5 min), with a final re-suspension in complete Schneider's medium and subsequent transfer to a six well plate ($0.1x10^6$ cells/well). This concentration was used to ensure contact dependent inhibition did not occur during the three day experimental period. Samples were collected at specified time-points by gently pipetting and re-suspending in 500µL FACS buffer. Mean fluorescence intensity in the V450 channel was measured using a FACSCanto II flow cytometer (BD Biosciences) compared to unstained and zero hour

stained time-point. Cells were gated to include single cells only using forward scatter (FSC)-Height and FSC–area.

2.2.35 Immunofluorescent Staining

Cells were cultured on 1.5mm round coverslips and fixed with 4% paraformaldehyde (methanol free) and permeabilised with 1% Triton X-100 detergent. Prior to antibody incubation cells were blocked with 1% BSA and then probed with primary and then secondary antibodies in 1% BSA for 1-2 hr. Finally, following 3x washes, cells were mounted onto glass slides using VECTASHIELD (Vector Labs) and imaged using a confocal fluorescent microscope.

2.2.36 Cell Cryopreservation

Cells were re-suspended in complete medium with 10% DMSO (at 4-8x10^6 cells/mL) and placed in a Mr Frosty freezing container at -80^{o}C for 24 hr before being transferred to liquid nitrogen (LN2) for long term storage.

Liver Cell Culture

2.2.37 Extracellular Matrix Coating

Extracellular matrix coating proteins (collagen I, collagen IV, fibronectin and laminin; Sigma-Aldrich) were diluted together in 0.1M bicarbonate buffer (pH 9.4)[150] and added to tissue culture plates or dishes so that each well contained 1µg of each protein with enough volume to cover the bottom surface. Subsequently plates were stored at 4^{o}C overnight and washed gently with complete DMEM twice before use. An alternative short protocol for coating involved plasma treating non-TC treated tissue culture plates for 30 sec followed by addition of coating solution for 15-30 min. All experiments with HepG2 and rat primary hepatocytes use these coated plates/dishes for experiments unless stated otherwise.

2.2.38 HepG2 Passage

Human HepG2 hepatoma cell lines were maintained in complete DMEM (10% FBS, 5% penicillin/streptomycin; Sigma-Aldrich) at 37^{o}C with 5% CO_2 in 175cm^2 filtered cap TC flasks. Cultures were seeded at the relatively high density of 60% to avoid clumping. Cells were passaged by trypsinisation (TrypLE, Thermo Sci) with 4-5mL for 15 min (37^{o}C, 5% CO_2) after washing with 1x PBS. Next 15mL complete DMEM was added carefully (without tipping the flask) to neutralise the trypsin, but not dislodge cells which come off in sheets. Cells were then dislodged using mechanical agitation and sucked slowly through a 18G syringe 3-4 times slowly to make separate cell clumps and flasks were seeded. Using this procedure maintained a suitable monolayer so that cells could be trypsinised without use of mechanical agitation of the syringe when seeding tissue culture flasks/dishes for experiments.

2.2.39 Primary Rat Hepatocyte Extraction and Maintenance

See supplemental section 8.1.3 for a detailed protocol. In summary, male Wistar rats [Crl:CD(SD), strain 001] were anesthetised and maintained using isoflurane during the

procedure. A 21G cannula was inserted into the hepatic portal vein and secured using tissue adhesive (3M) to prevent leakage. Firstly, liver perfusion medium (Thermo Sci; 37^{o}C) was pumped through the cannula at 10mL/min using a peristaltic pump and once the liver started to lighten (within 30 sec) the speed was adjusted to 20mL/min. Next the inferior vena cava was cut and over the next 5 min blocked 2-3 times and the pump increase to 40mL/min causing the liver to fill and flush out blood. Following successful perfusion, the media was exchanged for liver digest medium (Thermo Sci; 37^{o}C) and the same blocking procedure carried out for 8 min causing the liver to darken as the collagenase caused digestion. The liver was subsequently transferred quickly to 4^{o}C DMEM on ice and the following cell purification steps carried out on ice.

The liver was disrupted using the flat end of a syringe barrel in complete DMEM and the liquid passed through 100µM cell strainers into 50mL centrifuge tubes. The liver was washed with complete DMEM until clear and the resultant liquid filtered. For each liver about 160mL was used. The cell suspension was centrifuged (50 xg, 5 min, 4^{o}C) and the supernatant taken aside for non-parenchymal cell (NPC) extraction. For parenchymal cell purification (PC; hepatocytes) the pellets were washed twice in complete DMEM with a final re-suspension into two tubes of complete medium with a final volume of 19mL. 20mL sterile isotonic percoll (SIP) was added to each, mixed by gentle inversion three times and centrifuged (1.06g/mL, 100 xg, 10 min, 4^{o}C) to remove debris and dead cells (percoll purification modified from reference[151]). The resultant two pellets were washed twice in 40mL complete DMEM (50 xg, 3 min, 4^{o}C) and finally combined in 10-15mL 37^{o}C complete DMEM. Cells were counted using Trypan Blue (Sigma-Aldrich) and PC's added to pre-coated plates/dishes. Importantly the plates/dishes were not moved for 30 min to allow the cells to adhere evenly across the plate. They were then transferred to an incubator (37^{o}C, 5% CO_2) for 1-2 hr before medium was exchanged with serum-free hepatocyte growth medium (Promocell) which was exchanged every 12-15 hr.

The NPC suspension was pelleted (200 xg, 4^{o}C) and re-suspended to 20mL in complete DMEM. It was then transferred to a two-layer percoll suspension (15mL 1.066g/mL percoll on bottom, 20mL 1.037g/mL percoll on top, followed by 10mL NPC suspension) and centrifuged (800 xg, 15 min, 4^{o}C). The bottom layer was Kupffer cell enriched and the interface been both percoll densities was endothelial cell enriched[152]. Both were taken and washed in complete DMEM (800 xg, 10 min, 4^{o}C) twice before re-suspension in 5mL 37^{o}C complete DMEM and used to seed coated plates/dishes and transferred to the incubator (37^{o}C, 5% CO_2) for 1-2 hr before medium was exchanged with serum-free hepatocyte growth medium (Promocell) which was exchanged every 12-15 hr.

2.2.40 Cell Cryopreservation

HepG2 cells were cryopreserved as per method 2.2.36. Primary rat hepatocytes were re-suspended in Bambanker serum-free cell freezing medium (Wako) to 5x10^{5}-1x10^{7} cells/mL and transferred in cryovials to -80^{o}C and 24 hr later transferred to liquid nitrogen for long-term storage.

In Vivo Parasitology

2.2.41 Plasmodium Strains

All *Plasmodium berghei* strains used in this thesis had the wild-type ANKA background with gene additions of GFP or mCherry under the UIS4 promoter at the 230p neutral locus of chromosome 3 (*P. berghei*-GFP; 2227 cl6 GFP::Luc@Pbuis4_230p and –mCherry; 2204 uncloned mCherry@Pbuis4_230p) carried out using the 'Gene Insertion/Marker Out' system[153] by Dr Ahmed Salman and collaborators Dr Chris Janse and Dr Shahid Kkan (Leiden University, Netherlands) who kindly donated all strains.

2.2.42 Sporozoite Production

Cryopreserved parasitized RBC's (day five) were thawed and injected into naïve Balb/c mice by the intraperitoneal (i.p.) route and blood-stage parasitaemia monitored daily from day two as per method 2.2.43. Once infection levels of 1-2% were achieved with clear gametocytes the mice were anaesthetised (1:2:3 ratio of 20mg/mL xylazine, 100mg/mL ketamine and 1x PBS) with 25µL/10g body mass (usually ~20µL) intramuscularly (i.m.) and fed to pre-starved (2 hr) 7-10 day old female *Anopheles stephensi* mosquitoes. 7-10 days later the above feed was repeated using naïve Balb/c mice to increase sporozoite yields. Blood-fed mosquitos were maintained at 19^{o}C at 70% relative humidity for 19-22 days before sporozoites were extracted.

2.2.43 Monitoring Parasitaemia by Blood Smears

Blood-stage parasitaemia was monitored by tail-tipping infected mice to create thin blood smears. These were fixed in 100% methanol for 30 sec following by staining in 10% Giemsa (in dH_2O) for 45 min. Sides were rinsed, allowed to air dry and the number of infected RBCs counted by light microscopy using oil 100x magnification. For sporozoite production 5-6 fields of view were counted, for sporozoite challenge, 1000 RBCs were counted.

2.2.44 Mosquito Rearing

An. stephensi mosquitos used for experiments were raised at 28^{o}C, 70% relative humidity with a 12 hr light cycle. Larvae were fed with fish pellets and adults maintained on 10% fructose solution by Alex Fyfe (Jenner Institute Insectary, Oxford).

2.2.45 Sporozoite Challenge

P. berghei sporozoites were extracted from infected mosquitoes using one of the described methods in this thesis and diluted in dissection Schneider's medium (1% FBS, 4^{o}C) to achieve the desired sporozoite dose/50µL. Mice were placed in a 37^{o}C heat-box for 20 min prior to injection of 50µL intravenously (i.v.) into either lateral tail vein of restrained mice. From day five parasitaemia was monitored as per protocol 2.2.43 until three days of positive smears were obtained, mice were then sacrificed. Time to 1% parasitaemia was then calculated by linear regression. If parasites were not detected by day 14 the mice were sacrificed.

2.2.46 Merozoite Cryopreservation

To maintain cryopreserved blood stocks, sporozoite challenged mice (2.2.45) with a parasitaemia of ~5% were cardiac bled under terminal anaesthesia using a heparin coated 1mL syringe and blood mixed 50:50 with merozoite freezing medium before aliquots were frozen at -80^{o}C with long-term storage in LN2.

2.2.47 Sporozoite Cryopreservation

Sporozoites were dissected and pelleted by centrifugation (12,000 xg, 3 min, 4^{o}C) and re-suspended in one of the tested freezing buffers at 4^{o}C. Samples were frozen at either -5^{o}C/min using dry ice in ethanol as per reference[154] or -37^{o}C/min using liquid nitrogen vapour of a pre-determined volume in a polystyrene container as per the Jackson Laboratory sperm cryopreservation protocol[155] and stored in LN2 for at least two months. For use, samples were thawed quickly between hands and buffer exchanged for 4^{o}C dissection Schneider's medium.

In Vitro Parasitology

2.2.48 Hand Dissection of sporozoites

To obtain sporozoites by hand dissection, mosquitoes were sedated on ice for 10 min, then placed on a glass slide with 100µL dissection Schneiders medium and whole salivary glands removed by gently separation of the head using micro-forceps under an apochromatic stereo microscope with cold light LED bottom oblique adjustable mirrored illumination (Leica S8 APO). Both sets of glands were gently cleaned to remove other tissues and fat then placed into a glass tissue grinder on ice (which initially contained 40µL dissection Schneider's medium) using 2µL fresh medium with a 10µL pipette. The glass slide was cleaned between each dissection. Each dissection took approximately (45-90 sec) and was carried out for no more than 2-3 hr maximum to reduce loss of infectivity. To release sporozoites the salivary glands were homogenised with three gentle but firm grinds using the pestle. The sample was transferred to protein lo-bind Eppendorf (used to prevent loss of sporozoites by adhesion to plastic-ware) and mixed well before a sample was added to a haemocytometer and the average of four 16 square fields counted. Sample was diluted if too concentrated to accurately count.

2.2.49 Whole-Mosquito Homogenisation of Sporozoites

Mosquitoes sedated on ice were placed in a Petri dish with 2mL (per 400 mosquitoes) dissection Schneider's media and gently homogenised with the end of a 10mL syringe barrel for 30-60 sec. Liquid was removed and passed through a 100µM cell strainer in a 50mL centrifuge tube (gentle tapping of the tube on the table may be required). A further 1.5mL media was added to the petri dish, gently homogenised and passed through the 100µM filter. This was repeated twice more but with more vigorous grinding. Note, volumes used were adjusted based on number of mosquitoes used. Finally, the filter was washed with 1mL media. The filtrate was subsequently passed through a 70, 40 and 20µM filter and each washed with 1mL media. All steps were carried out on ice. On some occasions, the head and/or abdomens were removed before homogenisation. The resultant homogenate is referred to as 'MASH' or 'M' throughout the thesis.

2.2.50 Accudenz Gradient Sporozoite Separation

1mL of mosquito MASH was loaded onto a 3mL Accudenz cushion (4°C) in a 15mL centrifuge tube and centrifuged (2500 xg, 4°C) as per reference[156]. 400µL was then taken from the sporozoite enriched boundary at the 3mL mark (see results section for image). 1mL aliquots of Accudenz sporozoites were put into 2mL protein lo-bind eppendorfs (Eppendorf), made up to 2mL with dissection Schneider's media and centrifuged (12,000 xg, 4°C, 3 min). The resultant pellet was re-suspended in dissection Schneider's media. If the sample was to be used for free-flow electrophoresis (FFE) it was re-suspended to 200mq/mL (mosquitoes/mL; unless stated otherwise), which was based on the original number of mosquitoes homogenised and the final volume this was in (referred throughout as 'originating mosquito dose'). The resultant sporozoite suspension was referred to as 'MASH-ACC' or 'MA' throughout the thesis and in most cases was further purified by FFE.

2.2.51 Free-Flow Electrophoresis: Continuous Zone Electrophoresis (cZE)

Prior to sporozoite extraction the FFE machine was setup for cZE using a 0.5mm ZE spacer with a triethanolamine (TEA)-sucrose buffer system (see 2.1.3) using the setup detailed in Table 2-13. A more detailed protocol can be found in supplemental section 8.1.4. Briefly, the chamber was setup with dH_2O and the system flushed with 5% bleach then rinsed with dH_2O and exchanged with buffer. A stripe test (see results section) was carried out using SPADNS solution in buffer added to inlets two, four and six without voltage and the distribution of each stripe confirmed in 15±2 fractions. Secondly, SPADNS was pumped into the chamber via the sample inlet with voltage to ensure a left dislocation based on charge occurred.

MASH-ACC sample was mixed 1:1 with separation buffer (now at 100mq/mL) and injected into the chamber at 1600µL/hr and fractions collected 14 min after injection started and stopped 14 min after sample finished. Fractions were collected in 2mL protein lo-bind deepwell plates (Eppendorf). The peak sporozoite fraction(s) was identified by a haemocytometer (usually F2 and/or G2) and centrifuged in 2mL protein lo-bind tubes (max, 4°C, 3 min) and the pellet re-suspended in 100-500µL dissection Schneider's media (4°C). The resultant sporozoite suspension was referred to as 'MASH-ACC-FFE' or 'MAF' throughout the thesis.

Table 2-13 I FFE setup parameters

Aspect	Setup	Diagram
Mode	*cZE, Horizontal*	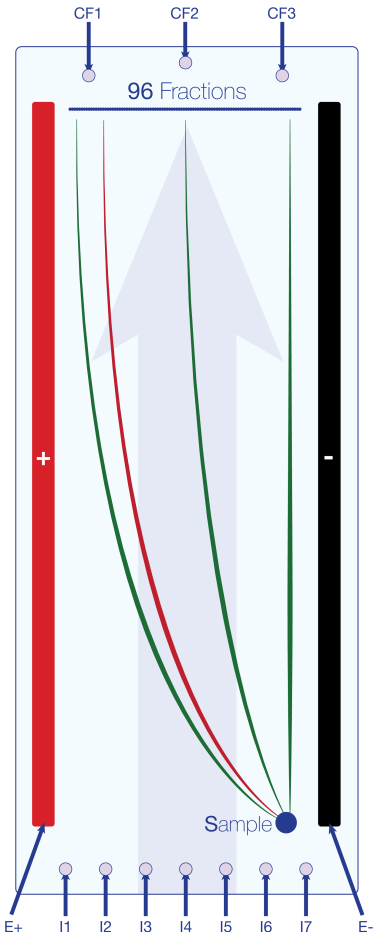
Chamber	*0.5mm ZE Spacer* *0.8mm Filter Paper* *4°C Chamber* *S4 Sample Inject, 0.25mm ∅* 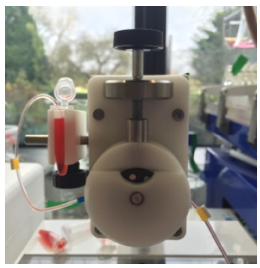	
Flow Rates	*Media: 300mL/hr* *Sample: 1600µL/hr*	
Separation	*750V* *150mA* *120W*	
Buffers (4°C)	*Separation Buffer* *Stabilisation Buffer* *Electrode Buffer*	
Buffer Inlets	*Stabilisation: Media Inlet 1+7* *Separation: Media Inlet 2-6* *Counterflow Inlet 1-3* *Electrode: Cathode & Anode*	

2.2.52 Sporozoite Challenge

In vitro sporozoite challenges were carried out on hepatocytes 24 hr after plating. Sporozoites in 4°C dissection Schneider's media were diluted in pre-warmed (37°C) DMEM (for HepG2; Sigma-Aldrich) or primary hepatocyte medium (for primary hepatocytes; Promocell) to achieve a desired ratio of sporozoite to hepatocyte (usually 1:1 or 1:2) and the culture media was exchanged with the sporozoite media. Cell cultures were carefully returned to the incubator to prevent swirling and an uneven distribution of sporozoites. Media was then no-longer exchanged for the remainder of the experiment.

2.2.53 Sporozoite Tracking

Sporozoites were added to 37°C complete DMEM and centrifuged (1,500 rpm, 4 min) in glass bottom tissue culture plates to sediment sporozoites. Fluorescent images were

captured at 2Hz (one every 0.5 sec) for 600 frames at 20x magnification. Motility was assessed using the ToAST ImageJ plugin[157].

2.2.54 Mass-Spectometry Analysis

Samples normalised by originating mosquito dose were lysed and denatured in 6M urea, 100mM tris (pH 7.8) and cysteine residues were reduced (5mM dithiothreitol, DTT) and alkylated (20mM iodoacetamide, IAA). Samples were diluted to a concentration of < 1M urea and protein digestion was carried out with sequencing grade trypsin (Promega) overnight (18 hr) at 37°C. Samples were acidified by addition of glacial acetic acid and peptides were isolated and desalted by reverse phase C18 solid phase extraction. Extracts were dried in a vacuum centrifuge and reconstituted in liquid chromatography tandem-mass spectrometry (LC-MS/MS) buffer (5% acetonitrile, 0.1% formic acid) prior to analysis by LC-MS/MS. Mass spectrometry output data was analysed using the Mascot algorithm (V2.4) and UniProt database. Mass spectrometry was kindly done by Dr Holger Kramer. A special acknowledgement to the Computational Biology Research Group (CBRG), MRC Weatherall Institute of Molecular Medicine and Radcliffe Department of Medicine for use of their services in this project. CBRG maintained and updated the MASCOT server which was used for proteomics database searches for protein identification.

Microfluidic Device Fabrication

2.2.55 Microfluidic Design and Photolithography

Microfluidic designs were made using AutoCAD (AutoDesk) and printed onto clear acetate with UV impregnable ink. The mask was placed onto a brass sheet coated with photoresist and exposed to UV light making the exposed parts of the photoresist resistant to acid treatment. Subsequent acid treatment created a brass mould. A special thanks to Dr Paul Pattinson for carrying out the photolithography process. The mould was bent and the edges soldered to create a tray or kept flat for making thin moulds

2.2.56 PDMS Mould

Polydimethylsiloxane (PDMS) was mixed with catalyst in a 9:1 weight ratio and subsequently poured into the brass moulds. PDMS was then degassed under vacuum for 1 hr before heating at 80°C for 20 min to cure. To make thin PDMS sheets a flat mould with degassed PDMS on was placed between two plates of glass coated in dried fairy liquid (to prevent PDMS sticking) and cured in the oven. Finally, holes were punch into the moulds for later addition of tubing.

2.2.57 Plasma Bonding

The microfluidic model contained three layers with PDMS-glass and PDMS-polycarbonate contacts which were adhered using different plasma bonding techniques. For the glass-PDMS adhesion both surfaces were cleaned with ispropanol, allowed to dry and placed into a plasma cleaner using ambient air for treated for 40 sec. Immediately after both materials were put together to bond. To bond PDMS and polycarbonate the surfaces were plasma treated and then treated with 1% (3-

aminopropyl)triethoxysilane (APTES) and 1% (3-glycidyloxypropyl)triethoxysilane (GPTES) for 20 min respectively. Subsequently, the surfaces were washed with isopropanol and bonded for 1 hr at RT[158,159]. Finally, tubing was added to the holes made earlier and sealed using epoxyresin.

2.2.58 Microfluidic Use

Chambers where coated overnight by injection of coating buffer into the chambers. The next day the chambers were syringe washed and cells injected into the chamber and allowed the adhere for 3-4 hr. Subsequently the chamber was attached to the microfluidic pump system (Ibidi) and buffer flowed through the chamber.

Imaging Techniques

2.2.59 Fluorescence Microscopy (Including Timelapse)

Timelapse imaging was carried out using 1.5mm glass bottom dishes/plates (Mattek) on a fluorescent microscope with LED fluorescence light source at 2Hz. Confocal microscopy was carried out on fixed cells grown on 1.5mm round coverslips mounted using VectaShield mountant (VectorLabs) and sealed with clear nail varnish.

2.2.60 Flow Cytometry

Flow cytometry was carried out use a FACScanto for 4a3b cells (2.2.34; 4a3b gating regime previously described) and an LSRII for hepatocyte cells. Hepatocytes were washed three times in 1x PBS and removed by gentle cell scraping. Hepatocytes were gated for single cell using FSC-H vs FSC-A and mCherry-*P. berghei* infected cells detected in the PE-Texas Red channel by comparing to the APC channel auto fluorescence. Uninfected hepatocytes were run as controls.

2.2.61 Electron Microscopy

4a3b cells were pelleted and fixed in 2% glutaraldehyde for 20 min and samples mounted prior to freezing in liquid nitrogen and sample freeze-fractured and imaged using transmission electron microscopy[160]. A special thanks to Dr David Ferguson, University of Oxford, for carrying out the sample preparation and imaging.

2.2.62 ImageStream

The ImageStream (Amnis) was used to measure autophagic flux in 4a3b cells as per reference[161], a method common used in Dr Kathrina Simons Lab (University of Oxford). 4a3b cells were collected by mechanical scraping after 2 hr treatment with bafilomycin, washed in cold FACS buffer and stained with live/dead marker (1:2000; Thermo Sci) for 10 min. After two washes in cold FACS buffer, cells were stained with LysoID (1:500; Enzolifesciences) for 20 min at 28^{o}C then washed twice in LysoID assay buffer followed by fixation 20 min and two washes in 1x cold permiabilisation (perm) buffer (EBiosciences). ATG8 was then stained by incubating the rabbit polyclonal (1:1000) in perm buffer for 20 min shaking (10 rpm). After a wash, cells were incubated with an Alexa Flour 488 anti-rabbit secondary antibody for 20 min shaking. Finally, cells were washed twice in FACS buffer and run on the ImageStream collecting 50,000 events. At

all steps cells were centrifuged at 1500 rpm for 5 min. Data was analysed using the IDEAS software (Amnis) and the level of co-localisation of ATG8 with lysosomes in double positive cells was measured, called bright detail similarity (BDS), with a BDS greater than 2.0 classed as co-localised. The mean BDS of double positive cells with a BDS greater than two was used to measure autophagic flux.

Vaccine Immunology

2.2.63 Animal Research

All animal work in this thesis was carried out according to the Animals (Scientific Procedures) Act 1986 Amendment Regulations 2012 (SI 2012/3039) with approval from the University of Oxford Ethical Review Committee. Rats and mice were kept in individually ventilated cages.

Conserve Vaccine Design

2.2.64 Java Program

The Conserve algorithm was converted into a computer program and UI using the Java SE Development Kit 8 (Oracle) with Phillip Kemlo.

2.2.65 NCBI Entrez

All protein sequences were obtained from the NCBI Entrez databases (NCBI).

2.2.66 Plotting

All data from the Conserve algorithm was plotted using Plotly 1.0 and 2.0[162].

2.2.67 Figures

All figures and drawings were created using the Adobe Illustrator software package.

Statistics

2.2.68 Statistical Analysis

All statistical analysis was conducted using Prism 6.0 (Graphpad, USA), R[163] or Plotly[162]. The method of exploratory data analysis (EDA) pioneered by John Tukey in 1977 was employed when carrying out statistical analysis[164]. As such, sample distribution of experiments was assessed by using a combination of, visual inspection of histograms, the Shapiro-Wilk formal normality test[165] and Q Q-plots which were used to determine whether a parametric or non-parametric test was used to compare groups. Equality of variance between groups was assessed by Fishers exact test or residual plots when comparing means (i.e. parametric data). Most parametric data was compared using a t-test with/without Welch's correction (dependent on equality of variance) and non-parametric using a Mann-Whitney U test. Experiments with more than one treatment were compared to control using a parametric t-test with Bonferroni correction (P value cut-offs divided by number of treatments) as an alternative to ANOVA and multiple comparison tests to avoid type I errors. When suitable, an ordinary one-way or two-way ANOVA was used on parametric data and a Kruskal-Wallis test

with Dunn's multiple comparisons test used for non-parametric data. Pearson's correlation coefficient was used to assess linear dependence in parametric data and Spearman's for non-parametric. Non-linear curve fitting was carried out using least squares regression. Survival curves were compared using Mantel-Cox test. A p value <0.05 was classed as significant *$p<0.05$, **$p<0.01$, ***$p<0.001$, ****$p<0.0001$.

3 Development of an Effective Workflow for the Investigation of Liver Stage Malaria *In Vitro*

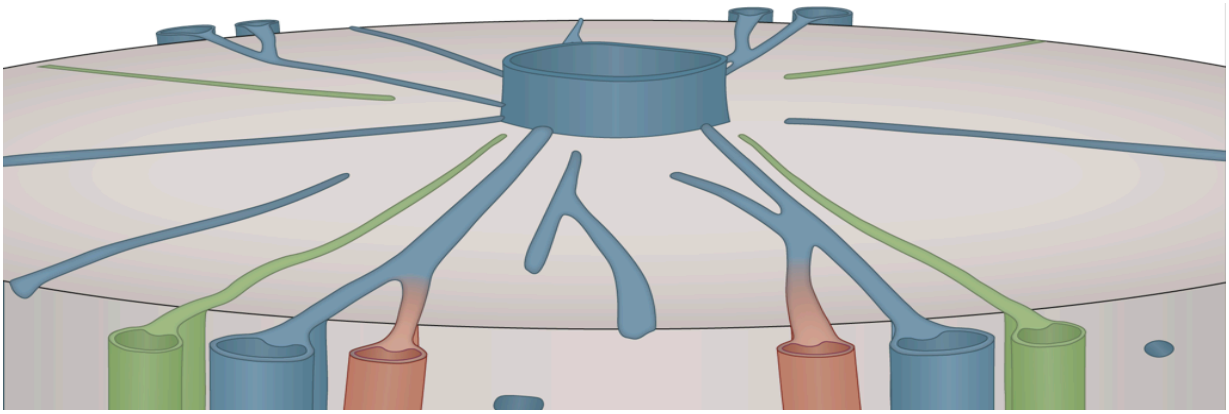

3.1 Introduction

Following a bite from an infectious mosquito the malaria parasite, in a form known as a sporozoite, is injected into the host dermis. Approximately 25% of these deposited sporozoites migrate until they reach a blood vessel[166], and from here arrest in the liver for 2-10 days, replicating within hepatocytes before their release into the blood, marking the start of the symptomatic period of infection[167]. It is estimated that an infectious bite will lead to approximately 24 infected hepatocytes in mice[168]. As such the liver stage of infection offers an attractive point of intervention due to its asymptomatic nature and low infection numbers[167,169]. However, since its discovery in 1948 by Shortt and Garnham[170] and the subsequent development of *in vitro* liver stage cultures[171], which provided the tools to study and manipulate the liver stage infection in detail, we still know relatively little about the infection process compared to the blood-stage[144,172]. This is especially true for *P. vivax* hypnozoites which remain dormant within hepatocytes[144]. Some recent progress has been made[138-140,173-175], however we still have considerable work to do in identifying effective liver stage intervention targets[142,144,172]. Furthermore, infection with irradiated sporozoites, which arrest within hepatocytes[176,177], provides protection against re-challenge[178-180], reaffirming the liver stage as an effective and attractive intervention point for drug and vaccines.

A review of the literature makes it evidently clear that a major stumbling block in understanding the liver stage and identifying new candidates is the inability to achieve **high numbers** of *Plasmodium* infected hepatocytes *in vitro*[142-144] for study and in some cases also *in vivo*[142]. Furthermore, being able to obtain sporozoites free from mosquito contaminants, have considerably hindered sporozoite proteomic studies[181-183] and is also associated with unwanted bacterial and yeast growth[156]. Table 3-1 illustrates the problem, listing many of these studies and the achieved infection rates, which are not always apparent or clearly stated.

Table 3-1 | Reported *in vitro* sporozoite hepatocyte infection rates.

Study	System Conditions	Reported % Hepatocytes Infected	Direct Quote
Kaiser, 2003[142]	N/A	N/A	*"Plasmodium hepatic stages are exceedingly difficult to study because they are rare and preparations are always contaminated with hepatocyte material"*
Sato, 2014[184]	*P. berghei* Huh7 Cells Microscopy Sporozoite Ratio: N/A	~0.1%♦ †	N/A
Bahont, 2005[173]	*P. berghei* HepG2 Microscopy Sporozoite Ratio: 1:1	Do not state (only show % of EEFs compare to WT)	N/A
Ishino, 2004[139]	*P. berghei* HepG2 Microscopy Sporozoite Ratio: 1:0.1-0.001	0.084-0.01%♦	N/A
Ishino, 2005[140]	*P. berghei* HepG2 Microscopy Sporozoite Ratio: 1:0.1	0.022%♦	N/A
Kariu, 2006[138]	*P. berghei* HepG2 Microscopy Sporozoite Ratio: 1:0.01-0.02	~0.1-0.3%♦ †	N/A
Coppi, 2011[169]	*P. berghei* Hepa-1,6 Microscopy Sporozoite Ratio: N/A	Could not determine from data available	*"limitations in the amount of material [infections] we can obtain for analysis preclude our being able to verify this hypothesis"*
Hollingdale, 1984[185]	*P. falciparum* HepG2 Microscopy Sporozoite Ratio: N/A	0.4-2.5%	N/A

Kennedy, 2012[156]	*P. falciparum* HC-04 Cells Flow Cytometry Sporozoite Ratio: 1:0.8	1.62%	*"Because of these contaminating microbes, the duration of many in vitro infections of permissive hepatocytes is often limited to only a few days"*
Sattabongkot, 2006[144]	*P. falciparum* HC-04 Cells Microscopy Sporozoite Ratio: 1:0.4-1	0.066% (0.041% *P. vivax*)	*"efforts are still needed for further improvement to provide sufficient experimental materials for studying EE gene expression and identifying novel liver stage vaccine candidates"*
Mazier, 1985[186]	*P. falciparum* Human Primary Microscopy Sporozoite Ratio: N/A	Max 1.3% (Used unground salivary glands)	N/A
Siau, 2008[187]	*P. falciparum* Human Primary Microscopy Sporozoite Ratio: 1:0.2	Typically 1.4-4.7% (3% Avg)♦	*"Sufficient quantities of parasite material necessary for such analyses cannot be obtained from in vivo infections"*
Zou, 2013[188]	*P. falciparum* Human Primary Sporozoite Ratio: 1:0.125	Typically 0.05-0.035% *(1 replicate of 6 gave 1.7%)*♦	*"The infection rates of the in vitro cultured cells by Malaria sporozoites and the transformation rates of the sporozoites into EE stages are generally low"*
Hovlid, 2016[133]	N/A	N/A	*"another screening bottleneck in liver-stage assays is their dependence on a supply of freshly harvested sporozoites from live mosquitoes. Methods to accelerate or even completely bypass this step could drastically improve the current capacity of liver-stage screens."*

Table of the reported percentage of hepatocytes infected (infection inside intact cells) in hepatomas or primary hepatocyte *in vitro* cultures and the ratio of sporozoites to hepatocytes used. ♦ = % not clearly shown in figures, had to be calculated from available data, † = infection rate estimated was not clearly described and not enough data provided. Sporozoite ratio is cells:sporozoite. EE; Exoerythrocytic.

3.1.1 The Malaria Lifecycle

To help understand the problems faced by the field it is important to have a clear idea of the malaria lifecycle (Figure 3-1). As the mosquito bites it injects saliva containing sporozoites, depositing around 50 sporozoites into the dermis[189]. Around 25% enter blood vessels to pursue effective host infections, while the remaining sporozoites stay in the dermis or enter the lymphatics[6,166]. The majority of sporozoites in the blood arrest in the liver[190], and cross the liver sinusoid by traversing either endothelial cells or Kupffer cells[191]. Known factors mediating this traversal are interactions with highly sulfated heparan sulfate proteoglycans (HSPG's) found in the liver space of Disse which protrude into sinusoids and on hepatocytes which interact with parasite CSP[192,193], and the recently discovered interaction of parasite glyceraldehyde-3-phosphate dehydrogenase (GAPDH) with Kupffer cell CD68[194]. Both sporozoite gliding motility and cell traversal are critical for sporozoites to migrate from the host dermis to hepatocytes[167]. Many key parasite proteins involved in this include perforin-like protein 1 (PLP1), sporozoite microneme protein essential for cell traversal (SPECT), phospholipase (PL), cell-traversal protein for ookinetes and sporozoites (CelTOS), TRAP-like protein (TLP) and gamete egress and sporozoite traversal (GEST)[138,139,173-175,195]. Sporozoites also traverse multiple hepatocytes before a successful infection[196,197]. This traversal was shown to protect against Kupffer cell phagocytosis[191]. However, traversal is not critical for actual productive hepatocyte invasion[139,140,198].

Hepatocyte invasion requires the host CD81 and SR-B1 receptors on *P. falciparum* and *P. vivax* respectively[199-201]. A key signal causing the switch to invasion may be the higher level of sulphated HSPG's on the hepatocyte surface[192]. Subsequently the parasite proteins thrombospondin-related anonymous protein (TRAP), apical membrane antigen (AMA-1), Pb36p and Pb36 help mediate the invasion of hepatocytes and development of a parasitophorous vacuole (PVM), a single membrane vacuole which the parasite resides in[6,140,202,203]. Pb36 appears to be important in mediating SR-B1 interaction[201]. Whereas, TRAP in particular mediates the movement into the host cell due to its attachment to the parasite actomyosin motor[204]. Additionally, proteins required for invasion are released from apical rhoptry and microneme vesicles via intracellular calcium[6,204].

Inside the PVM the sporozoite develops into an exoerythrocytic form (EEF) containing approximately 40,000 merozoites over 2-10 days by asexual replication[6]. The parasite up-regulated in infective sporozoites gene 3 (UIS3), UIS4 and Pb36p proteins are critical to development within hepatocytes[205-207]. During this process complex host-cell manipulations have been reported, for example inhibition of apoptosis[208,209].

Following asexual replication, parasites are released from the PVM[207] and kill their host cell in a unique parasite-dependent process[210], leading to the budding off of parasites in vesicles called merosomes to aid release into the blood circulation[6,211]. It has been suggested that merozoites are then released when merosomes enter the narrow lung capillaries causing them to burst open[212]. Merozoites subsequently invade red blood cells (RBCs) in a well characterised active process[213-215]. Parasite proteins involved in

this include merozoites surface protein 1 (MSP1)[216], erythrocyte binding antigens (EBA), reticulocyte binding homologs (RH)[6,217], AMA-1 and the rhoptry neck protein (RON) complex[218]. Following invasion the erythrocytic schizont divides forming approximately 24 merozoites and is followed by haemolysis of the RBC mediated by the parasite[6]. Parasites in RBCs have been shown to communicate between each other via release of vesicles[219,220]. During the cyclical merozoite schizogony some merozoites develop into gametocytes (male and female) and to complete the cycle they must be taken up by a mosquito in a blood feed[6]. During their development in humans they have been shown to reside in bone marrow[221].

Within the ingested mosquito blood-meal activated male and female gametes fuse and this fertilisation leads to the creation of a zygote, which develops into a motile ookinete that passes through the peritrophic matrix and traverses the mosquito midgut wall[222]. This traversal is the second critical bottleneck in the *Plasmodium* lifecycle[222]. On the basal laminal side the ookinete arrests and develops into a asexual replicating oocyst producing sporozoites[222]. These sporozoites are released into the haemolymph and the majority arrive at the salivary gland attaching and traversing acinar cells to reside within the glands in preparation for a blood feed[222].

The Plasmodium Lifecycle

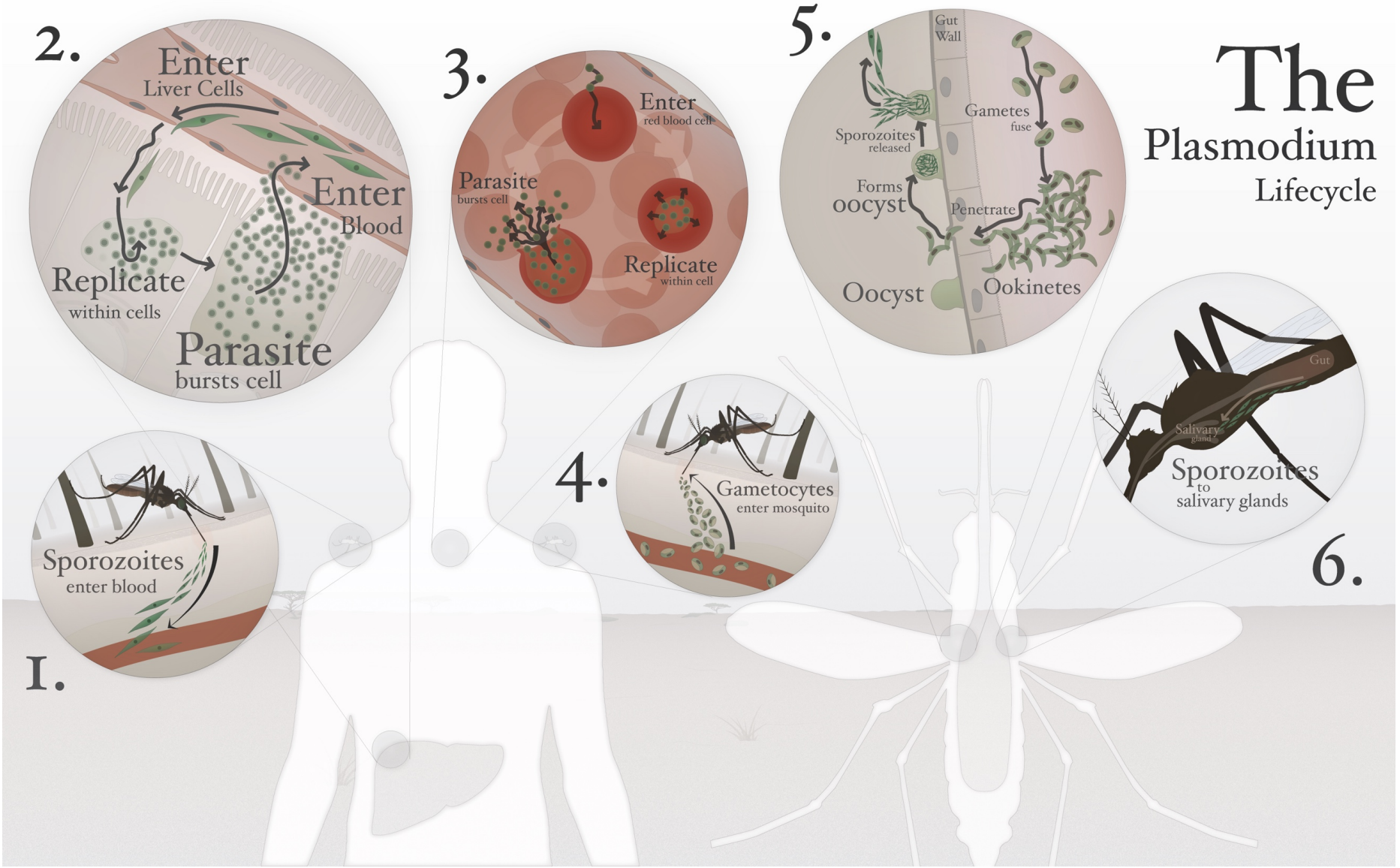

Figure 3-1 I The *Plasmodium* lifecycle. An infected mosquito transmits sporozoites which travel to the liver via the blood stream and infect hepatocytes. After 2-10 days merozoites are released into the blood stream and cyclically infected red blood cells. Gametocytes are taken up following a subsequent blood feed and activated to gametes which fuse to form a zygote which develops into ookinetes that traverse the midgut wall, developing into oocysts were sporozoites develop, migrating to the salivary glands[223].

3.1.2 Low Hepatocyte Infection Rates

To study liver stage infections *Plasmodium* sporozoites must be obtained from infected mosquitoes which have developed within the mosquito host over a period of days (21 days for *P. berghei*), until finally residing within the salivary glands[222]. Currently there is no successful published method for culturing sporozoites *in vitro*. All the studies in Table 3-1 obtained their sporozoites by manual salivary gland dissection, which is the de-facto protocol utilised worldwide for obtaining *Plasmodium* sporozoites originally described in 1964[224], with only small variations since[139,140,142,144,171,173,184,188]. It involves the laborious and time-consuming hand dissection of salivary glands under a microscope from infected mosquitoes and gentle homogenisation of salivary glands to release the sporozoites. The sporozoites are subsequently added to culture *in vitro* or injected *in vivo*.

Low hepatocyte infection rates *in vitro* can probably be attributed to many factors, including (Figure 3-2) but not exclusive, (i) inability to obtain high numbers of sporozoites quickly, (ii) low level of sporozoite purity (from mosquito associated protein, bacterial, yeast and lipids), (iii) poor sporozoite storage and length of time spent prior to addition to culture, and (iv) hepatocyte infectability, which are each discussed in more detail below. Factors (i) and (ii) are also highly relevant for *in vivo* infection too. Whilst factor (ii) is highly relevant to single cell omics on sporozoites. For example, recent proteomic studies with sporozoites suffered from excessive mosquito contaminates which made it difficult to identify parasite proteins[181-183].

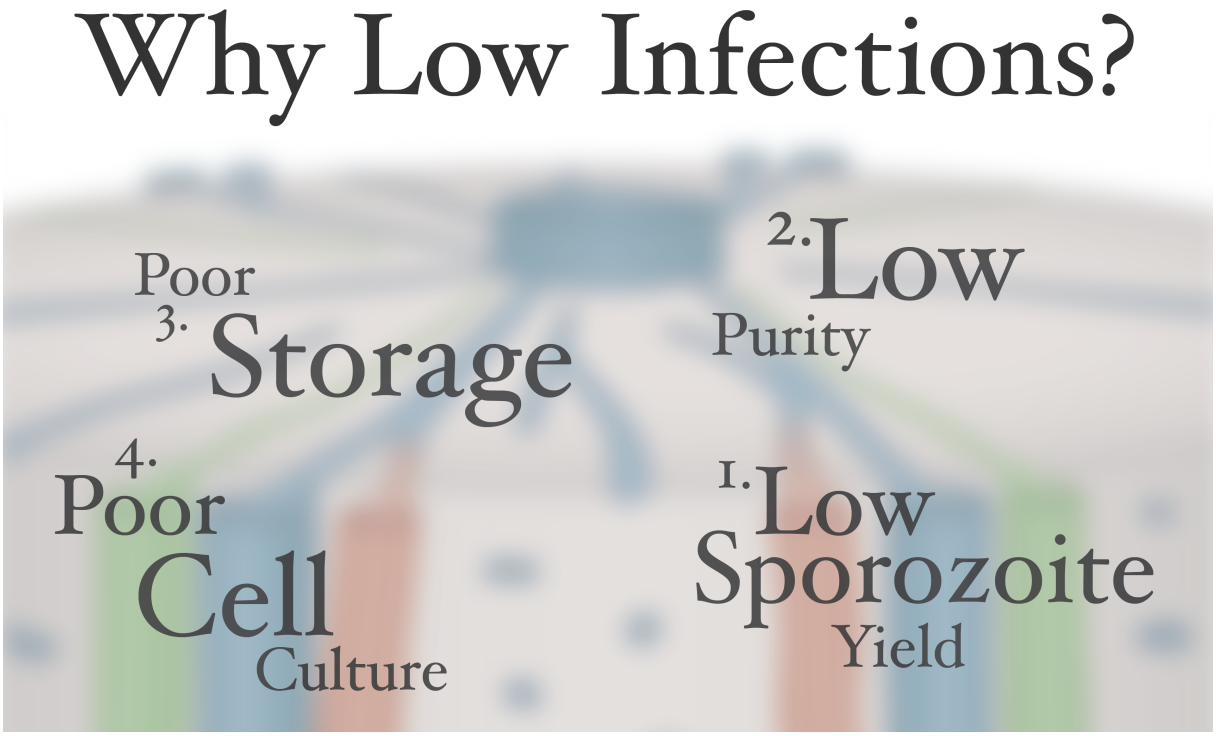

Figure 3-2 I Contributors to low *in vitro* hepatocyte infections. Hypothesised factors affecting the level of liver infections discussed in this thesis; poor sporozoite yield, purity, storage and poor hepatocyte infectivity. See main text for more details.

Many attempts have previously been made to develop improved protocols which focus on either reducing the time of purification, the level of purity or the number of sporozoites that can be purified at once. Early attempts included centrifugation through glass wool[225] or compression between glass plates[226]. However the poor purity of these methods led some to combine this with density gradients[227]. Discontinuous density gradients involving BSA-renografin[228-232] using either total mosquitoes or dissected salivary glands was also common practice. Later attempts at density-based separation included ficoll-hypaque gradients[227] and percoll gradients[187]. Although gradients gave high yields of sporozoites, they require long centrifugations and are commonly contaminated with mosquito material[233]. In 1978 sporozoites were even separated by ion exchange, however this gave poor yields[234,235].

More recently Mark Kennedy and colleagues[156] tested a multitude of different density gradients to develop a highly reproducible and relatively short density separation method using Accudenz, which reduced bacterial contamination, mosquito fats and debris and allowed separation of up to 10^7 sporozoites per gradient. However, the likely reduction seen in contaminants compared to earlier density-based attempts was probably due to the use of dissected salivary glands for the density separation instead of whole mosquitoes. This however adds considerable time to the process and requires numerous 'dissectors' to obtain 10^7 sporozoites within a reasonable time. Many of the studies in Table 3-1 use a low number of sporozoite to cell ratio which is likely due to the associated mosquito contaminants and time required to dissect large numbers of

sporozoites. Additionally, some groups have looked at improving culturing methods of primary hepatocytes[172].

3.1.3 Towards an Optimal In Vitro Liver Stage Assay

A new *in vitro* liver stage infection protocol should allow large amounts of starting mosquito material to be used to achieve high sporozoite numbers, allowing the infection of large numbers of hepatocytes. Earlier work showed that adding more sporozoites to the same amount of cells increases infection numbers up to an optimal 1:0.5 ratio of cells to sporozoites[188]. However, whether this is due to the manual dissection method use to obtain the sporozoites or other unidentified factors is unknown. When adding sporozoite sample to tissue culture one would assume that that the amount of extraneous contaminants would be inversely proportional to cell health. The mosquito-associated contaminants include, lipids, protein, bacteria and yeast[156]. The effect of bacteria and yeast on cell culture is well documented and is a major problem in sporozoite challenges[156]. Many papers use a combination of anti-fungal's and antibiotics against these contaminants[142,156,188], however the effect of these on sporozoite viability is currently unknown, though our lab has seen a drop in infection rate associated with high levels of antibiotics in the media (Carly Bliss Thesis, 2017). Interestingly, recent work reported that extraction of sporozoites in antibiotics failed to reduced bacterial load at later stages in experiments[156].

One area of *in vitro* culturing that has been well researched are the optimal storage conditions for extracted sporozoites before their addition to *in vitro* culture[142,187,236,237]. It is now well appreciated that the buffer used to dissect sporozoites into is critical to sporozoite survival, preserving hepatocyte infectivity and preventing the formation of EEF's outside of cells[142,187,236,237]. These studies have shown that bicarbonate ions and glucose promote the early EEF transformation, whereas albumin without bicarbonate prevents EEF transformation[236], thus supporting the use of insect cell medium as a suitable purification buffer[237]. Additionally, maintaining purified sporozoites at 4^{o}C until addition to hepatocyte culture is critical to maintaining sporozoite infectivity prior to addition to hepatocyte culture, preventing the formation of non-infective extracellular EEF's seen at higher temperatures[142,187,236]. Exemplified by the observation that just 2 hr at 37^{o}C prevents all *in vitro* hepatocyte infections[187]. Interestingly co-incubating sporozoites with keratinocytes or hepatocytes at 37^{o}C is able to maintain sporozoite hepatocyte infectivity for at least 1 hr[187]. Furthermore, the time spent outside of salivary glands has detrimental effects on sporozoite viability, which show a reduction in gliding motility[237]. However, many of these studies assess the effectiveness of media by only measuring sporozoite gliding motility, which does not necessarily correlate with *in vivo* infection ability when challenging intravenously[184,238]. How sporozoites are introduced to hepatocyte culture may also have an effect on infection rate. For example, when culturing hepatocytes in dishes centrifuging sporozoites down onto the hepatocytes has been shown to increase infections[188,239].

A final consideration for an *in vitro* assay is the hepatocyte culture setup. It is well accepted that primary hepatocytes give higher infection rates than hepatoma cell

lines[186,188] and is also evident from the studies in Table 3-1. However, this can vary depending on the *Plasmodium* species used[144], and whereas *P. berghei* can complete its EE stage in varied cell types[171,240-243], *P. falciparum* is more specific requiring primary hepatocytes or specific hepatoma lines such as HC-04[144,186]. Hepatomas lines however do not accurately represent true hepatocytes, showing abnormal signalling, gene expression and metabolism[172].

Although primary hepatocytes would be desirable for an improved *in vitro* setup they are difficult to culture long-term and to maintain their phenotype throughout the culture period. Fortunately, the recent boom in microfluidics has led to the development of artificial liver models to help enable long term culture of primary hepatocytes[172,244-249]. Hepatocytes with a highly mature phenotype may even promote increased infections. A combination of techniques have been shown to promote a mature phenotype *in vitro*. Critical to this is growing hepatocytes in narrow chambers approximately 200µM wide, which increases cell survival[248] and promotes the expression of maturity markers[245]. It has also been associated with cell polarity and even the formation of bile canaliculi[250]. Maintaining cells under a shear stress from media flow was also associated with improve maturity and bile canaliculi[251]. Additionally, non-parenchymal cells such as Kupffer cells and sinusoidal endothelial cells, which are important for *in vivo* infection[191], can be incorporated into a two layer microfluidic system[245].

It could be hypothesised that an artificial model containing these environmental cues could improve hepatocyte infectivity. Recently a micropatterned coculture (MPCC) system was used, where primary hepatocytes and fibroblasts cells were arranged to promote a highly mature phenotype as a system for *P. falciparum* and *vivax* infections[172,252]. Using this MPCC model the group reported higher infections than using unpatterned standard cultures[172], supporting the hypothesis that higher hepatocyte maturity promotes greater sporozoite infections. Furthermore, the parasites in MPCC culture developed into schizonts quicker than in HC-04 hepatoma lines and could achieve 0.01-0.1% and 0.3-0.6% infection rates for *P. falcparum* and *P. berghei* respectively, three days after infection using cryopreserved sporozoites[172]. However, using fresh *P. falciparum* sporozoites they could achieve a maximum of approximately 1.3%[172].

Each of these factors can be readily related to the sporozoite entry into hepatocytes (Figure 3-3), which experiences changes in shear stress[253-256] and has to cross the endothelial barrier involving contact with different cell types[191]. Therefore, in addition to maintaining maturity it may help to make sporozoites infective to hepatocytes by simulating the *in vivo* infection pathway.

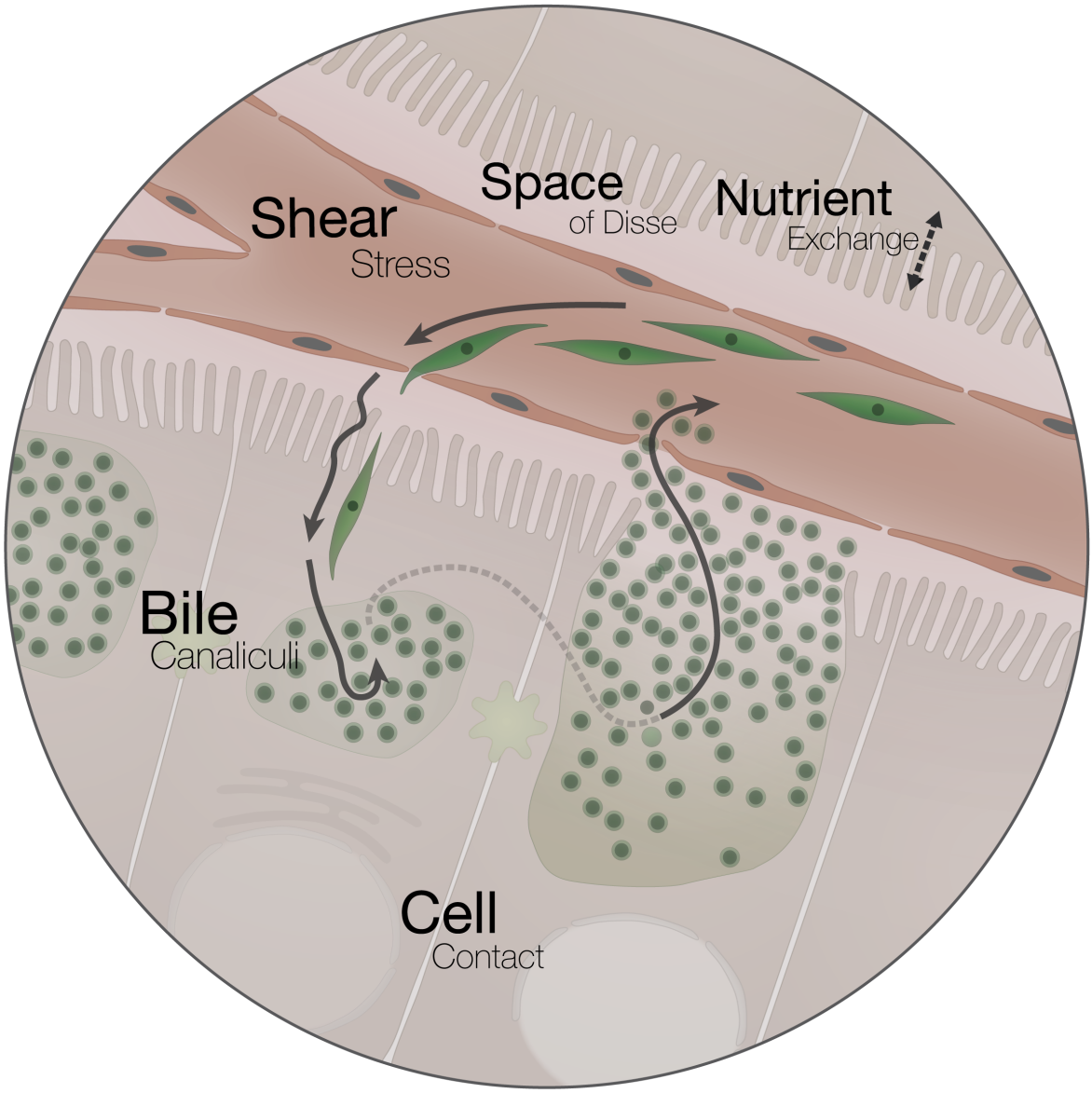

Figure 3-3 I Environmental cues in sporozoite liver infection. Sporozoites move from a high sheer stress environment in the liver sinusoids to the low sheer stress space of Disse[253-256]. During this change they traverse endothelial cells and subsequently hepatocytes[191].

3.1.4 A New In Vitro Liver Stage Infection Model

In 2010, Steven Hoffman published work reporting that they could purify aseptic attenuated sporozoites from mosquitoes to GMP level[178], which brought the advent of human clinical trials using an attenuated sporozoite vaccine[257-259]. Their 2011 study material and methods state the use of “size exclusion filters” after manual dissection of sporozoites. However, the details of this protocol are not available.[257] This means that there is still an opportunity and need to develop an optimal sporozoite purification protocol for the malaria research community. In 1983, Hans-G Heidrich and colleagues[233] demonstrated that sporozoites could be purified from mosquitoes using a method called free-flow electrophoresis (FFE). This is a liquid form of electrophoresis which at the time was commonly used to separate organelles, such as mitochondria,

under native conditions based on net surface charge. The group showed that they could separate sporozoites by FFE which were at least infective at high dose in animals[233]. Surprisingly, no subsequent publication utilising FFE to purify sporozoites has been reported even though there are now much more efficient machines available[260].

Interestingly the purification developed by Steven Hoffman[178] was used in the MPCC study[172]. The group used a high 1:3 ratio of cells to sporozoites not commonly seen in the field (Table 3-1). The use of a high sporozoite dose *in vitro* may be due to the purified nature of the sporozoites used and in addition to using more mature hepatocytes could partly explain the higher infection rates documents.

This thesis chapter attempts to improve the current state *Plasmodium in vitro* hepatocyte culture to enable a robust protocol for studying the malaria liver stage with improved numbers of hepatocyte infections. With the final aim of vastly improving the tools available to identify and test new liver stage candidates. To investigate this an improved protocol for extracting sporozoites from mosquitoes is developed, building upon initial work from Heidrich[233] and utilising new density separation techniques[156] to develop a complete workflow for the separation of large quantities of highly pure sporozoites in a short period of time. Additionally, this was combined with primary hepatocytes to investigate whether pure parasites and mature hepatocytes lead to significantly higher in infection levels *in vitro* (Figure 3-4).

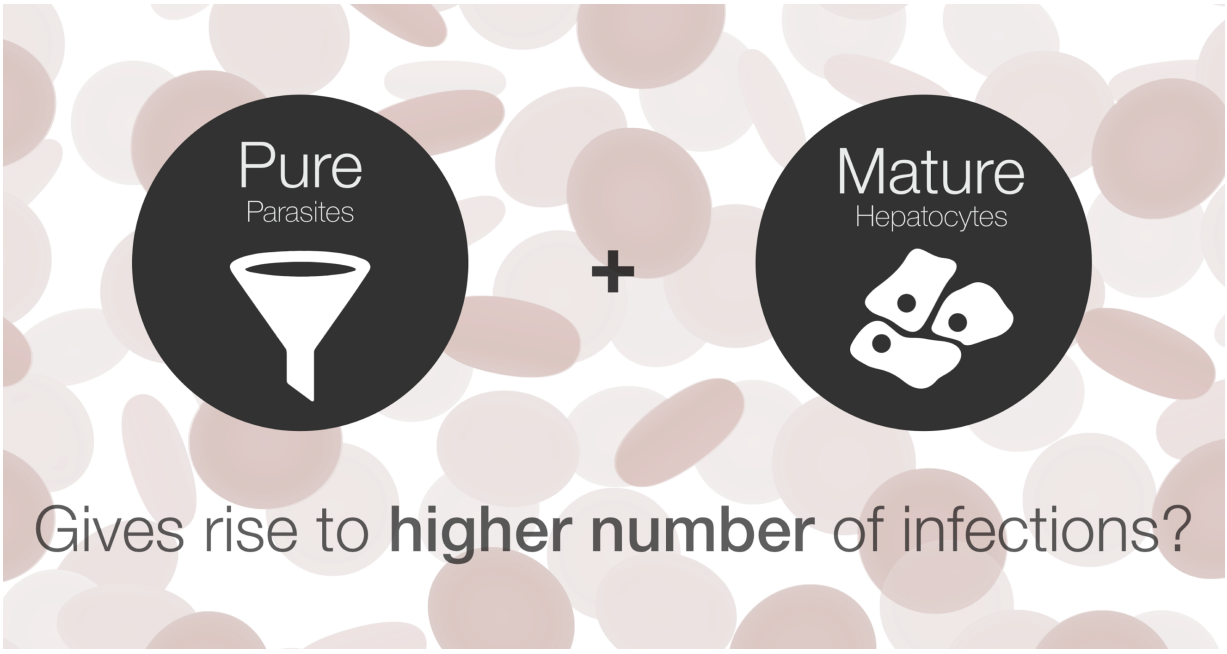

Figure 3-4 I The rationale. Do pure sporozoites and mature hepatocytes increase *in vitro* infections?

3.2 Results

3.2.1 In Vitro Liver Stage Plasmodium berghei Infection Using Existing Methods

In order to illustrate the constraints of existing *in vitro* methods, the standard method of *in vitro P. berghei* liver stage infection (with slight variations) was carried out[139,142,144,171,173,184,188,224], a protocol commonly used in our laboratory. Briefly, salivary glands were manually dissected from mosquitoes and mCherry expressing transgenic *P. berghei* sporozoites released by gentle tissue homogenisation over a period of 2 hr. The HepG2 hepatoma line was cultured in 24 well TC plates or 38mm dishes. Sporozoites in a 1:1 ratio of sporozoites:cells were added to cultures and infection monitored by fluorescent time-lapse microscopy at 2Hz. To demonstrate the problems of purity and sterility with manual sporozoite dissection the cultures were either maintained on 0.5% penicillin/streptomycin (P/S; Figure 3-5a), or the standard 1% P/S (Figure 3-5b). Figure 3-5a shows images taken at 10 min, 4 hr and 20 hr after addition of sporozoites. By 4 hr, bacteria growth is clearly visible and by 20 hr a large amount of cell death is visible and sporozoites showed an abnormal clumping phenotype with 0.5% P/S.

When infection was carried out in 1% P/S there was no visible bacterial growth by 20 hr and cells looked morphologically normal (Figure 3-5b) compared to HepG2 without sporozoites (Figure 3-5c). However, when primary rat hepatocytes were used with 1% P/S a significant change in cell morphology associated with cell stress is observed even with no visible bacterial growth (Figure 3-14). Changes in both cell types with and without P/S suggest there is considerable bacterial contamination and cell stress associated with using dissected sporozoites. Most importantly, in agreement with the literature (Table 3-1), when using this setup infection rates were on average below 1% by 40 hr (Figure 3-5d), which could be directly related to sporozoite purity and hepatocyte maturity. Interestingly the primary hepatocytes gave a lower percent infection rate compared to HepG2.

This therefore highlights the problems of time required to dissect and suggests contamination of cultures (purity) with mosquito contaminants is factor affecting infection rates.

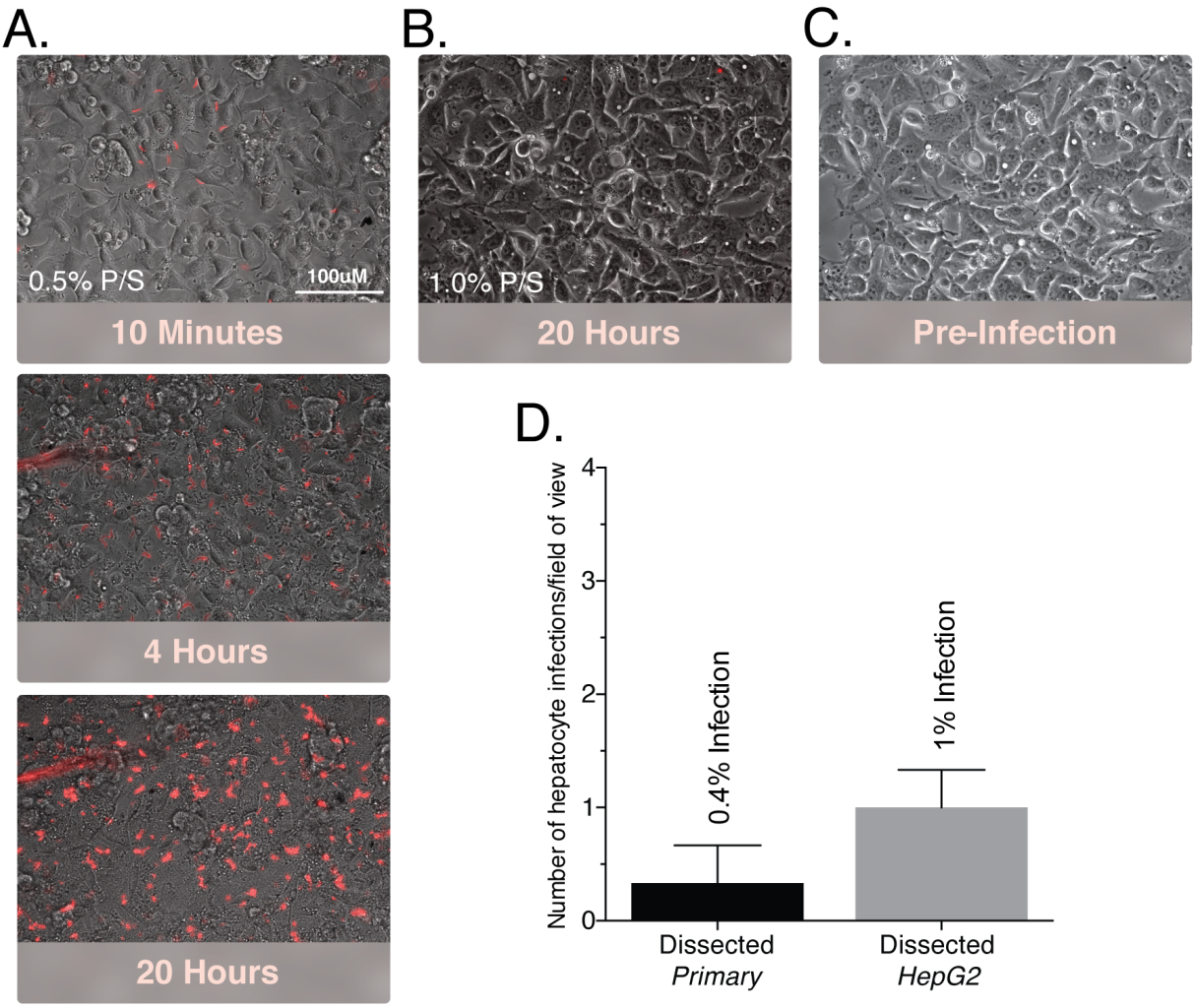

Figure 3-5 I Current *in vitro* methods in studying liver stage malaria. A) Three time-points from HepG2 cells infected with 1:1 ratio of cells:sporozoite taken from a 2Hz 48 hr time-lapse with 0.5% P/S. B) Same as (A) but with 1% P/S. C) HepG2 cells prior to addition of sporozoites. D) Mean percent infection rate of HepG2 and primary rat hepatocytes of three independent replicates, 40 hr post addition of sporozoites from 2Hz 48 hr time-lapses. Error bars represent SEM. All experiments used mCherry expressing *P. berghei* sporozoites isolated by hand dissection.

3.2.2 Developing an Alternative Approach for Sporozoite Purification

A different approach for the purification of sporozoites from mosquitoes was developed, which aimed to fulfil the criteria of (i) providing sporozoites highly purified from mosquito associated contaminants, including protein and microbiota, (ii) maintains the viability of sporozoites to *in vitro* hepatocytes and (iii) allows the processing of large quantities of mosquitoes in a short period of time. To achieve this a combinatorial approach was taken which included whole mosquito homogenisation, filtration, Accudenz gradient and FFE (Figure 3-6a). See material and methods (2.2.48-50) for detailed description. This protocol will allow investigation into whether sporozoite purity impacts on *in vitro* hepatocyte infection rates.

Firstly, the time taken from extraction of sporozoites to addition to culture has been show as critical for viability[237], which restricts the number of mosquitoes that can be dissected at once. Therefore, total mosquitoes were used as the sporozoite source and some experiments in this study used over 700 mosquitoes at once without any added inconvenience and minimal addition of time. Homogenisation of whole mosquitoes was chosen with subsequent filtering through 100 to 20µM filters to remove large debris as it allowed the release of sporozoites in a short period of time (Figure 3-6b). The homogenised sporozoites were then density centrifuged using the previously described Accudenz method[156] to remove larger mosquito associated debris and enrich for sporozoites (Figure 3-6c). Accudenz has previously been shown to maintain sporozoite viability *in vitro* and *in vivo*[156] justifying its use in this purification protocol.

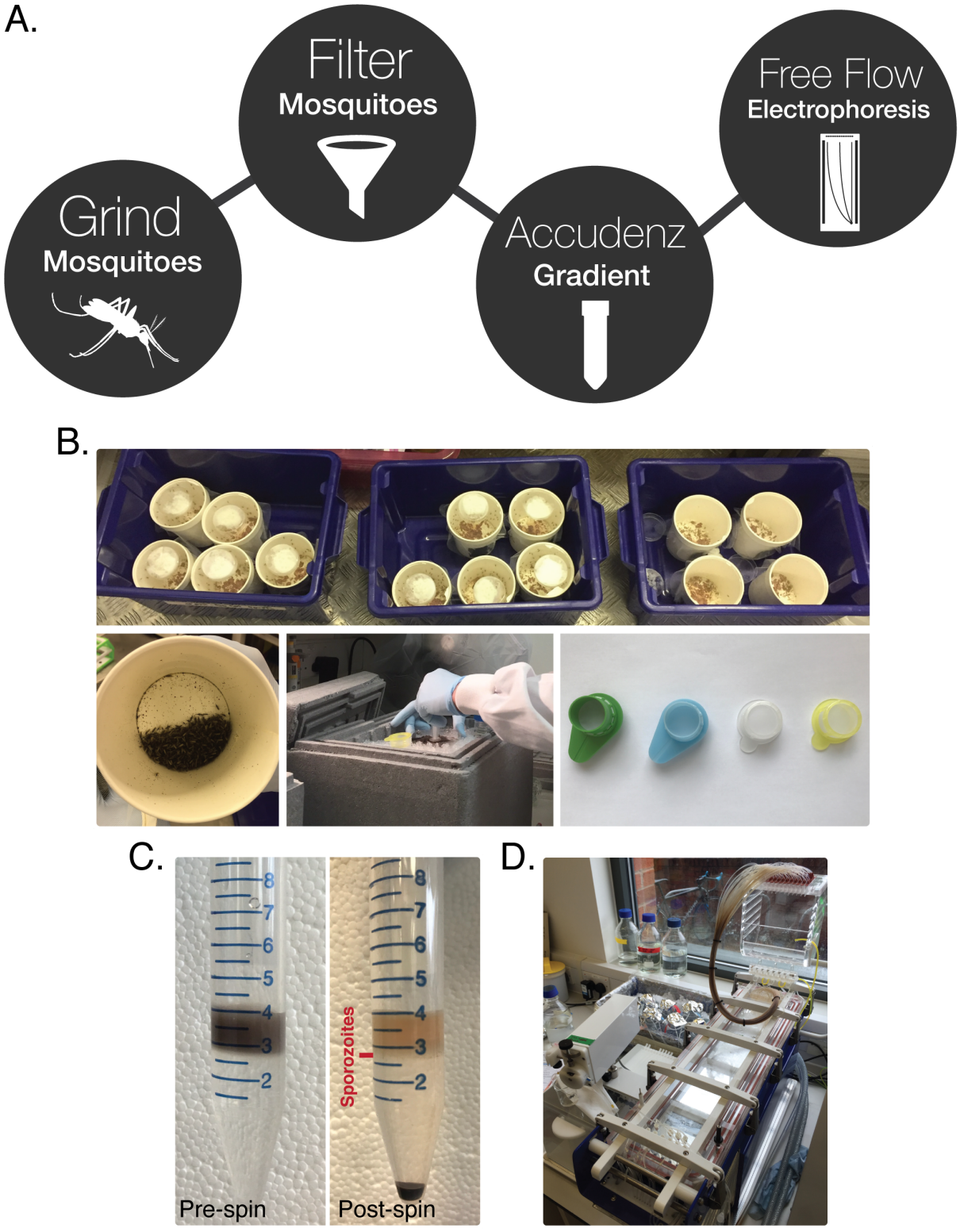

Figure 3-6 I Alternative method for sporozoite purification. A) The alternative sporozoite purification process. B) Mosquito homogenisation step. Upper and lower left panels; an example of using 700 mosquitoes at once. Bottom mid panel; mosquito homogenisation on ice. Bottom right; homogenate filtration. C) Photos of a homogenate loaded Accudenz gradient before and after centrifugation. D) FFE machine setup for continuous zone electrophoresis.

The resultant sporozoite band was finally purified by FFE (Figure 3-6d). FFE is an old, but versatile tool which can separate objects based on a multitude of characteristics, such as charge, density and isoelectric point (pI)[261], therefore it should increase sporozoite purity by separating from mosquito associated contaminants. FFE can also be conducted under native conditions and is relatively quick (10-15 min)[261], therefore making it a feasible option for maintaining sporozoite viability. Sporozoites were separated based on total net charge using the continuous zone electrophoresis (cZE) mode with a sucrose-TEA buffer system buffered at physiological pH.

In this mode an electrophoretic buffer was run through a chamber 0.5-0.1mm thick with a voltage applied across the flow (Figure 3-7a). Sample added to the start of the chamber is carried down the length of the chamber as a voltage is applied across, which causes the sample constituents to shift to their isoelectric point, effectively separating across the horizontal length of the chamber. The outflow from the chamber is separated into 96 outlets along the horizontal length of the chamber, effectively separating the sample into 96 fractions. A counter-flow buffer is applied into the top of the chamber to ensure that the sample leaves via the 96 outlet tubes. A stabilisation buffer with 10-fold molar concentration over the running buffer is run along each side of the chamber to prevent sample running into the electrodes. Separation can be modified by adjusting the buffer, buffer flow rate, chamber voltage and sample injection rate.

Prior to each run, correct functioning of the machine was assessed using the SPADNS dye in a: (i) stripe test; alternate media inlets are supplemented with SPADNS and linear flow assessed without voltage (Figure 3-7b). (ii) Shift test; SPADNS and pI marker dye are mixed and injected into the chamber via the sample inlet and dye separation assessed under voltage (Figure 3-7c). Once sporozoites had been separated the peak fraction was collected and sporozoites were re-suspended in media for use. Throughout the remainder of this chapter each stage of the purification process was characterised and the need for each step in this approach was investigated and justified.

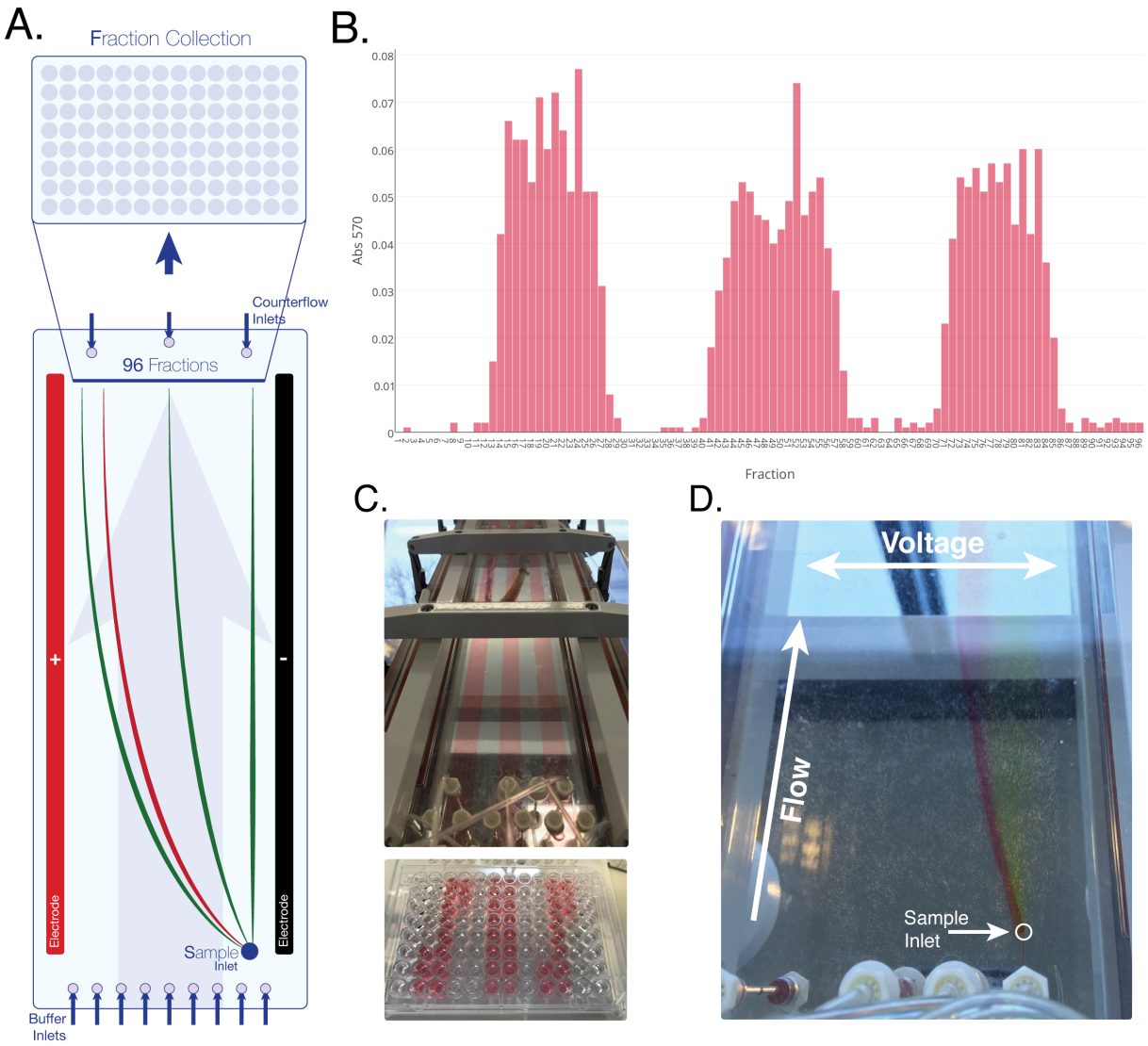

Figure 3-7 I Free-flow electrophoresis. A) Diagrammatic representation of sample separation by cZE mode. B) OD570 absorbance readings from each fraction after running a stripe test. C) Top; photograph of the FFE separation chamber during stripe test. Bottom; fraction output in 96 well plate during stripe test. D) Shift test; separation of dye mixture under voltage when injected via sample inlet. Arrows indicate voltage direction, media flow and sample inlet location.

3.2.3 Obtaining Sporozoites by FFE

Sporozoite extraction by total mosquito homogenisation followed by Accudenz (MA) was confirmed by visual microscopy. Subsequently, the ability of cZE to purify sporozoites was assessed using parameters described in method 2.2.51. Sporozoites from MA enrichment were injected into the FFE chamber from sample inlet four next to the cathode (Figure 3-8a) at four different doses of mCherry expressing transgenic *P. berghei* sporozoites (700, 3250, 7500, 8000 sporozoite/µL; spz/µL). These originated from mosquito infections of 7,600, 21,667, 33,333 and 53,333 sporozoites per mosquito (spz/mq) respectively. Therefore 92, 150, 225 and 150 mosquito worth of originating mosquito material was injected into the chamber per mL (mq/mL) respectively (Table

3-2). Subsequently the distribution of purified sporozoites (MAF) in the 96 fractions was assessed by light microscopy or mCherry fluorescent emission (610nm; Figure 3-8b-c).

Table 3-2 I FFE injected sporozoite and mosquito equivalents.

Injected FFE Sample	Sporozoite Infection Load Per Mosquito (spz/mq)	Dose injected into FFE Chamber	
		Sporozoite Dose (spz/mL)	Originating Mosquito Dose (mq/mL)
1	7,600	700	92
2	21,667	3,250	150
3	33,333	7,500	225
4	53,333	8,000	150

Variables from four different infected mosquito batches injected into the same FFE chamber setup.

Analysis showed that the majority of sporozoites from all concentrations tested (mean 75.4±5.1%) separate into a single fraction (15) with a characteristic tail that elongated as the dose loaded onto the FFE machine increased, containing a mean 20.8±6.3% of the total sporozoite dose. The second most abundant fraction (16) contained a mean 13.9±4.2% of the total sporozoites, with the remaining tail containing an average of 7.0±2.2% of the parasites. There was no correlation between the sporozoite dose and the overall percentage of sporozoites in fraction 16 (R^2=0.003035, p=0.9449) or in the remaining tail (> fraction 16) (R^2=0.01958, p=0.8601; Figure 3-8d) for any of the doses tested. However, there was a clearly positive but not significant correlation between the sporozoite dose and the length of the tail (R^2=0.8841, p=0.0598) but not the originating mosquito dose (R^2=0.7940, p=0.4669). Furthermore, although all samples contained different originating mosquito doses this did not change the peak fraction location (fraction 15). This suggested that sporozoite distribution was not affected by the level of mosquito contaminants. It was also apparent that different mosquito batches gave different doses of spz/mq.

In summary, this showed that up to 8,000spz/µL loaded onto FFE provides a high-resolution separation of sporozoites concentrated in one fraction with approximately 20% overspill into the adjoining fractions. Even though the tail elongated with increasing sporozoite dose, the percentage of total sporozoites within the tail deviated only 6.3% and showed no correlation with dose. Furthermore, the peak fraction location was independent of both sporozoite dose and dose of originating mosquito material. The peak fraction was used for all remaining experiments. On some occasions variations in the chamber setup between experiments caused small changes in the position of the peak fraction, however the distribution described above was representative of all FFE runs.

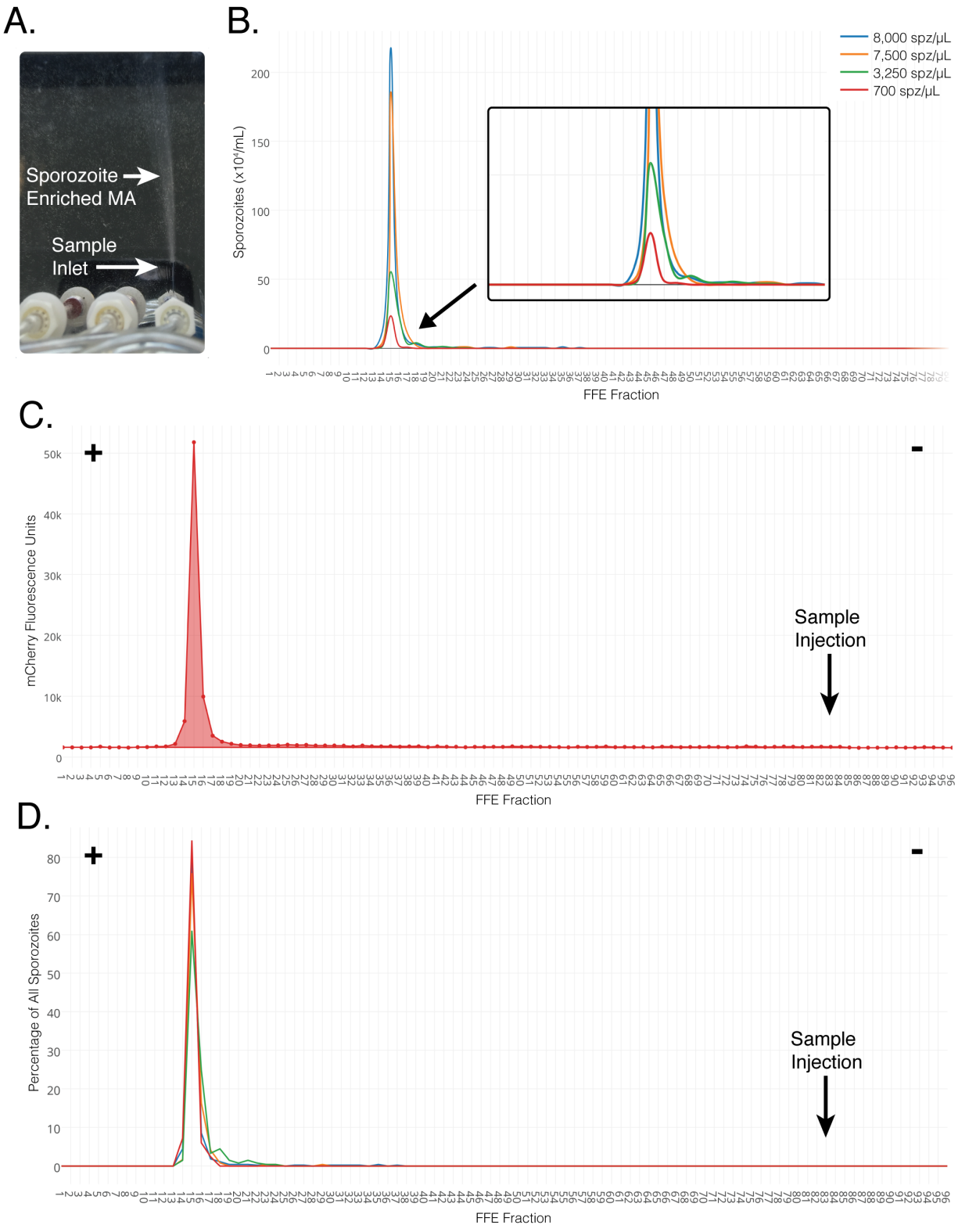

Figure 3-8 I Sporozoite FFE distribution. A) Photograph of a MA sample being loaded into the FFE separation chamber under voltage. B) Parasite distribution of FFE fractions when loaded onto the FFE machine at four different sporozoite doses (spz/mL). Quantified by haemocytometer count. C) 610nm emission intensity from 8000spz/µL dose loaded onto the FFE machine (equivalent to originating mosquito doses of 150 mq/mL from 53,333 spz/mq infections). D) Sporozoite distribution based on total percent of sporozoites per fraction for each sporozoite dose.

3.2.4 Sporozoite Purity: Separation from Mosquito Proteins

Following the characterisation of sporozoite distribution across FFE fractions, mosquito protein contaminants were assessed using a combination of approaches. To assess total protein contaminants naïve mosquitoes (not infected with *P. berghei*) and *P. berghei* infected mosquitoes were run on the FFE machine following MA at three different originating mosquito doses (300, 100 and 50mq/mL). Originating mosquito doses were calculated based on the original number of mosquitoes homogenised and the total volume in which this was done. For example, 400 mosquitoes were homogenised and filtered in 10mL media meaning 40mq/mL. This was loaded onto 10 Accudenz gradients and 400µL taken from each gradient (total 4mL) which gave 100mq/mL. The final 4mL was centrifuged and re-suspended to the desired concentration and loaded onto FFE.

The peak sporozoite fraction was the only fraction used and the FFE originating mosquito dose was calculated based on the volume collected in that one fraction. To enable reproducible results, the volume of media used for homogenisation was based on mosquito number (40mq/mL) and the volume taken from each Accudenz gradient was always 400µL. For the following experiments media without FBS was used to allow accurate assessment of protein levels. Samples were normalised by originating mosquito dose instead of sporozoite dose as sporozoite dose can vary between batches. Furthermore, it is the mosquitos which contribute the contaminants and the originating mosquito dose was shown not to affect the distribution of sporozoites (described in section 3.2.3). All remaining experiments were normalised in this way.

MA from naïve mosquitoes was loaded onto the FFE machine at 50, 100 and 300mq/mL with infected controls at each dose used to confirm location of the peak fraction, which for this setup was fraction 14. The same volume was injected and collected from the FFE machine for each treatment and total protein in each fraction quantified by bicinchoninic acid assay (BCA) (Figure 3-9a). All peak sporozoite fractions had undetectable levels of protein by BCA in naïve samples, with protein contaminants having lower electrophoretic mobility than the sporozoite peak fraction. However, protein contamination showed a greater shift towards the sporozoite peak with the higher mosquito dose.

To directly compare each step of the purification each stage was normalised to an originating mosquito dose of 200mq/mL and four mosquito worth of originating mosquitoes from each sample was run on a reducing SDS-PAGE and silver-stain conducted to assess protein levels. Dissected mosquitoes were used as a comparison to current methods. Comparing steps of purification using naïve mosquitoes (Figure 3-9b-c) it was evident that M and MA gave the highest total protein levels, followed by dissected, with MAF showing almost undetectable levels of protein contaminants. However, the level of contaminants was higher with increased originating mosquito dose (Figure 3-9b). Figure 3-9c shows the sporozoite positive FFE fraction in infected and naïve mosquitoes, showing the protein contributed by the sporozoites. A similar trend was seen when infected mosquitoes were used (Figure 3-9d), which also showed

that MASH followed directly by FFE (MF) contained more proteins than dissected sporozoites. This indicated that density centrifugation prior to FFE is desirable. However, as these were infected mosquitoes it was not possible to compare treatments, as the number of sporozoites contributing protein in each treatment may vary.

Finally, dissected salivary glands were used as the source for homogenisation instead of total mosquitoes (DISS-ACC; DA, DISS-ACC-FFE; DAF, DISS-FFE; DF) to assess its effect, although the time associated with this was considerably longer (Figure 3-9e). This showed a similar purification trend. A blot against *P. berghei* CSP protein for these fractions showed that there is a considerable amount of CSP protein degradation which was not present in steps involving FFE (Figure 3-9e). Furthermore, FFE purified treatments contained less full length CSP signified by a weaker band intensity, which could be possibly explained by shedding of CSP and/or the fact that each step of purification leads to a loss in sporozoites.

Based on these results it was clear that the higher the dose of originating mosquito material loaded onto the machine the greater the mosquito contaminants encroach on the sporozoite fraction. However, up to 300mq/mL, the peak sporozoite fraction was still free of detectable protein by BCA, but the adjoining fraction did have detectable levels. Earlier results and this section show that peak sporozoite fraction location is not affected by mosquito dose, therefore for the remainder of this study all FFE experiments were run using the originating mosquito dose of 100mq/mL injected into the chamber.

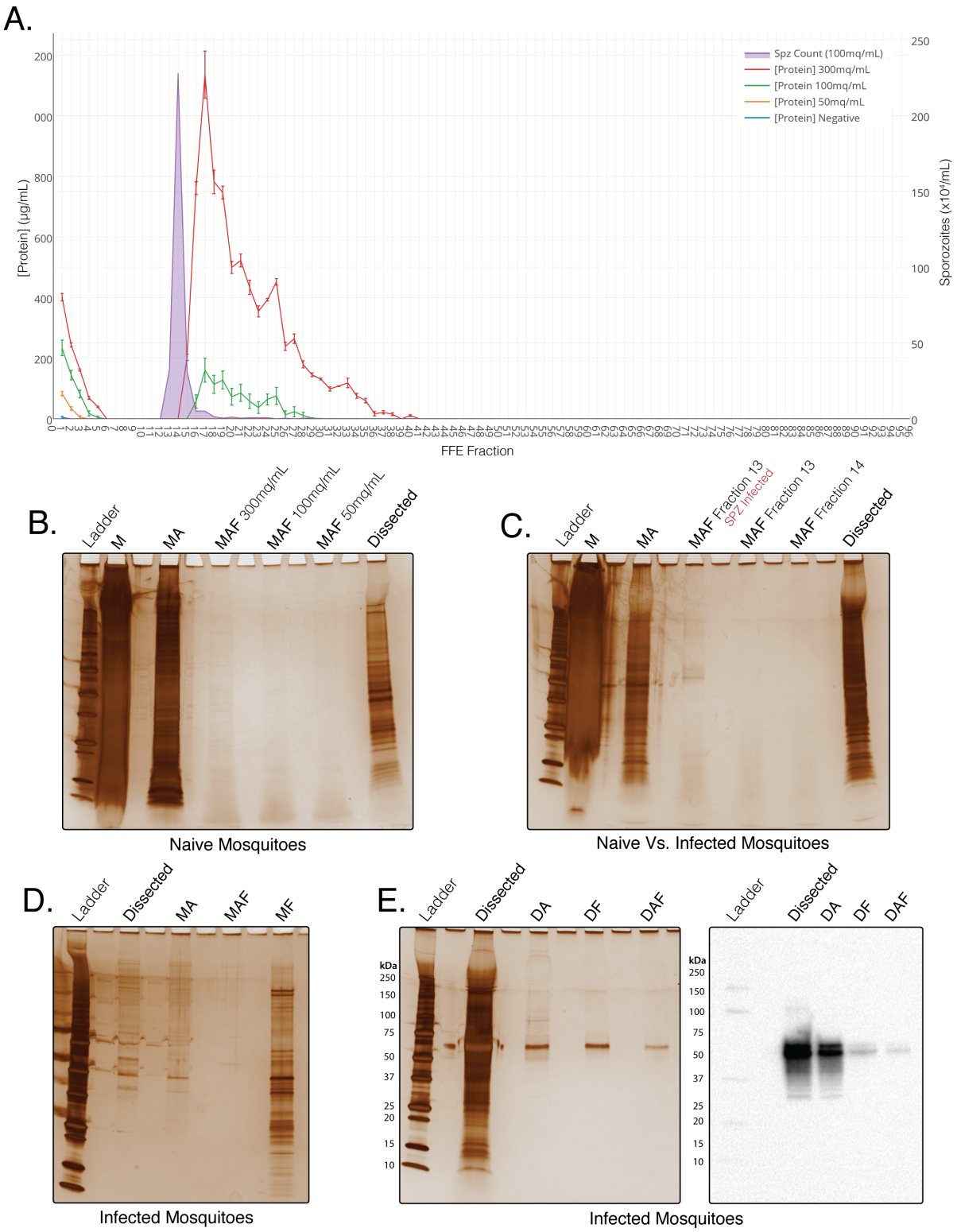

Figure 3-9 I Separation of mosquito associated protein contaminants. A) Protein concentration in each fraction after loading naïve mosquito MA onto the FFE machine at three doses of mosquitoes (MAF). Sporozoite distribution from infected mosquitos loaded at 100mq/mL at the same time as the naïve mosquitoes is marked to allow comparison of purification. B) Silverstain of naïve mosquitoes from each step of purification. Naïve MAF lanes are from the same fraction as the sporozoite peak fraction identified by running infected mosquitoes at the same time. C) Silverstain of naïve mosquitoes from each step of purification, with the MAF fraction from sporozoite infected mosquitoes (fraction 13) included (labelled

SPZ infected on the figure) and MAF fraction 13 and 14 from naïve mosquitoes. D) Silverstain of infected mosquitoes from each step of purification. E) Left; Silverstain of infected mosquitoes from each step of purification when using dissected salivary glands for homogenisation instead of total mosquitoes. Right; western blot against *P. berghei* CSP from the same samples as the silver stain (left). All silver stains are from reducing SDS-PAGE's with samples normalised by originating mosquito dose with four originating mosquitoes worth loaded onto each lane. MAF samples in C-E) where injected into the FFE machine at 100mq/mL.

To further illustrate the purity of samples obtained by FFE a sample from each stage of purification was pelleted by centrifugation (Figure 3-10a), which clearly showed a reduction in mosquito associated debris such as melanin from the cuticle. Samples from each MAF FFE fraction using infected mosquitoes injected at 100mq/mL were used to develop dot blots against CSP to identify sporozoites and mosquito actin as an example of an abundant mosquito protein (Figure 3-10b). The CSP distribution was similar to the manual counts, however the tail was considerable longer, possibly containing degraded CSP seen in Figure 3-9e instead of sporozoites.

Finally, liquid chromatography tandem mass spectrometry (LC-MS/MS) analysis of each stage was conducted to assess the protein purity of each stage of purification. LC-MS/MS raw data was searched against the Uniprot-Swissprot database using the MASCOT search algorithm (see methods). This led to the identification of several insect proteins across all three stages of purification (e.g. ATP synthase subunits α and β; Myosin heavy chain; ADP, ATP carrier protein ½) as well as other contaminating proteins (e.g. haemoglobin subunit β, specifically identified in MA). Importantly, *P. berghei* CSP protein was identified with three peptides exclusively in the fraction purified by MAF (Figure 3-10c). This suggested that parasites were sufficiently enriched, and mosquito as well as other contaminating proteins depleted to allow successful identification of this abundant parasite protein.

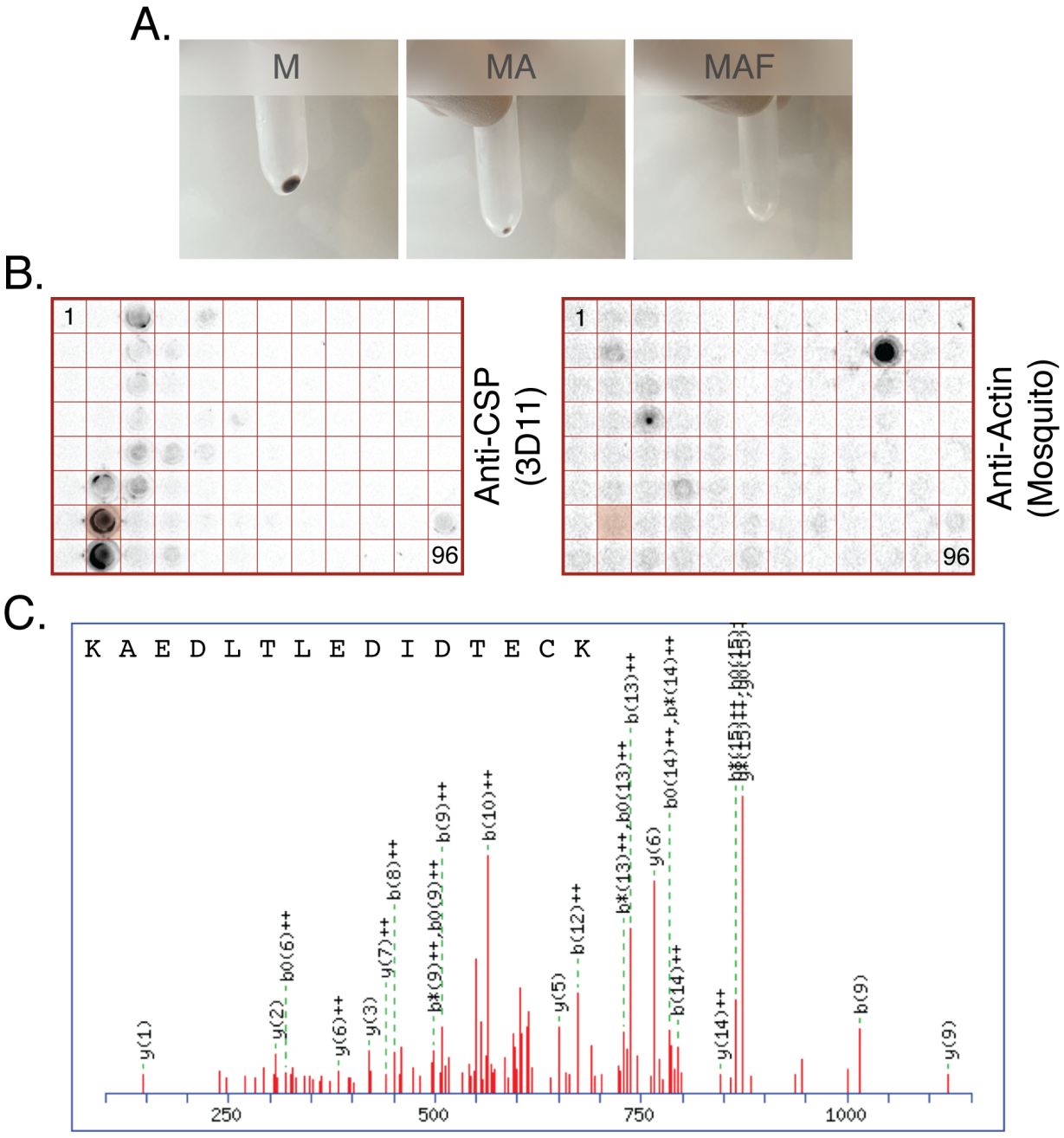

Figure 3-10 I Further characterisation of sporozoite purification from protein. A) Photographs of pelleted sample from M, MA and MAF purification stages. All pellets contain equivalent originating mosquito doses. B) Dotblots of FFE fractions against *P. berghei* CSP and mosquito actin proteins. Red well indicates the peak sporozoites fraction identified by manual count. C) Identification of tryptic peptide 297-312 from *P. berghei* CSP protein (Swissprot ID: P06915) with MASCOT score of 37 by mass spectrometry analysis. All samples normalised to 200mq/mL.

To visually assess the purification protocol, samples from dissected and MAF were diluted to the same concentration of sporozoites and visualised by brightfield microscopy (Figure 3-11). Large pieces of debris, including a whole salivary gland were seen in the dissected treatment but not in FFE. The morphology of the sporozoites from each treatment were similar.

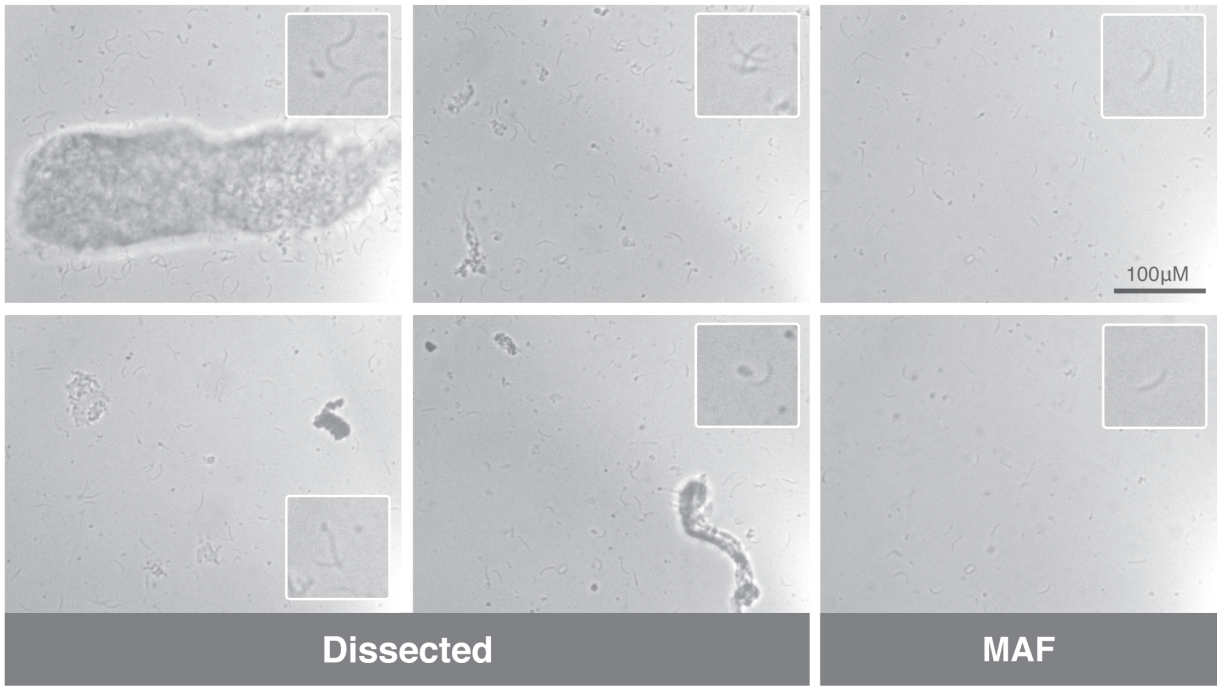

Figure 3-11 I Purified sporozoite microscopy. Brightfield images of sporozoites from MAF and dissection with a zoomed in portion. Both treatments normalised to same concentration of spz/mL.

3.2.5 Sporozoite Sterility: Separation from Mosquito Bacterial Biota

The second consideration when using sporozoites for both *in vitro* and *in vivo* experiments is their aseptic condition, as this may have considerable implications in experiments investigating innate immune responses in animals following intravenous injection and may require higher levels of antibiotics in tissue culture media. To assess bacterial contamination two methods of culture were used to maximise the growth of mosquito associated bacteria. Anaerobic bacteria were not considered, as using sporozoites in anaerobic conditions is not likely. Tryptic soya broth (TSB) is commonly used as non-selective media for growth of a large variety of aerobic bacteria[262] and was therefore chosen as an inoculum. A serial dilution of samples normalised by mosquito dose from each stage of purification was grown for 16 hr at 37^{o}C in TSB and absorbance at 600nm (OD600) measured (Figure 3-12a). Only MAF purified samples reached sterility during the seven dilutions, with MA and dissected showing similar absorbance levels.

Bacterial load across all 96 FFE fractions was assessed by inoculating each fraction from MAF injected at originating mosquito doses of 300, 100 and 50mq/mL into TSB for 24 hr. The time taken to reach 0.4 absorbance units was measured at OD600 and the reciprocal used to illustrate bacterial load, with sporozoite distribution from an infected control used to assess the purification from sporozoites (Figure 3-12b). Absorbance was also measured at 10 min intervals and used to create a heatmap (Figure 3-12c), which demonstrated that the majority of bacteria were in fractions 22-65, however bacteria growth was detected in the peak sporozoite fraction for all mosquito dilutions. Bacteria

growth showed a pattern with peak fractions of growth likely caused by the position of the seven separation buffer inlets.

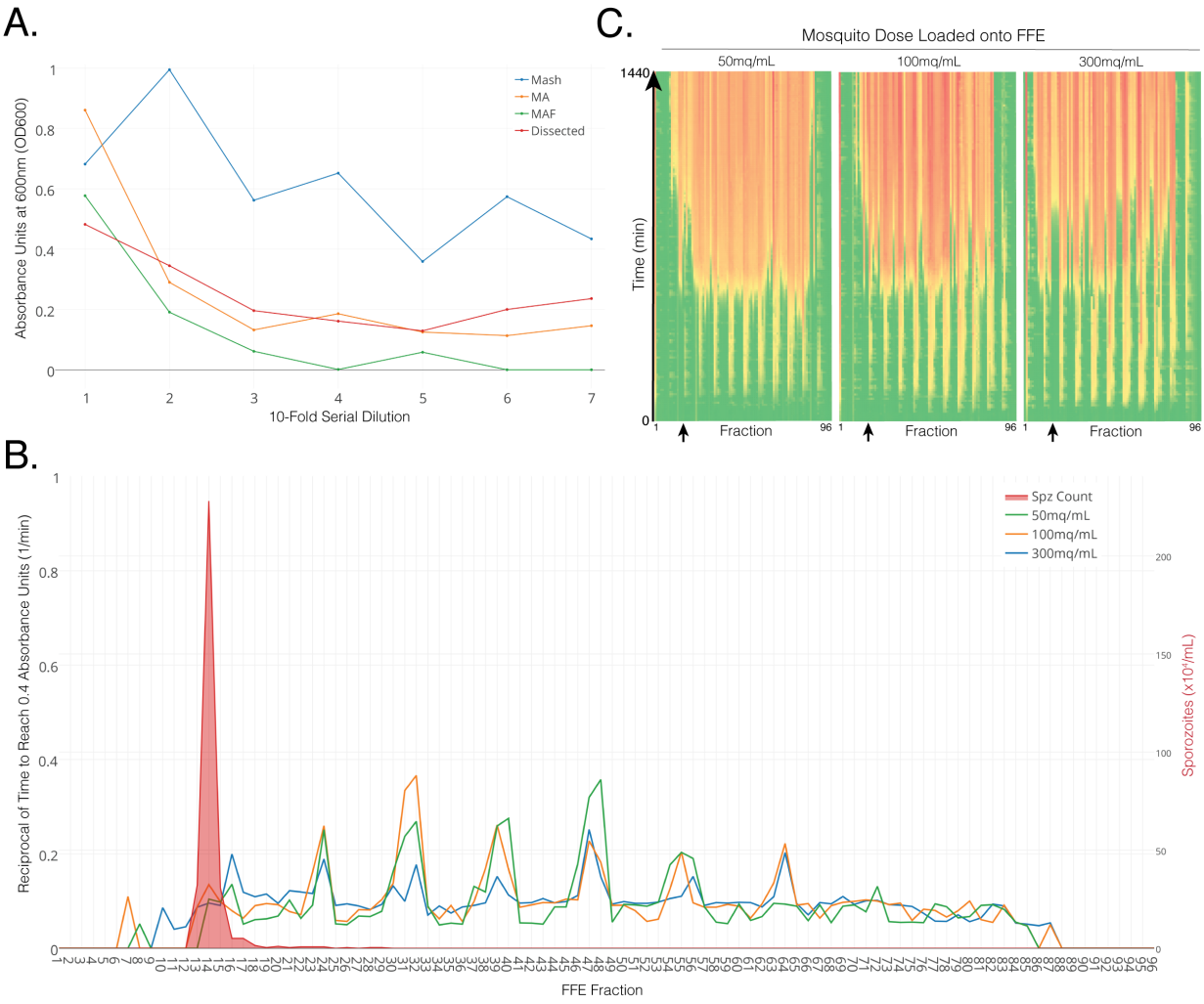

Figure 3-12 I Bacterial separation measured by TSB growth. A) End-point 16 hr serial dilution for each step of MAF purification. Absorbance of samples in TBS was measured at 600nm (OD600) 16 hr post-inoculation B) 24 hr bacterial kinetics in TSB. Bacteria load measured by reciprocal of time taken (min) to reach 0.4 absorbance units at 600nm. A value of 0 indicates no bacterial growth. TSB inoculated with 15µL of each fraction. Positive control of infected mosquitoes shown in red (z axis). Data representative of two independent replicates. C) 24 hr kinetics heatmap in TSB of MAF loaded at 50, 100 and 300mq/mL. OD600 absorbance measured every 10 min for each fraction and given a colour. Green represents no growth. Red represents high absorbance (i.e. growth). Arrow indicates peak sporozoite fraction. All growth conducted at 37°C, 300rpm. All experiments used mosquitoes blood fed on uninfected mice 21 days prior to MAF extraction.

For many experiments sporozoites are also injected intravenously (i.v.) into animals, therefore bacterial growth was also checked using growth on blood-agar plates with either naïve or infected mosquitoes normalised to 200mq/mL and bacterial colony forming units per mL (cfu/mL) determined. In naïve mosquitoes (Figure 3-13a) M from whole mosquitoes had the highest bacteria load (M: 12.0 log cfu/mL) which was reduced 1.7 fold by Accudenz centrifugation (MA: 7.0 log cfu/mL) but remained 1.1 fold higher

than using manual dissection (6.1 log cfu/mL). FFE purification of MA injected at 300, 100 and 50mq/mL caused a significant reduction of bacterial load compared to manual dissection (MAF: 300mq/mL: 1.2 fold, 4.9 log cfu/mL; 100mq/mL: 1.5 fold, 4.2 log cfu/mL; 1.6 fold, 50mq/mL: 3.9 log cfu/mL). With the lowest FFE injected dose causing the most significant drop in bacteria load of 1.6 fold (2.2 log cfu/mL). When mosquitoes were infected a similar trend was seen, with MAF loaded at 100mq/mL able to significantly reduce bacterial load by 1.3 fold (1.3 log cfu/mL) compared to manual dissection (Figure 3-13b).

If alternatively, dissected salivary glands instead of whole mosquitoes were used as homogenate then the complete DAF purification removed all bacteria detectable by blood-plate agar growth (Figure 3-13c). Accudenz purification (DA) significantly reduced the load by 1.4 fold (1.7 log cfu/mL) compared to dissected. However, if salivary gland homogenate was separated directly by FFE without density centrifugation (DF) it was more effective, reducing load by 1.6 fold (log 2.4 cfu/mL).

To confirm the trend of bacterial growth an alternative approach to normalisation was used based on mosquito and sporozoite numbers. Variability in mosquito sporozoite loads (spz/mq) meant it was unfeasible to normalise samples by sporozoite concentration. However, if mosquitoes have a higher sporozoite dose you effectively have a greater ratio of sporozoites to mosquito contaminants (sporozoite:mosquito). But, protein contaminants from the mosquito were found to be significantly low (Figure 3-9e), therefore this normalisation method may not be very useful. To determine this the ratio of originating mosquito dose per mL to sporozoite count per mL was used to normalise bacterial load. The same significant trend could be seen when using this normalisation method (Figure 3-13d) or when normalising by originating mosquito dose only (Figure 3-13e).

Both the bacterial and protein contamination studies indicated that injecting MA onto the FFE machine at 100mq/mL was a suitable compromise over time taken to run and the purity of the sample. Therefore, this dose was used for the remainder of experiments described in this chapter.

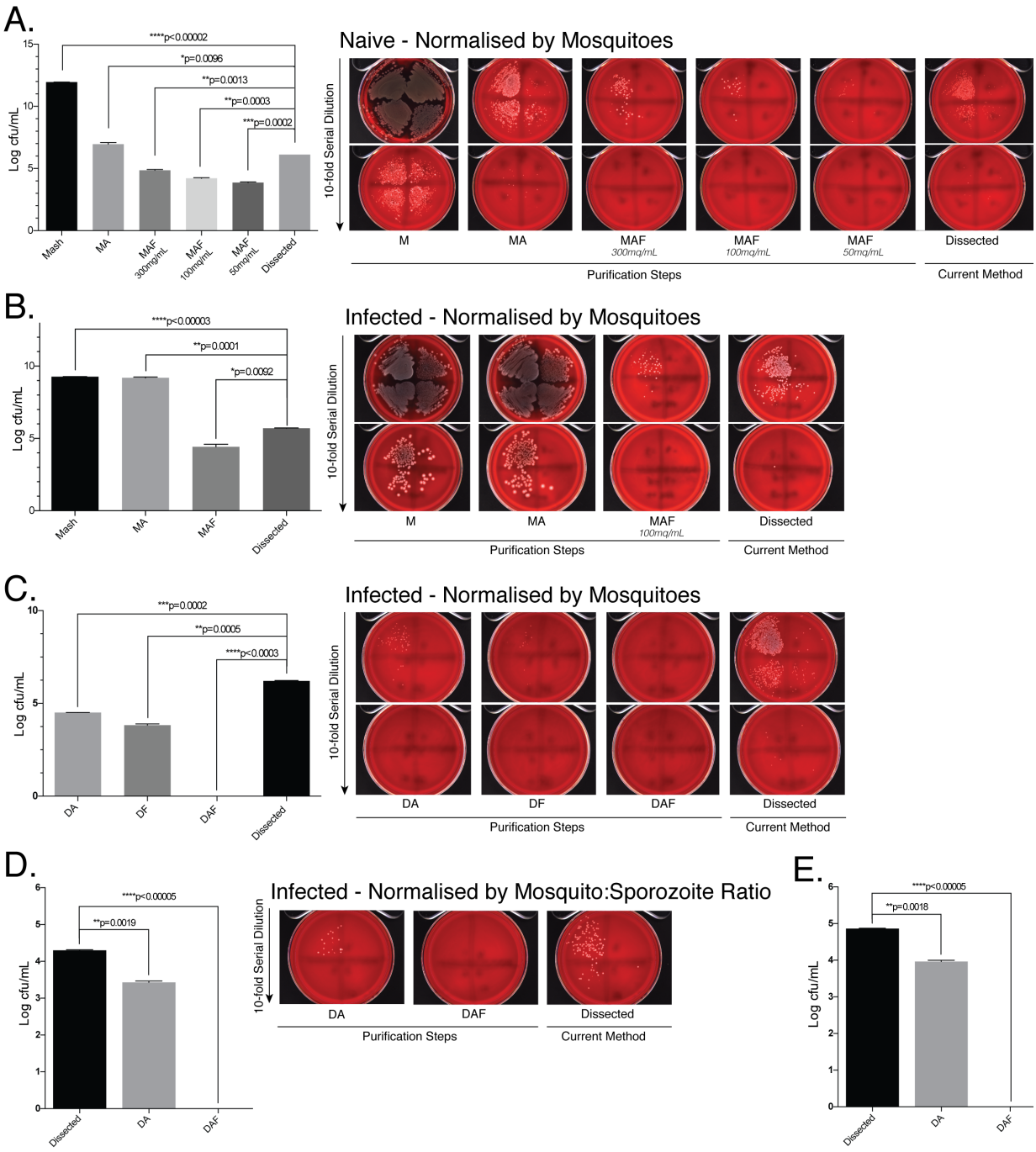

Figure 3-13 l Blood plate agar bacterial growth. A) Bacterial growth at different stages from uninfected MASH origin purification. Samples were loaded onto the FFE machine at three different originating mosquito doses. B) Bacterial growth at different stages from infected MASH origin purification. C) Bacterial growth at different stages from infected dissected salivary gland origin purification. D) As per (C) but samples normalised by normalised by originating mosquito:sporozoite dose ratio. E) As per (D) but samples normalised by originating mosquito dose only. All experiments show the mean of two technical replicates and error bars represent SEM. All treatments compared to dissected by unpaired two tailed t-test using Bonferroni correction (A: *p<0.01, **p<0.002, ***p<0.0002, ****p<0.00002; B-C: *p<0.017, **p<0.0034, ***p<0.00034, ****p<0.000034; D-E: *p<0.025, **p<0.005, ***p<0.0005, ****p<0.00005). Bacterial colony forming units log transformed. Samples (A-C & E) normalised to originating mosquito dose, (D) normalised by originating mosquito:sporozoite dose ratio.

Primary hepatocytes have been shown to be far more conducive to *Plasmodium* infection[186,188], making them a suitable candidate for FFE purified sporozoites (see supplemental 8.1.3 for development of extraction protocol). To assess the effect of MAF purification, sporozoites from either manual dissection or MAF were added to primary rat hepatocytes 24 hr after plating at a ratio of 1:1. 20 hr after the addition of sporozoites images were taken and morphology assessed (Figure 3-14). Hepatocytes with dissected sporozoites clearly showed considerable stress and cell death compared to hepatocytes cultured with MAF sporozoites. Some cell death in both may be attributable to cell traversal of sporozoites, however the greater number in the dissected treatment suggests contaminants associated with the sporozoites may be that cause of the poor cell morphology.

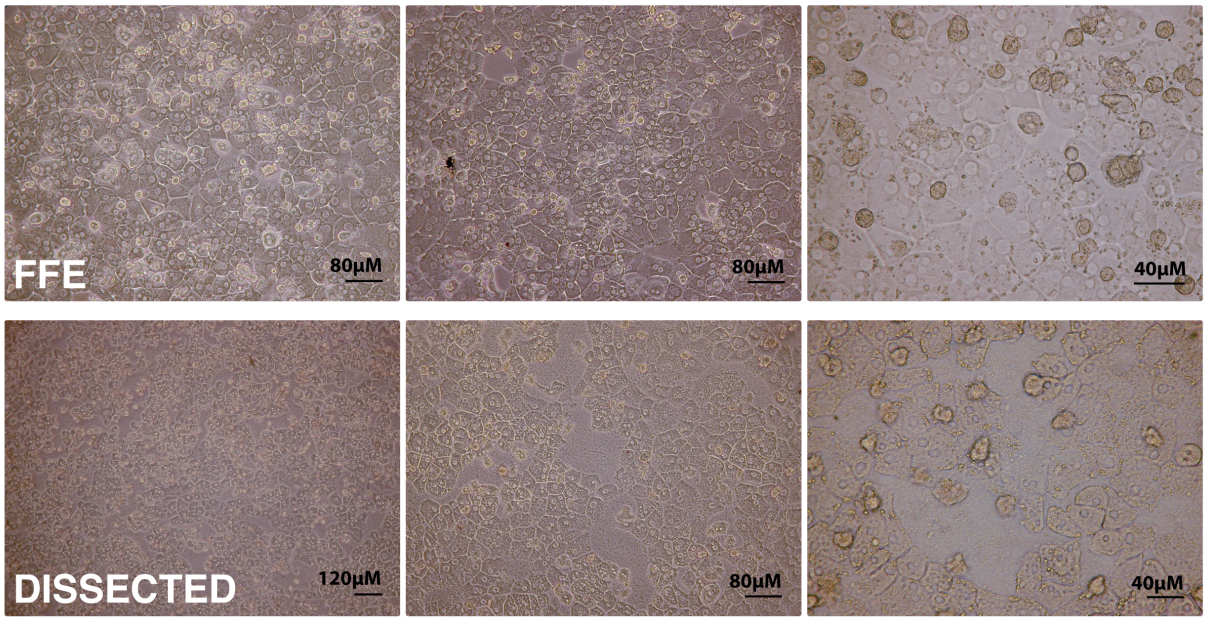

Figure 3-14 l Sporozoite-associated morphological changes in primary rat hepatocytes. Brightfield images of primary rat hepatocytes 20 hr after addition of sporozoites obtained by either manual dissection or MAF. Cultured in 1% P/S.

Thus far, characterisation of an FFE-based sporozoite purification protocol has shown that the MAF protocol is a feasible method for obtaining sporozoites with a superior reduction in mosquito derived protein and bacterial contaminants over the standard dissection method. This high purity alone lends itself well to studies which are reliant on purity such as proteomic and metabolic studies. Furthermore, when using the DAF method sporozoites were aseptic. Additionally, the MAF method is suitable for high throughput, enabling large quantities of sporozoites to be obtained in a few hours by one individual. For example, 700 mosquitoes can be processed to obtain over 40 million pure sporozoites within 2 hr, wereas using dissection a skilled person that can constantly dissect one mosquito per min would take nearly 12 constant hours. Thus, increasing productivity over 6 fold. To assess whether these sporozoites could be used for *in vitro* liver stage assays the viability of these sporozoites must now be assessed.

3.2.6 Sporozoite Viability: In Vitro

Following the assessment of sporozoite purification the effect on viability was assessed by a number of *in vitro* and *in vivo* techniques. The motility pattern of sporozoites is commonly used to assess viability[184,237] and MAF purified sporozoites were compared to manually dissected using the ToAST ImageJ Plugin[157]. The plugin classed sporozoite movement into attached static, attached waving or gliding (clockwise or counter clockwise) (Figure 3-15a-d). Sporozoites motility was compared by assessing both the mean velocity of sporozoites during each motility state (Figure 3-15b) and the overall percentage of motility states of sporozoites (Figure 3-15c-d) over a sliding average of nine frames for a total of 600 frames taken at 2Hz. Drifting sporozoites were excluded from analysis. There was no significant different between dissected and MAF purified sporozoites in any of the movement states based on either mean velocity or overall percentage.

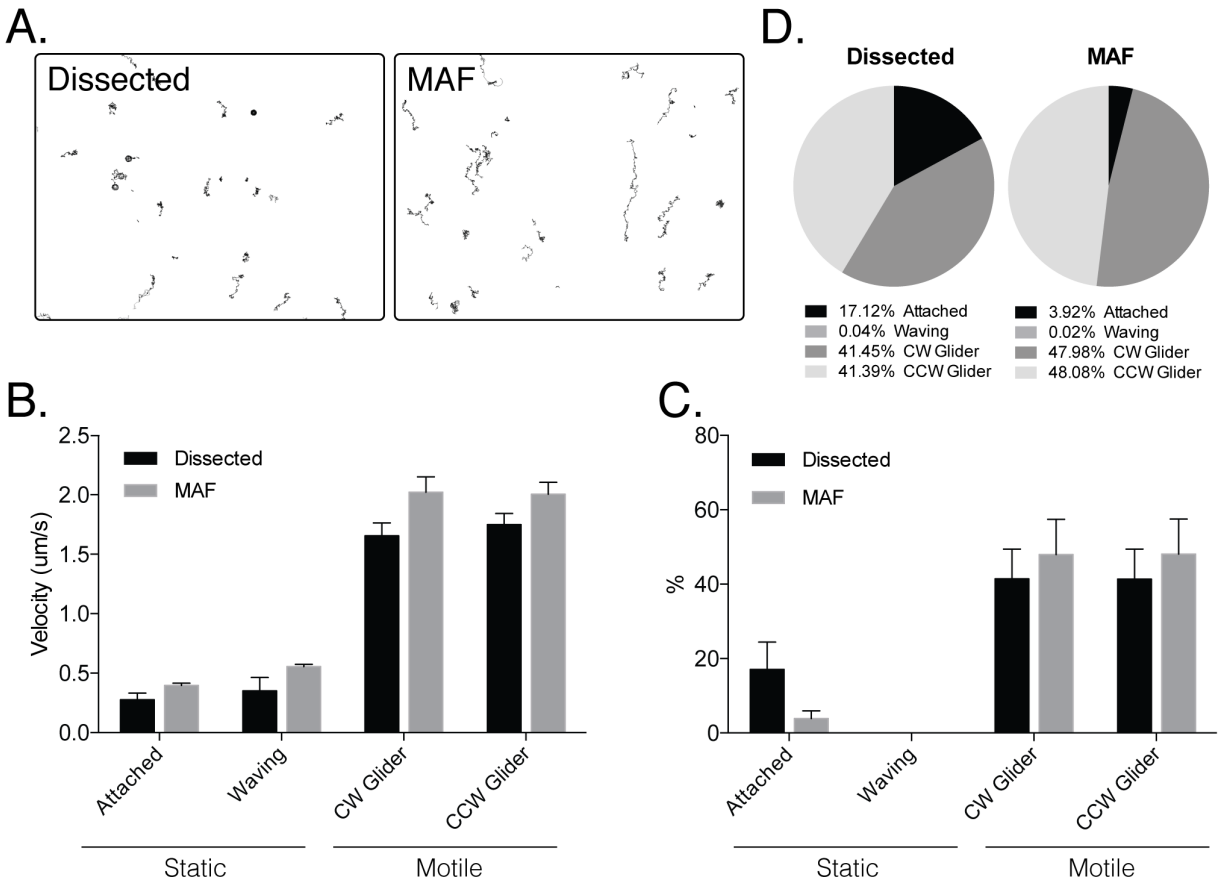

Figure 3-15 I Assessing sporozoite viability by *in vitro* infectivity and motility. A) Examples of movement trails from FFE and dissected sporozoites over 600 frames at 2Hz. B) Sporozoite gliding motility over 600 frames at 2Hz with a sliding nine frame average during each motility state over 600 frames at 2Hz. C-D) Comparison of the percentage of all sporozoites in each state. Sporozoite tracking represent mean of two independent replicates and six technical replicates. States were compared using an unpaired two-tailed t-test.

3.2.7 Sporozoite Viability: In Vivo

Murine challenges of sporozoites were used to assess the *in vivo* infectiousness by measuring time to reach 1% blood stage parasitaemia. Initially mice were challenge i.v. with an escalating dose of sporozoites purified using MAF, which showed that all mice developed blood stage infection, with only the 500 sporozoite dose showing reduced infectivity (Figure 3-16a). Subsequently, to assess whether purification was associated with a reduction in infectiousness, mice were challenged i.v. with 5000 sporozoites purified by either MA or MAF and compared to manual dissection. Gliding motility, which is commonly used to assess sporozoite viability, has been shown to decline over time when left in the dissection buffer[237]. Therefore, to allow direct comparison with groups, including the dissected control, all sporozoites were kept outside of the mosquito host for the same amount of time before injection. All mice reached 1% parasitaemia (Figure 3-16b). Sporozoites from MA and MAF however caused a significant median delay of 0.66 and 0.59 days respectively compared to dissected (Figure 3-16c). There was no significant difference between MAF or MA. As both treatments used MA, this suggests that either using Accudenz or obtaining sporozoites from whole mosquito MASH may cause a reduction in infectiousness. A more detailed challenge was therefore conducted to assess the effects of different combinations of purification methods.

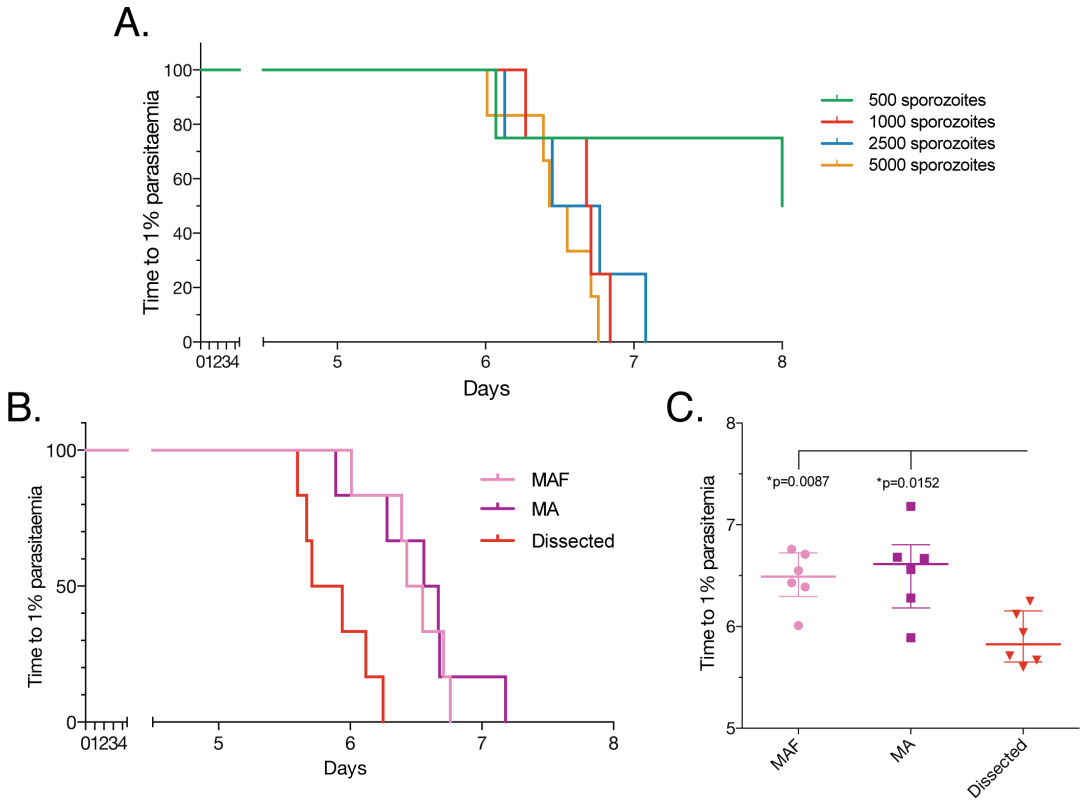

Figure 3-16 I Accudenz and FFE sporozoite challenge. A) Kaplan-Meier survival curve of mice challenged i.v. with increasing doses of sporozoites from MAF. Endpoint classed as 1% parasitaemia. B) Kaplan-Meier survival curve of mice challenged i.v. with 5000 sporozoites from different purification steps. Endpoint classed as 1% parasitaemia. C) Box blot of time to reach 1% parasitaemia from challenge (B), with treatments compared to dissected sporozoites using Mann Whitney test with Bonferroni correction (*p<0.025, **p<0.005, ***p<0.0005, ****p<0.00005). Error bars show median with IQR.

Mice were challenged i.v. with either 1000 (Figure 3-17a) or 5000 (Figure 3-17b) sporozoites from each stage of purification using either whole mosquitoes or dissected salivary glands as homogenate. As before all groups were kept outside of the mosquito host for the same amount of time. The longest treatment being DAF (approximately 3-4 hr). This may offer an explanation for the failure of one mouse in the dissected group from the 1000 sporozoite challenge to establish blood stage infection and also the differences between challenge doses. Both challenges show a significant difference between time to reach 1% parasitaemia with different treatments (Mantel-Cox Test, 1000spz: *p=0.0272, 5000spz: ****p<0.0001), indicating as shown before (Figure 3-16) that purification may be associated with a significant drop in sporozoite infectiousness.

Compared to dissected, all MASH origin treatments caused a significant delay in time to reach 1% parasitaemia, except MA with 1000 sporozoite dose (Figure 3-17a-b). Furthermore, there was no significant difference between MA and MAF treatment in all experiments (Figure 3-16b, Figure 3-17a-b). This indicates that using sporozoites from whole mosquito MASH is associated with a possible reduction in sporozoite infectiousness. However, using dissected sporozoites followed by Accudenz (DA) only was not associated with a significant delay, whereas combining with FFE (DAF) did cause a significant delay (Figure 3-17). This suggests that FFE may also cause a reduction in sporozoite infectiousness, but by an alternative way than that observed with MASH origin sporozoites.

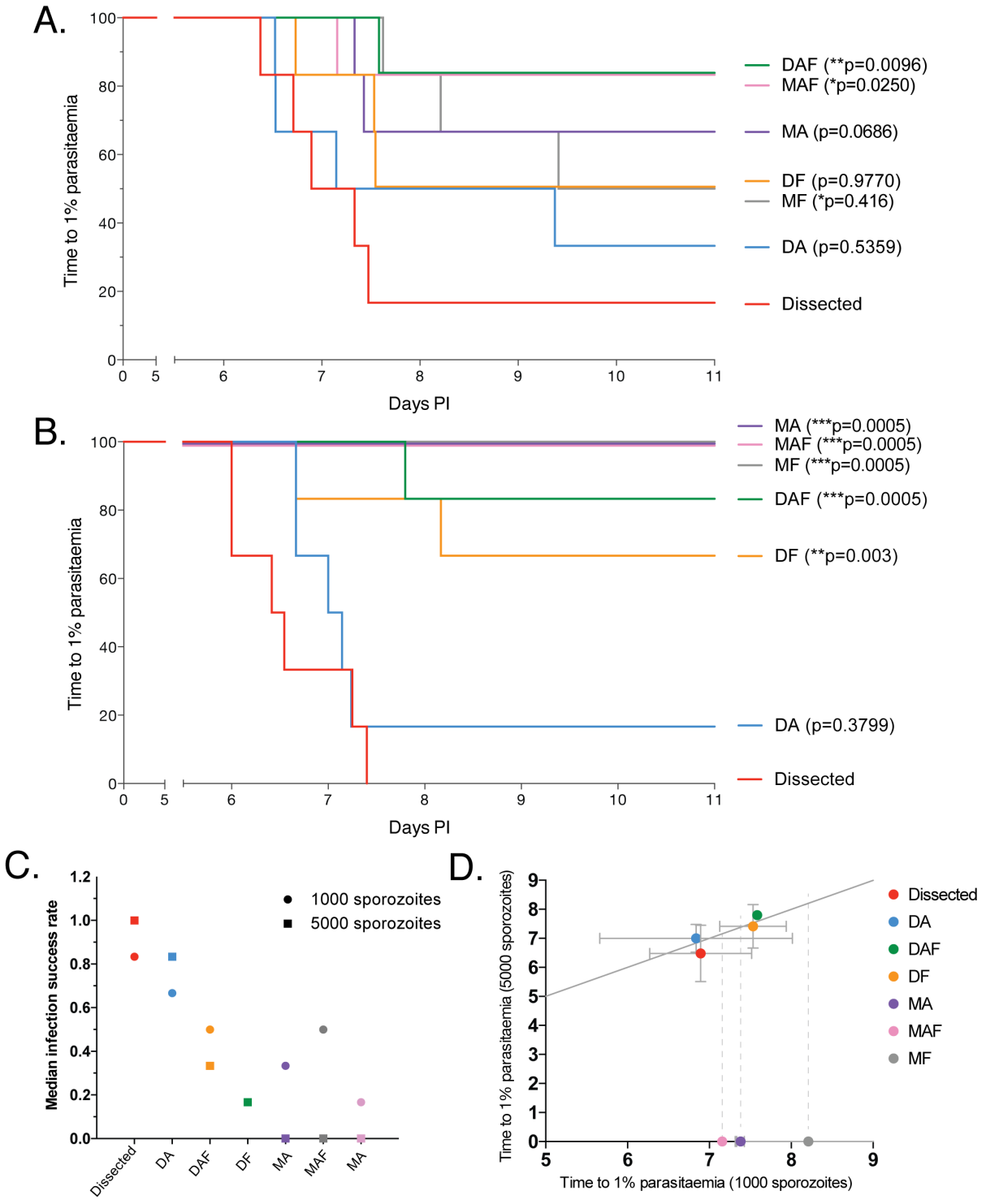

Figure 3-17 I *In vivo* murine sporozoite challenge. A) Kaplan-Meier survival curve of mice challenged with 1000 sporozoites from different purification steps. Death classed as 1% parasitaemia. B) Kaplan-Meier survival curve of mice challenged with 5000 sporozoites from different purification steps. Death classed as 1% parasitaemia. C) Median infection success rate for the 1000 and 5000 sporozoite challenges A) and B). D) Median time to reach 1% parasitaemia of 1000 sporozoite challenge plotted against the 5000 sporozoite challenge. Solid line shows y=x, an interpolating dashed line is draw for treatments with no successful infection after 5000 sporozoite dose. Error bars represent interquartile range. Survival curves compared using Mantel Cox statistical test.

To investigate the cause of MASH-associated blood stage delay the effect of effect of sporozoite source (haemocoel, salivary gland or oocysts) was investigated. Different part of mosquitoes were homogenised followed by Accudenz and FFE and mice challenged with 1000 sporozoites (Figure 3-18a). No delay was observed by prior removal of the abdomen (to remove oocysts and some haemocoel sporozoites) compared to manually dissected sporozoites (Figure 3-18b). Unfortunately, both removal of abdomen and decapitation lead to loss of salivary glands on many occasions so this treatment was not carried out. This suggests that oocysts or haemocoel sporozoites are less infective.

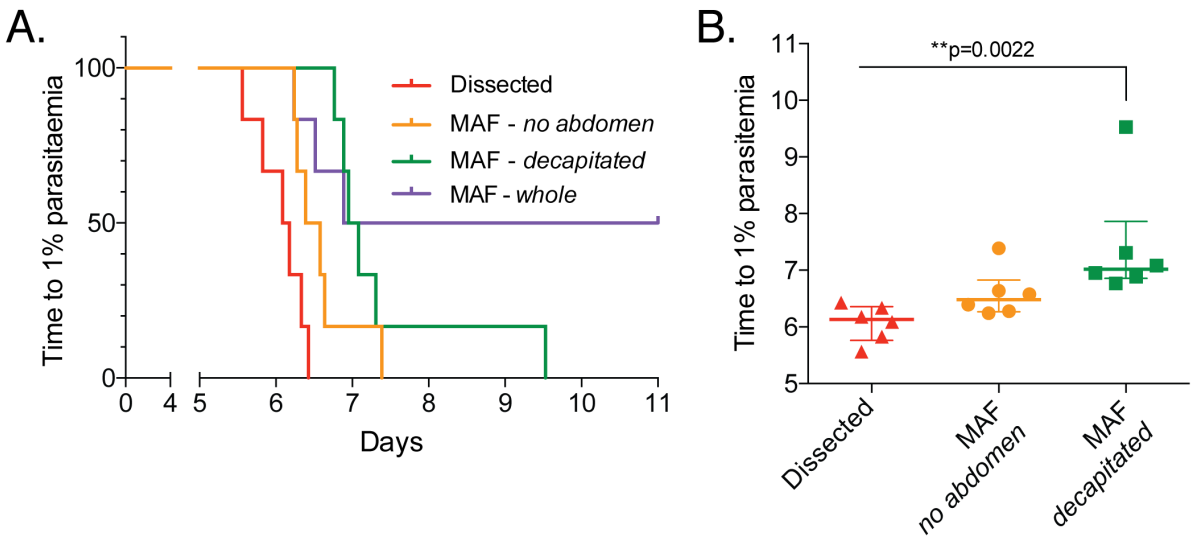

Figure 3-18 I Decapitation and abdomen removal. A) Kaplan-Meier survival curve of mice challenged with 1000 sporozoites from different sources followed by MAF. Death classed as 1% parasitaemia. B) Box blot of time to reach 1% parasitaemia from challenge (A). Treatments compared to dissected Mann Whitney test using Bonferroni correction. Error bars show median with IQR.

Surprisingly, no cumulative delay in parasitaemia is observed when MASH and FFE techniques were combined (Figure 3-16b, Figure 3-17a-b). A possible reason for this could be that sporozoites from the salivary gland are more resilient to stress compared to sporozoites from haemocoel and oocysts that are obtained when the whole mosquitoes are homogenised. In corroboration with this, no significant delay is observed when abdomens were removed prior to MAF (Figure 3-18). Additionally, salivary gland dissection followed directly by FFE was not consistently associated with a significant delay in these experiments (Figure 3-17). Also, the median infection success rate was higher in treatments starting with salivary gland homogenate than mash homogenate (Figure 3-17c). Nevertheless, the fact that a delay in blood stage parasitaemia was observed with the DAF treatment (Figure 3-17a-b) but not following abdomen removal with MAF treatment suggests that viability from the FFE protocol may be variable. Therefore, different sources of stress that may influence parasite infectivity need to be further investigated.

3.2.8 Assessment of the Purification Protocol on Infection Rate in Hepatocytes

The infection rate of MAF purified sporozoites was assessed in HepG2 hepatoma and primary rat hepatocytes using RT-PCR, microscopy and flow cytometry. Absolute copy number of *P. berghei* HSP70 DNA were measured using RT-PCR with a DNA plasmid standard curve in both HepG2 (Figure 3-19a) and primary rat hepatocytes (Figure 3-19b) using sporozoites from manual dissection or MAF. Copy numbers were normalised to 1000 HSP70 copies for the dissected treatment. MAF purified sporozoites showed a 1.5 and 2.1 fold increased in HSP70 copy numbers compared to manually dissected sporozoites in HepG2 and primary hepatocytes respectively.

Relative *P. berghei* HSP70 mRNA transcript levels were measured using RT-PCR at 11 and 40 hr post addition of purified and dissected origin sporozoites in primary rat hepatocytes (Figure 3-19c). By 40 hr MAF treatment had a mean significant increase in HSP70 transcripts of 1.6 times compared to dissected and MA had a non-significant mean decrease of 0.76 times. No significant difference was detected at the 11 hr time-point. MA appeared to be detrimental to liver-stage infection rates, possibly linked to the lower purity shown earlier. 24 hr time-lapse videos were taken of primary rat hepatocytes and successful hepatocyte infections identified by counting EEF's still present at 24 hr. Treatments from MAF sporozoites showed a significant 5.4% infection rate compared to 0.4% when using manually dissected sporozoites (Figure 3-19d). This data suggests that FFE-based sporozoite purification may increase *in vitro* infections, however further work will be required to confirm full liver stage schizogony occurs with MAF sporozoites.

Finally, 36 hr after addition of MAF mCherry sporozoites to primary rat hepatocytes the number of infected cells was quantified by flow cytometry (Figure 3-19e). After gating for single cells the percentage of mCherry positive cells was determined by gating mCherry fluorescence against either FSC or the APC channel giving infection percent of 8.37% (235 out of 2808 cells) and 10.37% (302 out of 2808 cells) respectively.

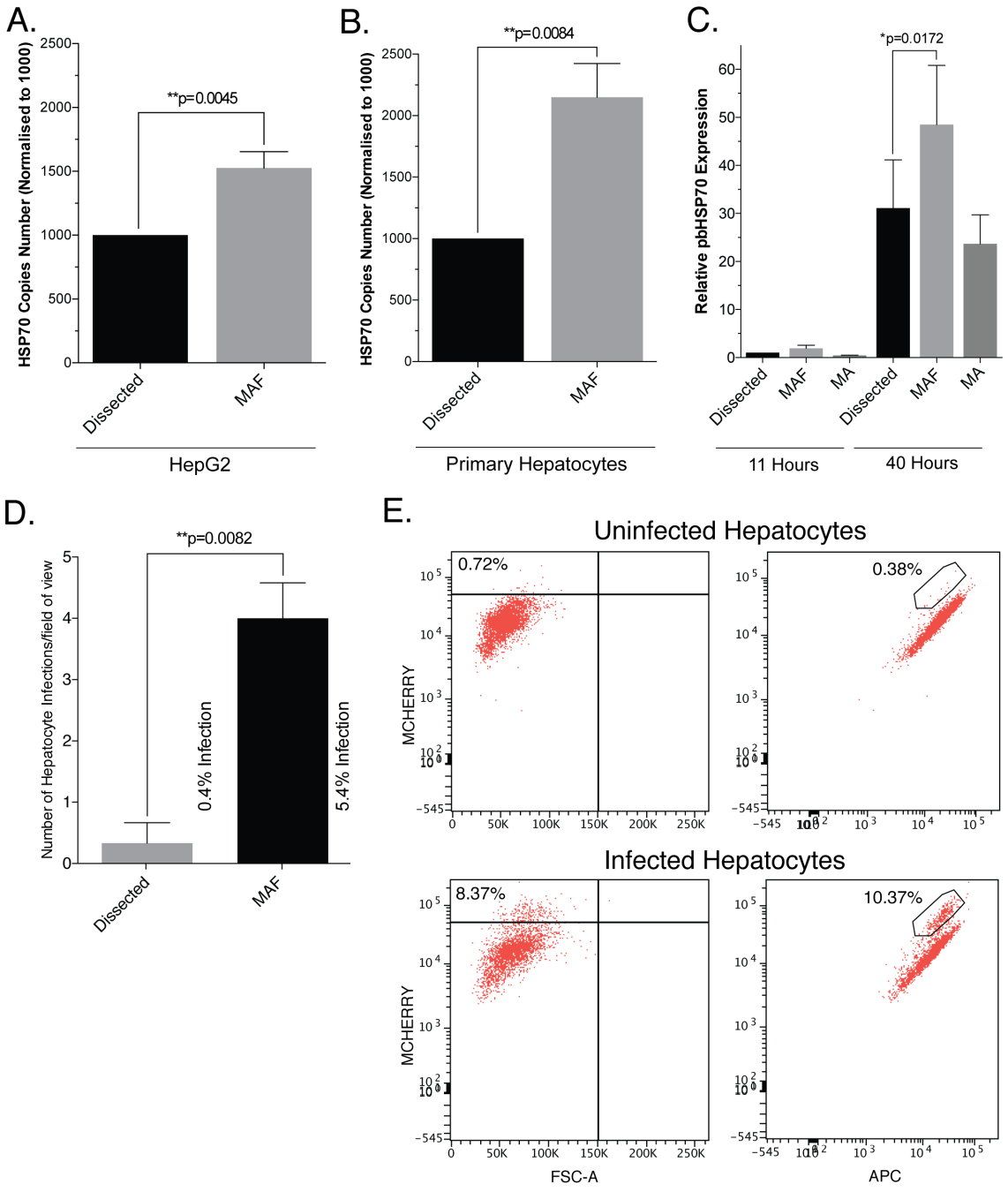

Figure 3-19 I Assessment of FFE sporozoite infection rate. A) Absolute RT-PCR quantification of parasite HSP70 DNA copies normalised by host HSP60 gene in HepG2 cells. Three independent replicates. B) Absolute RT-PCR quantification of parasite HSP70 DNA copies normalised by host HSP60 gene in primary rat hepatocytes. Three independent replicates. C) Relative RT-PCR quantification of parasite HSP70 relative to host HPRT1 transcript at 11 and 40 hr post addition of sporozoites from different purification methods. D) Manual counts of successful hepatocyte infections in primary rat hepatocytes measured by visual identification of six fields of view over 24 hr time-lapse from three Independent replicates. E) Flow cytometry quantification of mCherry expressing transgenic *P. berghei* infected primary rat hepatocytes 36 hr post addition of sporozoites (total 2808 cells in treatment, 3906 cells in control). Data representative of three technical replicates. Groups in all panels compared using two-tailed paired t-test. Cut off values for panel (C) were adjusted using Bonferroni's correction (*p<0.025, **p<0.005, ***p<0.0005, ****p<0.00005). Bars represent means and error bars the SEM.

As an alternative to direct *in vitro* infections the ability of *in vivo* challenge parasites to infect hepatocytes *in vitro* and grow *ex vivo* was investigated. A rat was i.v. challenged with 30 million GFP transgenic sporozoites purified from 400 mosquitoes and 14 hr later hepatocytes extracted by liver perfusion. Infected hepatocytes were sorted and plated for up to 30 hr. Sorting identified 2.83% GFP positive cells (Figure 3-20a, b).

A.

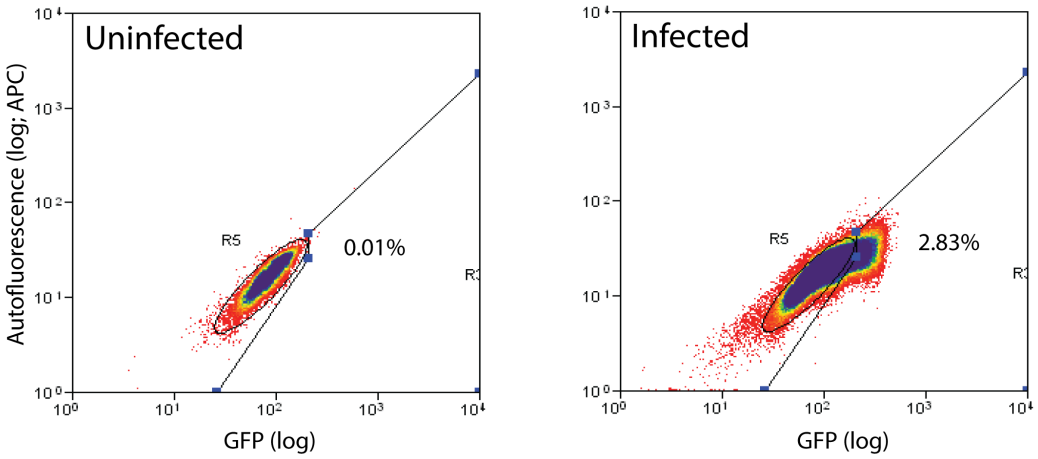

B.

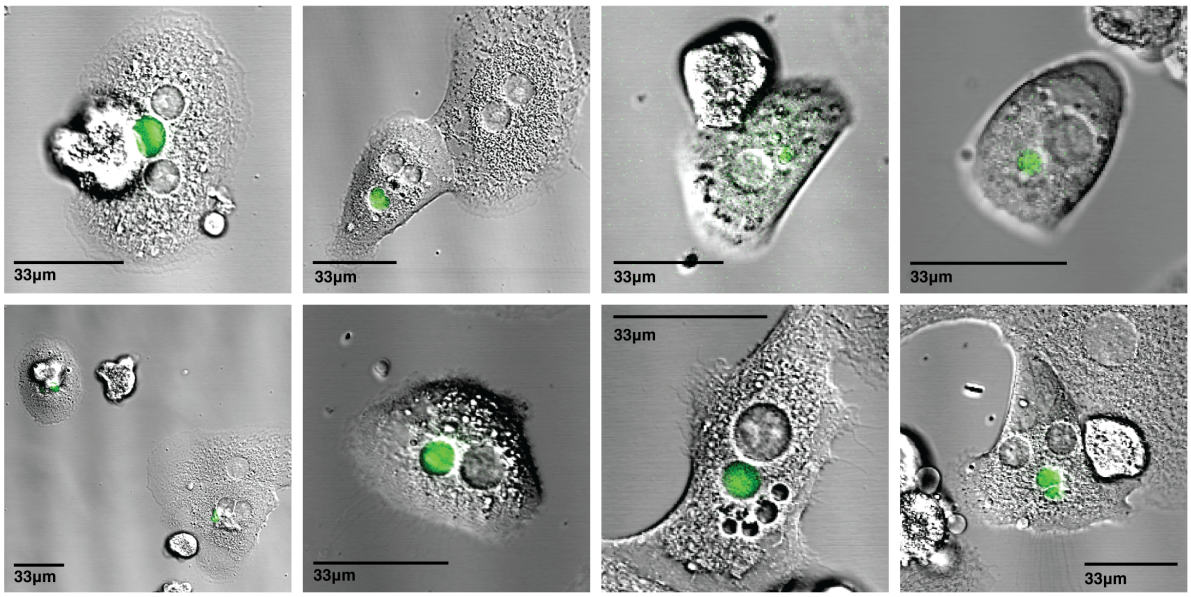

Figure 3-20 I *In vivo* challenge to create *in vitro* infection. A) Gating strategy for sorting infected primary hepatocytes from uninfected. Left; Uninfected rat, right; infected 30 million challenge rat. B) Fluorescent microscopy images of GFP positive gated cells 24 hr after liver extraction.

Hepatocyte maturity has been associated with increased hepatocyte infection[172]. Microfluidic liver models offer a relatively recent method by which to simulate a liver and improve hepatocyte maturity[244-249]. Based on previous work[245,246] an artificial microfluidic liver was created, however due to time constraints it could not be tested with sporozoites (see supplemental 8.1.4 for its development).

3.2.9 Sporozoite Cryopreservation

Following the optimisation of a method of purifying large quantities of sporozoites a natural progression would be to cryopreserve the sporozoites. Eight different freezing solutions were investigated based on a combination of previous buffers for freezing cells, cattle sperm and other organics[154,263-266]. Two freezing rates were investigated -37°C/min (Figure 3-21a) and -5°C/min (Figure 3-21b). Dissected sporozoites were frozen at 6.2x10^6 spz/mL in 1mL of pre-chilled buffer and stored in liquid nitrogen for two months prior to rapid thawing, resuspension in DMEM and i.v. injection of 10,000 sporozoites into two mice. Only 50% FBS freezing solution in Schneider's *Drosophila* media, frozen at -37°C/min gave detectable blood-stage parasitaemia. This cryopreservation procedure was repeated and mice challenged with three doses and a 1000 sporozoite dissected control (Figure 3-21c). Only the 1,180 cryopreserved sporozoite dose showed no infectivity. However, a 100,000 fold increase in cryopreserved sporozoites was needed to achieve a similar time to 1% parasitaemia. This shows that much more work is needed on this area to obtain satisfactory infectivity and viability of sporozoites after cryopreservation.

A.

Method	Parasites Detected (2 mice)
10% HES	N
50% FBS	Y
10% FBS	N
30% Glycerol	N
30% Glycerol, 50% FBS	N
20% Egg Yolk, 10% Glycerol	N
Bambanker	N
10% DMSO, 30% FBS	N

B.

Method	Parasites Detected (2 mice)
10% HES	N
50% FBS	N
10% FBS	N
30% Glycerol	N
30% Glycerol, 50% FBS	N
20% Egg Yolk, 10% Glycerol	N
Bambanker	N
10% DMSO, 30% FBS	N

C.

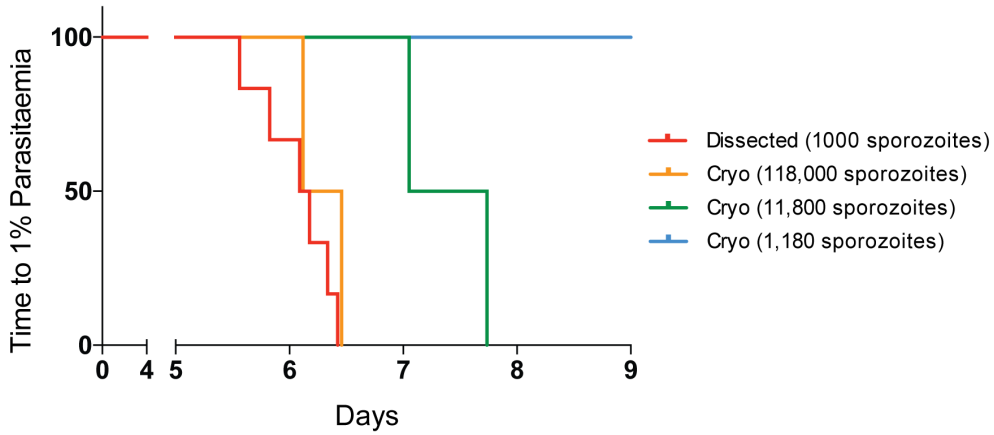

Figure 3-21 I Cryopreservation of sporozoites. A-B) Detection of infected RBCs following BL6 mice challenge with 10,000 sporozoites cryopreserved using one of eight buffers. A) Freezing rate of -5°C/min. B) Freezing rate of -37°C/min. C) Survival curve of time to reach 1% infected red blood cells following challenge with escalating doses of sporozoites cryopreserved using 50% FBS at -37°C/min.

3.3 Discussion

Although the pre-erythrocytic stage of malaria is an attractive intervention point to prevent the development of clinical malaria in human hosts, the field has struggled to understand and identify possible intervention targets of this development stage[95]. A major contributor to this has been the limited success of *in vitro* liver stage systems, which provide low numbers of infected hepatocytes (Table 3-1)[267,268]. However, *in vitro* systems do have great potential for drug-screening and identifying novel vaccine targets[143,172,183,188]. In particular, they provide opportunities for high throughput phenotypic studies against drug candidates[127-134] and identification of suitable new vaccine candidates by enabling a better understanding of pathogen physiology. For example, the first high throughput drug screen for malaria was carried out using *in vitro* asexual blood cultures[135], due to the relative ease of using this culture system for this stage of *Plasmodium*[133]. More recently, other blood stage candidates have been identified[127,132]. However lower infection rates with *in vitro* liver stage cultures have hindered such studies in this part of the *Plasmodium* lifecycle[142-144]. Four of the possible explanations for this low *in vitro* hepatocyte infectivity are discussed in this thesis (Figure 3-2): low sporozoite yield, low purity, poor sporozoite storage and hepatocyte culture methods.

The data presented in this chapter demonstrate the development of a complete workflow for the purification of sporozoites in large quantities and with a high purity. Fulfilling two of the above criteria, purity and high yields. Additionally, based on previously published work, an optimal storage condition was provided for sporozoites between extraction and infection of primary hepatocytes[142,184,186-188,236,237]. The purification workflow alone improved infection rates, suggesting purity may be a key factor affecting *in vitro* infection rate. Furthermore, this setup allowed unseen levels of sporozoites to be purified at once with little added time and minimal workforce, for example 40 million sporozoites were purified in one go within only 2-3 hr.

The first stage in developing an FFE-based protocol was to optimise and characterise the separation of sporozoites and ensure the hypothesised requirements were met. Importantly, the protocol needed to use whole mosquitoes instead of dissected salivary glands to reduce the time for extraction and enable the use of large quantities of mosquitoes. After the homogenisation of whole mosquitoes, the sample was filtered to remove large objects that would affect charge-based separation by disrupting FFE buffer laminar flow. After optimisation, FFE separated ~80% of sporozoites in one fraction in a highly reproducible manner that was independent of both sporozoite and originating mosquito dose. However, it was anticipated that the sample may also require density gradient centrifugation prior to FFE separation. The well characterised Accudenz gradient[156] was used for this over other methods such as percoll[142] as it required only a 20 min spin and had previously been shown to have no effect on sporozoite viability (assessed by *in vivo* and *in vitro* infections)[156].

The data also demonstrated that culture of sporozoites in HepG2 using only 0.5% P/S was associated with considerable bacterial growth, which was only controlled by >1% P/S for 48 hr. However, our lab has found that elevated levels of P/S reduces hepatocyte invasions (Carly Bliss DPhil Thesis, 2017). Furthermore, *P. falciparum* cultures can take at least seven days to complete the infection cycle making control of bacterial growth more challenging. The addition of dissected sporozoites was also associated with considerable morphological cell stress but no apparent bacterial growth, indicating that other mosquito associated contaminants such as protein may be responsible.

Sporozoite purity from mosquito contaminants was assessed at both a protein and bacterial level. MAF was the most effective method at separating sporozoites from mosquito-associated protein. Leading to almost undetectable levels of protein by silver stain which detects a minimum of 0.25ng of protein. Manual dissection contained significantly more protein, comparable to MA levels. M only contained the highest total protein content. Protein contaminants in each FFE fraction was assessed by BCA which has a sensitivity of 5µg/mL and indicated that the peak sporozoite fraction migrated slightly ahead of the protein contaminants. However, the higher the originating mosquito dose injected the greater the overlap. If using dissected salivary glands as the sporozoite source a similar trend is seen. Immunoblotting of each separation stage against parasite CSP from infected mosquitoes highlighted two phenomenon's. First that there was a reduction in total CSP following each step, indicating that there is a loss of sporozoites at each stage. Secondly, steps prior to FFE separation contained CSP fragments as detected by blotting with the anti-CSP antibody (3D11[269]) which binds to the central repeats within CSP[270].

Some of these additional bands may be non-specific antibody binding, which has been documented previously, however these were mostly at a lower molecular weight[269] to the bands seen here. The majority of these small fractions are likely degradation products which were removed by FFE. A dot blot of all FFE fractions showed that CSP had a longer tail in the FFE fractions than the sporozoites supporting this hypothesis. It also showed the effective separation of the highly abundant mosquito actin from the sporozoites.

CSP is expressed on the surface of sporozoites and during hepatocyte infection it becomes proteolytically cleaved, triggered by HSPG's on the hepatocyte surface and is therefore dependent on hepatocyte contact[192,271]. Genetically modified sporozoites which express the cleaved form invade more hepatocytes *in vitro*[169]. The 3D11 antibody is able to bind both cleaved and uncleaved CSP which have sizes of approximately 45 and 55kDa respectively[271] Following MAF purification two clear bands were seen with the same size by 3D11 blotting, which may be the cleaved and uncleaved forms. Interestingly if this is the case the ratio of uncleaved:cleaved was 1:1.76 and 1:7.30 for dissected and MAF purified sporozoites (assessed by densitometry) respectively. This would indicate that MAF purified sporozoites have 4.1 times more cleaved CSP on their surface, and could therefore be another factor contributing to improved infectivity seen with FFE.

Previous sporozoite proteomics analyses have suffered from poor sporozoite yields and purity which has made it difficult to identify parasite specific peptides compared to the large number of mosquito associated hits[181-183]. Mass spectrometry analysis of each stage of purification showed that only the MAF stage was able to detect a significant hit for a parasite protein, CSP. Suggesting this method would be highly suitable for such proteomic analyses. Finally, visual inspection of the peak sporozoite MAF also showed a significant reduction in mosquito associated debris compared to dissection.

Kennedy and colleagues[156] showed that Accudenz-based density centrifugation of dissected sporozoites was able to significantly reduce bacterial load using LB-Agar. Similarly, this thesis showed that DA reduced bacterial contamination by 1.4 fold compared to dissected using blood-agar. However, using FFE instead of Accudenz (DF) was more effective, reducing bacterial load by 1.6 fold and when combined (DAF), no detectable bacterial growth was observed. When using M as the sporozoite source Accudenz failed to reduce bacterial load below standard dissection. MAF however reduced bacterial load by up to 1.6 and 1.3 fold for naïve and infected mosquitoes respectively.

These results indicate that if mosquitoes can be dissected quickly enough that DAF could be used to avoid the use of antibiotics. Therefore, the purification process was updated to include dissection as an optional starting material (Figure 3-22).

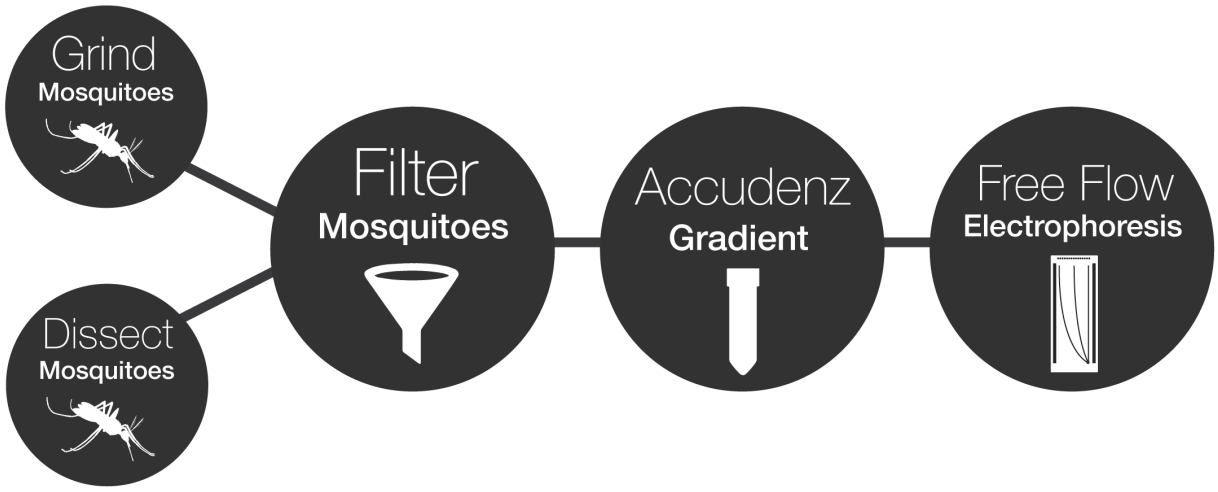

Figure 3-22 | Updated FFE-based sporozoite purification protocol.

Following characterisation of purity, the viability and infectiousness of the sporozoites was assessed by a combination of *in vitro* and *in vivo* assays. MAF purified sporozoites showed an increase in parasite HSP70 mRNA expression *in vitro*. Also *in vivo* challenged MAF purified sporozoites were shown to successful infect hepatocytes and develop using an *ex vivo* setup. Blood stage infection was also achieved *in vivo*, however significant drops in infectiousness was observed when compared to manually dissected sporozoites.

Sporozoites from MA and MAF were associated with a delay to patency in all experiments compared to dissected control, except in one experimental. This delay was not significant between the two treatments in any experiment. Indicating that MA and not the proceeding FFE was associated with a drop in infectiousness *in vivo*. However, DA was not associated with a significant delay compared to dissected, as similarly seen by the Kennedy study[156], but DAF was associated with a significant delay in all experiments. Furthermore, there was a significant difference in delay between DA and DAF treatments in one of the experiments. This would suggest both MASH origin and FFE treatment were together associated with a drop in sporozoite infectiousness.

Sporozoites develop in oocysts on the outside of the mosquito midgut and from here enter the haemolymph and travel to the salivary glands were they mature before entering a host during a blood feed[169]. At day 20 post infection of mosquitoes, a study by Coppi and colleagues[169] reported that 54% of sporozoites were found in salivary glands, 18% in the haemolymph and 28% midgut associated. Studies on the infectiousness of each of these sporozoite stages has shown that oocyst sporozoites are over 1000-fold less infectious than salivary gland sporzoites by i.v. challenge[272]. Therefore, this may offer a possible explanation for the decrease in *in vivo* infectiousness with MASH origin sporozoites as some of the injected sporozoites are poorly infective.

Some groups use motility as a measure of sporozoite infectiousness to hepatocytes[157,184,237], based on the observation that the poorly infective oocyst sporozoites show no or little gliding motility[157,184,272] and that the gliding phenotype increases through haemolymph sporozoites to salivary gland sporzoites which show greater than 80% gliding[157,184]. In support of this Vanderberg[272] found that haemolymph sporozoites showed considerable levels of *in vivo* infectivity which in some cases matched time to patency of salivary gland sporozoites, however it was observed that the EEF's showed lower development *in vivo*[272]. More recently, *in vitro* infections have shown that haemolymph and salivary gland sporozoites have the same level of hepatocyte infectivity but a reduction in traversal and in agreement with Vanderberg[272], the number of EEFs was reduced at 24 and 48 hr post infection[184]. The same group show however by RT-PCR that at 48 hr post infection *in vivo* EEF infections were the same between salivary gland and haemolymph sporozoites[184]. Vanderberg[272] reported a considerable variability of the *in vivo* infectivity of haemolymph sporozoites compared to salivary gland sporozoite infectivity, which may explain the inconsistency between these studies. Also, the different methods used to measure parasite infectivity likely contributes to variations between studies.

To address this point, the gliding motility of dissected and MAF sporozoites was assessed. In contradiction to previous groups[157,184] the gliding speed and percentage of gliding sporozoites did not vary between dissected and MAF. Unfortunately, the unpurified MASH material was too dirty to reliably characterise sporozoite motility. One possible explanation for this could be that mixing sporozoites from different stages changes motility. Alternatively, the homogenisation of total mosquitoes may release

materials that effect gliding motility, or the buffers used may affect motility. However, a study reported that sporozoite gliding was critical to navigating the skin but not infection of hepatocytes[238].

To further investigate the infectivity of different sporozoite sources, *in vivo* patency studies were conducted using MAF sporozoites from different MASH sources. This included removal of the abdomen to remove oocyst sporozoites (and some haemolymph sporozoites) and removal of the head (the salivary glands remained in the thorax). Only removal of the abdomen reduced the delay to 1% blood-stage parasitaemia to salivary gland dissected levels. Based on earlier work[272] this corroborates the hypothesis that oocyst sporozoites are the main contributor to the delay seen in *in vivo* patency with MASH origin sporozoites.

The challenge data in this thesis therefore suggests that the *in vivo* delay observed is possibly a combination of the FFE procedure and the MASH source. The MASH likely contributes poorly infective oocyst sporozoites, however the effect of haemolymph sporozoites on infectivity may be negligible[184]. Interestingly, the data presented here showed that delay in blood stage parasitaemia associated with MASH sporozoites and FFE purification were not cumulative. One possible explanation may be that sporozoites originating from salivary glands are more resilient to stress caused by FFE compared to haemolymph sporozoites. Supported by the fact that dissected homogenate purified treatments had a higher infection success rate compared to mash origin treatments. Furthermore, DA treatment was not consistently associated with a delay in all experiments. Interestingly, The variability in infectiousness of haemolymph sporozoites between studies noted by Vanderberg[272] supports the hypothesis of the lower resilience of haemolymph sporozoites. Vanderberg's suggestion that this may offer an explanation for the variability been studies may also explain why removal of abdomens prior to MAF remove delay but DAF does not. Haemolymph sporozoites are likely physiologically the same as salivary sporozoites during the development of EEF's, as a study by Sato and colleagues[184] showed that irradiated haemolymph sporozoites still gave sterile protection. Therefore, MAF purified sporozoites are still suitable sporozoites to use for investigating intervention methods.

Also, during all experiments sporozoites were extracted in Schneider's *Drosophila* medium due to its low bicarbonate levels with 1% FBS at 4^{o}C to promote viability and maintain infectivity as previously reported[142,187,236,237]. During the development of this protocol, Lupton and colleagues[237] confirmed the use of an insect medium as a suitable solution to purify sporozoites. When conducting *in vitro* infections sporozoites were re-suspended in 37^{o}C serum-free hepatocyte growth medium. A serum-free media was used to prevent the clumping of sporozoites as observed in Figure 3-5a. The higher bicarbonate within the hepatocyte medium and temperature increase was theorised, based on the literature, to promote hepatocyte infections. For example, an increase in temperature to 37^{o}C causes the release of microneme proteins which are associated with hepatocyte infection[187,203], whereas culture at room temperature reduced infections[187]. Sporozoites were then immediately added to culture, as co-incubation with

hepatocytes at 37°C prevents loss of *in vitro* infectivity for a period[187], a behaviour also seen *in vivo*[273,274]. The final consideration was the used of primary hepatocytes, which are known to provide higher infection rates[186,188].

Using this method with MAF sporozoites led to a significant increase in successful infections from 24 to 40 hr after invasion, measured by either RT-PCR or microscopy. Furthermore, infection rates of 8.37-10.37% were observed by flow cytometry. MA alone had no significant effect on the *in vitro* infection rate, as similarly seen using Accudenz in the Kennedy study[156]. Compared to dissected sporozoites, MAF sporozoites were shown to be associated with a considerable drop in mosquito origin protein and bacterial contaminants. MA sporozoites were associated with similar levels of protein contaminants to dissected sporozoites but greater bacterial contamination. This would suggest that reduction in mosquito protein could be a major contributor to the increased *in vitro* infections observed here. Using DAF instead of MAF sporozoites may increase *in vitro* EEF numbers further by excluding haemolymph sporozoites which are shown to develop less EEF's[184]. Further experiments will need to be done to investigate this as well as to confirm full EEF development occurs *in vitro* with MAF/DAF purified sporozoites.

During the final stages of this project a report by Billman and colleagues[275] corroborated the purity-based hypothesis, showing that dissected sporozoites without purification by Accudenz density centrifugation caused a reduction in pre-primed sporozoite (boost) specific CD8 T-cell responses. High levels of mosquito contaminants could also cause innate upregulation *in vivo* which may mask the effects of vaccination studies. Further work could investigate the effect of FFE-based purification on *in vivo* malaria immune responses which this thesis shows achieves greater purity than Accudenz alone which was used in the Billman study. The data in this chapter also demonstrates that FFE allows the challenge of animals with large doses of sporozoites.

Combining FFE-based purification with the microfluidic liver model could potentially increase infection rates further, and provide a complete workflow for assessing or identifying liver-stage intervention strategies. For example, the MAF protocol is highly appealing for immunopeptidomics to identify parasite specific peptides presented by MHC molecules on the surface of infected on hepatocytes. Currently the MAF-based purification protocol is being applied to immunopeptidomics with Dr Paulo Bettencourt in the Jenner Institute, Oxford. The microfluidic liver could also allow for *in vitro* CD8 killing assays.

Finally, the ability to obtain large quantities of pure sporozoites makes the ability to cryopreserve them highly attractive, as it can reduce variably by freezing multiple batches from one preparation. It also avoids the need to infect mosquitoes and wait 21 days for sporozoite development. A set of eight different buffers with two different freezing rates were chosen which identified 50% FBS with a freezing rate of -37°C/min as the only method to produce *in vivo* infections. However, to achieve a similar patency to freshly dissected sporozoites the dose had to be 100 times greater, indicating that

much more work is needed. In 2017 the John Adams group published comprehensive work on a method using CryoStor CS2 solution (Stem Cell Technologies) for cryopreserving sporozoites, providing promising results[276].

In conclusion, the work presented here shows the development of a new protocol for purification of sporozoites, which provides higher purity sporozoites compared to dissected and is associated with an increase in *in vitro* hepatocyte infections. However full EEF development in hepatocytes needs to be confirmed to enable studies looking at full schizont development. This purification method highlights mosquito associated contaminants probably as a major determinant of infectivity. Furthermore, the procedure allows purification of much higher numbers of sporozoites in a short period which has been shown to improve viability. This method is therefore very promising as a means to improve current *in vitro* studies helping to solve one of the major problems within the preerythrocytic malaria field and will hopefully translate to the identification of many new intervention candidates. It is also a promising approach to single cell omics studies requiring large amounts of highly pure sporozoites.

4 Physiological Host - Interactions of *Wolbachia* on the Malaria Vector *Anopheles gambiae*

4.1 Introduction

The bacteria *Wolbachia* are probably one of the most widespread endosymbionts in the world[68,69], infecting arthropods and filarial nematodes[67]. In arthropods the bacterium is spread by vertical transmission from mother to offspring[67]. Fundamental evolutionary biology dictates that vertical transmission by infection of the female germline selects mutualism to aid survival of the symbiont which depends on the host for replication and survival[67]. However, unexpectedly *Wolbachia* detrimentally manipulates the reproduction of arthropods to enhance its transmission[277], which may explain the high global prevalence.

The type of reproductive manipulation varies between *Wolbachia* strains and hosts, however all work by increasing the number of infected females[67]. In the field of human mosquito-borne diseases, cytoplasmic incompatibility (CI) is the most relevant form of reproductive manipulation[75,79,278]. In CI, infection of the male germline renders the sperm inviable unless the male mates with an infected female carrying the same strain, 'rescuing' the sperm[279]. Infected females however can mate with both infected and uninfected males, therefore female infection is a selective advantage (Figure 1-5)[279]. This also means that *Wolbachia* can have other virulent effects on the host without such a selective disadvantage, for example lifespan reduction[75]. However, beneficial effects have also been reported, some with minimal or no reproductive manipulation. For example, *Wolbachia* provides vitamin B for *Cimex lectularius*[280]. Additionally, vertically transmitted symbionts are predicted in the context of co-host infection of horizontally transmitted pathogens to evolve to protect the host from these pathogens[281-283], providing another host fitness advantage which may promote *Wolbachia* host virulence.

As such, *Wolbachia* is associated with host protection against many insect pathogens[70-72]. Of particular relevance is protection against human pathogens including dengue,

chikungunya[70], zika[71] and *Plasmodium*[72,73]. Pathogen inhibitory phenotypes of these infections are in non-native mosquito trans-infections.

Wolbachia-based interventions against malaria have focused on two *Wolbachia* strains, *w*AlbB and *w*MelPop[72,73,284,285]. *w*AlbB originates from *Aedes albopictus*[286] and *w*MelPop originates from *Drosophila melanogaster*[287]. The key distinguishing factor between both strains is that *w*MelPop is a high replicating strain[75]. Both strains have been shown to reduce *P. falciparum* oocyst load[73]. The method by which *Wolbachia* mediates pathogen inhibition is not fully understood but is believed to be a combination of lifespan reduction (in *w*MelPop)[75], resource competition[70] and immune priming[72,73].

Gene expression studies between both strains in *An. gambiae* somatic infections and cell lines have shown variations in immune gene expression. For example, in Sua5B (*An. gambiae*) cell lines using a microarray the majority of immune cells were down regulated with *w*AlbB infection[286]. However, in MOS55 (*An. gambiae*) cells *w*MelPop infection caused an upregulation in the six immune genes investigated[72] of which five showed no change in expression levels in the *w*AlbB microarray, only DEF1 was upregulated in both papers. In somatic *An. gambiae* infections, *w*MelPop but not *w*AlbB initially caused a moderate increase in the expression of the 11 immune genes assays, however by day 10 post-infection both strains downregulated the majority of the 11 genes[73]. Though, both strains caused a robust reduction in *P. falciparum* oocyst levels[73], indicating in this experiment that immune priming may not play a protective role.

Competition for resources may also be a key method by which *Wolbachia* mediates pathogen inhibition[70]. This is important as mosquitoes carry very little nutrient storage[288] and therefore only during a blood feed are there considerable nutrients, and as malaria enters a mosquitoes in a blood meal the availability of these nutrients could be used by *Plasmodium* for its development. Normally these nutrients are needed by the fat body to produce the yolk proteins used for egg development[3,289,290]. Interestingly, somatic *Wolbachia* infection in *An. gambiae* is focused in the fat body[73], therefore it could prevent nutrient use by *Plasmodium* and instead ensure nutrient use for egg development which is required for *Wolbachia* transmission[67].

Finally, the high-replicating strain *w*MelPop is associated with reduced lifespan, which is enhanced by blood feeding[75,284]. The enhancement after blood feed could be due to a reduction in anti-oxidant gene expression[73,286]. Lifespan reduction is important as *Plasmodium* has a 14-21 day incubation period in the mosquito before it is infective to humans[169] therefore, reducing lifespan can reduce the chances of transmission.

Unfortunately, these studies were in somatic *An. gambiae* infections, as no vertical transmission has yet been established. Without CI, a *Wolbachia* intervention program against malaria cannot be considered. However, if achieved, the success of trials in *Aedes aegypti* targeted against dengue which show effective inhibition of DENV transmission by field *w*Mel-infected mosquitoes[66,77,78] indicate that it could be a highly effective intervention method. Infection of the female germline is crucial for maternal

transfer, however in somatic infections *Wolbachia* is primarily located in the fat body and haemocytes[73,291]. Suggesting that the pathogen inhibitor phenotype may be mediated via these two organs. A vertically transmitted *w*AlbB infection has been achieved in *Anopheles stephensi* which reduced *P. falciparum* oocyst loads[79] providing hope for *An. gambiae*. However, a better understanding of underlying mechanisms in *An. gambiae* may help to establish a stable infection of *An. gambiae* mosquitoes and to replicate or improve the pathogen inhibitory phenotype and provide other methods to target the malaria parasite.

All three of the theorised inhibitory phenotypes of *Wolbachia* can be linked hypothetically to the target of rapamycin (TOR) signalling axis, which has been shown to modulate lifespan, immune responses and nutrient release[3,289,290,292,293]. It could therefore be hypothesised that *Wolbachia* modifies the TOR axis to aid its survival within mosquitoes.

4.1.1 The TOR Axis

Responding to the changing environment is critical to the survival of any cell and the organism it resides in, enabling it to regulate its metabolism, maintenance, growth and immune defence[292,294-296], with likely many more undiscovered responses. It is therefore of no surprise that such a critical signalling pathway regulating this is conserved across eukaryotes, including mammals, insects and yeast[292,295,297]. The pathway in question is the TOR signalling cascade, which has at its centre the TOR protein, a phosphatidylinositol kinase-related kinase (PIKK), which forms two complexes, TOR complex (TORC) 1 and 2, and can be broadly categorised as modulating cell survival by controlling the 'when' and 'where' respectively[294,295]. TORC1 regulates the cellular level of anabolic/catabolic flux, by promoting activities such as protein synthesis, whereas TORC2 is a regulator of cytoskeletal organisation and cell survival[294,295].

These complexes are not fully understood however[298,299], and whilst TORC1 activities are much better characterised, TORC2's activities and cross-talk with TORC1 signalling is only recently being appreciated, which may eventually render the above framework an oversimplification. For example, until recently mammalian (m)TORC2's activity on protein kinase B (PKB/AKT), which signals to mTORC1, was highly controversial in the field[300-304]. Another consideration is that even though the pathways are well conserved there are some variations between organisms (for example yeast contains two TOR proteins[298]), and when working with species less well characterised such as the focus of this study, *An. gambiae* mosquitoes, some extrapolation is required. Table 4-1 shows the currently identified *An. gambiae* homologs of the key TOR signalling proteins predicted from mammalian and *D. melanogaster* genes.

Table 4-1 | Predicted *An. gambiae* TOR pathway homologs.

Name	VectorBase ID	Description	Predicted Ortholog (Ensembl)
*ag*TOR	AGAP007873	Target of rapamycin	Human, *Drosophila*
*ag*S6K	AGAP007333	P70-S6 kinase	Human, *Drosophila*
*ag*InR	AGAP012424	Insulin Receptor	--
*ag*ILP3	AGAP010602	Insulin-like peptide 3 precursor	--
*ag*ILP4	AGAP010601	Insulin-like peptide 4 precursor	--
*ag*TSC2	AGAP011123	Tuberous sclerosis complex 2	Human, *Drosophila*
*ag*S17	AGAP004887	40S ribosomal protein S17	Human, *Drosophila*
*ag*RAPTOR	AGAP010035	Regulatory-associated protein of mTOR	Human, *Drosophila*
*ag*mLST8	AGAP001036	Mammalian lethal with SEC18 protein 8	Human, *Drosophila*
*ag*Deptor	Not Found	DEP domain-containing mTOR-interacting protein	Human
*ag*Lobe	Not Found	--	Human (PRAS40), *Drosophila*
*ag*mSIN1	AGAP008831	Stress-activated map kinase-interacting protein 1	Human, *Drosophila*
*ag*RICTOR	AGAP001035	Rapamycin-insensitive companion of mTOR	Human, *Drosophila*
*ag*PRR5	Not Found	Proline-rich protein 5	Human

Predicted homologs TOR to S17 are from Arsic *et al*[289] and the remainder identified using Ensembl and Flybase searches.

The TOR axis integrates signals from an assembly of sources; growth factors/endocrine, nutrient levels, energy levels and stress signals. TORC1 and 2 respond by modifying a multitude of cellular processes some of which have only recently been identified, including but likely not limited to actin cytoskeletal rearrangement, translation, transcription, cell survival, cell cycle, autophagy and metabolism (e.g. lipid metabolism, amino acid synthesis) (Figure 4-1)[292,294,295,305,306].

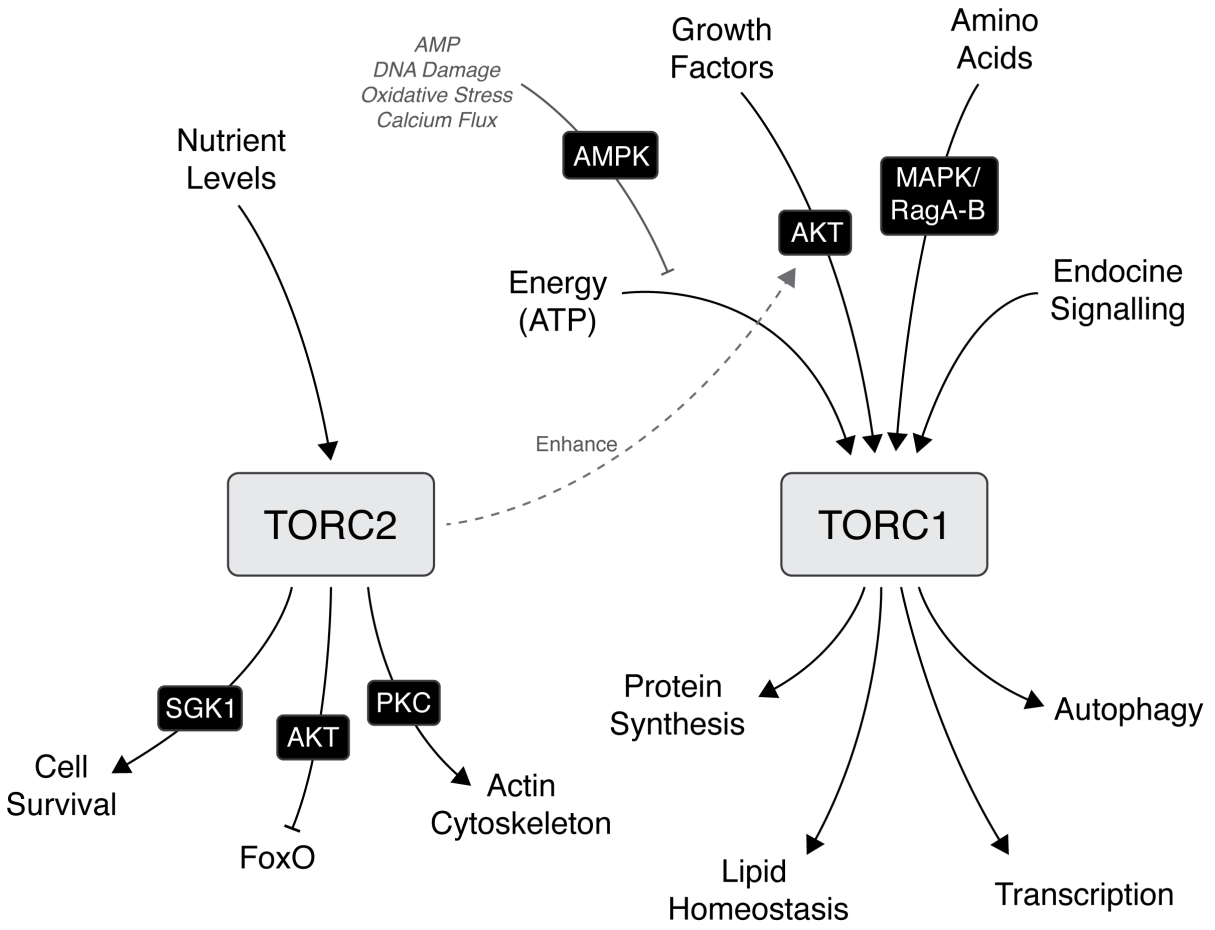

Figure 4-1 I TOR inputs and outputs. The inputs and outputs of the TORC1 and TORC2 complexes. Facilitating proteins are in black boxes. Refer to text for references.

The TOR protein was discovered in 1991[307] and since then both TOR complexes have been characterised in mammals and insects[295,308]. The TOR protein functions as a serine/threonine kinase which is located at the C-terminal[295,308]. However, multiple other proteins interact with TOR to form TORC1 and 2, through multiple other domains on TOR which include FAT, FATC, FKBP12-rapamycin binding (FRB) and HEAT domains.[295,308] The TOR protein has been identified in mosquitoes and contains a similar domain structure[309]. Table 4-2 shows the complex components in mammals and identified orthologs in *Drosophila*. See Figure 4-2 for a summary of the TOR signalling pathway.

Table 4-2 I Constituents of the TOR complexes in mammals and *Drosophila*.

Complex	*Drosophila*	Mammals
TORC1	RAPTOR	RAPTOR
	LST8	mLST8
	LOBE	PRAS40
	---	Deptor
TORC2	RICTOR	RICTOR
	SIN1	mSIN1
	LST8	mLST8
	---	Deptor
		PRR5/PRR5L

Orthologous proteins which complex with TOR in mammals and *Drosophila*[294,310].

4.1.2 TOR Axis Inputs - AKT

A critical input for TORC1 comes from the AKT axis, which promotes TORC1 activity[305]. AKT is one of many AGC kinases that play a role in the TOR axis, the others include S6 kinase (S6K), protein kinase C (PKC)[302] and mitogen-activated protein kinases (MAPK)[305]. AKT a serine/threonine kinase contains three important phosphorylation motifs (i) Turn Motif (TM; Threonine[450] Mammal/Thr484 *Drosophila*), (ii) A-loop (AL; Thr308 mammal) and (iii) Hydrophobic Motif (HM; Serine473 mammals) the role of which until recently was hotly debated[302]. These sites are conserved in *An. gambiae* and the TM experimentally shown in *Drosophila*[302] and *Aedes aygepti*[311]. Phosphorylation of this site during AKT translation prevents ubiquitination and destruction in mammals[302,312]. Initially, AKT is recruited to the membrane by phosphatidylinositol-3,4,5-triphosphate (PIP3) which is generated by the class I phosphatidylinositol 3-kinase (PI3K) following stimulation by a receptor tyrosine kinase (RTK)[305]. In *Drosophila*[313,314] and *Anopheles*[315] this RTK is the single insulin receptor (InR), which is stimulated by insulin-like peptides (ILP's) released in response to nutrients, of which five have been identified in *An. gambiae*[315]. In mosquitoes ILP release and InR stimulation could be due to nutrients from a blood meal[289,315].

Subsequently, AKT is activated by phosphoinositide-dependent kinase-1 (PDK1) on the AL motif[302] which is also recruited by PIP3 and enables the kinase to activate TORC1[295]. This is done by inhibiting the tuberous sclerosis complex (TSC) 1 and 2 complex which in-turn inhibits the TSC1/2 complex GTPase activating protein (GAP) activity allowing Rheb to activate TORC1 using its GTPase activity[294,316-318]. Although AL phosphorylation is crucial for AKT activity, HM phosphorylation increases AKT activity 4-fold[300,302,303,319,320]. HM phosphorylation has been shown to occur by TORC2, also in a nutrient-dependent manner[302]. Furthermore, TORC2 also controls TM

phosphorylation in a nutrient-independent manner[302], however there is conflicting data[320] showing that AKT does function without TORC2 indicating that the TM may not be as critical as thought[302,312]. Furthermore, TORC2 activity ablation does not appear to effect the TORC1 downstream effector activity, S6K[303,319,321], suggesting that there may be two functional states of AKT dependent on its phosphorylation state. In support of this, TORC1 inhibition in *Drosophila* ablates apoptosis mediated by forkhead box (FOXO) indicating TORC2 activated AKT may mediate its activities via FOXO[321].

4.1.3 TOR Axis Inputs - AMPK

Another critical TORC1 input is 5'-adenosine monophosphate-activated protein kinase (AMPK), which has traditionally been associated with responding to cellular energy levels in the form of 5'-adenosine monophosphate (AMP)[295,322]. Unlike AKT, AMPK inhibits TORC1 activity by enhancing TSC2 GAP activity, responding instead to energy depletion[295,322]. It has been hypothesised that AKT modulates AMPK energy response by maintaining high ATP levels, positively reinforcing TORC1 activation, indicating that cross-signalling occurs between both pathways[323,324]. A similar cross-over occurs via FOXO (only one FOXO in *Drosophila*[325]) which can be inhibited by AKT[320,326,327] preventing FOXO-mediated transcription of AMPK activators including Sestrin[328] and P53[295]. With the recent appreciation of TORC2 activity, evidence shows that AKT requires TORC2 phosphorylation on the HM motif (which is nutrient stimulated TORC2 activity), as well as PDK1 AL motif phosphorylation (which needs InR stimulation) to inhibit FOXO[302,320,326,327].

Conversely, signals associated with excess TORC1 activation including DNA damage, oxidative stress and calcium flux activates FOXO causing AMPK activation in a negative feedback loop[295]. For example, oxidative stress sensed through a c-Jun N-terminal kinase (JNK) elevates sestrin expression via FOXO[329]. P53 activated by DNA damage directly activates AMPK[330] and conversion of PIP3 to PIP2 inhibiting AKT activation via PTEN[330,331]. AMPK has also been shown to directly activate FOXO in humans[332] and *Caenorhabditis elegans*[333]. In addition, the growth factor stimulated Ras-Raf-MEK1/2-Erk1/2 MAPK cascade has been shown to directly inhibit TSC1/2 activity in mammals[334,335].

4.1.4 TOR Axis Inputs – Amino Acids

Amino acid levels are another critical input onto TORC1, however the signalling pathways are debated and likely need further research. In *Drosophila* and mammals the MAPK, MAP4K3, stimulated by amino acids activates TORC1 independent of TSC1/2 and appears to be dominant to the TSC1/2-TORC1 pathway, suggesting that TSC1/2 inactivation also requires MAP4K3 activity to activate TORC1[335,336]. However, Gao and colleagues[337] show that inactivating TSC1/2 does not need amino acid stimulation for TORC1 activity. Furthermore, it is shown that activating Rheb without amino acids simulates TORC1 activity[338,339]. Leucine has been revealed to cause an increase in insulin levels supporting a TSC1/2 method of regulating TORC1[340]. Some evidence suggests that the class III PI3K VPS34 may act upstream based on amino acid levels[341,342], however this has been excluded in *Drosophila*[343]. It is likely that there are

multiple methods of amino acid sensing. Additionally the Ras GTPases RAG1/2 have been shown to sense amino acids and to recruit Rheb on lysosomal membranes where TORC1 is located[344,345], therefore enhancing TORC1 activation. Finally InR-AKT-TORC1 signalling can regulate amino acid uptake by increasing amino acid transporter uptake[324,346,347].

4.1.5 TOR Axis Inputs - Others

The WNT, HIPPO and Notch signalling pathways have also been show to modulate the TOR pathway[306,336]. Other modulating factors on TOCR1 activity in *Drosophila* have also been identified, such as translationally controlled tumour protein (TCTP) and proteasomal degradation[294].

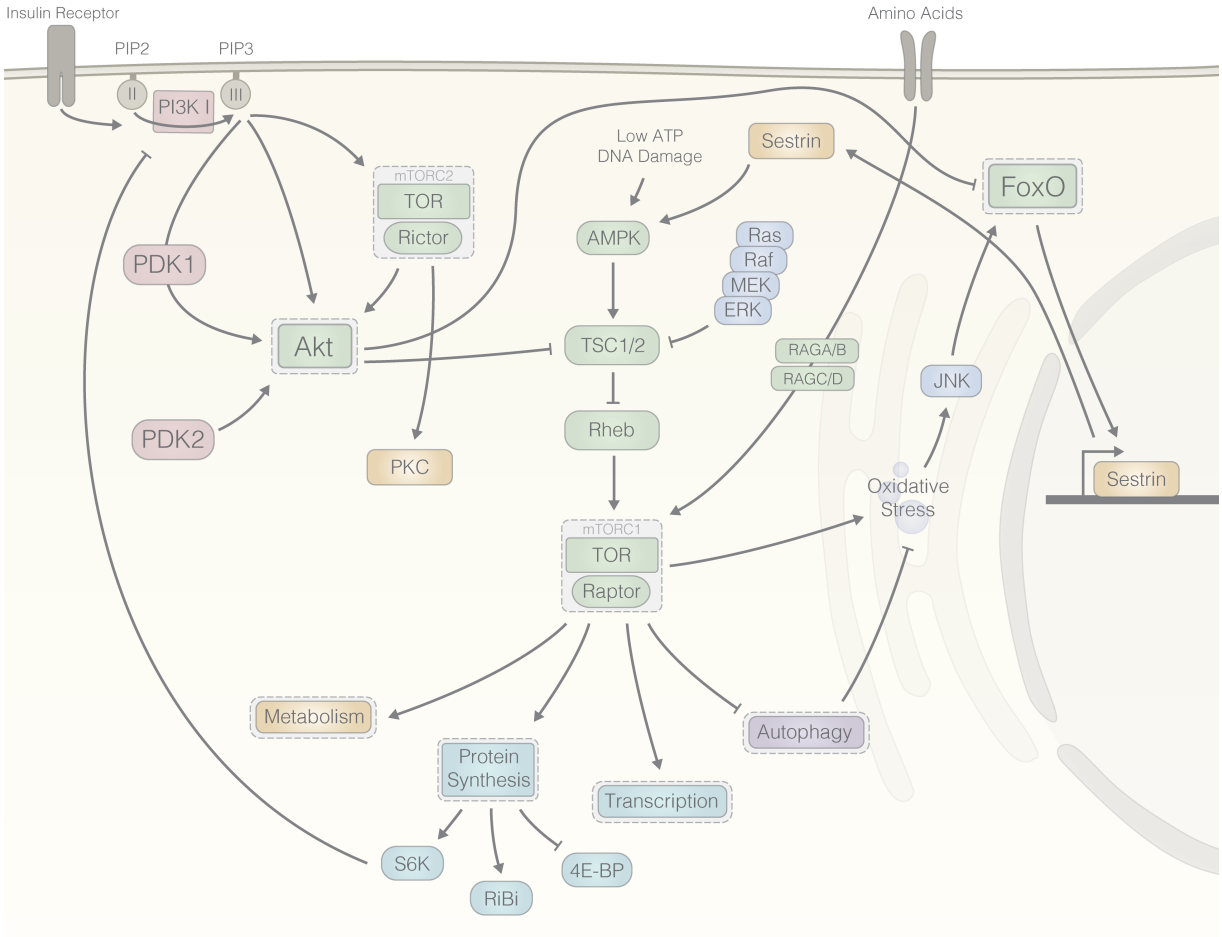

Figure 4-2 l mTOR axis signalling pathway. The TOR signalling cascade consist InR-AKT-TORC1 and AMPK-TORC1 pathways. Refer to references in main text.

4.1.6 TOR Axis Outputs – TORC2

All of these inputs combine to elicit a cellular response either through TORC1 or 2. In addition to TORC2's previously described effect on AKT activity, actin cytoskeletal rearrangement has historically been a canonical activity associated with TORC2. As such RNAi KD's of TORC2 in mammals have shown actin abnormalities[319,348] and furthermore, nutrients have been shown to affect the actin cytoskeleton suggesting the

effect of TORC2 is likely nutrient stimulated[349,350]. Actin rearrangement is theorised to occur via the activation of PKC, RhoA/Rac1 and Paxillin[294,336]. However, more recent research using TORC2 complex knock-outs (KO's)[326] and drug based inhibition[300] have failed to show a change in cytoskeletal integrity. TORC2 has however been shown in mammals and *C. elegans* to activate serine/threonine protein kinase 1 (SGK1) which is important for cell survival regulating processes such as sodium transport[294,351-353], and furthermore the inhibition of FOXO via AKT activation also prevents the expression of pro-apoptotic proteins[336].

4.1.7 TOR Axis Outputs – TORC1

Translation upregulation is a critical activity of TORC1 and is believed to be mediated by both increased ribosomal biogenesis and an increase in overall mRNA translation[306]. Characterised mediators of this are the downstream TORC1 effectors, S6K and eIF4-E binding protein (4E-BP) which are found in mammals and *Drosophila*[294,354,355]. S6K, which is also phosphorylated by PDK1, phosphorylates the S6 protein of the 40s ribosomal subunit[295] and has been indicated as increasing translation of 5' terminal oligopyrimidine tract (5'-TOP) mRNAs which encode proteins involved in translational machinery[354]. However, later evidence suggested that this was not the case as S6K inactivation did not affect 5'-TOP translation[356,357], even though the upstream TORC1 has been shown to promote 5'-TOP translation[306,358]. Nonetheless, more recently SK6 KO in mice did reduce the translation of 78% of ribosome biogenesis (RiBi) genes[359], although total protein synthesis did not appear to be effected[359,360], but may be explained by cell compensation inhibiting 4E-BP[359].

4E-BP is a translational inhibitor by binding translational initiation factor 4E (IF4E) in mammals and *Drosophila*[355]. Upon TORC1 phosphorylation 4E-BP is released from IF4E enabling mRNA cap binding, initiation of translation[354,361] and was recently shown by ribosome profiling to be the protein modulating 5'-TOP translation as well as mRNA containing pyrimidine rich translational elements (PRTE)[358,362]. There is also some evidence that TORC2 modulates translation[306]. One of the most well characterised feedbacks in this pathways is the inhibition of the InR by S6K in mammals and *Drosophila*[363-367].

In *Drosophila* the MYC transcription factor has been shown to stimulate RiBi gene expression, and its transcription is regulated by the epidermal growth factor receptor (EGFR) via Ras and surprisingly TOR[368-370]. Transcriptional regulation of genes by TOR has more recently been appreciated and shown by transcriptional and metabolomic studies to particularly modulate expression of genes involved in biomolecule synthesis and metabolic pathways[371,372]. For example, starvation or TORC1 inhibition in humans and mice down-regulated anabolic processes such as lipid, nucleotide and protein synthesis[371]. Of interest, the profile of transcription varies depending on whether amino acids are removed or TORC1 is inhibited by the rapamycin drug supporting the idea that multiple factors control the TOR pathway and some nutrient based signalling occurs independent of TOR[371].

Furthermore, the use of TSC1/2 KO's identified mTORC1 as controlling the expression of genes in lipid synthesis, pentose phosphate pathway and glycolysis[372]. This is likely achieved by TOR-mediated activation of transcription factors or regulatory proteins. In 2010 a study identified sterol regulatory element-binding protein (SREBP) 1 and 2 transcription factors, which are activated by S6K, as increasing the expression of pentose phosphate pathway (PPP) and lipogenic enzymes[372]. A similar effect may be mediated by mTORC2[373]. Also the prefoldin, unconventional prefoldin RPB5 (URI), has been shown to interact with RNA polymerases and modulate gene expression under the control of TOR[374].

The outcome of TORC1 controlled transcription is metabolic regulation of membranes and energy storage by lipid synthesis and of nucleotides synthesis via the PPP[306,372]. For example, TOR inhibition in *Drosophila* caused increased loss of body fat[327]. These above effects are important in modulating cell **growth**, which is seen as distinct from cell **proliferation**[307]. Cell growth can be visually appreciated by increases in cell size[375].

Early belief was that TOR controlled cell cycle progression, however it later came to be appreciated that lack of TOR mediated cell **growth** indirectly inhibited cell cycle progression (**proliferation**) in the seminal work of Nik Barbet[307,376]. Later studies further supported this, showing that the translational control proteins, S6K and 4E-BP1, controlled G1 phase progression in mammals[377] and in *Drosophila*[378]. In the G1 stage cells prepare for the DNA proliferation that occurs in the proceeding S phase[379]. Although, the TOR axis may still have some direct role on cell cycle progression as suggested by some groups[377,380-382].

The final characterised process that TORC1 modulates is autophagy. Macroautophagy, henceforth referred to as autophagy, is a highly conserved process[383-385] which involves the engulfment of cytoplasmic material in double membrane autophagosome vesicles and its degradation in lysosomes[386]. Originally thought of as a starvation defence mechanism, its intricate role in the immune response regulation and pathogen defence is more recently being appreciated[387,388] (Figure 4-3). Paradoxically, this means that many intracellular pathogens adapt to and modulate autophagy for their own benefit[389,390]. Broadly speaking the autophagic interactions with pathogens can be (i) true xenophagy; the direct uptake of cytoplasmic pathogens into forming autophagosomes via interaction with adapter proteins (sequestosome 1-like receptors; SLRs) and pathogen recognition receptors (PRRs), (ii) non-specific upregulation of autophagy by pathogen-associated molecular patterns (PAMPs), and (iii) LC3-associated phagocytosis (LAP); the recruitment of autophagy machinery to vesicles and fusion with lysosomes[387,388]. In mammals, due to autophagy's vast interaction with the immune signalling pathways it can modulate many aspects such as inflammation and antigen presentation[387,388]. *Salmonella* for example, releases the deubiquitinase SseL via its type III secretion system (T3SS) to reduce autophagy[391]. Interestingly, *Salmonella* has also been shown to use the host autophagy to repair damage to the single membrane vacuole that it resides in, preventing release into the cytoplasm and destruction by the autophagy machinery[392]. Like-wise the *Shigella* effector IcsB inhibits

LC3 recruitment to *Shigella* vacuoles[393]. Therefore, *Wolbachia* may modulate autophagy to aid its survival, possibly via its T4SS[394].

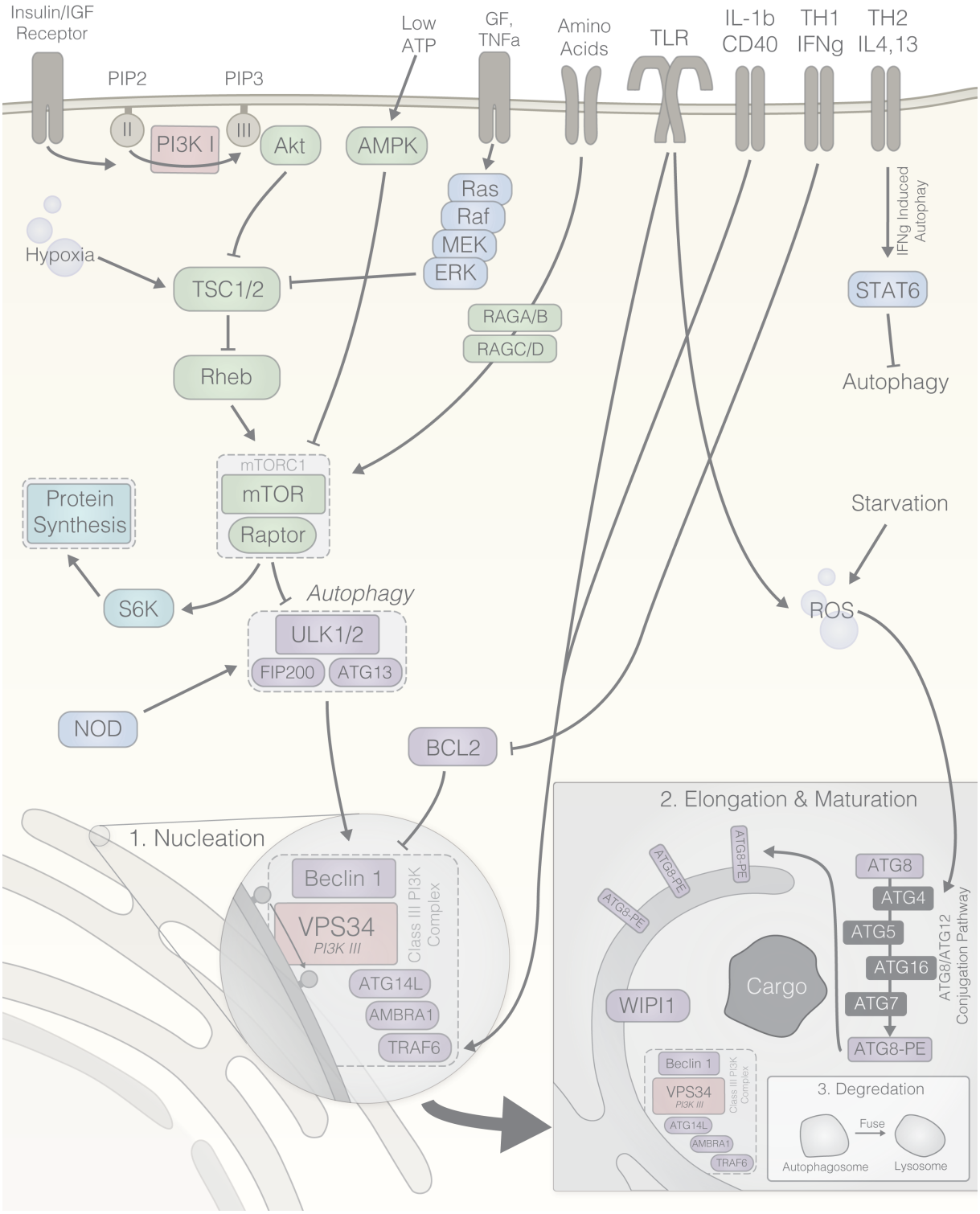

Figure 4-3 I The autophagy pathway with a mammalian focus. Broadly the initiators of autophagy can be nutrient related or immune related[388]. Nutrient signals can be from growth factors which signal via class I PI3K's[385], or AMP/ATP levels via AMPK signalling. Many of these converge upon mTOR leading to the regulation of autophagy initiation via the ULK1/ATG1 complex[386-388]. Additionally immune signals from PRR's such as NOD's and cytokines have been shown to modify autophagy[387,388,395]. Downstream

of these signals the ULK complex including the PI3K class III VSP34 translocates to the ER and via cooperation with other proteins leads to the formation of a phagophore; an isolation membrane[387,388,396]. Following this, the phagophore membrane is extended via two ubiquitin-like conjugation systems that lead to the addition of phosphatidylethanolamine (PE) to the C-terminus of ATG8-like proteins allowing it to insert into the membrane of the expanding phagophore[386-388]. This protein works in concert with others to close the phagophore, forming an autophagosome around the cytoplasmic material[386-388]. In some cases of xenophagy, adapter proteins (SLRs) recruit pathogens[388]. Unlike in yeast and *Drosophila* which has only ATG8, in mammals there are many paralogs, such as LC3A/B/C and GABARAP[388]. Following this maturation the double membrane vesicle fuses with lysosomes[388]. Figure created using information from[306,383,386-388,397-403].

4.1.8 Mosquito TOR Implications

In anautogenous mosquitoes an important nutrient source is blood obtained through blood feeding, which is a requirement for egg development and is associated with increased TOR signalling in ovaries of *Anopheles*[289] and the fat body of *Aedes*[3]. Furthermore, many mosquito-borne pathogens are obtained from a host blood feed[5,12,13]. This therefore suggests that TOR may play an important and relevant role during mosquito infection due to its temporal upregulation.

Taking a blood meal is associated with both distention[289] of the abdomen and upregulation of TOR in the midgut which increases the translation of early trypsin enzymes[290] and protein breakdown with subsequent release of amino acids into the haemolymph[404]. This TOR activation is itself likely amino acid mediated, but also appears to require an additional signal, possibly stomach distention, for the trypsin translation to occur[290,404]. This is supported by the fact that saline feeding in *An. gambiae* increased ovary TOR activity, however albumin with amino acids gave a much stronger activation[289].

In *Aedes*, proceeding a blood meal the neurosecretory cells in the brain[311,405,406] and possibly midgut cells[315], likely stimulated by stomach distension[289] and other blood constituents, release ILPs and ovarian ecdysteroidogenic hormone I (OEH-I) which act on the ovaries, likely by InR signalling, to cause the synthesis of ecdysteroid hormones from ovaries[311,315,407]. In *Anopheles,* five ILPs have been identified[315]. In *Aedes,* InR expression has been shown to increase after a blood meal[408], and insulin stimulates the production of ecdysteroids[408,409]. Furthermore, ILP-InR-TOR activation is important for the expression of late stage trypsin to further digest the blood bolus which is enhanced by amino acid presence[407]. This is associated with an elevation in TOR activation and likely due to the neuropeptides[3].

The ecdysteroid hormones act on the fat body to cause the production of yolk proteins using the blood derived amino acids which are needed by the developing eggs, a process called vitellogenesis[3,410]. However, expression of these genes has been shown to need priming of the fat body with amino acids from the blood mediated via TOR activation; evidence suggests both InR-dependent and -independent signalling is involved[3,411,412].

Figure 4-4a shows a hypothetical TOR response from mosquitoes to a blood meal. It can be hypothesised that InR and TOR signalling therefore acts as a switch stimulated by a blood feed to change a mosquitoes state from reproductive arrest to active (Figure 4-4b). The consequences of this for both the mosquito and blood-borne pathogen development can be appreciated by modifying TOR in insects. For example, inhibition of parts of the InR and TOR cascade in *Drosophila* extends lifespan[292,413]. Also in *An. gambiae,* eggs fail to develop with just an amino acid food bolus, likely requiring other factors such as lipids found within a blood bolus[289]. This my possibly be as *Anopheles* mosquitoes have lower energy reserves and need the fat and other metabolites for vitellogenesis[288]. Furthermore, removal of the head post-blood feed prevents egg development and is restored by ILP injection in *Aedes*, indicating a critical role of InR/TOR signalling in the ovaries for egg development[405,407,414]. Work in *Drosophila* also suggests that TOR signalling increases hunger and food consumption[415] and may therefore regulate mosquito blood feeding.

This evidence suggests that the TOR axis in the aspect of nutrient availability may exert considerable effect over *Plasmodium* development which enters the mosquito via a blood meal. Likewise, TOR-axis manipulation by either *Plasmodium* or for example *Wolbachia* could promote or inhibit *Plasmodium* development respectively. In support of this, *Anopheles* mosquitoes fed on infected blood supplemented with insulin showed increased parasite yield[416], suggesting TOR activation is beneficial to the parasite. *Plasmodium* also causes apoptosis in ovaries of *Anopheles* mosquitoes[417] which increases the amount of blood-based nutrients as the follicles become resorbed and in theory increases the amount of nutrients available for parasite development[315].

Furthermore, *Plasmodium* development requires approximately 14-21 days to develop in the mosquito[169], therefore anything which modifies the mosquitoes lifespan or increases its survival such as modifying feeding behaviour could affect transmission. Both these features have been shown above to be associated with TOR-axis activity. Finally, TOR may also modify innate immune genes[418].

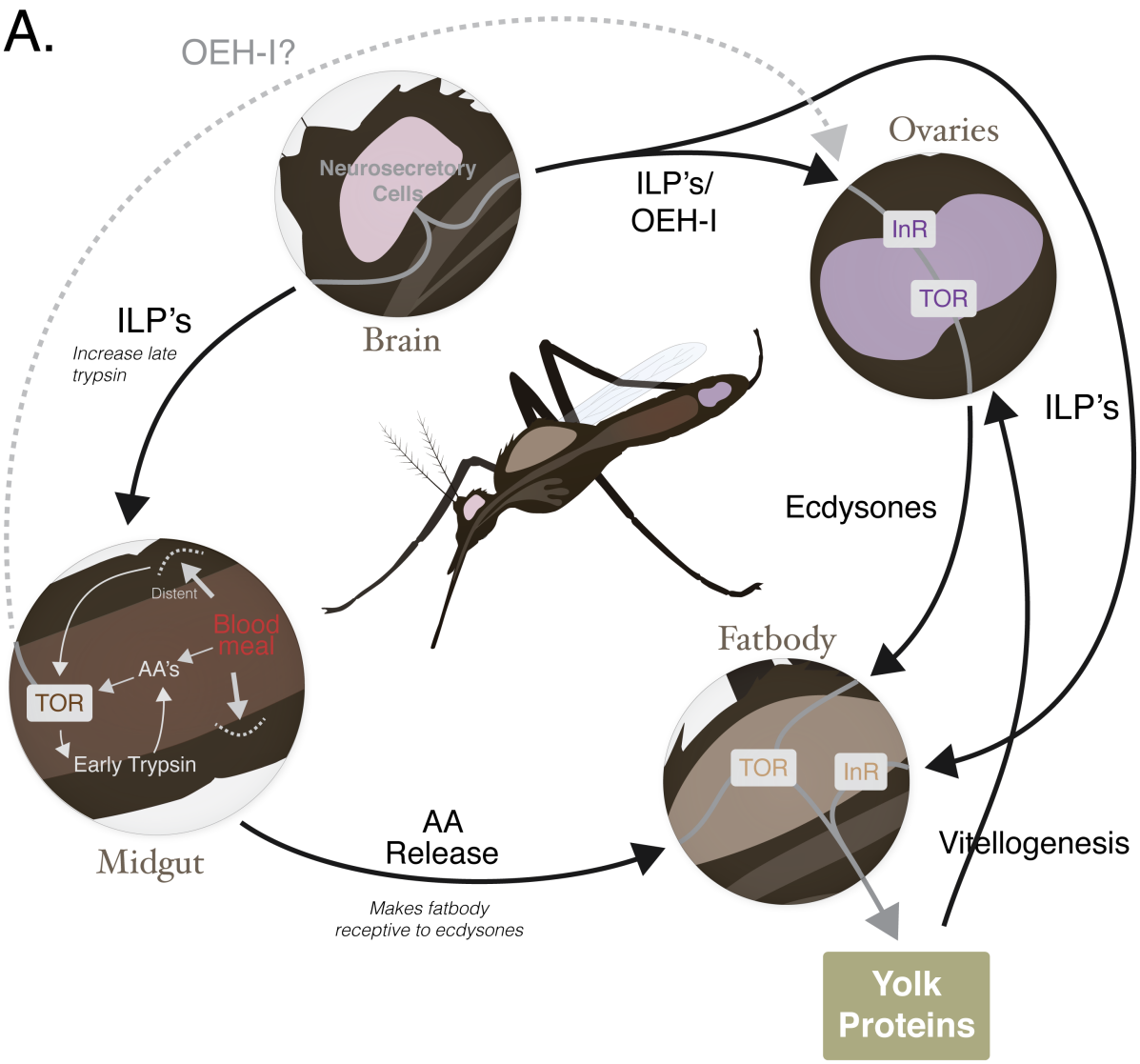

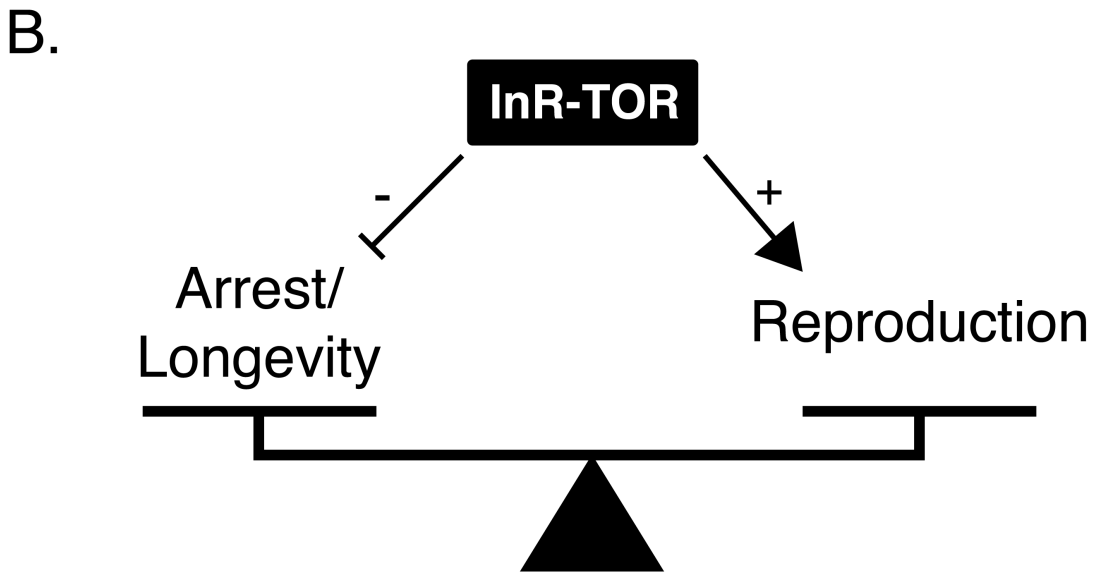

Figure 4-4 I Mosquito InR-TOR-axis signalling. A) Theorised bloodmeal InR-TOR signalling in mosquitoes. Refer to main text for references. B) The reproductive balance in mosquitoes between longevity and reproduction.

Wolbachia infection has been associated with decreased lifespan[75], nutrient competition[70], and immune priming[72,73] and is found in ovaries and the fat body[73,419]. Therefore, the TOR-axis was investigated in *An. gambiae* cell lines to try and elucidate a possible mechanism for *Wolbachia's* anti-malarial phenotype and possibly to help investigate the difficulty with establishing a stable infection in *An. gambiae* mosquitoes.

4.2.1 Assessing Wolbachia TOR-axis Modulation

The effect of stable *Wolbachia* infection with *w*MelPop and *w*AlbB on the TOR axis in *An. gambiae* 4a3b cells lines was initially investigated. TORC1 activity was assessed by measuring the activation level of the direct downstream S6 ribosomal protein[295]. Activated S6 was measured by western blotting against activated S6 phosphorylated at serine positions 235/236 (S6p) using a monoclonal antibody (Figure 4-5a). Densitometry showed that *w*MelPop caused a significant increase in activated S6 indicative of elevated TORC1 activity. In contrast, *w*AlbB infection was not associated with a change in TORC1 activity from basal (Figure 4-5b), possibly as *w*MelPop is a high replicating strain[287], confirmed by electron-micrographs of *Wolbachia* infected 4a3b cells which show a much higher infection load in *w*MelPop infected 4a3b cells (Figure 4-5c). Unfortunately, due to a lack of suitable antibodies specific to *An. gambiae*, TOR activity could only be assessed using one antibody (S6p). A list of all the failed antibodies tested in 4a3b cells can be found in supplemental Table 8-1. Therefore, the accuracy of the S6p antibody as a measure of TORC1 activity was confirmed by treating cells with TOR inhibiting drugs (Figure 4-6) to show a reduction in S6p levels.

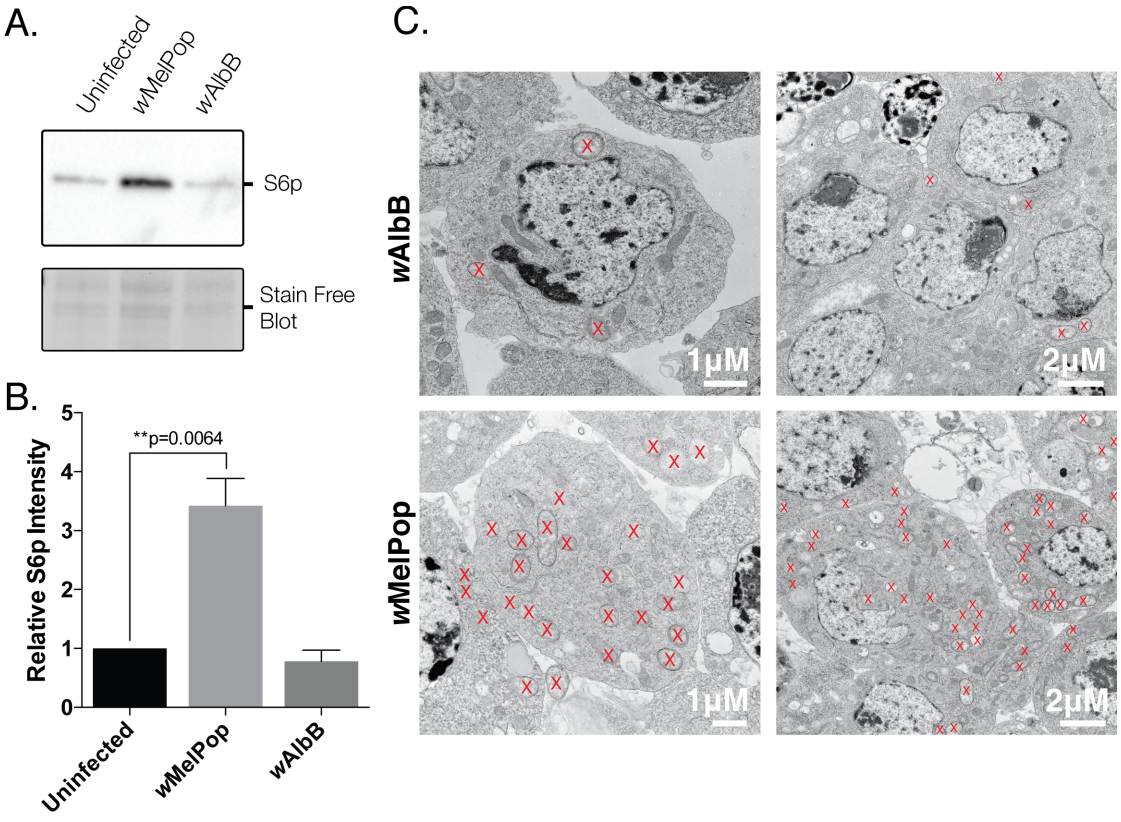

Figure 4-5 I Infection with *w*MelPop increases basal mTORC1 activity. A) Reducing SDS-PAGE western blot against phosphorylated S6 ribosomal protein (S6p; size 39kDa), representative of five replicates. Equal loading was assessed by BioRad Stain-Free™ blot. B) Mean relative S6p band intensity compared to uninfected from five replicates. C) Electron-micrographs of *w*AlbB and *w*MelPop infected 4a3b cells. *Wolbachia* marked with red X. Error bars represented SEM, groups compared using a two-tailed paired t-test.

4.2.2 Investigating the Effect of Drug-based TOR Modulation on Wolbachia

To investigate whether upregulation of TORC1 activity is a possible survival strategy during infection of 4a3b cells, TOR complexes were directly inhibited using pharmacological methods. Rapamycin is a commonly used drug for the allosteric specific inhibition of the TORC1 complex[300,420], believed to function by using its association with FK506-binding protein 12 (FKBP12) in the TORC1 complex[421] to prevent substrates from binding correctly to the catalytic domain[421,422]. The effectiveness of 5µM rapamycin on uninfected 4a3b cells was tested over a 96 hr period showing effective inhibition of TORC1 activity measured by undetectable S6p levels (Figure 4-6a). *w*MelPop infected cells treated with 5µM rapamycin for 48 hr showed a significant drop in *w*MelPop *Wolbachia* density relative to control, with effective inhibition confirmed by S6p blot (Figure 4-6b-c). Rapamycin had no effect on *w*AlbB levels (Figure 4-6b).

Rapamycin mainly acts upon TORC1 in mammals and yeast[421,423], but has been suggested to have a limited effect on mTORC2 over long-periods of use in mammals[301,424]. Rapamycin has also been shown to have only a limited effect on mTORC1 mediated 4E-BP activation in mammals[420]. As such PP242, a second-generation mTOR kinase domain inhibitor that has a stronger TORC1 inhibition with effective IF-4E inhibition and TORC2 inhibition was also used [300,425]. To avoid cellular toxicity two doses (300, 800nM) of PP242 were tested for 3, 10 and 48 hr by measuring S6p levels (Figure 4-6d) and 300nM selected for treatment of *w*MelPop cells for 48 hr. This caused a significant drop in *w*MelPop density relative to control (Figure 4-6e).

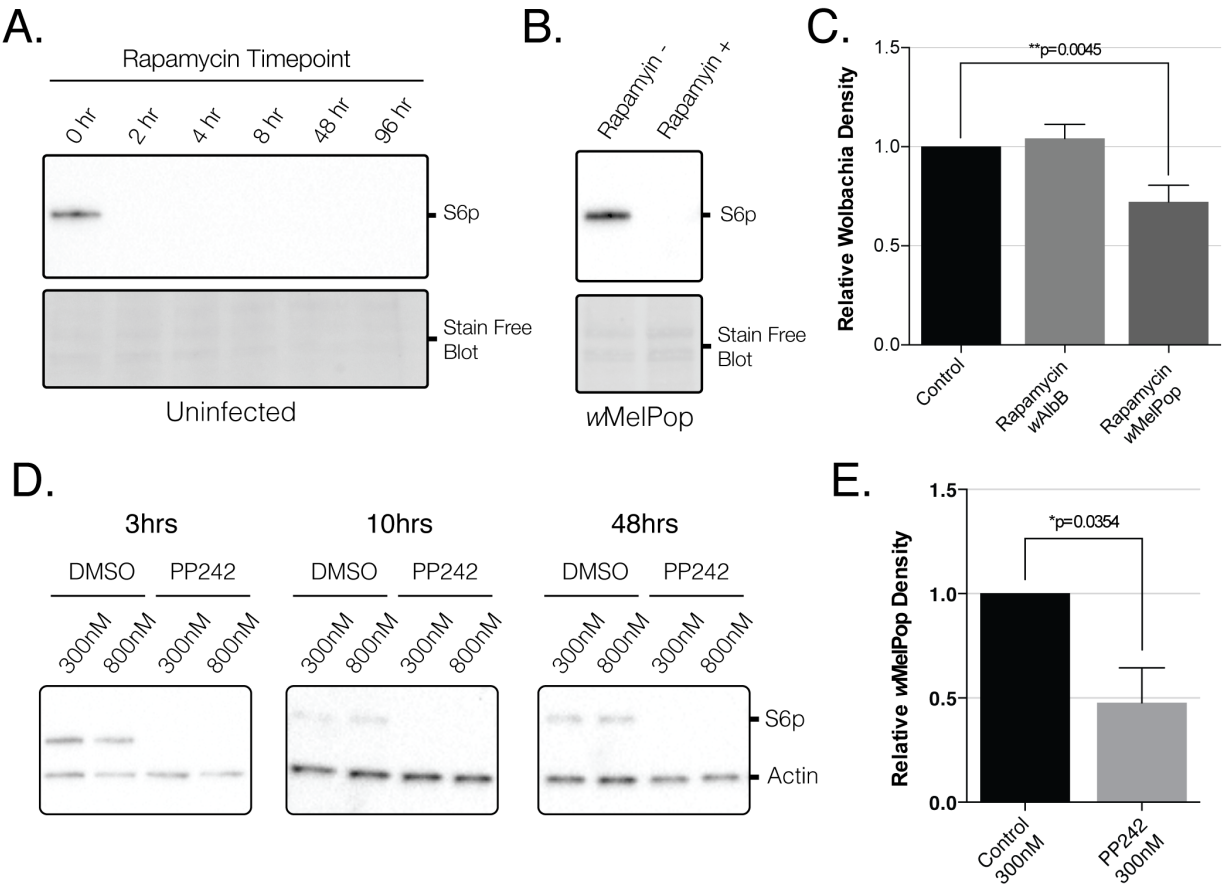

Figure 4-6 I Treatment of 4a3b cells with TOR inhibitors. A) Denaturing SDS-PAGE western blot against S6p in uninfected 4a3b cells treated with 5µM rapamycin collected at time-points up to 96 hr. 0 hr sample is DMSO vehicle control. B) Denaturing SDS-PAGE western blot against S6p in *w*MelPop infected 4a3b cells treated with 5µM rapamycin after 48 hr. C) Mean *Wolbachia* density of *w*AlbB and *w*MelPop infected 4a3b cells after treatment with 5µM rapamycin for 48 hr. Four Replicates. D) Denaturing SDS-PAGE western blot against S6p in uninfected 4a3b cells treated with 300nM or 800nM PP242 collected at time-points up to 96 hr. E) Mean *Wolbachia* density of *w*MelPop infected 4a3b cells after treatment with 300nM PP242 for 48 hr. Three Replicates. All drugs controls are DMSO vehicle controls. Bar charts show mean with error bars representing SEM. Groups compared to control by two-tailed paired t-test.

4.2.3 Investigating the Effect of RNAi-based TOR Modulation on Wolbachia

To further confirm the drug-based results, RNAi was used to knock-down (KD) targets to decrease TORC1 and TORC2 complex activity. This involved the synthesis of a 185 bp double stranded RNA (dsRNA) fragment against TOR (dsTOR), preventing TORC1 and 2 complexes forming. *w*MelPop and *w*AlbB infected 4a3b cells were treated with dsRNA using Lipofectamine for seven days, KD efficiency and *Wolbachia* density was measured by absolute RT-PCR and western blot against S6p (Figure 4-7a-b). Seven days was chosen as this time-point gave the most effective KD (data not shown). dsTOR gave a mean KD of 58%±5.4 which lead to a significant mean drop of 12%±4.1 in *w*MelPop density, whereas *w*AlbB infection showed a non-significant decline (Figure 4-7c)

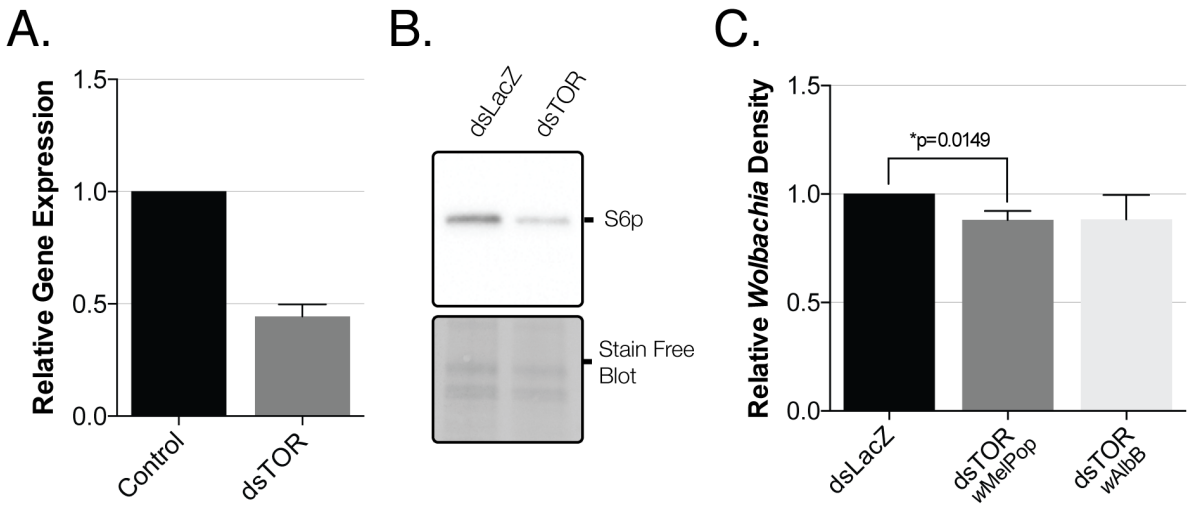

Figure 4-7 I Treatment of 4a3b cells with dsRNA. A) Relative RT-PCR quantification of TOR gene expression compared to S7 housekeeping gene, seven days after dsRNA treatment. Four Replicates. B) Reducing SDS-PAGE western blot of 4a3b wMelPop cells treated with dsLacZ or dsTOR. Equal loading assessed by BioRad Strain-Free blot. C) *w*MelPop and *w*AlbB density compared to dsLacZ control after seven days dsRNA treatment. *w*MelPop treatment is three replicates, *w*AlbB is four replicates. Bar plots represent means and error bars represent SEM. Treatments compared to dsLacZ or siScrambled controls using two-tailed paired t-test.

4.2.4 Investigating the Effect of Starvation-based TOR Modulation on Wolbachia

TORC1 activity is regulated by available extracellular nutrients levels via multiple pathways including the ILP stimulated PI3K/AKT starvation axis and the amino acid sensing RagA/B and MAPK cascades[335,344,345] (Figure 4-8a). *w*MelPop infected 4a3b cells were starved of amino acids for seven days in FBS-reduced Schneider's Medium (2% FBS, 5% P/S) which caused a significant 14%±4 reduction in *Wolbachia* density (Figure 4-8b). The starvation was not associated with morphological cell stress and similar to work by Denis Voronin[426] it had minimal effect on cell growth .

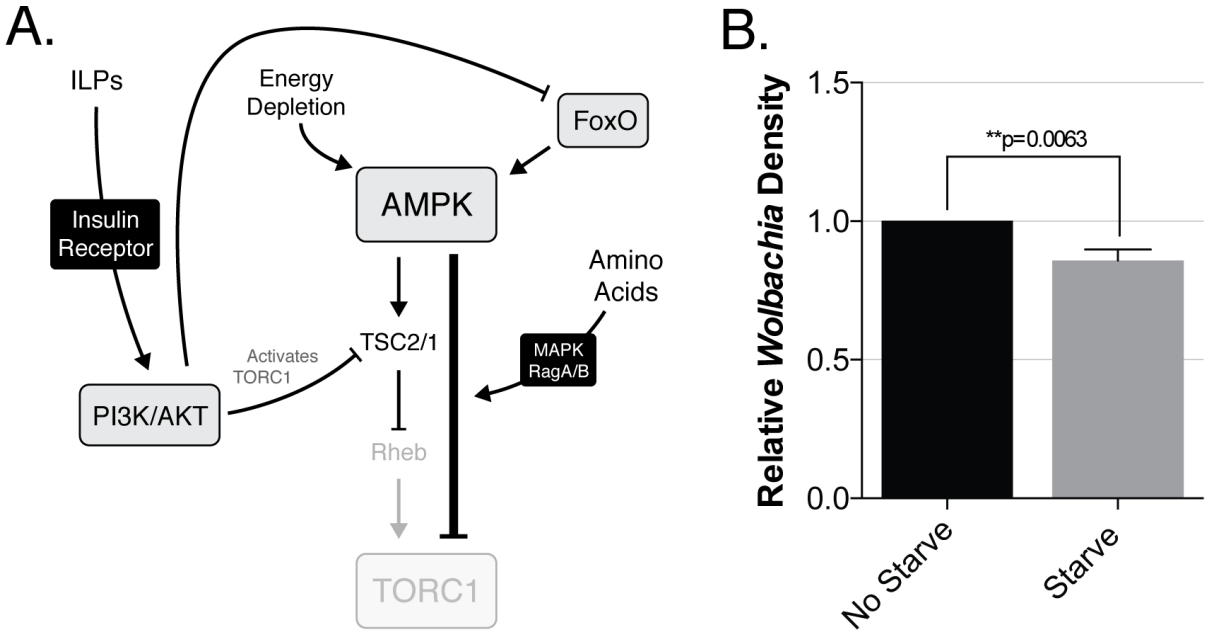

Figure 4-8 l Starvation of 4a3b cells to modulate TOR activity. A) Diagrammatic representation of the starvation PI3K/AKT axis. B) *w*MelPop density after seven day starvation compared to control. Three replicates. Bars represent sample mean, error bars SEM. Groups compared using two-tailed paired t-test.

4.2.5 Physiological Consequences of Constitutive mTOR Activation - Proliferation

TORC1 is critical in modulating many host cell anabolic processes including indirectly affecting cell proliferation by modulating the availability of host cell building blocks[376-378]. Therefore, the effect of *Wolbachia* infection on cell cycle progression was investigated using a cell tracing assay. *Wolbachia* infected 4a3b cells were stained using a fluorescent dye which bound cellular amines and the mean decline in fluorescent intensity, as the cells divided asynchronously, was measured every 24 hr. Cells were allowed to proliferate before cell contact inhibition occurred. Non-proliferating controls were maintained on either AICAR, an AMPK activator or PP242, a TOR inhibitor. Fluorescent intensity histograms showed a declining shift in intensity after three days in both uninfected and *w*MelPop infected cells when compared to 0 hr staining. However, this shift was lower in AICAR treated cells (Figure 4-9a). This decline was significant in all treatments over 72 hr (Figure 4-9b; ordinary two-way ANOVA $p<0.0001$).

Proliferation between uninfected and *w*MelPop infected cells was assessed by comparing both the normalised mean fluorescence and shift in mean fluorescence after 72 hr (Figure 4-9c, d). *w*MelPop infected cells had a significantly higher mean fluorescence and showed a significantly lower shift than uninfected cells (Figure 4-9c-d) indicating lower proliferation in *w*MelPop infected 4a3b cells. A significant difference in mean fluorescence shift with and without *w*MelPop infection was also observed following treatment with AICAR and PP242 but became non-significant when considering mean fluorescence at 72 hr.

Using non-linear exponential growth curve fitting, doubling time was estimated for groups (Figure 4-9e). Uninfected and *w*MelPop infected cells had doubling times of -0.5516 and -0.5256 (rate of fluorescence drop per day) respectively. As expected AICAR treated cells had much lower doubling time compared to untreated (uninfected AICAR: -2.636; *w*MelPop AICAR: -3.162). However, PP242 showed similar doubling times to untreated (uninfected PP242: -0.5203; *w*MelPop PP242: -0.4879). Only AICAR caused a significant increase in mean fluorescence compared to untreated (AICAR vs. uninfected $p<0.0001$ or *w*MelPop $p<0.0001$, two-tailed t-test not shown on graph) and not PP242 (PP242 vs. uninfected $p=0.8973$ or *w*MelPop $p<0.4869$ two-tailed t-test not shown on graph) (Figure 4-9c-d). This showed that PP242 had a limited effect on decreasing cell proliferation.

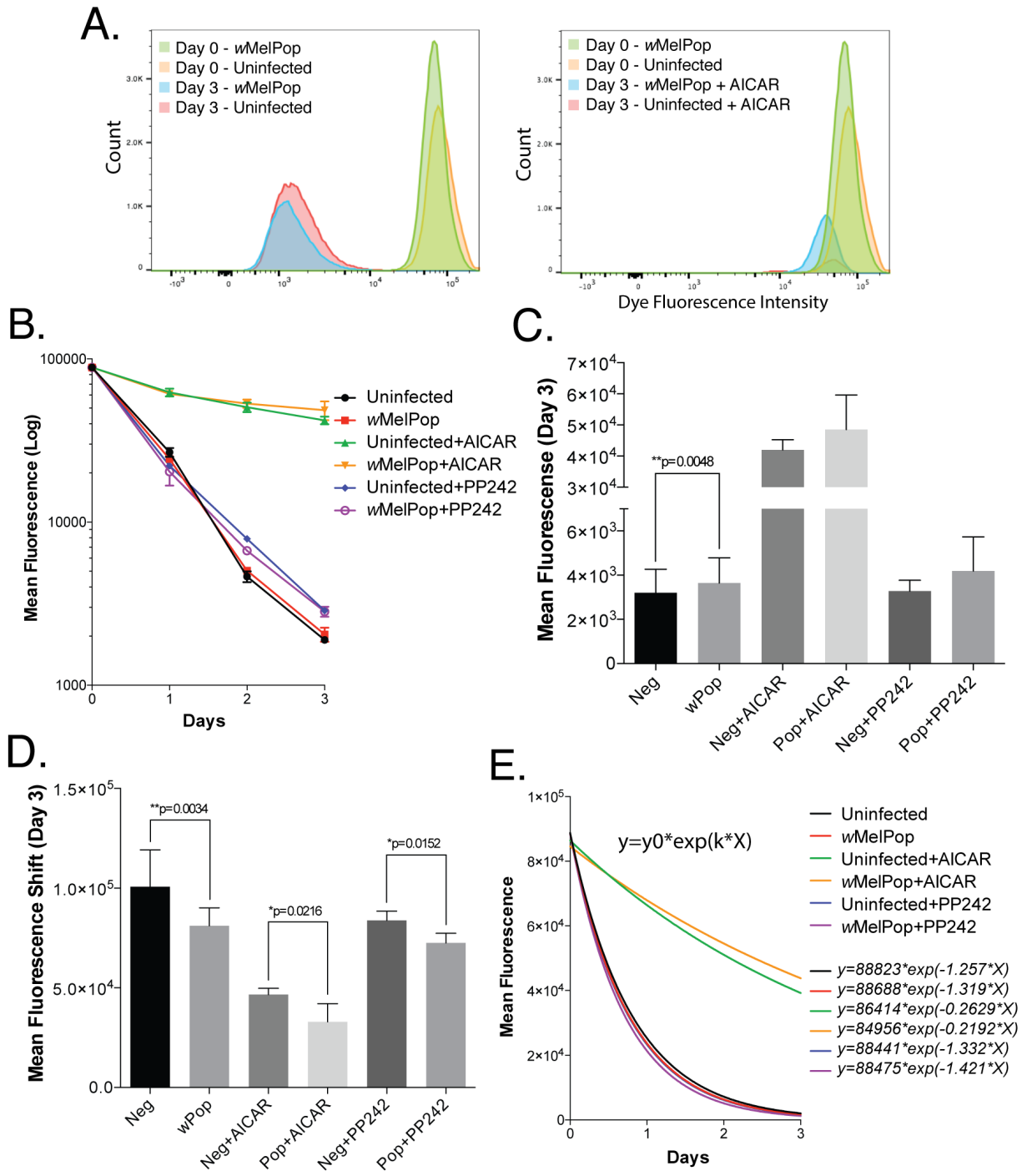

Figure 4-9 I Cell proliferation in *Wolbachia* infected cells. A) Histogram of day zero and day three fluorescent channel. B) Log10 mean fluorescent intensity of cells normalised to day zero readings every 24 hr. Two replicates. C) Mean fluorescent intensity of cells normalised to day zero readings 72 hr after staining. Two-tailed paired t-test used to compare uninfected vs. *w*MelPop infected for each treatment. Seven experimental replicates. D) Mean shift in fluorescent intensity of cells normalised to day zero readings 72 hr after staining. Two-tailed paired t-test used to compare uninfected vs. *w*MelPop infected for each treatment. Seven experimental replicates. E) Non-linear exponential curve fitting of mean fluorescent intensity samples in (B). Errors bars represent 95% CI. 100,000 cells collected for each sample.

4.2.6 Physiological Consequences of Constitutive TOR Activation – Autophagy

Autophagy is a critical downstream effector of TOR activity. TORC1 activation leads to inhibition of autophagy, however oxidative stress caused by TOR's anabolic activities leads to inhibition of TOR activity and elevated autophagy to remove oxidants and damaged organelles[388]. Autophagy has been shown to play a role in *Wolbachia* infection of *Aedes* mosquitoes cells[426].

Autophagy levels are commonly assessed by measuring the level of ATG8 lipidation that occurs[427]. It is important when measuring ATG8 lipidation that it is compared to the same treatment but with lysosomal degradation inhibited so that the level of ATG8-II breakdown can be assessed, this is known as autophagic flux (AF)[427]. To investigate autophagy in 4a3b cells a polyclonal antibody raised against *Drosophila* ATG8 (*dr*ATG8), kindly donated by Barth and colleagues[147], was tested and worked successfully. In response to this, a large enough quantity of polyclonal antibody was raised using the orthologous peptide sequence from *An. gambiae* (*ag*ATG8) which shared 87% homology with the *D. melanogaster* peptide (Figure 4-10a) and gave the same bands; a non-lipidated ATG8 (ATG-I; ~18 kDa) and lipidated ATG8 (ATG8-II; ~14 kDa).

Autophagic flux in uninfected, *w*MelPop and *w*AlbB infected cells was assessed by reducing SDS-PAGE western blot using the agATG8 polyclonal antibody. Samples were treated with E64D and Pepstatin A (AF+) to prevent ATG8-II breakdown, or vehicle control (AF-) 2 hr prior to protein extraction of cells. Blots (Figure 4-10b) and densitometry analysis (Figure 4-10c) showed a significant decrease in AF+ *w*MelPop and *w*AlbB infected ATG8-II levels not seen in uninfected cells, indicative of reduced autophagy.

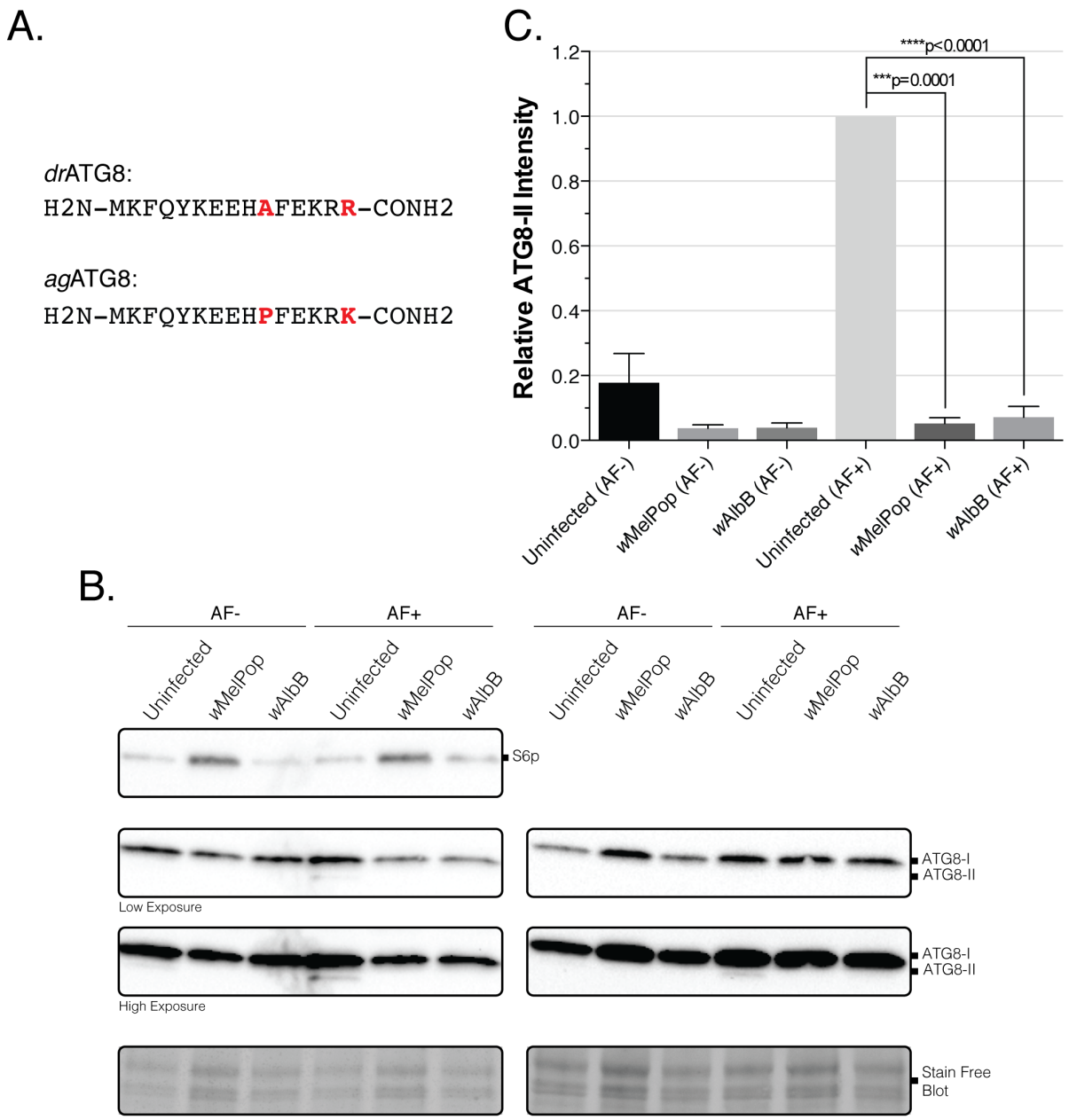

Figure 4-10 I Measuring autophagy in 4a3b cell using ATG8 antibody. A) Comparison of peptide sequences used to raise polyclonal anti-ATG8 antibodies against *Drosophila* and *Anopheles*. Non-matching residues marked in red. B) Reducing SDS-PAGE western blot using anti-*ag*ATG8 and anti-S6p from infected and uninfected 4a3b cells with and without AF. Samples normalised using StainFree Blot. Example of two replicates shown side-by-side. C) Mean relative ATG8-II densitometry of infected and uninfected samples with and without AF. All samples normalised to uninfected AF+ samples. Mean of four replicates, error bars show SEM. Groups compared to the respective uninfected AF treatment using two-tailed paired t-test.

Autophagic flux was also assessed using ImageStream fluorescent cytometry, which measured the number of ATG8 foci in cells and the level of localisation of these bright foci with lysosomes in AF+ cells as per the previously described protocol[161] (Figure 4-11a-b). The level of localisation was measured on the ImageStream using the BDS

value; a measure of localisation strength between two fluorophores. The mean BDS of samples positive for ATG8 and lysosomes with a BDS value greater than two was used to assess autophagic flux. ImageStream analysis showed that *w*MelPop caused a significant decrease in localisation indicative of decrease autophagy (Figure 4-11c). *w*AlbB showed a non-significant decrease in mean BDS compared to uninfected.

Double membrane vesicles are a common feature of ATG8-coated autophagosomes[427], therefore electron microscopy was used to assess intracellular *Wolbachia* associated host membranes (Figure 4-11d). This showed *Wolbachia* to be surrounded by a single membrane vesicle. During this investigation however, novel ring shaped structures were observed surrounding *Wolbachia* (Figure 4-11e), which resembled Septin rings (See figure 1a from reference[428]). Septin rings have been show to play an important role in host defence against intracellular bacteria, which is partially mediated by interaction with the autophagy machinery[390,429]. To confirm this hypothesis anti-Septin antibodies were tested by western blot but none specific for *An. gambiae* could be found. Therefore, further investigations of this will be necessary in the future to elucidate these unknown rings.

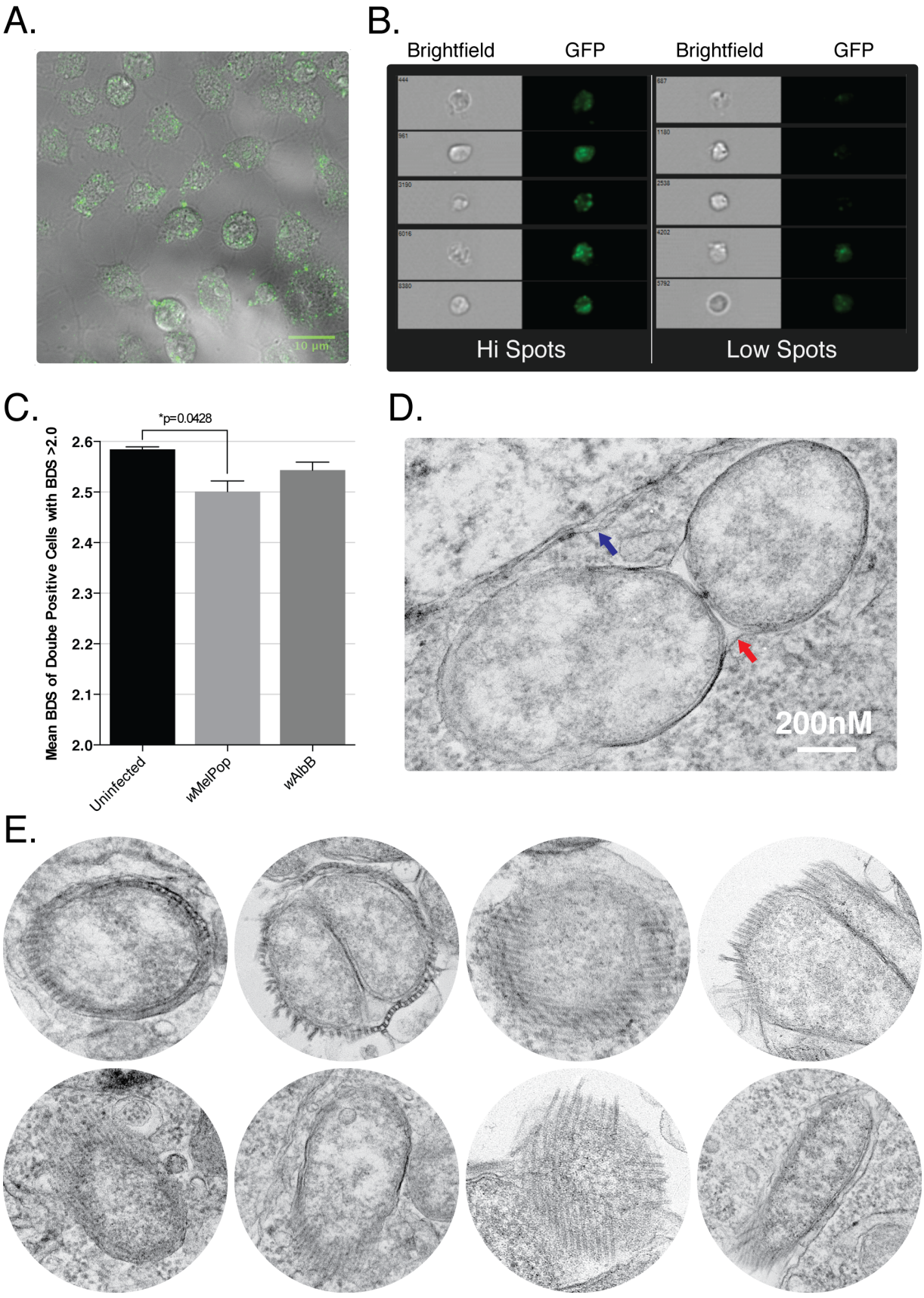

Figure 4-11 I Quantifying *Wolbachia* by ImageStream and vesicular location. A) Confocal fluorescent microscopy of anti-*ag*ATG8 foci using 488 secondary antibody in 4a3b cells overlaid with brightfield. B) Example of ImageStream quantification of ATG8 spots (high; left, low; right) with brightfield

channel. C) Quantification of mean BDS of double positive cells with BDS >2.0. Mean of three replicates (100,000 cells). Error bars represent SEM. Groups compared using two-tailed paired t-test. D) Electron micrograph of two *Wolbachia* in a single membrane vesicle. Single membrane around dividing *Wolbachia* indicated by red arrow. Double membrane of host cell indicated by blue arrow. E) Multiple electron micrographs of ring-like structures surrounding *w*MelPop.

Autophagy is critical to the removal of old damaged mitochondria (mitophagy)[388]. In order to investigate this in *Wolbachia*-infected cells the structural integrity of mitochondrial was assessed by EM, which showed a build-up of dysfunctional mitochondrial in *w*MelPop infected cells. Characterised by disorganised cristae and abnormal shapes which could be a significant cause of host cell oxidative stress, and their lack of clearance suggests a defect in their autophagic removal (Figure 4-12a).

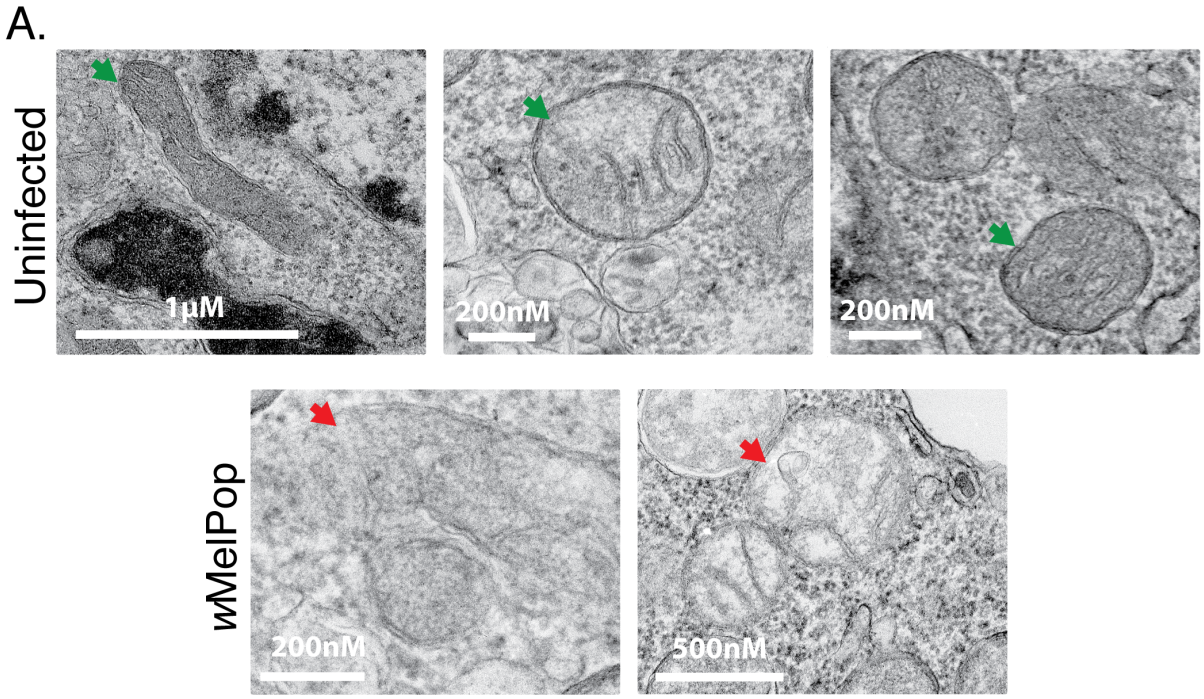

Figure 4-12 I 4a3b mitochondria integrity. A) EM images of mitochondrial from uninfected and *w*MelPop infected 4a3b cells. Green arrows indicate normal mitochondria, red arrows indicate abnormal mitochondria.

4.2.7 Modifying Autophagy Levels

To assess the effect of autophagy on *Wolbachia* infection a combination of autophagy manipulating drugs and RNAi KD's were used to modify autophagy levels in 4a3b cells. Three autophagy modulating drugs, 3-methyladenine (3MA), papamycin (RAPA) and wortmannin (WORT) were used on *w*MelPop and *w*AlbB 4a3b cells. The effect of each drug was confirmed by assessing ATG8 autophagic flux using western blot (Figure 4-13a).

RAPA is a TOR inhibitor therefore enhances autophagy[427]. Treatment with 5µM RAPA caused a detectable increase in ATG8-II with AF treatment confirming elevated

autophagy. 3MA is a PI3K class III inhibitor which inhibits early autophagy, however It is known to promote autophagy by PI3K class I inhibition when treated for extended periods (>4 hr) due to loss of its strong PI3K class III inhibition[430]. The same phenomenon was seen in 4a3b cells treated for 48 hr, which showed an increase in ATG8-II after AF treatment and a reduction in S6p levels. Furthermore, when 4a3b cells were treated for multiple time-points autophagy levels only become elevated after 4 hr treatment, a phenomenon observed previously by You-Tong Wu and colleagues[430] (Figure 4-13b).

Cells were also treated with 5μM WORT, which was not shown to have the same effects as 3MA[430]. WORT treatment was not associated with an increase in autophagic flux. Its inhibitory effect on autophagy was confirmed by the reduction in S6p indicating reduced TORC1 activity which under normal physiological conditions would be associated with elevated autophagy.

The effect of these drugs on *Wolbachia* density was assessed in *w*MelPop and *w*AlbB infected 4a3b cells (Figure 4-13c). 3MA caused a significant drop in *w*MelPop and *w*AlbB 4a3b cells. RAPA also caused a significant drop, but only in *w*MelPop infection. WORT failed to cause a change in *Wolbachia* levels, which correlated with a low level of autophagy flux seen on ATG8 blots (Figure 4-13a).

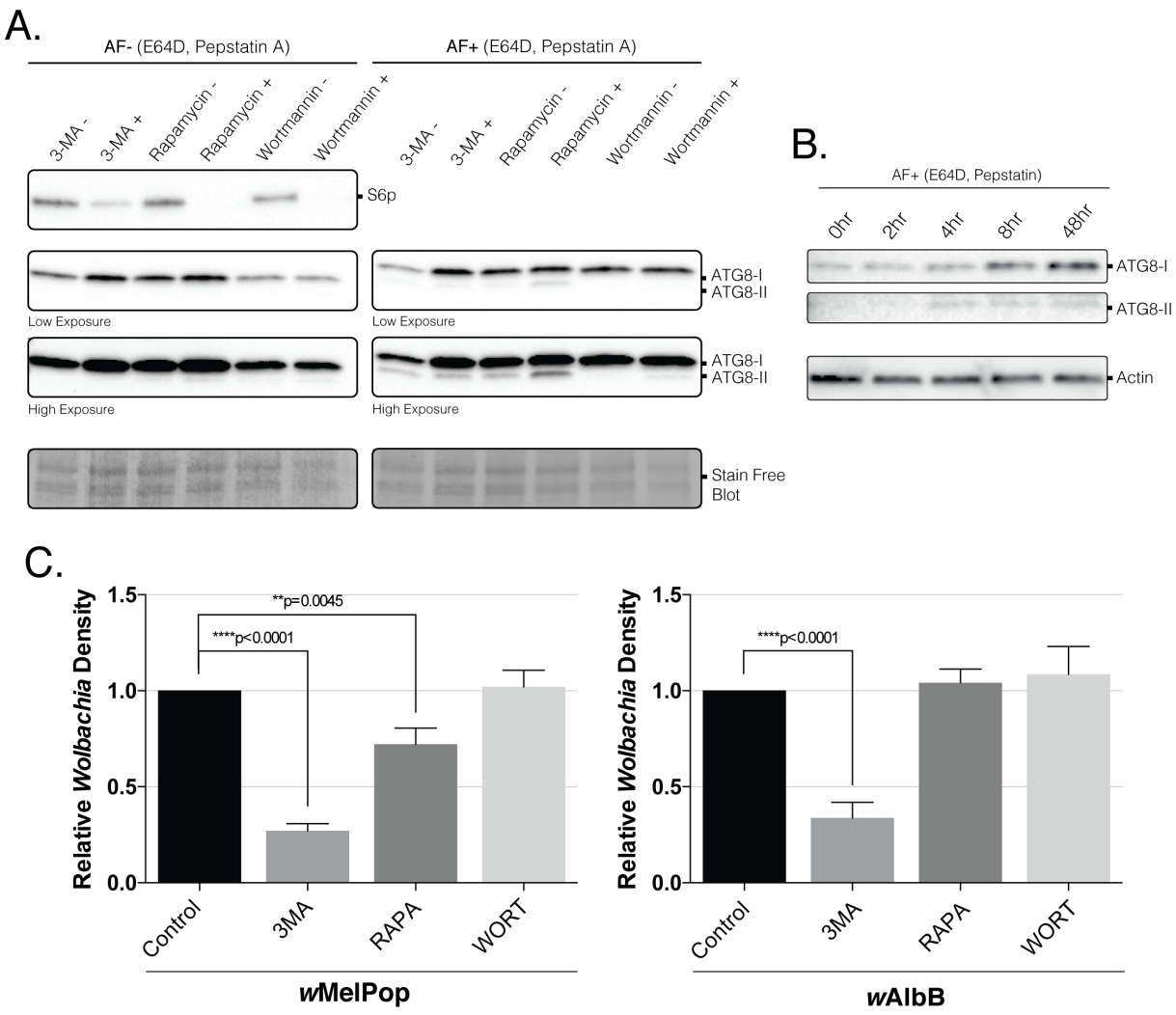

Figure 4-13 I Drug-based autophagy manipulation. A) Reducing SDS-PAGE western blot of *ag*ATG8 and S6p in AF- and AF+ conditions in *w*MelPop cells. Two exposures are shown on ATG8 bands to see both the stronger ATG8-I and weaker ATG8-II. Equal loading checked by StainFree blot. Representative of two replicates. B) Reducing SDS-PAGE western blot of *ag*ATG8 in AF+ conditions after treatment with 10mM 3MA at different time points. Equal loading compared by actin housekeeping. C) Mean *Wolbachia* density after treatment for 48 hr with autophagy manipulating drugs. 3MA and RAPA from four replicates, WORT from three replicates. Error bars represent SEM. Groups compared to control by two-tailed paired t-test.

As an alternative method, autophagy was modified by a genetic approach using RNAi. *w*MelPop infected cells were treated with double stranded RNA against ATG1 (dsATG1) for seven days to decrease autophagy levels. This efficiently reduced expression levels by 85%±2.2 (Figure 4-14a) but did not lead to a significant change in *w*MelPop density; Figure 4-14b).

To further confirm the findings, short-hairpin RNA expressing constructs were created against ATG5, ATG14 and ATG8. These however failed to produce effective KD's (data not shown). Instead, siRNA against ATG8 was designed to downregulate autophagy and cells electroporated using an Amaxa due to improved efficiency (see supplemental

8.1.2 for development of protocol for 4a3b cells). Pre-made siRNA was used to perform these KD's due to difficulty in synthesising enough dsRNA. siATG8-2 gave a KD efficiency of 94±6.1% after 48 hr (Figure 4-14c) and a reduction in total ATG8 translation (Figure 4-14d). However, this failed to significantly affect *w*MelPop density (Figure 4-14e).

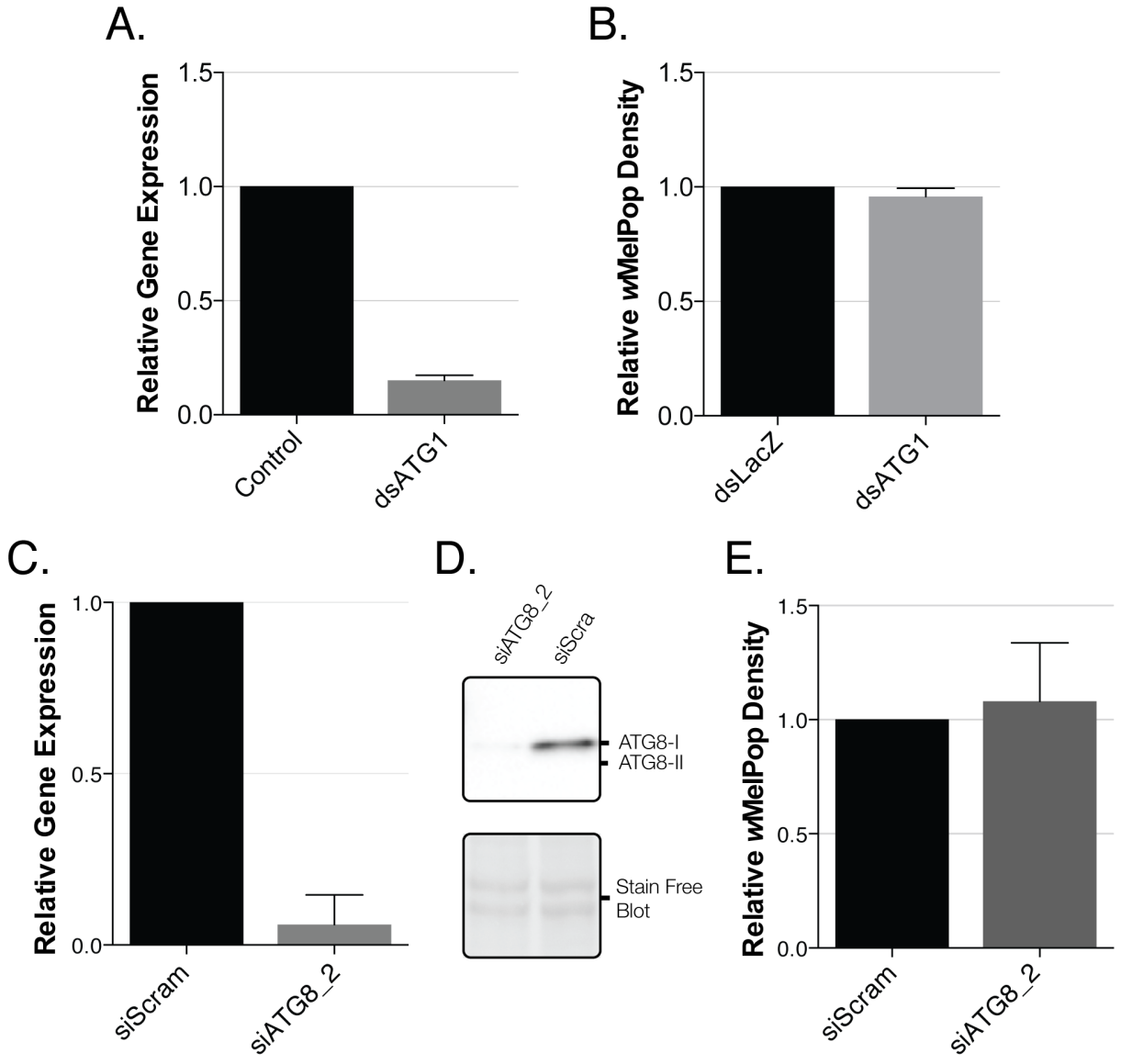

Figure 4-14 I dsRNA and siRNA-based autophagy manipulation. A) Relative RT-PCR quantification of ATG1 expression seven days after dsRNA treatment in *w*MelPop infected 4a3b cells. Mean of four replicates. B) *Wolbachia* density seven days after dsRNA treatment in *w*MelPop infected 4a3b cells. Mean of four replicates. C) Relative gene expression of ATG8 after treatment with siATG8-2 for 48 hr compared to siScrambled control respectively. D) Reducing SDS-PAGE western blot against agATG8 in AF-*w*MelPop infected cells. E) Mean *w*MelPop density following treatment with siATG8 for 48 hr. Mean of two Replicates. Bars represent sample mean, error bars SEM. Groups compared using two-tailed paired t-test. siScram; SiScrambled.

4.2.8 Investigating the TORC1 Regulator Sestrin During Wolbachia Infection

Next, possible mechanisms that *w*MelPop might use to modify TORC1 were investigated. Sestrin is a key control point acting upstream of TOR via activating AMPK to prevent cell damage caused by excessive TOR activity[328](Figure 4-15a). When 4a3b cells were treated with the TOR inhibitor PP242 for 48 hr, as expected this caused a reduction in *An. gambiae* Sestrin (*ag*Sesn; AGAP007169) expression (Figure 4-15b).

Sestrin has previously been shown to be differentially expressed in *Wolbachia* infection using whole-genome microarrays[286,431]. Since *w*MelPop infected 4a3b cells showed elevated TOR activation levels the transcript levels of *ag*Sesn in 4a3b cells was investigated. *w*MelPop infection caused a statistically significant reduction of 79%±2.6 compared to uninfected 4a3b cells (Figure 4-15c). Attempts to look at translational levels of *ag*Sestrin proved unsuccessful due to the inability to find a successful antibody, both commercially and from previously published work[328].

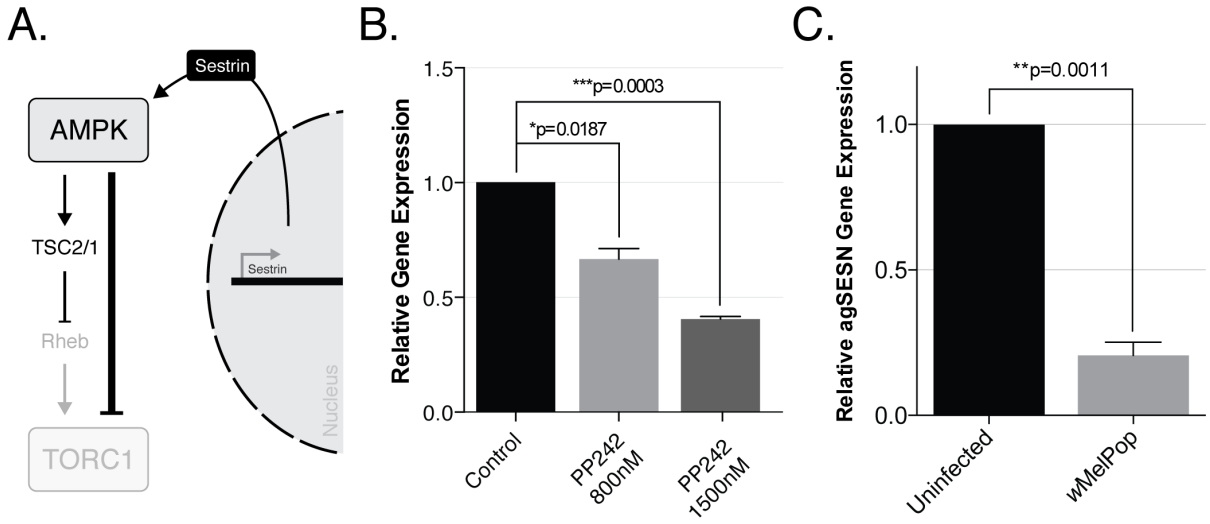

Figure 4-15 l Sestrin transcriptional levels in 4a3b cells. A) The Sestrin signalling pathway. B) Relative gene transcript levels of *ag*Sesn in 4a3b cells treated with 800nM or 1500nM PP242 compared to control treatment for 48 hr, assessed by RT-PCR. Mean from three replicates. C) Relative gene transcript levels of *ag*Sesn in *w*MelPop infected 4a3b cells compared to uninfected cells. Mean from three replicates Bars represent means, error bars represent SEM. Groups compared to control using two-tailed paired t-test.

4.2.9 Overcoming Sestrin Inhibition by Ectopic Expression

To elucidate Sestrin's effect on *Wolbachia* infection *ag*Sesn was cloned into an expression vector for intracellular expression. The *An. gambiae* homolog was identified from the *D. melanogaster* Sestrin gene (drSesn; FBtr0113114)[328]. RNAseq data on VectorBase suggested that the gene was incorrectly annotated as having an extra exon at the 5' end, which was confirmed by PCR amplification. Uninfected and *w*MelPop infected cells were AMAXA electroporated and cells collected for analysis after 48 hr. Relative RT-PCR showed electroporation caused a mean 8257- and 2179-fold increase in *ag*Sesn transcription compared to empty vector in uninfected and *w*MelPop infected cells respectively (Figure 4-16a). The ectopic protein had a C-terminal His-tag which

allowed translational expression to be confirmed by reducing SDS-PAGE western blot using an anti-His tag antibody (Figure 4-16b).

Ectopic expression of *ag*Sestrin however, only caused a non-significant decrease in *w*MelPop density ($p=0.1455$; Figure 4-16c). A significant difference in cellular morphology was observed between different treatments 48 hr post electroporation, indicating different cell viabilities (Figure 4-16d). This suggested that elevated levels of *ag*Sesn caused a dramatic loss in cell viability compared to empty vector. This loss in viability was lower in *w*MelPop infected cells. Electroporation with the empty vector in uninfected cells induced some loss in viability but not to the same degree, suggesting that the main cause of cell death was elevated levels of *ag*Sesn, but that *Wolbachia* infection may also make cells less vulnerable to this effect.

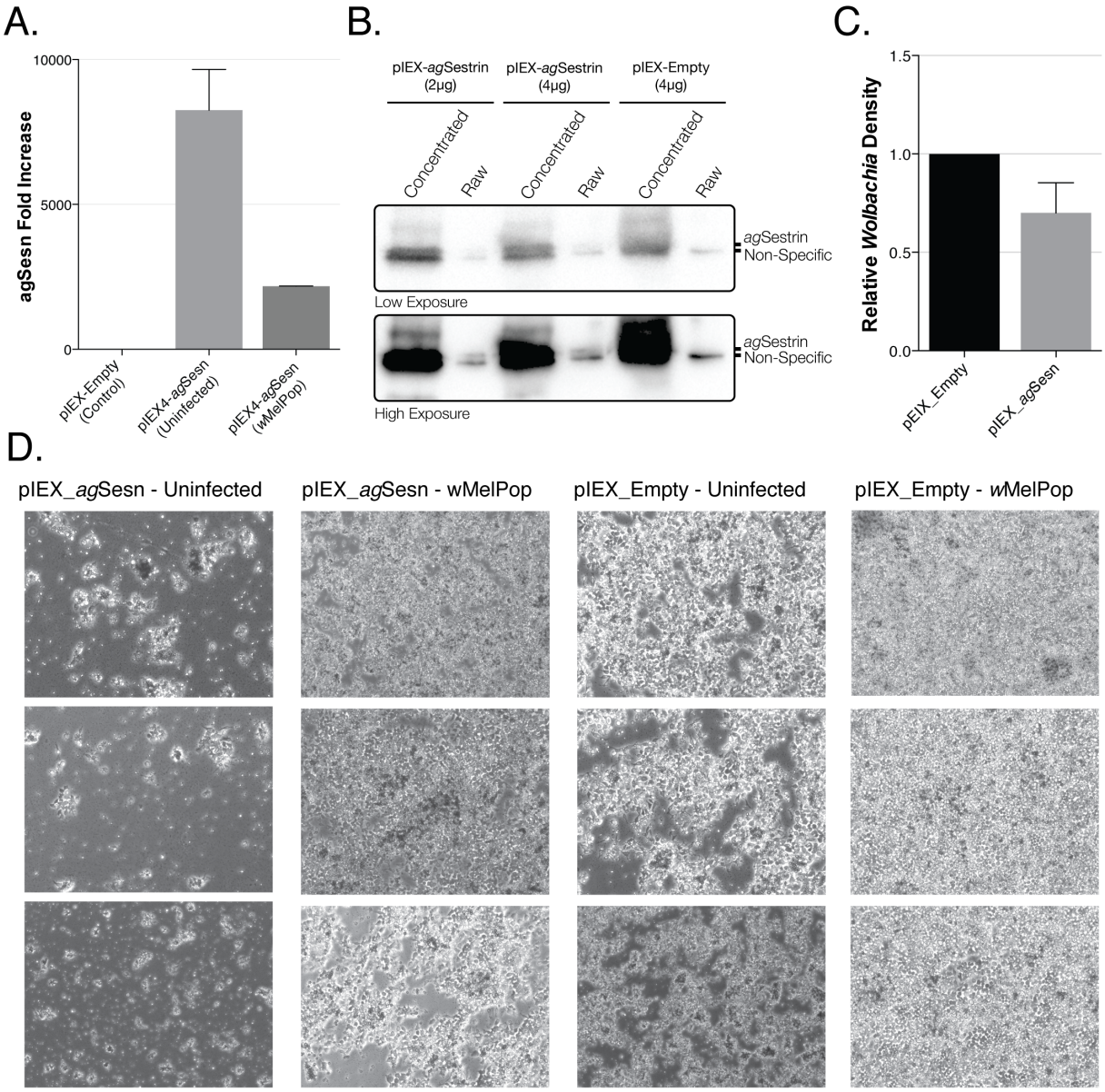

Figure 4-16 | Ectopic expression of *ag*Sesn in 4a3b cells. A) RT-PCR of relative *ag*Sesn expression levels compared to empty vector 48 hr after electroporation. Mean of two replicates. B) Reducing SDS-PAGE western blot using anti-His primary antibody to detect ectopic *ag*Sesn. C) RT-PCR quantification of *w*MelPop cells 48 hr after electroporation with pIEX4 constructs. Mean from four replicates. D) Brightfield images of 4a3b cells 48 hr after electroporation with either pIEX4_Empty or pIEX4_*ag*Sesn. Bars represent mean, scale bars SEM. Treatments compared using two-tailed paired T-test.

4.2.10 Overcoming Sestrin Inhibition by AMPK Activation

As an alternative to ectopic *ag*Sesn expression and to confirm that the AMPK-TORC1 axis does not affect *Wolbachia*, *w*MelPop infected cells were treated with the AICAR drug. AICAR is an activator of AMP analog which causes the activation of AMPK and the subsequent inhibition of TORC1 activity[295]. As expected, uninfected 4a3b cells treated with AICAR caused a downregulation of agSesn transcription (750µM, 41±18% drop; 1000µM, 75±8% drop; Figure 4-17a). To assess its effect on *An. gambiae* TOR1 activity, the activity of S6 protein was measured by western blot against S6p in *w*MelPop

infected cells after treatment for 50 hr with either 500µM or 750µM AICAR. As expected this decreased S6p to undetectable levels (Figure 4-17b). However, it failed to cause a significant drop in *w*MelPop density (Figure 4-17c).

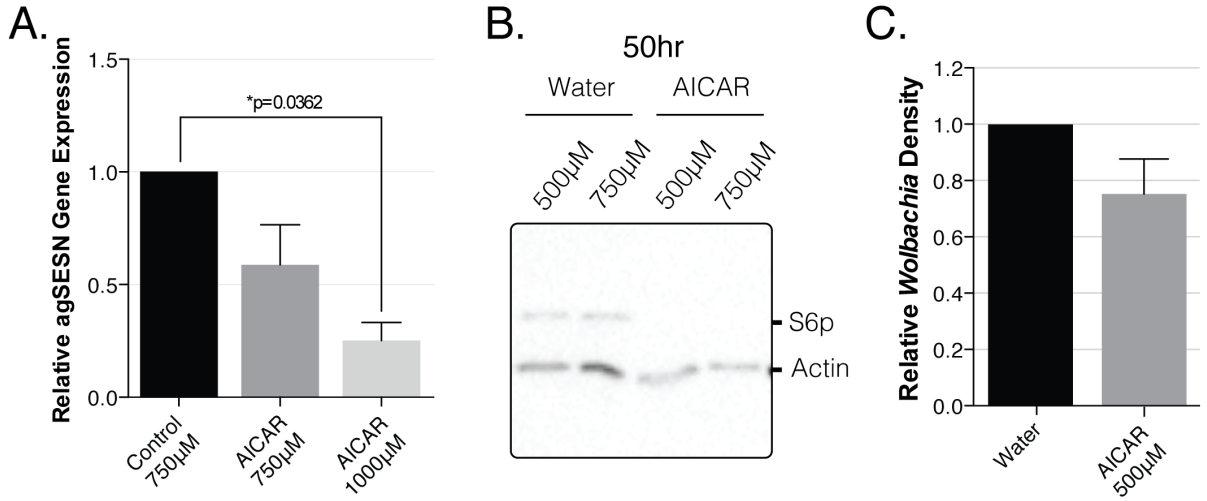

Figure 4-17 I AMPK activation with AICAR. A) Relative *ag*Sesn gene expression in uninfected 4a3b cells after treatment with 750 and 1000µM AICAR compared to vehicle control. Mean of three replicates. B) Reducing SDS-PAGE western blot of S6p in *w*MelPop infected cells treated with 500 and 750µM AICAR for 50 hr. C) RT-PCR quantification of *w*MelPop density in cells treated with 500µM AICAR for 50 hr. Mean of five replicates. Bars represent mean, scale bars SEM. Groups compared using two-tail paired t-test.

4.2.11 Investigating TORC2 Mediated Wolbachia Effects

The non-significant decrease in *Wolbachia* following AMPK modulation suggested that TORC2 and not TORC1 could instead mediate the effect on *Wolbachia*. siRNA against Rheb, a direct TORC1 upstream activator[295] was therefore used to determine whether direct TORC1 or TORC2 effects *Wolbachia* density. 48 hr following electroporation with siRheb cells showed a mean 60%±1.4 reduction in Rheb gene expression (Figure 4-18a) and reduction in S6 activation (Figure 4-18b). However, this failed to cause a significant change in *w*MelPop density (Figure 4-18c).

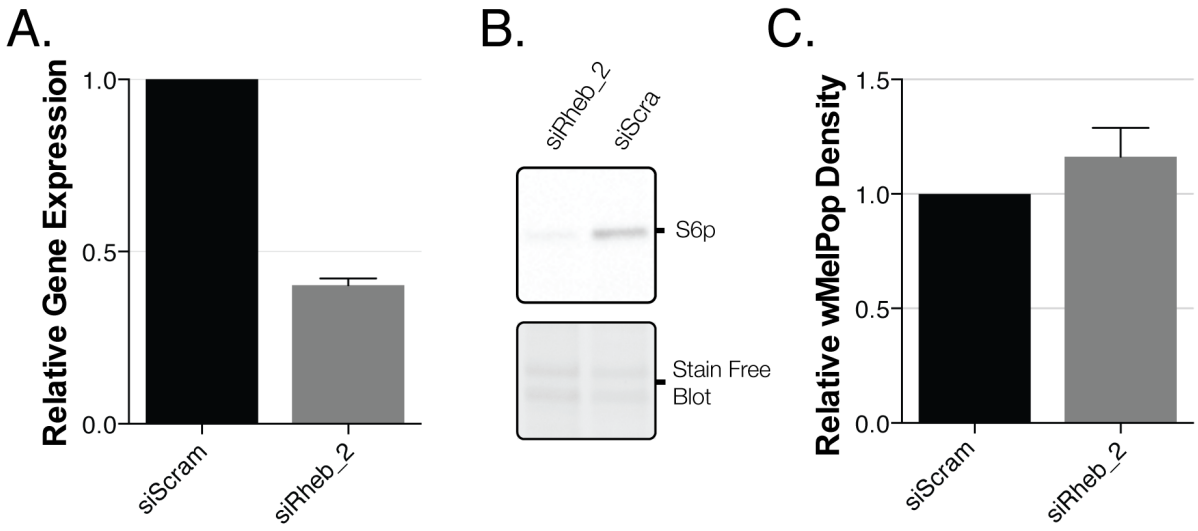

Figure 4-18 l TORC1 inhibition by Rheb KD. A) Relative gene expression of Rheb after treatment with siRheb-2 for 48 hr compared to siScrambled control. B) Reducing SDS-PAGE western blot against S6p in *w*MelPop infected cells. C) Mean *w*MelPop density following treatment with either siRheb or siScrambled for 48 hr. Two Replicates. Bars represent sample mean, error bars SEM. Groups compared using two-tailed paired t-test.

4.3 Discussion

Non-native *Wolbachia* infections are commonly associated with pathogen inhibition in insects[67]. Theories of how this is mediated include, life shortening[75], resource competition[70] and immune priming[72,73]. In *An. gambiae,* somatic infections have been shown to inhibit *Plasmodium*[73], however vertical transmission has yet to be achieved. All three of the theorised inhibitory phenotypes of *Wolbachia* can be linked theoretically to the TOR-axis. For example, TOR-axis inhibition in *Drosophila* has been shown to increase their lifespan[292]. It is also critical to the regulation of blood meal derived nutrient release, storage and utilisation for egg development in mosquitoes[3,289,290]. Finally, it has also been shown in mammals to modify innate immune effectors[293]. TOR manipulation could therefore make the mosquito host unsuitable for *Plasmodium* development and effect egg development. Therefore, TOR signalling in *Wolbachia* infection was investigated.

To address this, two strains of *Wolbachia* were used, *w*AlB from *Aedes albopictus*[286] and *w*MelPop, a high replicating strain from *Drosophila melanogaster*[287]. Both strains are associated with unique phenotypes, for example although both inhibit *P. falciparum*[73], *w*AlbB has been shown to increase *P. berghei* oocyst load[284]. Furthermore, gene expression profiles in somatic *An. gambiae* and cell line infections between strains show distinct differences[72,73,286]. Finally, *Wolbachia* induced virulence after blood feeding in *An. gambiae* is only seen in *w*MelPop and not *w*AlbB infection[73]. These differences suggest both strains may have different mechanisms of manipulating the host and were chosen for this reason.

*w*MelPop infection was associated with a 3.5 times increase in the level of activated S6 ribosomal protein in *An. gambiae* 4a3b cells. S6 activation is mediated by S6K which is itself activated by the TORC1 complex[295]. This would suggest that *w*MelPop infection is associated with elevated TORC1-axis activity. Unfortunately, a suitable activated TOR antibody for *An. gambiae* could not be found, however the function of the S6p antibody as a output of TORC1 was confirmed by treatment of cells with the TORC1 inhibitor rapamycin[300].

S6K activation is associated with increased protein translation mediated by increased ribosome biogenesis[359,369], suggesting that in *w*MelPop infection there is elevated protein synthesis. Infection of 4a3b cells with *w*AlbB was not associated with a change in S6 phosphorylation state. This difference may be explained by the higher *w*MelPop density in 4a3b cells. Unlike *w*AlbB, *w*MelPop is a fast replicating high density strain and the density of *Wolbachia* has been associated with its anti-viral activity[432-435], however somatic *An. gambiae* infections with *w*AlbB and *w*MelPop suggests that density does not correlate with anti-malaria activity[73,284]. Nonetheless, the higher density in 4a3b cells would indicate that *w*MelPop requires a considerably greater amount of host-derived nutrients than *w*AlbB and therefore increased TOR activity and protein synthesis in *w*MelPop infections could be beneficial to the bacterium.

To investigate whether TORC1 activation was beneficial to *w*MelPop infection a combination of approaches were used to inhibit TORC1 activity. Both rapamycin, which is a TORC1 specific inhibitor and PP242, which inhibits both TORC1 and 2 complexes[300], reduced *w*MelPop density significantly. PP242 was more effective at reducing density and has been shown to be a far more effective TORC1 inhibitor than rapamycin which may explain the difference, for example rapamycin is a poor inhibitor of 4E-BP activity but not PP242[300]. Genetic KD of the TOR protein in both complexes also reduced *w*MelPop density showing drug specificity against TORC complexes. The specificity of rapamycin for TORC1 and not TORC2 compared to the other approaches would suggest that TORC1 signalling is beneficial for *w*MelPop survival. *w*AlbB density was not affected by TOR KD or rapamycin treatment, which in combination with the lack of S6p modification would suggest that TOR activity may be irrelevant or have a limited effect on *w*AlbB survival.

Starvation by amino acid (aa) withdrawal was also used to modify TORC1 status in *w*MelPop infection. Aa's have been shown to act at multiple points in the TOR axis, however this is still not fully understood. This includes InR signalling via ILPs *in vivo* and directly via RagA/B *in vitro*[335,344,345]. Since experiments were conducted in cell culture the main method would likely be RagA/B and not InR signalling. Unfortunately, an anti-AKT antibody that recognised activated *An. gambiae* AKT to check InR-AKT signalling *in vitro* could not be found. Starving cells for seven days caused a significant 14% reduction in *w*MelPop density. In corroboration with genetic and drug-based inhibition this suggests that TORC1 activity promotes *w*MelPop survival.

Possible beneficial outcomes of increased TORC1 signalling include increased anabolic activities and decreased autophagy[295]. Host-cell nutrient availability is a critical factor in determining the level of cell proliferation and as a consequence TOR activity is indirectly associated with cell cycle progression, as it provides the building blocks for G1 progression[376-378]. Unexpectedly, *w*MelPop infection was associated with a reduction in cell proliferation. In the context of elevated TOR activity this could suggest that *Wolbachia* infection may affect the availability of the building blocks required for cell cycle progression, such as DNA synthesis, preventing S-phase progression. Alternatively, it could be associated with elevated cell stress which prevents cell cycle progression[436]. In support of this, *w*MelPop infected cells showed morphologically damaged mitochondria, which are associated with causing oxidative stress[388]. Damaged mitochondria are commonly associated with reduced autophagy levels preventing their clearance[388].

There is considerable active work showing that autophagy plays a critical role in the survival of many intracellular bacteria such as *Salmonella* and *Shigella*[391-393] and some initial studies suggest that autophagy may play an important role in *Wolbachia* survival[426,437]. Control of autophagy by TORC1 has been well characterised in mammals and *Drosophila*, where TORC1 activity inhibits autophagy[294,295]. To measure autophagy in 4a3b cells a polyclonal antibody was raised against *An. gambiae* ATG8.

As expected from increased TORC1 signalling, *w*MelPop infection was associated with decreased autophagic flux measured by immunoblot and ImageStream. However, in disparity with its TORC1 status *w*AlbB infection results were mixed, showing decrease autophagic flux in the immunoblot but a non-significant trend in ImageStream analysis. A possible explanation for the disparity with *w*AlbB could be that the ImageStream technique only assesses ATG8-II that is in proximity to lysosomes, whereas western blots look at total ATG8-II. From this it could be hypothesised that *w*MelPop infection is associated with a reduction in ATG8 lipidation and autophagosome-lysosome fusion, however *w*AlbB infection is associated with reduced ATG8 lipidation but the level of fusion with lysosomes is similar to uninfected. The outcome is that only *w*MelPop infection causes a reduction in the degradation of autophagosome material. This highlights the requirement for using multiples methods to assess autophagy, with the ImageStream method measuring the important physiological event, degradation of autophagosomes material.

An alternative hypothesis may be that the host cell attempts to mount a non-canonical form of autophagy called LC3-associated phagocytosis (LAP) against *Wolbachia*, which uses the same autophagy machinery as canonical autophagy but is independent of the TORC1 downstream ULK1 (ATG1 in insects) signalling[438,439], and that *w*MelPop and *w*AlbB are able to inhibit the autophagy machinery that is shared between both canonical and non-canonical autophagy. In LAP, bacteria in single membrane vesicles become coated with ATG8-II using the autophagy machinery[388] and fuse with lysosomes[440]. This is supported by the fact that *w*MelPop and *w*AlbB were found in single membranes instead of the classical double membrane vesicles associated with autophagy[388] and by the fact that *w*AlbB was associated with a reduction in total ATG8-II but no change in TORC1 activity. However, although LAP autophagy is poorly understood, LAP is unlikely in these infections as rapamycin, which inhibits TORC1 which is directly upstream of ULK1/ATG1 has been shown to increase ATG8 lipidation of bacteria containing phagosomes[441,442], indicating that TORC1 signalling is needed for LAP too.

To investigate whether decreased autophagy was an irrelevant consequence of elevated TORC1 or beneficial to *Wolbachia's* survival, autophagy levels were manipulated using both drugs and RNAi. Rapamycin was used to increase autophagy by TORC1 inhibition, whereas 3MA and wortmannin were used to decrease autophagy by inhibiting the class III PI3K. However, in 4a3b cells 3MA also increased autophagy after more than four hours treatment. This phenomenon probably occurs as 3MA also has class I PI3K activity, which regulates AKT activity[427,430] and *in vitro* is known to lose its class III PI3K activity after four hours treatment[430].

Upregulation of autophagic flux by rapamycin and 3MA treatment was associated with a significant reduction in *w*MelPop density. The ability of rapamycin, which acts on TORC1, to increase autophagy in *w*MelPop infected cells suggests that *Wolbachia* is unable to directly inhibit the autophagy machinery. Inhibition of autophagy by wortmannin did not affect *Wolbachia* density. Interestingly, 3MA but not rapamycin

treatment reduced *w*AlbB density. A possible reason for the mixed results in *w*AlbB infection could be due to the low infection density and/or limited sensitivities of the TOR and autophagy assays used. Furthermore, the lack of a reduction in *w*AlbB density with rapamycin, which has been shown to reduce LAP[441,442] provides further evidence against LAP.

To confirm the effects of these drugs were mediated by autophagy, ATG1 (ULK1 in mammals) and ATG8 were KD to decrease autophagy. ATG1 KD would not affect LAP[439]. Similar to wortmannin treatment, this had no effect on *w*MelPop density. A possible explanation for this could be that as *Wolbachia* infection is associated with decreased autophagy that further treatments that act to inhibit autophagy may have no further effect. Alternatively, the anti-*Wolbachia* activities of 3MA and rapamycin may be non-autophagic. For example, 3MA has also been associated with modifying lysosomal acidification, mitochondrial permeability and glycogen metabolism[430].

Denis Voronin[426] however found that genetic KD of autophagy by siATG1 in *Drosophila* did increase *w*MelPop density. A possible explanation for the disparity with these results could be as *w*MelPop is a natural infection in *Drosophila* but not mosquitoes[287] or that autophagy is not important for *Wolbachia* survival in 4a3b cells. Similar to these results they also showed that rapamycin reduced *w*AlbB in *Aedes albopictus* cell lines, however 3MA increased *w*AlbB levels[426]. But they failed to use autophagic flux drugs to confirm that 3MA decreases autophagy, showing only decreased ATG8 fluorescence as evidence that in these cells 3MA inhibited autophagy. Therefore, an effect on AKT via class I PI3K activity cannot be ruled out. They also found that starvation of cells reduced *w*AlbB levels.

During the assessment of *Wolbachia* in electron micrographs a distinct striated structure was seen surrounding *Wolbachia* and has not been described in *Wolbachia* before. These structures resembled Septin rings (See figure 1a from[428]). Septins are guanidine-nucleotide (GTP)-binding proteins which organise into filaments[443] to mediate many process involving membrane remodelling[444]. More recently is has become appreciated that Septins ‘cage’ some intracellular bacteria and has been shown to prevent actin motility of *Shigella* and aid autophagosome formation and recruitment of autophagy proteins such as ATG8 around the bacteria[429]. Whether Septin rings can also be used by bacteria to also defend themselves is unknown[445]. The IcsB protein released by *Shigella* from its T3SS prevents the formation of Septin cages around cytosolic *Shigella* and therefore prevents recruitment of the autophagy machinery[429,446]. The presence of Septin rings surrounding *Wolbachia* vacuoles suggests that it is unable to prevent Septin ring formation. Alternatively, they may be beneficial to *Wolbachia’s* survival such as helping with division in cells.

The second aim of this study was to investigate in more detail how *Wolbachia* might be elevating TORC1 activation. Interestingly, *Wolbachia* has a T4SS which may allow it to modify the TOR signalling pathway[394]. The high level of conservation found for the components of *Wolbachia* T4SS has been reported, suggesting that the T4SS may be

functionally important for survival within the host[447]. Many T4SS expressing bacteria have been shown to secrete host modifying proteins[448], such as *Helicobacter pylori* which secretes CagA that modifies the activation of many host signalling proteins including those involved in actin rearrangement[448,449]. Some *Rickettsiales* express the T4SS secreted protein RalF which acts as a guanine nucleotide exchange factor[450], however a BLAST shows that this protein is not present in *Wolbachia.*

Elevation of TORC1 signalling occurs in excess nutrient levels promoting anabolic processes[295]. The FOXO transcription factor is a key regulator of TORC1 activity, as a result FOXO can be activated by many of the detrimental effects of excess TORC1 activation such as oxidative stress[329]. Therefore, *Wolbachia* may possibly inhibit this feedback loop, unfortunately a suitable FOXO antibody could not be located to assess its activation level. A key method that FOXO uses to downregulate TORC1 activity is via promoting the expression of Sestrin, an AMPK activator[328]. Interestingly, sestrin has been found to be differentially expressed in *Wolbachia* infection. For example, in *An. gambiae* Sua5B cells *w*AlbB infection is associated with a down-regulation of Sestrin[286]. *w*MelPop infected *Aedes aegypti* mosquitoes were also associated with a drop in Sestrin expression, which was upregulated in *w*Mel infected mosquitoes[431]. Like *w*AlbB, *w*Mel is a lower replicating strain[431]. In 4a3b cells, agSesn gene transcription showed a 79% reduction with *w*MelPop infection. This however could not be confirmed at the protein level as a Sestrin antibody against *An. gambiae* could not be found. Decreased *ag*Sesn expression would suggest reduced FOXO activation. Sestrin has been characterised in *Drosophila*[328] and its negative feedback inhibitory effect on TORC1 was confirmed in 4a3b cells.

To investigate whether Sestrin downregulation was a requirement for *Wolbachia* survival *ag*Sesn was ectopically expressed. *ag*Sesn over expression was associated with considerable cell death, which was reduced in *w*MelPop infection, suggesting that *w*MelPop may prevent death by reduced TORC1 signalling by keeping TORC1 activity high. In support of this, ectopic a*g*Sesn expression only caused a non-significant reduction in wMelPop density. To simulate Sestrin activity cells were also treated with AICAR to activate AMPK, this also caused a non-significant reduction in *w*MelPop density and produced a reduction in S6p TORC1 activity indicating effective TORC1 blockade. This is in contrast to earlier results showing that TORC1 and autophagy manipulation modifies *Wolbachia* density, suggesting that either modulating the AMPK-axis is not effective at inhibiting TORC1 activities associated with *Wolbachia* survival, as for example some TORC1 drugs such as rapamycin only inhibit certain TORC1 activities[300], or that TORC1 activities are not critical to *Wolbachia* survival.

Considering the latter theory, TORC inhibition by rapamycin, PP242, dsTOR and starvation, and autophagy activation by 3-MA was associated with reduced *w*MelPop. However, TORC inhibition by AMPK activation was associated with a non-significant decrease in *w*MelPop. One key difference between these intervention methods is that the former treatments can also have TORC2 activities, whereas the latter is TORC1 restricted. For example, PP242 has been shown to inhibit AKT activity by preventing

TORC2 from phosphorylating the HM motif[300]. HM motif phosphorylation is required for AKT-mediated FOXO inhibition [302,320,326,327]. The HM phosphorylating activity of TORC2 is also known to be nutrient stimulated, suggesting starvation may inhibit TORC2 activity[302]. TORC2-mediated AKT activity could therefore partially promote *w*MelPop survival via FOXO inhibition. In support of this Sestrin gene expression was reduced in *w*MelPop Infection. Furthermore, long-term rapamycin treatment has also been hypothesised to inhibit TORC2 activity by reducing the availability of active TOR protein available to form TORC2 complexes[319]. TOR KD would also effect both TORC1 and TORC2 complexes.

Finally, 3MA prevents recruitment of AKT to the membrane and its activation via its PI3K class I inhibition[430], therefore the decline in *Wolbachia* may not be due to autophagy. This can be further supported by the lack of an increase in *Wolbachia* density following autophagy inhibition, as Voronin[426] showed an increase in *Wolbachia* density following autophagy inhibition in *Aedes* cells. Also, *Wolbachia* were found in only single membrane vesicles and there was no evidence to support LAP.

Another function of TORC2 activity is in promoting cell survival[295]. Interestingly, in *Brugia malayi* loss of *Wolbachia* causes large amounts of cell apoptosis[451], suggesting another possible benefit of TORC2 activation for *Wolbachia*.

Although *w*AlbB was not associated with a detectable increase in TORC1-S6p activation, manipulation of host cells by 3MA was associated with a decrease in *w*AlbB density, suggesting that *w*AlbB may be dependent on AKT signalling but this may not be FOXO mediated. Interestingly *w*AlbB infection has been associated with a downregulating of HSP proteins[286]. HSP proteins have been shown in mammals to protect AKT from ubiquitin degradation when not phosphorylated by TORC2 at the TM motif (T450)[302]. Therefore, *Wolbachia* could indirectly modulate AKT activity.

To conduct a preliminarily investigation of this hypothesis the direct upstream TORC1 activator Rheb was KD. Rheb KD failed to significantly reduce *w*MelPop levels which suggests that rapamycin may be mediating its effects via TORC2 and not TORC1, and that TORC1 activation mediated by AKT may be irrelevant to *Wolbachia* survival. This therefore suggests that TORC1 activation may be an effect of other possible TORC2-AKT manipulation such as FOXO inhibition. *Wolbachia* has been shown to modulate Chico expression[452], which is part of the InR signalling in *Drosophila*[354], therefore *Wolbachia* could upregulated AKT activity via this method. Furthermore, it has been shown that *Wolbachia* infection in *Drosophila* reduces the physiological effects of InR KO and this was associated with maintenance of AKT activity compared to InR KO without *Wolbachia*[453]. Whether this also happens in mosquitoes is unknown.

To further investigate this, FOXO and AKT KD's will be needed and suitable antibodies against these proteins must be created to enable monitoring of their activation levels. However, AKT KD in *Aedes aegypti* cells has been shown to decrease *Wolbachia* levels (Kirsty Stainton, unpublished data). If *Wolbachia* does modulate FOXO activity its effect on *Wolbachia* density is likely not via AMPK-TORC1. FOXO is however associated with

controlling many different effects in cells such as apoptosis, cell cycle arrest and oxidative responses[454].

In summary, the data presented here provides early evidence suggesting that elevated TORC1 activity seen in *w*MelPop infection in *An. gambiae* may not be a major contributing factor to its survival, but a consequence of host cell manipulation. Modification of the AMPK-TORC1 axis failed to affect *w*MelPop density. However, drug, genetic and starvation mediated modification suggests that AKT signalling may be beneficial to *Wolbachia* survival, possibly mediated by FOXO or other pathways, which could explain the elevated TORC1 activity. *w*AlbB however failed to modify TORC1 activity which may be explained by its low density in cells. This work therefore lays the ground work for further investigations into possible TORC2 mediated *w*MelPop survival. The interactions of *Wolbachia* and the TOR axis are likely to be complex.

In vivo Setting

Another consideration is that although TORC1 may not directly affect *Wolbachia* density in 4a3b cell lines, *Wolbachia* TORC1 modulation may still be beneficial in an *in vivo* setting. Serbus and colleagues[455] for example highlights the problems with extrapolating results from *in vitro* culture to *in vivo*, showing that in *Drosophila* TOR signalling in **somatic tissues** controlled the density of *Wolbachia* in oocytes in **ovarian tissues**. Elevating TOR in somatic cells but not in the ovaries decreased oocyte *Wolbachia* density. They also showed that diet was able to modify TOR via InR signalling in somatic cells (particularly in the fat body) and therefore modify oocyte *Wolbachia* density. However, this had the opposite effect in somatic cells, causing an increase in *Wolbachia* density. Interestingly, if *w*MelPop also upregulates TOR in somatic *An. gambiae* infections as it does in 4a3b cells, this could possibly explain why we cannot establish infections in the ovaries *in vivo*[73].

Furthermore, excessive TORC1 activity has been associated with some of the *in vivo* anti-pathogenic phenotypes accompanying *Wolbachia* infection, in particular the life-shortening phenotype[292]. Interestingly, *w*AlbB is not associated with lifespan reduction[73,284] and in infection in 4a3b cells is not associated with an increase in TORC1 activity. Reduced Sestrin expression has also been associated with tissue dysmorphia such as wing bending in *Drosophila*[328] and could be the cause of proboscis bending seen in *Wolbachia* infection which reduced feeding ability[456,457].

TOR is a critical signal for the extraction and utilisation of nutrients from blood for the development of eggs by production of yolk proteins in the fat body (vitellogenesis)[3,289,290]. In particular TOR signalling occurs in response to a blood meal and is required in the midgut, ovaries and fat body to mediate the production of yolk proteins (Figure 4-4a)[3,289,290]. It therefore makes sense that the parasite within the blood meal must utilise these proteins for its own nutrient demanding development, however it would be competing with the fat body and its production of yolk proteins for the developing follicles[3]. It has been shown that *Plasmodium* causes apoptosis in the developing follicles and their reabsorption[417]. A suggested reason for this has been to

release the limited nutrients instead to the developing *Plasmodium* oocysts[315]. Interestingly, *Wolbachia* has been shown to protect the ovaries from apoptosis[451,458,459]. Therefore, it may prevent nutrient release to developing parasites. However, in somatic *An. gambiae infections* the germline is not infected.

Wolbachia in somatic *An. gambiae* infections is found concentrated in the fat body. *w*MelPop infection of 4a3b *An. gambiae* cells elevates TOR levels above physiological levels and could be seen as causing a similar TOR profile in mosquitoes to blood-fed mosquitoes. Interestingly, supplementing *An. gambiae* mosquitoes with an ecdysone agonist reduced lifespan and reduced *Plasmodium* development[460], phenotypes seen in *w*MelPop infection[73]. This provides support for fat body mediated TOR activation by *Wolbachia* mediating some of *w*MelPop's inhibitory effects. Furthermore, in somatic infection of *w*MelPop in *An. gambiae* the life shortening phenotype is only seen after a blood feed[73], further implicating TORC1 in *Wolbachia's* host manipulations. In further support of this *Wolbachia* infected *Drosophila* produce more eggs under low nutrient conditions than flies without *Wolbachia*[461,462].

In summary, this suggests that modification of TORC1 in an *in vitro* setting may have implications for the anti-*Plasmodium* activity and egg development in *An. gambiae.*

5 A Bioinformatics Approach for the Design of a CD8 T-cell Based Dengue Vaccine

5.1 Introduction

Approximately 75% of all dengue infections are subclinical. However, the remainder experience a spectrum typified by acute fever that after defervescence can develop into severe haemorrhagic dengue fever characterised by dangerous plasma leakage and hypovolaemic shock which can progress to organ failure and vascular haemorrhage[103,463]. Unfortunately, there is no effective treatment for severe disease[103], therefore a dengue vaccine is a highly attractive prospect. This introduction will thus have a strong emphasis on vaccine design in the context of dengue.

5.1.1 Lifecycle

The virus itself is a 50nM virion constructed from Capsid (C), preMembrane/Membrane (prM/M) and Envelope (E) protein in a lipid envelope[463]. Inside is a 10.7kb positive sense capped RNA (+RNA) genome which also encodes seven non-structural proteins (NS1, NS2A, NS2B, NS3, NS4A, NS4B and NS5; Figure 5-1)[463]. Following a bite from an infectious *Aedes aegypti/albopictus* mosquito[463] the virus is released into the host via the saliva[464]. The mosquito would have previously been infected by taking a blood meal from an infected human, where the virus then enters the haemolymph and replicates before localising to the salivary gland in high numbers[465].

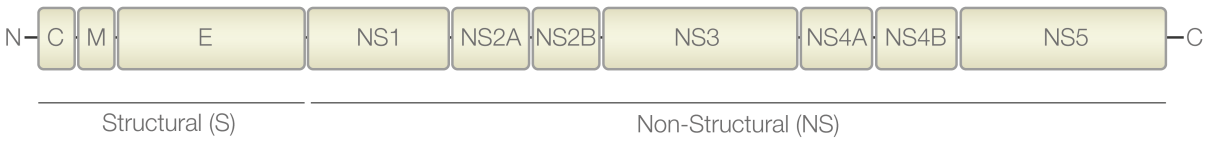

Figure 5-1 I Dengue. The DENV proteome.

In the human host the virus has an assorted cell tropism, particularly dendritic cells, macrophages and monocytes[463]. Binding and entry of these cells is mediated by the E protein[466] and although many binding proteins have been suggested (heparan sulfate, DC-SIGN, mannose receptor, TIM/TAM receptors, laminin, HSP90/70) the receptor

mediating entry remains elusive[463]. The virus enters host cells by clathrin-mediated endocytosis, although there may be alternative entry methods in some cell types[467]. Acidification of the endosomes and the E protein are critical to fusion with the host membrane and release of the viral genome into the cytoplasm. The E protein is a three domain protein (EDI, EDII, EDIII) and acidification causes the E protein to trimerise to reveal a fusion loop within EDII which mediates this fusion[466,468-470]. The EDIII domain distinguishes the four serotypes[471].

Subsequently, the viral RNA is translated by the host machinery as a single polyprotein anchored in the endoplasmic reticulum (ER) membrane[466,472] and the polyprotein is cleaved into its constituent proteins mostly by itself using the NS2B/NS3 protein on the cytoplasmic side, but also by host proteases in the ER luminal side[473-475] (Figure 5-1). NS2B is critical to NS3's serine protease function[476] and recognition[477]. The RNA genome contains both 3' and 5' UTR hairpin loops which modulate viral replication[478]. Processed viral proteins with some host factors form a complex that mediates the replication of the viral genome via a negative-strand intermediate. Most importantly the NS5 RNA-dependent RNA polymerase (RdRp) synthesises the negative-strand RNA which it uses to produce the positive sense RNA with a double stranded intermediate[479,480]. NS3 and NS5 mediate the 5' capping of the nascent +RNA[480]. NS3 also functions during replication via its helicase activity[481].

The capped RNA is then packaged with the capsid protein and localises with E and prM heterodimers which bud from the ER[472] as immature virions made from 180 prM/E dimers in 60 trimeric complexes[482]. prM acts to prevent the fusion loop from being revealed while in the host[471], however as virions traverse the Golgi, prM is cleaved into the pr fragment and M by host furin followed by a realignment of the E proteins into anti-parallel dimers[483]. Following budding from host cells the pr fragment is released, mediated by the change in pH forming mature virions[484]. Furin cleavage is however inefficient, leading to a mixture of prM containing virions[484]. The roles of the remaining non-structural proteins are less well characterised. NS4A is believed to be important in formation of replicative complexes[485], structures where viral RNA replication occurs[486]. NS1 functions in RNA replication and virion production[487]. NS2A and NS4B are also important in replication[488].

5.1.2 Correlates of Protection

Understanding the correlates of protection for complex pathogens is critical to successful vaccine design in the modern era. They help us to engineer and tailor vaccines to specifically elicit these protective aspects of the immune system in a memory response. Consequently, a rudimental understanding appears only successful for some cases (e.g. smallpox[489]) and may even lead to disease enhancement with life-threatening consequences[490,491]. Unfortunately, a brief look at the literature indicates that dengue falls within the latter group[463,471], and a recent phase III dengue vaccine trial showed increased disease severity in young children[108]. This unfortunate side-effect is however not unexpected. The development of severe dengue following acute fever, epitomised by increased vascular permeability[463,492], almost elusively occurs

during a secondary infection with a unique serotype to the primary infection[54-56]. Furthermore, infection with each serotype elicits long-term protection to the respective serotype, but only short-term (~2 months-3 years) protection to other serotypes[493-497].

It was therefore hypothesised that infection with one serotype enhanced the infection of a subsequent heterotypic serotype[56,471,494,495]. In support of this, increased viremia was shown to correlate with severe disease[498,499]. In 1988, Srisakul Kliks and collegues[500] provided direct evidence that maternal dengue antibodies both provided immunity in infants from dengue infection and that their decline correlated with severe dengue symptoms. The lack of T-cells in this situation suggested antibodies as the main mediator of protection and disease severity. Early *in vitro* work showed that antibodies could enhance infection via Fc receptors (FcR)[501].

Since then, considerable work has expanded knowledge on this phenomenon referred to as antibody-dependent enhancement (ADE); described as cross-reactive IgG antibodies from a previous infection with poor neutralizing capability which bind the heterologous serotype and enhances its uptake via FcR's into host cells[492,502]. This is likely a mediator of increased viremia mediated through increased host cell infection[502].

Most work has however been inferred from *in vitro* or animal models[501,503-507]. Increased binding and uptake has been show in P338D1 cells[508] and THP-1 cells[509]. Recent *in vitro* work suggests that in some FcR-containing cell types the increase in infected cells and viremia in ADE may in fact be mediated by enhanced fusion within endosomes and not increased host cell binding and uptake[508].

Recent work has shown that FcR binding in ADE may modulate the antiviral response. For example, THP-1 monocyte cells infected via ADE showed that FcR signalling reduced type I IFN and pro-inflammatory cytokine production, Toll-like receptor (TLR) expression and nitric oxide radicals, which was paired with an increase in IL-10 expression. This lead to enhanced viral production[509-511], however, in macrophages IL-10 induction has not been found[512]. Considerable work shows or suggests that high viremia is associated with vascular leakage[510,513-515], offering a possible correlate of severe disease. An *in vivo* mouse model with maternal antibodies, found increased TNFα and linked this to vascular leakage[516]. In humans with severe dengue TNFα levels have been found to be elevated[517,518].

An antibody that causes ADE can be defined as one which binds viral particles but does not prevent viral entry into host cells[492,503]. This is dependent on not only whether it binds to neutralising epitopes, but also circulating levels, its affinity, and how accessible the epitope is[471,502,519-522]. As such a neutralising antibody could theoretically become disease enhancing in low levels[471,502,519-522]. A key factor is obviously cross-reactivity (heterotypic) with the secondary infecting serotype, but heterotypic antibodies can be neutralising[523] and heterotypic neutralizing antibodies have been associated with reduced symptoms[524].

Severe disease determinants include the natural decline of heterotypic neutralising antibodies but not homotypic neutralising antibodies over time[502]. Also the presence of anti-prM antibodies which may enable non-infectious immature DENV particles to infect host cells[503,525,526]. Finally, DENV particles are extremely dynamic undergoing a process known as viral 'breathing' which can affect the ability of neutralising antibodies to bind[103,463]. These indicate that ADE predisposition is likely a dynamic process dependent on a combination of factors.

During a primary infection the majority of antibodies are cross-reactive and non-neutralising (not protective)[504,527], most of these antibodies are anti-E antibodies against the conserved EDII fusion loop suggesting that they are non-neutralising[471,527]. During secondary infection however, anti-fusion loop antibodies are strongly neutralising[523]. Many of the best neutralising anti-E antibodies have been shown to bind complex epitopes dependent on the quaternary structure[528-532]. Included within this are antibodies that interact with the fusion loop[528-532].

High levels of poor-neutralising prM antibodies are also found during secondary infection with *in vitro* ADE activity[503,527]. A few antibodies have also been detected against other proteins, including non-structural[533,534]. Antibodies against NS1 have been shown to enhance NS1's complement activation activity which may contribute to vascular leakage[535], however antibodies against NS1 have also been shown to reduce vascular leakage[515]. This may be explained by differences in the amounts or type of antibodies raised against NS1.

In-terms of vaccination this suggests that raising high levels of neutralising antibodies against E would be protective, these could be homotypic or heterotypic. However, a decline in the heterotypic levels could be detrimental. Avoiding prM antibodies may be beneficial to prevent immature virions becoming infectious. In hindsight it is therefore not surprising that the tetravalent Sanofi CYD-TDV vaccine consisting E and prM caused increased virulence[108]. This could have been mediated by prM antibodies acting on immature virions or the tetravalent nature possibly encouraging cross-reactive antibodies? Alternatively, competition between each virus type may cause certain vaccine serotypes to replicate more skewing the antibody response, which has been seen in mosquitoes and humans[536,537]. It may also explain the differing levels of serotype protection seen[108,110].

However, in a Phase II trial, neutralising antibodies against all four serotypes were detected but there was no DENV2 protection[538]. Another explanation for the limited efficacy could be a lack of appreciation for CD8 T-cell responses. As most dominant CD4 epitopes have been found in the C, E and NS3 proteins, whereas most CD8 epitopes have been found in NS3, NS4B and NS5[112,539-542], which are missing from the CYD-TDV vaccine[108]. There are however only a few MHCII epitopes currently identified[110,542] therefore a bias towards C, E and NS3 cannot be strongly concluded as yet.

Until recently the same could be said for MHCI epitopes, however the recent seminal work of Daniela Weiskopf and colleagues[112] increased the number of CD8 epitopes by over 83%, and the Immune Epitope Database and Analysis Resource (IEDB)[543] now has over MHCI 350 human epitopes. This, until recent scarcity of epitopes may partly explain the recent paradigm shift in CD8 correlates, driven partly by the Weiskopf group[110].

Traditionally CD8 T-cells are associated with protection from viral infections by a mixture of antiviral activities, including cytotoxicity and the release of pro-inflammatory and anti-viral cytokines, which can be enhanced by CD4 T-cells[110,544-546]. However in dengue, CD8 T-cells have historically been associated with severe disease and capillary leakage, and many refer to Juthathip Mongkolsapaya[547] on this. The only early evidence really excluding a role for CD8's in severe disease was the discovery that maternal antibodies in infants without a pre-existing T-cell response was associated with increased severity[500]. Only recently there has been a considerable increase in evidence for a non-pathogenic or protective role of CD8 T-cells in dengue infection[112,516,548-551].

The predicted detrimental effects of CD8 T-cells have been referred to as antigenic sin and is defined as the domination of cross-reactive memory CD8 T-cells from the original serotype during a heterotypic infection which have low avidity[110]. This proliferation of cross-reactive CD8's instead of naïve CD8's in secondary infection is likely as memory T-cells have a lower activation threshold and are present in higher frequency[552]. Antigenic sin is theorised to be mediated by the released of vasodilators leading to vascular leakage[553,554]. For example, T-cell secretions such as IFNα and IL-2R have been correlated with disease severity[518], however the concentration of blood products due to plasma leakage may confound such results[507]. Furthermore, although TNFα has been implicated in disease[555], TNFα has also been implicated in disease in primary infection of mice with maternal antibodies[516]. Suggesting pre-existing cross-reactive CD8's may not be a predisposing factor.

Most of the literature report dengue specific CD8 T-cells during the acute phase[547,548] and thus before the onset of severe disease, providing the premise that they could cause pathogenesis[548]. Commonly groups will however refer to the work by Nguyen Thi Phuong Dung and colleagues[507] who only detect dengue specific CD8's after the onset of vascular leakage. Although tempting, this does not necessarily mean CD8's play no role in pathogenesis as they may be sequestered in tissues or enhance vascular leakage in late stages[507]. Alternatively, these differences may reflect host genetic backgrounds as all use the same NS3 epitope and HLA-A11 MHC[507,547,548]. This does however highlight the restraints of using only a restricted number of HLA and epitopes to draw conclusions.

Interestingly, Heather Friberg[548] reported that dengue specific CD8 T-cells reach peak frequency slightly earlier in primary than secondary infection. This observed difference may be explained by increased apoptosis of CD8's in secondary infection, which has been reported using an NS3 epitope measuring Ki67 positive cells[547]. In further support

of a pathogenic CD8 role, the epitope- and HLA-independent CD96 measure for CD8 proliferation has shown that during the acute febrile phase there is an increase in total activated CD8 T-cells in patients that developed vascular leakage[556]. Heather Friberg[548] however showed no difference in the frequency of dengue specific CD8 or their activation level (CD38) in acute phase for primary or secondary infection and used multiple epitopes and HLAs.

In further support of antigenic sin, evidence exists to suggest that cross-reactive MHC binding doesn't necessarily elicit an effective CD8 response[113,552]. These cross-reactive CD8's are obviously able to bind epitopes across serotypes and in many cases due to serotype variability (25-30%) these will have sequence differences (epitope variants)[552]. Considerable work on epitope variants (mostly with the NS3 GTS epitope and its variants) have shown that although stimulation with a heterotypic variant induces proliferation these T-cells are low avidity[547] and have reduced cytotoxic degranulation with elevated cytokine release[552]. Furthermore, Heather Friberg and colleagues[113] extensively characterised the activation of dengue specific CD8 T-cells and showed that some heterotypic epitope variants showed an atypical mono-functional CD8 response characterised by MIP-1b release whereas other heterotypic variants of the same epitope and the homotypic variant were associated with a polyfunctional response (MIP-1b, degranulation, TNFα, IFNγ)[113]. A poly-functional response is associated with protection in other viruses[557,558]. Consequently, this suggested that the heterotypic serotype that a person gets challenged with could affect the type of cross-reactive CD8 response they get i.e. the order if serotype infection[113]. In support of this greater numbers of dengue specific CD8's producing TNFα, IFNγ and IL-2 prior to heterotypic infection was associated with an asymptomatic infection[550].

Heather Friberg[113] suggested that as the release of the CD8 mediators was sequential starting with MIP-1b that the mono-functional response maybe due to inherent features of the epitope variant sequence effecting the length of TCR interaction, a process referred to by the Weiskopf group[110] as altered peptide ligands (APL)[559]. It has been suggested that cross-reactive CD8's may preferentially bind to heterotypic epitope variants[547], however this is not the case and instead epitopes preference is due to inherent properties of the peptides affecting HLA avidity[548].

Finally, Daniela Wesikopfs[112] retrospective study which identified considerable numbers of new CD8 epitopes, showed that during primary infection most CD8's targeted serotype-specific epitopes, however this changed to mostly targeting cross-serotype conserved epitopes in secondary infection with a different serotype. Therefore, there is some skewing of CD8 responses dependent on what epitopes are conserved between the two serotypes you have been infected with. However, these conserved epitopes were of high avidity and produced a poly-functional response (INFγ, IL2, TNFα). However, they did conduct a meta-analysis which linked HLA as a risk factor in disease severity which was associated with low CD8 response magnitude, showing that a low magnitude response was associated with a mono-functional response.

In summary, the combination of supporting evidence for both a protective and detrimental role for CD8's suggests that CD8's may play a multifaceted role in disease, which may depend on CD8 epitope characteristics in the context of epitopes variants and level of antigen presentation enhancement by ADE. This may have detrimental implications for the other two most progressed vaccines from NIH and Inviragen which contain dengue proteins targeted by both antibodies and CD8 T-cells (see 1.2.2 for details of vaccines)[110,111]. Furthermore, the tetravalent nature of these vaccines[111] may promote cross-reactive CD8's against epitope variants with unpredictable responses. The evidence therefore suggests that a vaccine based on cross-serotype conserved CD8 epitopes may more predictably raise protective poly-function CD8 responses.

An alternative/additional explanation for the considerable contradiction and confusion with the literature regarding CD8 function during dengue infection is likely due to the different methods, HLA's and epitopes used, the quick dynamics of immune cells[113,548], lack of standardised assays[471] and the problem with obtaining human samples especially at different time points during infection (acute or severe). Another consideration is the limited availably of animal models to study infection which can fully simulate a human infection[516].

5.1.3 Viral Evolution and Dynamics

Although early serological work identified four distinct circulating dengue viruses, more recent genetic analysis has identified distinct genotypes within each serotype which consist of further clades[560]. These are commonly geographically separated[560], however some 'cosmopolitan' lineages are found in multiple continents[560-562] and in some cases more than one lineage is present in the same region[563].

Dengue dynamics in endemic regions are complex, characterised by continual lineage turnover and changes in prevalence[564,565]. These lineage turnover dynamics have however been classified on a genetic level as following two non-mutually exclusive patterns, (i) an incremental spectrum of dead end variants within lineages and (ii) dramatic replacements of lineages[562,565]. Recent phylogenies based on E genome sequences have identified five genotypes in DENV1 & 2, and four genotypes in DENV3 & 4[560,566].

DENV lineages have been associated with varying disease severity[567] and transmission rates[565,568], therefore an understanding of these dynamics would greatly aid future intervention methods including vaccine design. However, in the field there is considerable controversy regarding the factors modulating lineage dynamics, with many papers supporting alternative hypothesises[560,562,564,565,568-571]. However, most agree that as yet we do not have a firm enough grasp to predict these dynamics. Within the field, three different factors have each been hypothesised to control dengue dynamics; (i) genetic fitness, (ii) population immunological status and (iii) stochastic events, each with supporting evidence from the field[560,562,564,565,568-571]. This controversy is likely a consequence of the multifactorial nature of dengue infection dynamics. Coincidently, recent work[560,562,564,572] is starting to appreciate that all three factors likely contribute in

a complex cross-talk. Using the current sphere of knowledge, a hypothetical diagrammatic representation of this complex dynamic process has been created (Figure 5-2), which is discussed in detail below.

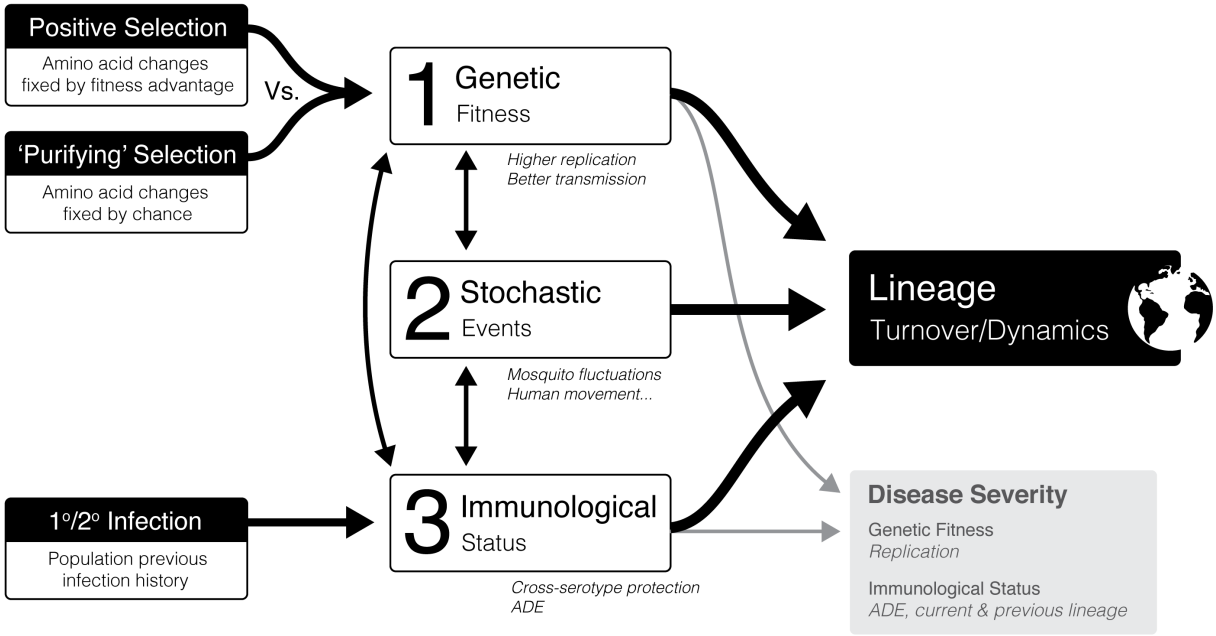

Figure 5-2 I Dengue dynamics and its implications for vaccine design. Lineage turnover and dynamics depend on three key factors; genetic fitness, population immunological status and stochastic events. 1) Genetic fitness linked to increased transmission and out competition of other lineages has been associated with positive selection of non-synonymous mutations[560,562,564] and purifying/negative selection by introduction of mutations fixed by chance that have fitness advantages in a immunological context[562]. 2) Stochastic events such as mosquito population fluctuations, human movement and seasonality may influence lineage dynamics[560,571]. 3) The immunological status of the population in context of previous dengue infection likely effects lineage dynamics by balancing between ADE-mediated infection enhancement and short-term cross-serotype protection[571,573-575]. Both viral replication rates and previous serotype/lineage infections have been associated with disease severity[564].

(i) **Genetic Fitness** is one of the most controversial areas. This is the idea that 'fitter' or more 'virulent' strains will outcompete and increase in prevalence and replace the weaker lineages (positive selection)[565]. A fitter virus can be seen as one with greater transmission, which is theorised to be related to increase replication in the vector or host and thus more 'virulent'[576,577]. Recent work supports this showing that more virulent South East Asian DENV2 strains outcompete less virulent strains in mosquitoes co-infected with both[578].

Importantly, increased DENV viral replication has been associated with more severe disease[498,579]. Evidence for positive selection and its association with virulence has been reported. For example, a replacing clade in Thailand in the 1990's was found to have higher viral titres within the mosquito hemocoel, suggesting increase transmission[565]. Furthermore, the replacing DENV2 lineage in Vietnam during the late 1990's was associated with increase viral titres in humans which was linked to increased

transmission[568]. Also, in Nicaragua a replacing DENV2 clade had nine amino acid substitutions not found in the old clade, two of which were found in the NS5 RdRp region which may affect its RdRp activity (R401K & T290I)[564]. Positive selection of non-synonymous amino acid substitutions, assessed by maximum-likelihood, has also been associated with replacement clades. For example, minor positive selection has been identified for NS2A[562,580,581], E protein[561,572] and NS1[570]. Mutations in E for example may affect cell tropism or cell fusion[572].

Positive selection of mutations is not surprising since RNA viruses lack a proofreading RdRp and are estimated to introduce one mutation per replication[560,568]. However, paradoxically and controversially, most the DENV genome has been shown to be under purifying selection, shown by low non-synonymous (dN/dS) substitution rates[569,582]. It is hypothesised that having to replicate alternately in two hosts puts significant genetic restraints on the virus, hence purifying selection. In support of this a group showed that virus, cycling in 10 alternating passages between insect and mammalian cells caused an increase in fitness in their respective cells[581]. This was not seen with one cycle alternating culture, indicating that using two hosts restricts fitness to balance effective replication in both hosts[560]. Suggesting that mutations are deleterious to survival and therefore 'purified'[570]. Consequently, this provides support for use of a conservation-based approach to design a vaccine.

Groups that support purifying selection suggested that clade replacements are instead due to stochastic bottlenecks[563,583-586]. Some possible (ii) **stochastic events** likely playing a contributing role in lineage dynamics include human population movements, mosquito population dynamics and other environmental factors[562,587]. Indicating that controlling these may have implication for vaccine efficacy by effecting the pool of genetic variants (i.e. lineages) that hosts need to be protected against.

However, it has been suggested that some amino acid substitutions fixed by chance during purifying selection, i.e. not positively selected could actually be associated with a fitness advantage when an (iii) **immunological selection pressure** is present within the population[562]. Although serotype protection is serotype-specific[103], cross-protection between serotypes has been reported for a short period after a DENV infection[103,564,571]. In support of this hypothesis a study in Thailand in the late 1990's found that a DENV1 clade replacement was associated with an overall decline in DENV1 prevalence, but increase in overall DENV4 prevalence, suggesting that the surviving DENV1 clade may have had initial less-cross protective immunity with DENV4 than the preceding DENV1 clade[562]. In further support of this, they found that amino acids changes between the two DENV1 clades were not under positive selection[562]. Furthermore it has been suggested that the replacement of DENV1 and 2 in Iquitos with DENV3 was due to low population immune protection against DENV3, which lead to increased DENV3 infections, which in turn lead to short-term cross-protection against DENV1 and 2[588].

Conversely, an increase in prevalence of lineages has been associated with infection enhancement by ADE in secondary infection using models[589], which coincidently has

been linked to increased chances of severe disease[564]. In support of this, OhAinle and colleagues[564] showed that a replacing DENV2 clade in Managua was associated with more serve disease. Interestingly, they found that disease severity risk was associated to which DENV2 clade they become infected with following a primary DENV3 infection[564]. Intriguingly a model which includes cross-protection suggests that cross-protection causes the more unpredictable dramatic lineages changes[571].

Models supporting both these scenarios have predicted that ADE enhancement and serotype cross-protection are large factors controlling dengue lineage dynamics (including replacement) and prevalence[571,573-575,590]. This considerable evidence for positive selection above, and this, suggest that both positive and purifying selection may play role.

5.1.4 Requirements of a Dengue Vaccine

The above discussion has shown that the clinical outcome of dengue infection (1^o or 2^o) in individuals likely depends on a considerable set of factors both (i) **dengue specific**, such as dengue immunological status (previous infections, order of infections)[110] and genetic fitness of the lineages infected[565,567,568], and (i) **patient specific**, such as age, HLA status and unknown genetics[553]. Furthermore, the dengue specific factors would be considerably effected by viral dynamics (Figure 5-2).

These factors also have key implications for vaccine design, which as well as eliciting life-long protection against all four serotypes, must do so without clinical symptoms in subsequent DENV infections or based on previous infections. A consequence of this has been seen in the Sanofi antibody-based vaccine, eliciting ADE[108]. Considerable evidence[110,112,113], although mixed[547,552] suggest eliciting a carefully targeted CD8 response, possibly one with MHCI interactions involving long TCR engagement that elicit polyfunctional responses and/or against epitopes conserved across serotypes without variants[112,113,547] could achieve this goal. Unlike the current poor efficacy Sanofi B-cell based vaccine[104]. To this end a conservation-based approach was used to identify inter-serotype conserved fragments with the aim of creating a vaccine with conserved epitopes able to elicit protective immune responses.

5.2 Results

5.2.1 Initial Development of an Algorithm for the Design of a Conservation-based Vaccine

The initial aim was to develop a method to identify regions of conservation across the dengue proteome, which could also be utilised by others with limited bioinformatics skills to design vaccines for other mosquito-borne viral diseases as well as dengue. To achieve this a sliding window approach was developed to assess and identify highly conservation regions.

When assessing conservation, the most important consideration is that the sequence input is a reliable representation of the population. Thus, the more sequences that can be included within the assessment the more likely the whole pathogen population can be represented both spatially and temporally i.e. obtain sequence from as many lineages as possible. Thus, globally and publically contributed sequence database are a suitable source. However, this introduces the problem of collection bias and redundancy where some lineages are over or under represented[591], due to for example a major sequencing project initiated in one country. This is important for many pathogens including dengue whose lineages are geographically based[560]. As a consequence, this bias can cause the false over-representation of amino acids at each position and give a falsely high sequence conservation. Therefore, the vaccine will only represent the lineages with which a greater number of sequences have been obtained and not the lineages where only a few sequences exist.

One approach to avoid this is to conduct phylogenetic analysis and attempt to pick representative sequences of the global population. However, this can suffer from human bias and considerable user input. Alternatively, sequences can be weighted avoiding the need for such sequence selection, and have been shown to be very effective[592,593]; whereby more diverged sequences are given a greater weighting compared to more similar/redundant sequences, allowing distant relationships greater importance[591]. In the context of dengue this would allow lineages from different geographical regions to be well represented, independent of the number of sequences available. However, an assumption must be made that lineages with few sequences from one geographical region are representative of that lineage.

Weighting methods can commonly be defined as tree-based[592,594,595], pairwise distance-based or position-based[591,596]. Tree and pairwise methods are based on the distance of each sequence from a root or specified sequence, whereas positon-based methods determine weights on positions instead of whole sequences[591]. The Henikoff position-based method was chosen due to the lack of assumptions needed (e.g. do not need to assume that the tree created is representative of the population, do not need to select a sequence/root to measure distance between) and minimal compute power needed[591].

The Henikoff position-based weighting method was therefore incorporated into a sliding window-based approach to assess conservation on an aligned sequence set. A two-step protocol was developed in the case of dengue where, (1) sequence conservation was assessed within each serotype (intraserotype conservation) which, (2) was used to cross-reference regions of shared (interserotype) conservation. Serotype conservation was assessed separately so that each serotype would be equally represented.

To assess intraserotype conservation, each sequence was first given a weighting determined by calculating a Henikoff position-specific matrix from aligned sequences[591]. The weightings for all sequences sum to 1. Sequence conservation was then determined on an incrementing window-basis with conservation at each position in the window calculated by incorporating the sequence weightings with amino acid prevalence to determine amino acid frequency (patent pending), and the mean value calculated per window. A value of 0 indicated no conservation and a value of 1 indicated fully conserved. Gaps were treated as a special amino acid character. An example is illustrated in Figure 5-3. To illustrate the effect of weighting in a real sequence set the intraserotype conservation per window from the weighted and unweighted methods using dengue sequences was plotted against window position. The 1st quartile (Q1) of the mean window conservation values was used as an arbitrary conservation cut-off and red circles used to illustrate windows where the conservation values move to the opposite side of the cut-off (Figure 5-4).

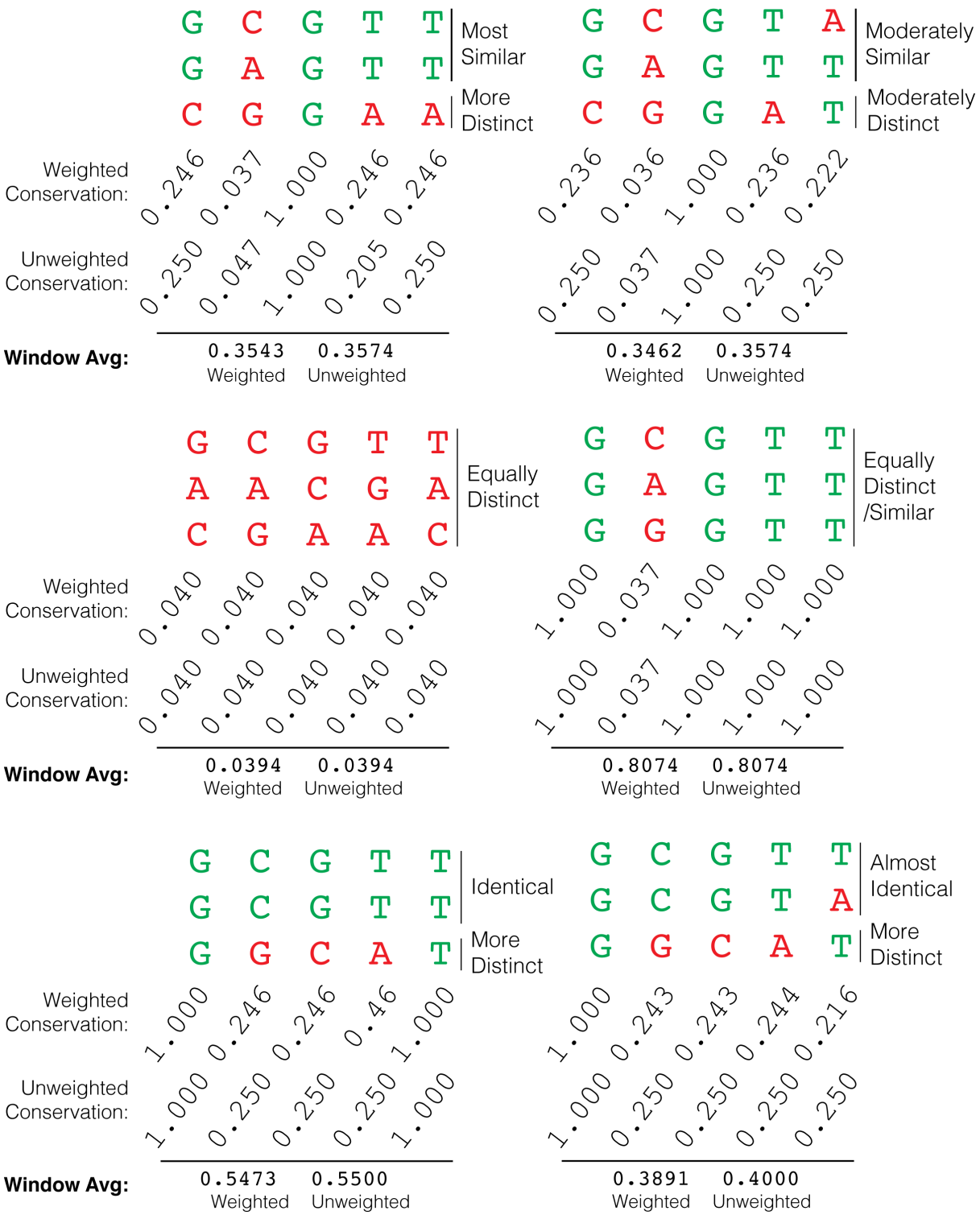

Figure 5-3 l Conservation analysis of an example window. One window with three fictional sequence were used to illustrate the beneficial effect of using weighting within the conservation algorithm. Scenarios include sequences which are of different degrees of distinctiveness. The conservation value per position and the final window average are calculated. Note that differences associated with weighting in the example are small due to using only three sequences. Red = position not conserved in majority of sequences. Green = position conserved in majority or all sequences.

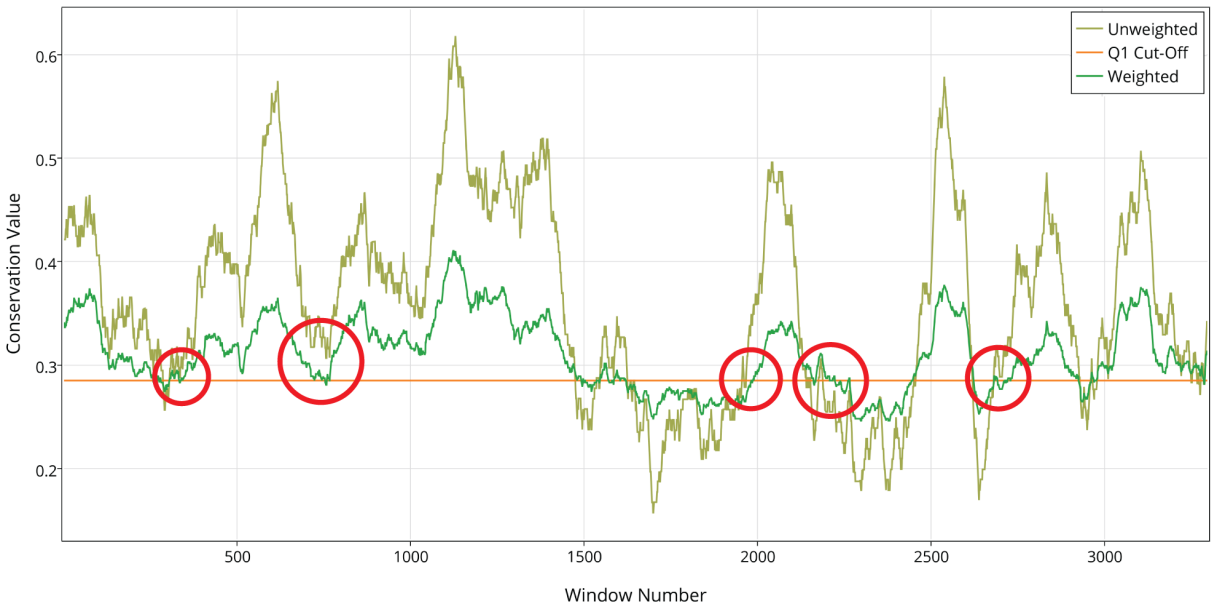

Figure 5-4 l Comparing the effect of sequence weighting using dengue. Conservation plot of DENV1 sequences with and without incorporation of sequence weighting. Red circles indicate windows which fall on the opposite side of the Q1 after weighting.

After assessing intraserotype conservation the program utilises the sequence weightings to create a weighed consensus sequence for each serotype, which can be directly compared and used in the subsequent inter-serotype conservation analysis.

Subsequently, intraserotype conservation outputs are used to assess conservation between sequence serotypes and produces a 'cumulative conservation' value per window, which is a measure of the level of shared conservations between serotypes. The value is created by first identifying windows which are all below their respective threshold for each serotype and with greater than 75% sequence identity shared between serotypes. Subsequently, the degree of deviation from the 1st quartile is calculated as a percentage of the total range of all window conservation values for each serotype. These are then combined to create a cumulative conservation value. Additionally, the program conducts the same calculation for windows conserved in only three and only two serotypes.

Using this data the weighted consensuses from each serotype is then used to create a combined inter-serotype conserved consensus using the most common residue shared between consensuses at each window with inter-serotype conservation. The final sequence output was designed to be versatile and could output regions only conserved across all serotypes, or create a mosaic based on regions conserved in only two, only three and in all four serotypes. The complete process is illustrated in Figure 5-5a. The algorithm was built into a Java-based program with user-interface (UI) to enable effective vaccine design (Figure 5-5b)

Figure 5-5 I Vaccine design program. A) Flow diagram of the vaccine design process. Sequences are collected for each serotype and manually audited before alignment. Audited sequences are processed by the program giving each a weighting value before assessment of intra- and inter-serotype conservation and final output. B) UI of Java program.

5.2.2 Sequence Collection, Sanitisation and Alignment

Sequences for the four serotypes were collected from the NCBI protein database in January 2014. Initially the NCBI Taxonomy Browser was used to obtain sequences from each of the four serotypes using their Taxa ID's; 11053, 11060, 11069 and 11070 respectively. Subtree links were used, via stating [Organism:exp] in the search. The search queries were modified to include human origin full length sequences only. Following this, sequences were reviewed to check that, (i) data only contained full length sequences, (ii) sequences with strings of X's were removed, and (iii) sequences were from natural human dengue viruses and not mosquito or laboratory modified. Table 5-1 shows the queries used and the number of sequences before and after auditing for each serotype. Following auditing the full-length sequences were subsequently aligned together using ClustalOmega command line v1.2.0 with default settings[597].

Table 5-1 I Dengue sequence collection.

DENV1			
Query	(((((txid11053[Organism:exp]) AND "Homo sapiens") NOT vaccine) NOT vaccinia)) NOT partial	***Sequence Number Pre-audit:***	1268
		Sequence Number Post-Audit:	1257
DENV2			
Query	(((((txid11060[Organism:exp]) AND "Homo sapiens") NOT vaccine) NOT vaccinia)) NOT partial	***Sequence Number Pre-audit:***	894
		Sequence Number Post-Audit:	893
DENV3			
Query	(((((txid11069[Organism:exp]) AND "Homo sapiens") NOT vaccine) NOT vaccinia)) NOT partial	***Sequence Number Pre-audit:***	660
		Sequence Number Post-Audit:	660
DENV4			
Query	(((((txid11070[Organism:exp]) AND "Homo sapiens") NOT vaccine) NOT vaccinia)) NOT partial	***Sequence Number Pre-audit:***	120
		Sequence Number Post-Audit:	119

Queries with NCBI taxa ID used to collect sequences with the number of sequences collected and the number after auditing.

Sequence metadata, including collection location and date was also collected for further analysis. Sequences missing metadata variables were excluded. Sequences were from 29, 28, 31 and 14 countries for DENV1, DENV2, DENV3 and DENV4 respectively, representing the Americas, Africa and Asia-Australasia (Figure 5-6a-b). The majority of DENV1 sequences were from Asia, particularly Vietnam which accounted for 67% of the total sequences. DENV2 and 3 sequences contained similar numbers of America and Asia-Australasia sequences and DENV4 mainly America sequences. Assessing sequence collection date showed that the majority of sequences were collected within the past 10 years, indicating that only relatively new lineages will be present (Figure 5-6c).

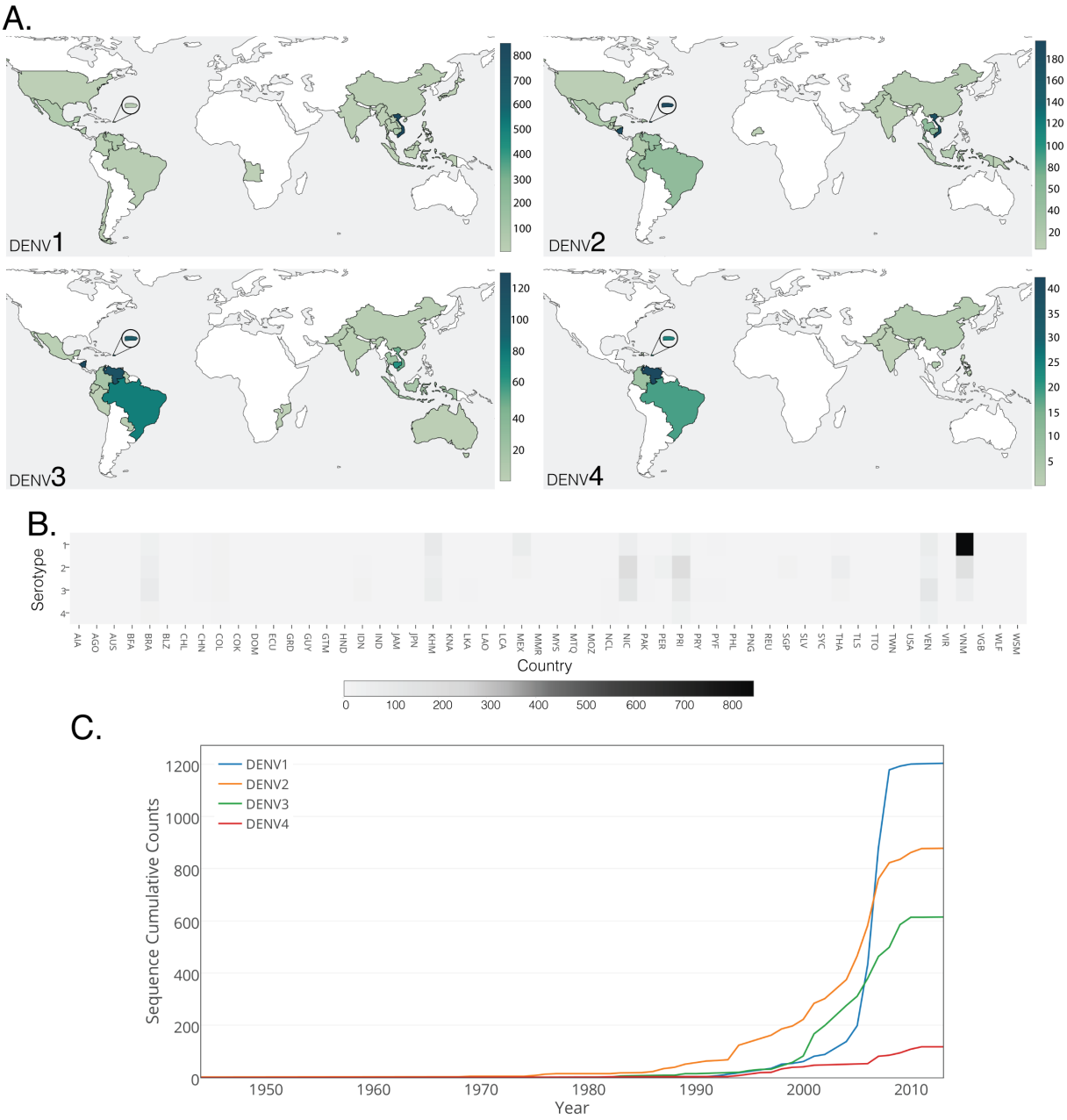

Figure 5-6 I Sequence characteristics. A) Choropleth maps showing the number of sequences per country for each serotype. B) Heatmap showing the number of sequences collected from all countries for each serotype. C) Cumulative sequence count per year for each serotype.

5.2.3 Intra-Serotype Diversity Calculations

Aligned full length sequences from each serotype were separated and processed individually using the Henikoff weighted sliding window method to determine intra-serotype conservation. To allow comparative analysis of Henikoff weightings between serotypes, the Henikoff sequence weightings from each serotype were normalised based on the number of sequences. Henikoff weightings for each serotype showed a non-normal distribution with a left median shift from the expected mean/median (median=mean) if all sequences had the same weighting value, with deviations from the expected mean of -11.6%, -7.3%, -4.2% and -2.6% for DENV1 to 4 respectively (Figure

5-7a), with normalised median weighting values of 0.8957, 0.9317, 0.9600 and 0.9751. A median of 1 would indicate equal weighting of each sequence and thus equal sequence variance. This indicated a greater number of similar sequences in the DENV1 sample and the least in DENV4. Consequently, this meant DENV4 contained more unique/distinct sequences. Normalised medians were found to be significantly different by Kruskal-Wallis (****$p<0.00001$).

A key benefit of the weighting method is to prevent large numbers of sequences of certain lineages from biasing the results and thus providing poor representation of all dengue lineages. Geographical location is a key determinant of dengue genetic lineage dynamics and as such lineages are generally geographically based[560]. It would therefore be expected for countries with large numbers of sequences to have a low median sequence weighting due to relatively high conservation. To investigate this, sequences were stratified by country of origin and the median weighting per country calculated (Figure 5-7b). An inverse correlation between median sequence weight per country and the number of sequences per country was identified for all serotypes (Figure 5-7c), supporting this hypothesis.

The benefits of weighting were illustrated in DENV1 where Vietnam contributes 67% of the total sequences but has a median weighting within the lower quartile (Figure 5-7b), indicating limited sequence variation and therefore without weighting would over-represent this particular lineage and bias conservation calculations.

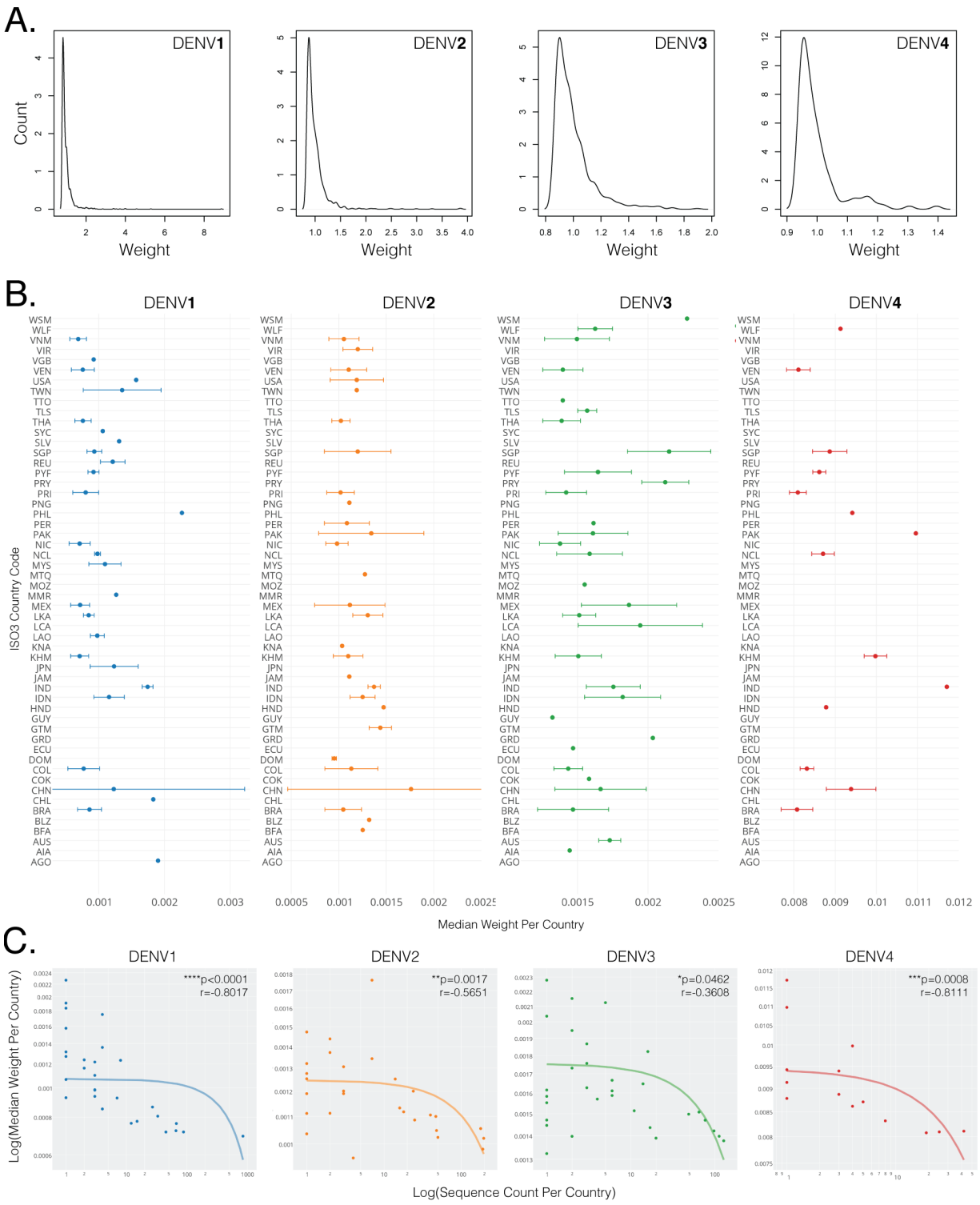

Figure 5-7 I Weighting stratified by country of origin. A) Histograms of Henikoff sequence weighting values for each serotype. Weighting values were first normalised by sequence number to allow comparison between serotypes. B) Median sequence weighting values stratified by country of origin. Error bars represent IQR. C) Log of median country weight against log sequence count per country with linear regression (y=mx+c). Correlation was assessed using non-parametric Pearson's correlation.

Initially, serotype conservation was assessed using a sliding window size of 100 amino acids (aa) to identify trends across serotypes (Figure 5-8). All four serotypes shared a

similar diversity signature upon visual inspection, however DENV1, 2 & 3 had the greatest median diversity and IQR, indicating greatest diversity across the length of the proteome compared to DENV4 (DENV1: 0.33±0.20; DENV2: 0.27±0.20; DENV3: 0.20±0.20; DENV4: 0.07±0.11; Median±IQR).

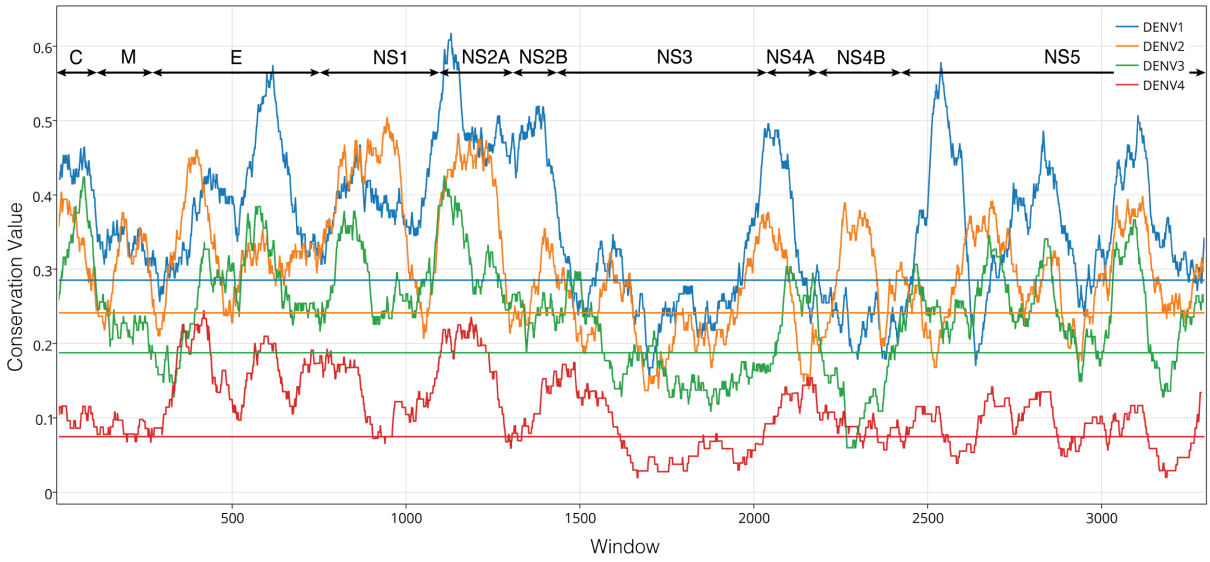

Figure 5-8 I Comparing serotype conservation. Intra-serotype conservation window values across DENV1-4 proteome using window size of 100 amino acids. Lines represent Q1 for each serotype. Arrows indicate individual proteins.

Serotypes were then processed using a windows size of 15 aa to best represent MHC peptides (Figure 5-9a-d). The 1st quartile (red line) was used as an arbitrary cut off for conservation, with windows below classed as conserved within their respective serotypes. For each serotype (DENV1-4), only 3%, 4%, 4% and 3% respectively of the windows below the Q1 threshold were located within structural proteins, indicating that the structural proteins showed less conservation than non-structural proteins.

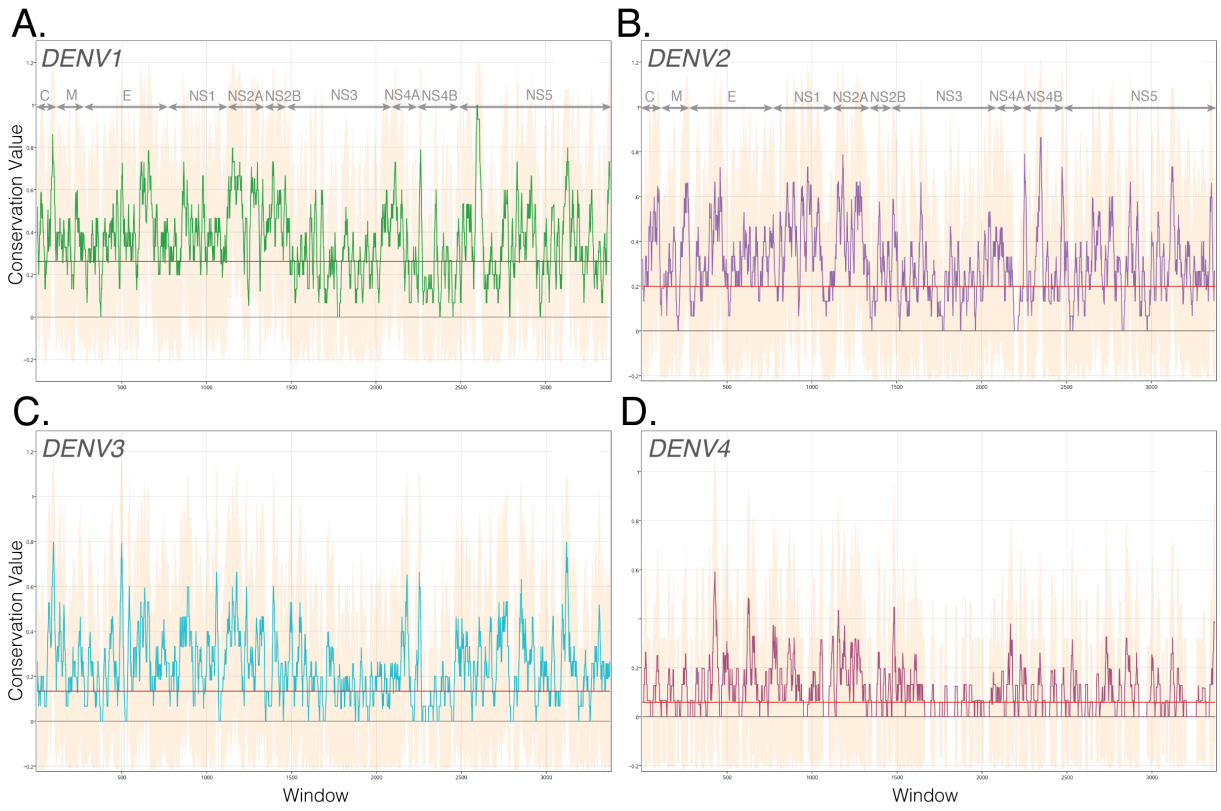

Figure 5-9 I Intra-serotype dengue conservation. A-D) Intra-serotype conservation for DENV1-4 respectively with window standard deviation in orange and 1st quartile as red line. A window size of 15 aa was used

Finally, the sequence weightings were used to create a weighted consensus sequences for each serotype. To do this each position was assessed for the most common residue but incorporating the Henikoff weighting to determine the representation of each residue and provide a consensus sequence representative of the population for each serotype. The shared percentage identity of the four weighted intra-serotype consensuses was then compared using a 15 aa sliding window to provide an early assessment of sequence similarity across serotypes (Figure 5-10). This showed that NS2A in particular, had limited cross-serotype conservation. However, regions of shared consensus identity do not necessarily indicate that the regions are conserved within each serotype. To assess this the window conservation values were also considered using the cumulative conservation algorithm explored in the next section.

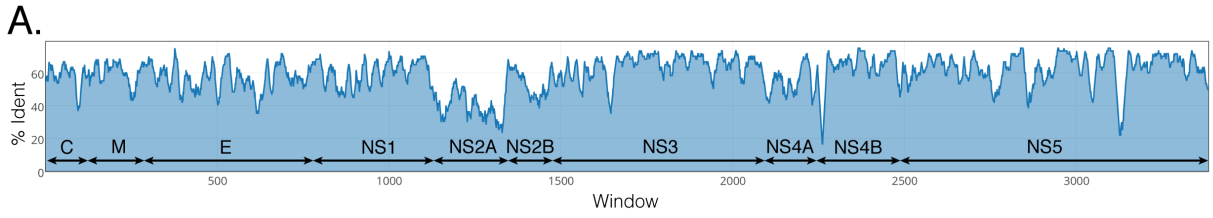

Figure 5-10 I Inter-serotype consensus percent identity. Percentage of identity of each weighted serotype consensus assessed by a 15 aa sliding window.

5.2.4 Inter-Serotype Diversity Calculations

To assess inter-serotype conservation 'cumulative conservation', which combines whether windows are below their respective serotype thresholds and their magnitude from each serotype was assessed. Corresponding windows conserved in either all four (4Sero), only three (3Sero), or only two (2Sero) serotypes were identified and the relative degree of conservation below their respective thresholds was calculated as a cumulative conservation value (Figure 5-11a-d).

Four distinct regions with high levels of cumulative conservation in all four serotypes were found in NS1, NS3, NS4 and NS5, but not in the structural proteins (Figure 5-11b). The clustering suggested a functional correlation. Cumulative conservation shared between two and three serotypes identified a greater number of regions which still clearly clustered with the four non-structural proteins in three serotypes but also showed limited cumulative conservation in the three structural proteins, mainly C and M (Figure 5-11c). Cumulative conservation between two serotypes showed a similar trend with a small degree of cumulative conservation in the E protein (Figure 5-11d). However, of all the proteins the E protein showed the lowest level of cumulative conservation. The highest level of cumulative conservation was identified in NS3, in a region conserved in all four serotypes with a value of -69 (out of -100).

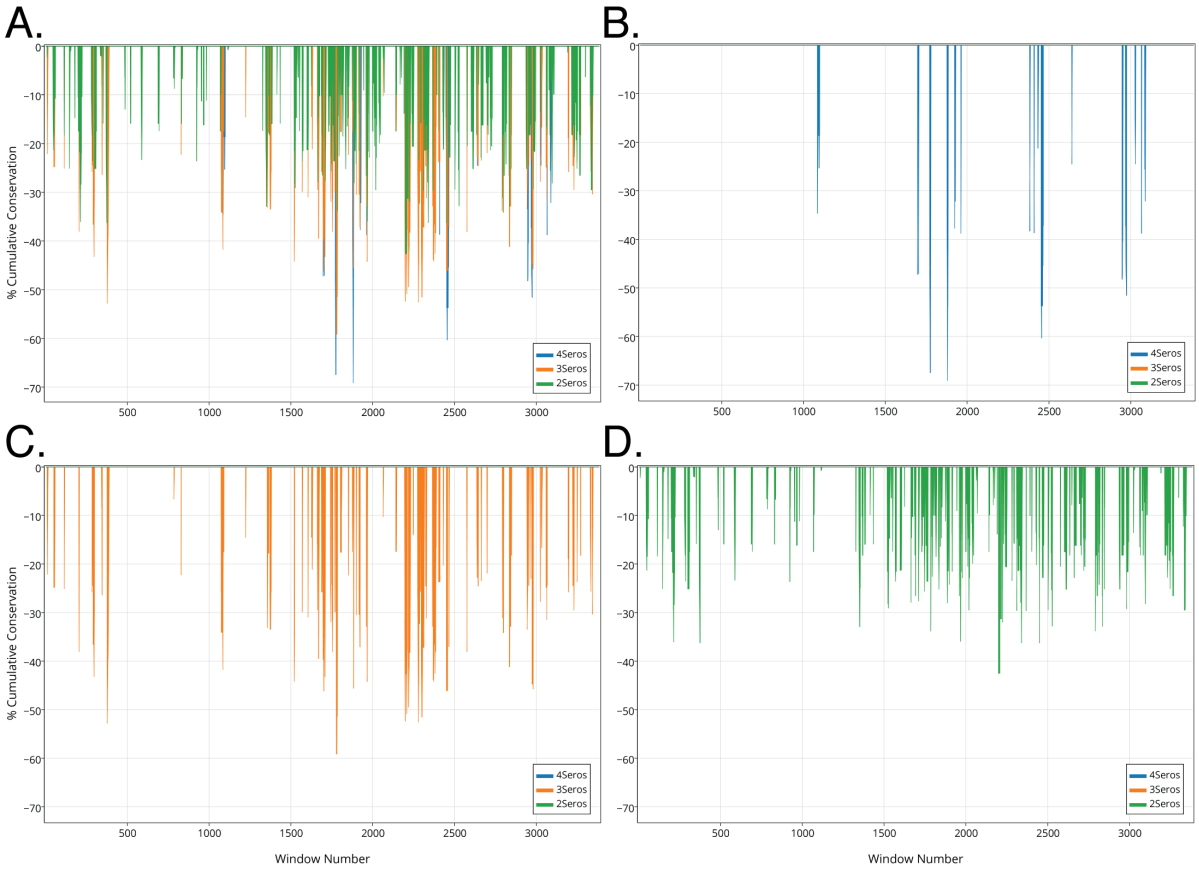

Figure 5-11 I Cumulative conservation across dengue serotypes. A) Cumulative conservation in windows conserved in four, three, and two serotypes. B) Cumulative conservation in windows conserved in four serotypes. C) Cumulative conservation in windows conserved in three serotypes. D) Cumulative conservation in windows conserved in two serotypes.

5.2.5 Creating a Representative 'Smart' Consensus

Following the identification of window positions conserved across different combinations of serotypes a 'smart' consensus was created (Figure 5-12); a mosaic which combined windows that showed cumulative conservation from the weighted consensus from each serotype. The serotypes combined depended on which serotypes showed cumulative conservation; four, three or two serotypes. For example, a window with cumulative conservation in all four serotypes (4Sero) would use all four weighted serotype consensuses to create the inter-serotype consensus. A window with cumulative conservation in only DENV1 and 2 would only be based on those two weighted serotype consensuses. This created a mosaic of 2269 aa, totalling 87 fragments. 16 fragments (total 319 aa) were conserved in all four serotypes. The percentage identity of each fragment conserved in all four serotypes was compared to the four weighted consensus sequences and had a mean % identity of 92%±3.6.

```
----RKKAAKPSFNMLKRARNRVSTV-------------------LVMAFIAFLRFLAIP
PTAGILARWGQFKK-------------------------------------MAFHLTTR
DGEPHMIVA----------------NKCTLIAMDLGELCEDTITYKCP----------DC
WCNATDTWVTYGTC---GEHRREKRSVALAPHVGMGLETRTETWMSSEGAWKHAQRVESW
ALR-----------------------------------GMRCVGVGNRDFVEGLSGATW
VDVVLEHGGCVTTMAKDKPTLDFEL-------LALLRKLCIEAKISNITTDSRCPTQGEP
SLNEEQ--NFVCKHTFVDRGWGNGCGLFGKGSLVTCAKFKC-------------------
ITVHTGDQHQVG---------------------------------------------LLK
M--KAWLVHKQWFFDLPLPWLPGA--------------TFKNAHAKKQDVVVLGS-----
-----------------------------------------GKFKIDKEMAETQHGTT
LVK-----------------------------------------------------------
---------------------------GAKRMAILGDTAWDFGSVGGL------------
-----------------------------------AM-----------------------
-NWKGKELKCGSGIFVTNEVHTWTE----------------------GVCGIRSATRLEN
LMWKQIANELN---------------------------------------------------
----------------------RAWNSLEVEDYGFGVFTTNIWL-------ELCDHRLMS
AAIKDEKAVHADMGYWIESEKNGSWKIEKASLIEVKTC---KSHT---------------
-------------------------------------------HRGPSLRTTTASG
KLITEWCCRSCTLPPLRFRGEDGCWYGMEIRPLKEKEENLVKSLVSAGHGE-----LG--
-----------------------------------------------------------
----------------------LTSRELLLLTIGLAL-----------------------
-----------------------------------------------QQKADWI
PLAAGILGAKPLAIFLMTLMK-AK-RSWPLNEAIMAVGLVSILASSLLKNDVPMAGPLVA
GGLLIACYVITGRSADLELE-------------SGSSPIIEIKIDEDG-FRIKDDEEENI
LTILIKTALITVSGIFPLAIPATAAAWHLWQVK-TQRSGVLWDVPSP-----AELD----
----------SQIGAGVFKEGVFHTMWHVTRGAVLMHQGKRIEPSWADVKKDLISYGGGW
RLEGEWDEGEEVQVIAVEPGKNPKAVQT---------GEIGAIALDFKPGTSGSPIVNRE
G--VGLYGNGVVTKSGAYVSAIAQT--------------FRKRNLTIMDLHPGAGKTKR
YLPAIVREAIKRRLRTLILAPTRVVAAEMEEALKGLPIRYQTTAIKAEHTGKEIVDLMCH
ATFTMRLLSPVRVPNYNLIIMDEAHFTDPASIAARGYISTRVEMGEAAAIFMTATPPGSA
```

```
DAFPQSNAPIEDEEREIPERSWNSGFDWITDFAGKTVWFVPSIKAGNDIANCLRKNGKKV
IQLSRKTFDTEYPKTKLNDWDFVVTTDISEMGANFKADRVIDPRRCLKPVILTDGPERVI
LAGPMPVTAASAAQRRGRIGRNHKKENDQYIYMGQPLNNDEDHAHWTEAKMLLDNINTPE
GIIPALFEPEREKSAAIDGEYRLRGEARKTFVELMRRGDLPVWLSYKVASAGFQYKDREW
CFDGERNNQILEENMDVEIWT-EGE-KKKLRPRWLDARTYADP----------------
--------------------------------------HALEELPETLETLLLLALLG-
-----FLFFLSGKGIGKMSIGLCCIIAAS-LLWMAEIQPHWIAASIILEFFLMVLLIPEP
EKQRTPQDNQLAYVVIGILTLAAAIAANEMGLLETTKKDLGIG----------AILDVDL
HPASAWTLYAVATTIITPMLRHTIENSTANVSLTAIANQAAVLMGLDKGWPISKMDLGVP
LLALGCYSQVNPLTLT--------HYAIIGPGLQAKATREAQKRTAAGIMKNPTVDGIMA
IDLDPIPYDPKFEKQLGQVMLLILC-SQILLMRTTWALCEALTLATGPITTLWEGNPGKF
WNTTIAVSMANIFRGSYLAGAGLAFSLIKN-----------GETLGEKWKRQLNQLDKS-
FEEYKKSGILEVDRTEAKEAI------------------------MV-----VIDLGCGR
GGWSYYCAGLKKVR---GYTKGGPGHEEPIPMATYGWNLVKLHSGVDVFF---EKCDTLL
CDIGESSPNPTIEEGRTLRVLKMVEPWLKG-NQFCIKILNPYMPSVIE-LEKLQRKHGGM
LVRNPLSRNSTHEMYWVSNGTGNIVSAVNMISRMLINRFTMAHK----------------
------------------------------DEDNPYKTWAYHGSYEVKATGSASSMVNGV
VKLLTKPWDVVPMVTQMAMTDTTPFGQQRVFKEKVDTRTPEA------------------
----------------------------QDENGWKSA------------------LHLE
GKCESCVYNMMGKREKKLGEFGKAKGSRAIWYMWLGARFLEFEALGFLNEDHWFSRENSL
SGVEGEGL--LGYILRDISKIPGGAMYADDTAGWDTRITEDDLHNEEK-----------L
AKAIFKLTYQNKVVKVQRPTPRGAVMDIISRKDQRGSGQVGTYGLNTF-TNMEAQLIRQM
EAE-----------------------------------------------------------
----------QWEPSKGWHDWQQVPFCSHHFH-IFMKDGRKLVVPCRNQDELIGRARISQ
GAGWSLRETACLGKSYAQMWQLMYFHRRDLRLASNAICSAVPSHWVP-SRTTWS----HE
WMTTEDMLAVWNRVW-------------HSWEDVPYLGKREDQWCGSLIGLTSRATWAKN
           I-----------GNEEY---------------------
```

Figure 5-12 I Mosaic consensus sequence. Mosaic consensus sequence generated from regions conserved in four, three or two serotypes. Dashes (-) represent regions either conserved in one serotype only or not conserved at all. Grey highlight indicates regions conserved in all four serotypes.

5.2.6 CD8 Epitope Analysis

The aim of this vaccine was to raise a protective CD8 response, therefore *ex vivo* identified CD8 DENV epitopes were mapped onto the 'smart' consensus and characterised. The IEDB was queried to return MHCI epitopes associated with *ex vivo* human CD8 responses irrespective of HLA type from published literature. The majority (83%) of known epitopes (including variants) were however recently identified by Daniela Weiskopf and colleagues in a 2013 study[112]. Weiskopf epitopes were obtained by measuring *ex vivo* IFNγ responses against over 400 predicted epitopes from Sri Lankan individuals seropositive for dengue, independent of whether it was homologous or heterologous; which they found did not affect spot forming cell (SFC) responses[112]. They identified 25 epitopes (and any variants between serotypes) which they classed as being in immunodominant regions (mostly NS regions) of the DENV proteome. The

remaining IEDB epitopes were identified by either chromium cytotoxicity assay, or intracellular cytokine staining (ICS). The 25 epitopes from Weiskopf *et al*[112] and the remaining 10 from IEDB were collected and cross-referenced with the collected DENV sequences to identify 15 unique epitopes (with their variants) present within the raw sequences and within a window below the conservation threshold of the respective serotype(s). These are illustrated in Table 5-2 by a green cell with a tick. These matched epitopes covered 13 HLA alleles.

Table 5-2 I Epitopes found below threshold in at least one serotype.

Epitopes	Position	In 'Smart' Vaccine	Serotype found in (Below Threshold)				% of Seqs Below Threshold	Total % of Seqs	Individual T-cell Response	HLA Types
			1	2	3	4				
Wesikopf Epitopes										
LPVWLSYKV	2013	✔	✓	✗	✗	✓	49.9		313	B*5101
APTRVVASEM	1694	✘	✓	✗	✗	✗	25.0		607	B*0702
APTRVVAAEM		✔	✗	✓	✓	✓	75.0		1623	B*0702/3501
TPEGIIPAL	1971	✔	✓	✗	↑	✗	25.0	74.8	2396	B*0702
TPEGIIPALF		✔	✓	✗	↑	✗				B*3501
TPEGIIPSM		✘	✗	✓	✗	✗	24.9		4686	B*3501/5301
TPEGIIPSMF		✘	✗	✓	✗	✗				B*0702/3501
TPEGIIPTLF		✘	✗	✗	✗	✓	25		2914	B*3501/0702/5301
GEARKTFVEL	1999	✔	↑	✓	✗	✗	0.1	25	1330	B*4001
GEARKTFVDL		✘	✗	✓	✗	✗	24.9		1405	B*4001
GEQRKTFVEL		✘	✗	✗	✗	✓	25.0		1050	B*4001
GEFRLRGEQR	1993	✘	✗	✗	✗	✓	25		1373	B*4001
DPASIAARGY	1762	✔	↑	✓	✓	✗	49.9	55.4	2383	B*3501
DTTPFGQQR	2834	✔	↑	✓	✓	✓	74.9	99.9	3260	A*6801/3301
IANQATVLM	2309	✘	✗	✓	✗	✗	24.9		1518	B*3501
ATGPITTLW	2438	✔	↑	✗	✓	✗	25.0	50.0	505	B*5801
TPMLRHTIEN	2291	✔	✗	✗	✓	✓	50		388	B*0702
IEDB Epitopes										
SVKKDLISY	1541	✘	✓	✗	↑	✗	25.0	48.8	N/A	B62
ILLMRTTWA	2422	✔	✓	✗	✗	✗	25.0		N/A	A2
VLLMRTTWA		✘	✓	✗	✗	✗	0.1		N/A	A2
FLDLPLPWT	486	✘	✓	✗	↑	↑	25	48.7	N/A	A2
TPEGIIPAL	1971	✔	✓	✗	↑	✗	25	49.9	N/A	B35/*0702
TPEGIIPSM		✘	✗	✓	✗	✗	24.9		N/A	B*3501/5301/0702
TPEGIIPSL		✘	✗	✓	✗	✗	0.1		N/A	B35
TPEGIIPTL		✘	✗	✗	✗	✓	25		N/A	B*3501
ALRGLPIRY	1705	✘	✗	✓	✗	↑	25	49.7	N/A	B62/*0301
GTSGSPIINRE	1605	✘	✗	✗	✓	✗	29.9		N/A	A11

Epitopes conserved in at least one serotype, their position, whether they are present within the 'smart consensus', which serotype they are conserved in (green box + ✔ = conserved, red box + ↑ = present but not above the Q1 threshold, grey box + ✗ = not present), the percentage of sequences they are found in (total % of sequences = the number of sequences in all 4 serotypes that the epitope is found in, % sequences below threshold = how many of the sequences in all 4 serotypes that the epitope is found in below the Q1 threshold) and HLA types that the epitopes were tested against. The T-cell responses from the Weiskopf *et al*[112] were also included.

Epitope 1694 with its variant was the only epitope found in all serotypes below the conservation threshold. Epitope 1971, 2834 and their variants were found conserved in three serotypes and epitopes 2013, 1999 and 1762 were found conserved in two serotypes. The remaining four were only found below the threshold in one serotype. Four of the epitopes contain variants and thus only one variant was present in the smart consensus. Other epitopes were not present as they were only found in one serotype below the threshold and in the remaining serotypes they were above the threshold.

The epitope variants were restricted by serotype and found present in >97% of sequences of that serotype. The only exception was GEARKTFVEL which was a rare variant (0.1%). Furthermore, the ILLMRTTWA epitope had one rare variant, which were all found in serotype 1. Excluding variants, 10 (67%) of the epitopes were found in the smart consensus.

Epitopes below the threshold in at least one serotype were mapped onto the cumulative conservation plots (Figure 5-13a-b) and compared to experimental *ex vivo* IFNγ (SFC) data from Weiskopf *et al*[112] (Table 5-3). Only epitopes found below the threshold in two or more serotypes are associated with a cumulative conservation value. Epitope 1694, which was present in all four serotypes and gave the highest cumulative conservation value (-47.3) did not give the highest SFC (Table 5-3). The two highest responders, 1971 and 2834 correlated with cumulative conservation in two and three serotypes respectively in NS3 and NS5.

Although, all but one IEDB epitope was found in only one serotype below the threshold, three matched with cumulative conservation (Table 5-3). This suggested that the other serotypes may contain unreported variants of these epitopes, similar to the Weiskopf epitopes.

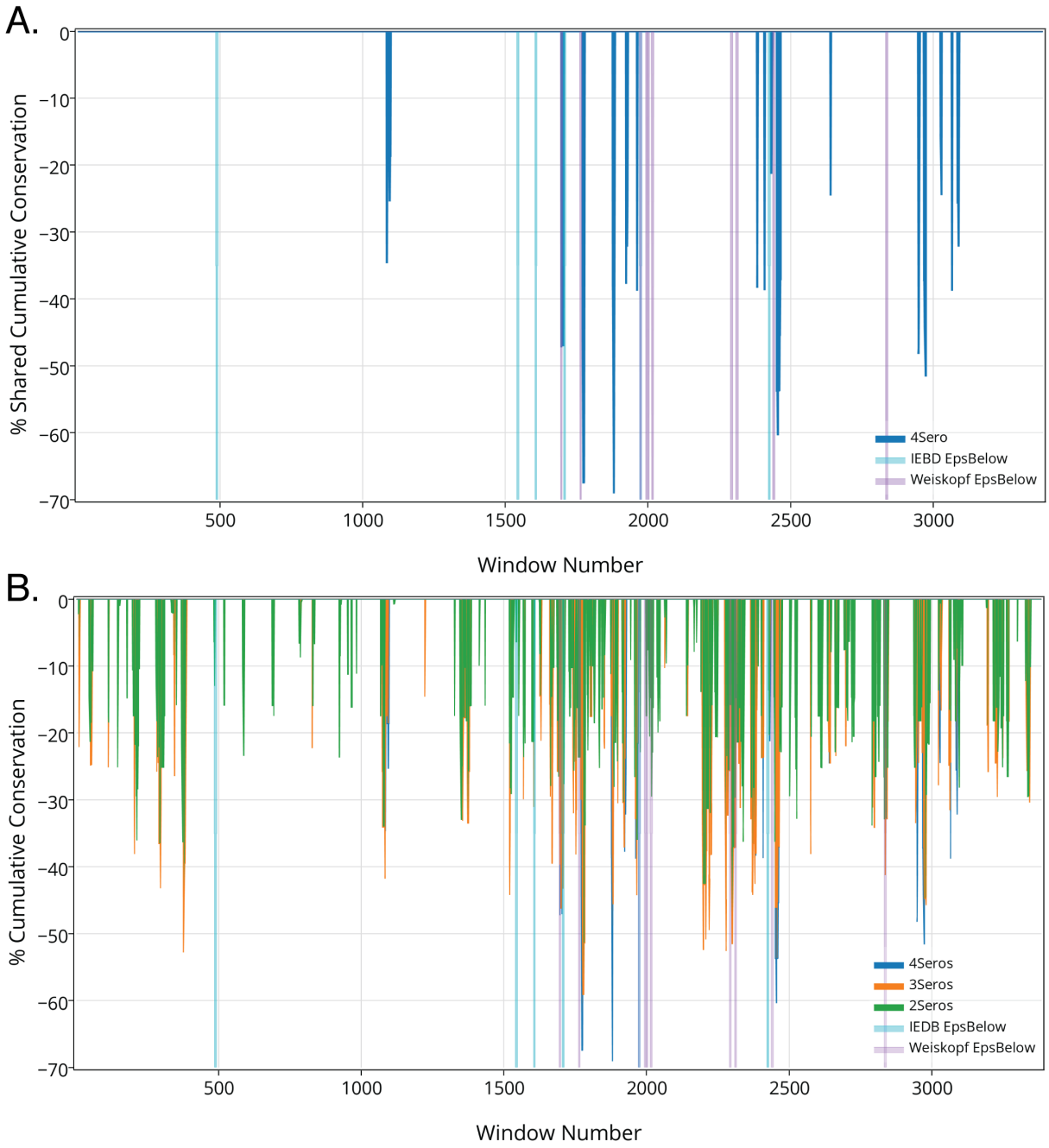

Figure 5-13 I Epitopes conserved in at least one serotype. A) Cumulative conservation for regions conserved in all four serotypes with epitopes from Table 5-2 mapped. B) Cumulative conservation for regions conserved in all four, three and two serotypes with epitopes from Table 5-2 mapped.

Table 5-3 I Cumulative conservation vs. T-cell response.

Epitopes (inc Variants)	Number of Serotypes Present in Below Threshold	Mean T-Cell Response	Cumulative Conservation Value (2-4 Serotypes)			Protein
			2Sero	3Sero	4Sero	
Weiskopf						
2013	2	313	**-22.3**	0	0	NS4A
1694	4	1115	0	0	**-47.3**	NS3
1971	3	3341	**0**	**-16.4**	0	NS3
1999	2	1261.7	**-17.5**	0	0	NS3
1993	1	1373	0	0	0	NS3
1762	2	2383	**-23.6**	0	0	NS3
2834	3	3260	0	**-36.2**	0	NS5
2309	1	1518	0	**-29.7**	0	NS4B
2438	1	505	0	0	0	NS4B
2291	2	388	**-15.74**	0	0	NS4B
IEDB						
1541	1		**-6.4**			NS3
2422	1		0	0	0	NS4B
486	1		0	0	0	E
1971	3		**0**	**-16.4**	0	NS3
1705	1		0	**-35.7**	0	NS3
1605	1		**-19.1**	0	0	NS3

Cumulative conservation value, mean epitope T-cell response of all variants from Weiskopf *et al*[112] and location of epitope locations found conserved within the smart consensus. Epitopes from Table 5-2.

There was no correlation between cumulative conservation and mean individual T-cell response for the Weiskopf epitopes (Pearson's: r^2=0.07160, p=0.2676; Figure 5-14a) and no significant difference between the mean T-cell response of Weiskopf epitopes in conserved and non-conserved windows (Mean±SEM in conserved windows: 1546±351.2, in non-conserved windows: 1897±234.8; Figure 5-14a-b). All epitopes in non-structural regions were found in NS3, NS4 and NS5.

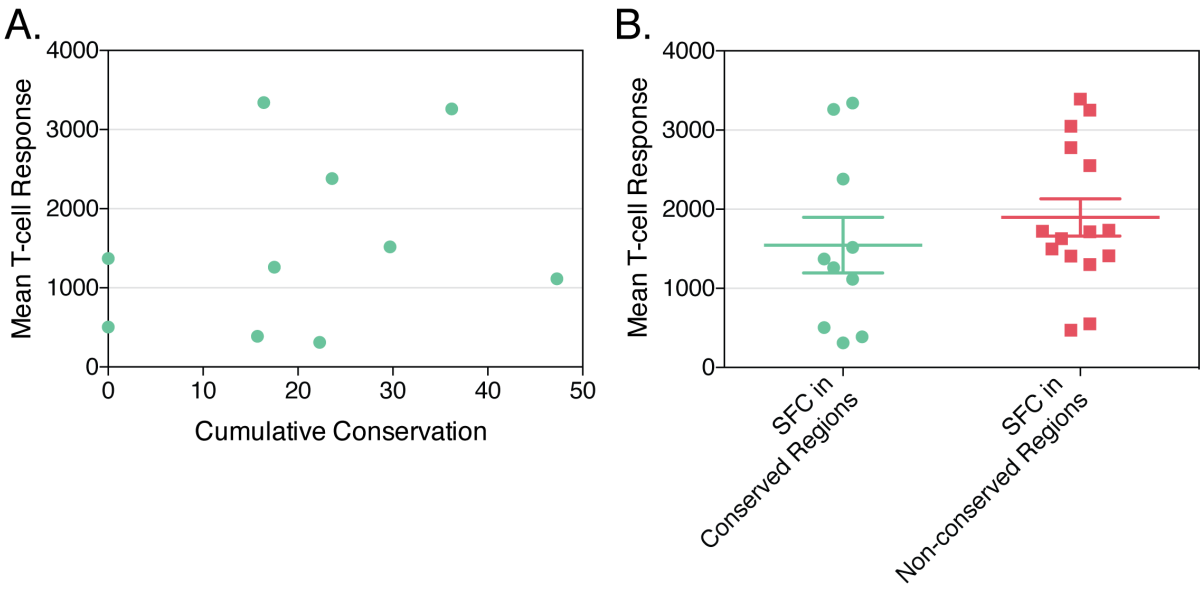

Figure 5-14 I T-cell correlations. A) Cumulative conservation value against mean T-cell response[112] from epitopes found in conserved windows. B) Mean T-cell response[112] from epitopes found in either conserved or non-conserved windows. Groups compared using unpaired two-tailed T-test. SFC; Spot-forming cells.

Finally, Syfpeithi[598] was used to predict any remaining epitopes within the 4Sero fragments in the smart consensus using nonamers and all available MHCI types, with a score >21 classed as significant (Table 5-4). Syfpeithi predicted 26 epitopes, two within the previously experimentally discovered epitope (APTRVVAAEM). 31% of the predicted epitopes were found within all four serotypes. The remaining epitopes contained variants within the other serotypes.

Table 5-4 I Syfpeithi predicted epitopes in 4sero cumulative conservation consensus.

Windows	4sero Cumulative Consensus	Syfpeithi Predicted Epitopes	HLA [Score]	Serotypes In
1085	EWCCRSCTLPPLRFR	RSCTLPPLR	HLA-A*11:01 [22]	1,2,3
		CTLPPLRFR	HLA-A*68:01 [22]	1
		CRSCTLPPL	HLA-B*27:05 [22] HLA-B*39:01 [23]	1,2,3
1087	CCRSCTLPPLRFRGE	RSCTLPPLR	HLA-A*11:01 [22]	1,2,3
		CTLPPLRFR	HLA-A*68:01 [22]	1
		CRSCTLPPL	HLA-B*39:01 [23]	1,2,3
1091-8	CTLPPLRFRGEDGCWYGMEIRP	None		--
1697	LILAPTRVVAAEMEE	LILAPTRVV	HLA-A*02:01 [25]	1,2,3,4

		ILAPTRVVA	HLA-A*02:01 [22] HLA-A*03 [25]	1,2,3,4
1703	RVVAAEMEEALKGLP	EMEEALKGL	HLA-A*26 [24]	3
		MEEALKGLP	HLA-B*45:01 [23]	3
1771-1776	SIAARGYISTRVEMGEAAAI	VEMGEAAAI	HLA-B*44:02 [23]	4
1877-82	LNDWDFVVTTDISEMGANFK	DISEMGANF	HLA-A*26 [23]	1,2,3,4
1924-8	PMPVTAASAAQRRGRIGRN	ASAAQRRGR	HLA-A*11:01 [23]	1,3,4
		VTAASAAQR	HLA-A*68:01 [24]	1,3
1962	DHAHWTEAKMLLDNI	EAKMLLDNI	HLA-B*08 [22]	1,2,3,4
2383	KRTAAGIMKNPTVDG	None		
2408	YDPKFEKQLGQVMLL	KQLGQVMLL	HLA-B*13 [22]	2,3,4
2432-4	MRTTWALCEALTLATGP	ALCEALTLA	HLA-A*02:01 [22]	2,3
2452-5	LWEGNPGKFWNTTIAVSM	None		--
2457-65	PGKFWNTTIAVSMANIFRGSYLA	AVSMANIFR	HLA-A*11-01 [25] H:A-A*68-01 [22]	1,2,3
2640	LCDIGESSPNPTIEE	None		--
2948-51	YNMMGKREKKLGEFGKAK	KLGEFGKAK	HLA-A*03 [28]	1,2,3
		KREKKLGEF	HLA-B*27:05 [27]	1,2,3,4
2967-73	SRAIWYMWLGARFLEFEALGF	YMWLGARFL	HLA-A*02:01 [23]	1,2,3,4
		ARFLEFEAL	HLA-B*14:02 [27] HLA-B*27:05 [26] HLA-B*27:09 [23]	1,2,3,4
		SRAIWYMWL	HLA-B*39:01 [22]	1,2,3,4
3026-29	MYADDTAGWDTRITEDDL	DTRITEDDL	HLA-A*26 [24]	1,3,4
2065	FKLTYQNKVVKVQRP	LTYQNKVVK	HLA-A*03 [22] HLA-A*11:01 [25]	3,4
3085-9	VMDIISRKDQRGSGQVGTY	DIISRKDQR	HLA-A*68:01 [22]	2,3,4

Epitopes predicted using Syfpeithi from smart consensus fragments conserved across all four serotypes (4Sero). The Syfpeithi score is given in [square] brackets with the predicted HLA type. Serotypes that the epitopes are found in is given. Experimentally defined epitopes highlighted in grey.

5.2.7 Functional Domain Analysis

4Sero regions were analysed for critical domains to investigate whether this explained their high level of inter-serotype conservation (Table 5-5). Fragments were located within NS1, NS3, NS4B & NS5 and found within critical catalytic domains in NS3 and NS5 (Figure 5-15). 4Sero fragments were mapped onto the crystal structures for NS3 (associated with ADP) (PDB ID: 2JLZ)[481,599] and NS5 (PDB ID: 2J7U)[600] in cyan (Figure 5-16a-b).

NS3 carries out multiple functions during viral replication mediated by its serine protease, NTPase/Helicase and RNA triphosphate activity[601]. Five conserved regions were identified exclusively within the NTPase/Helicase, which consists of three structural domains (DI-III) containing six motifs (1-6)[601]. Conservation was identified in all domains and within motifs 1a, 5 and 6. Magnesium ion interaction within motif 2 is critical for function. NTP interactions have been predicted in Domain DI and II (inc Motifs 1, 2, 5, 6) and RNA interactions in DI an II (Inc Motifs 1a, 4)[601-603]. Furthermore, residues in motif 6 have been identified as critical for NTPase and Helicase activity[604].

NS5 has methyltransferase and RdRp activities important in viral RNA replication[605]. Six conserved regions in NS5 were identified both within the methyltransferase domain and the RdRp domains. The conserved region in the methyltransferase was part of the KDKE catalytic site[605]. The RdRp folds into a right hand structure with a central palm and finger and thumb domains[605]. NS4 is not well characterised[485], however the cumulative conservation pattern shown for NS3 and NS5 domains would suggest a possible active site for NS4B.

Table 5-5 I 4Sero cumulative conservation sequences and identified domains.

Windows	4sero Cumulative Consensus	Cumulative Weight	Region/Domain	
1085	EWCCRSCTLPPLRFR	-34%	NS1	
1087	CCRSCTLPPLRFRGE	-18%	NS1	
1091-8	CTLPPLRFRGEDGCWYGMEIRP	-21%	NS1	
1697-703	LILAPTRVVAAEMEEALKGLP	-47%	NS3	Helicase – Domain I, Motif 1a
1771-1776	SIAARGYISTRVEMGEAAAI	-61%	NS3	Helicase – Domain I
1877-82	LNDWDFVVTTDISEMGANFK	-56%	NS3	Helicase – Domain II, Motif 5
1924-8	PMPVTAASAAQRRGRIGRN	-30%	NS3	Helicase – Domain II, Motif 6
1962	DHAHWTEAKMLLDNI	-38%	NS3	Helicase – Domain III
2383	KRTAAGIMKNPTVDG	-38%	NS4B	
2408	YDPKFEKQLGQVMLL	-38%	NS4B	
2432-4	MRTTWALCEALTLATGP	-18%	NS4B	
2452-65	LWEGNPGKFWNTTIAVSM ANIFRGSYLA	-55%	NS4B	
2640	LCDIGESSPNPTIEE	-25%	NS5	Methyltransferase (KDKE Motif)
2948-51	YNMMGKREKKLGEFGKAK	-40%	NS5	Chain A, Ns5 RNA dependent RNA polymerase Domain
2967-73	SRAIWYMWLGARFLEFEALGF	-44%	NS5	
3026-29	MYADDTAGWDTRITEDDL	-22%	NS5	Chain A, NS5 RdRp Domain
2065	FKLTYQNKVVKVQRP	-39%	NS5	Chain A, NS5 RdRp Domain
3085-9	VMDIISRKDQRGSGQVGTY	-27%	NS5	Chain A, DENV Serotype 3 RdRp

Functional regions identified within fragments conserved in all four serotypes by NCBI conserved domain database (CDD)[603] and references[601,605].

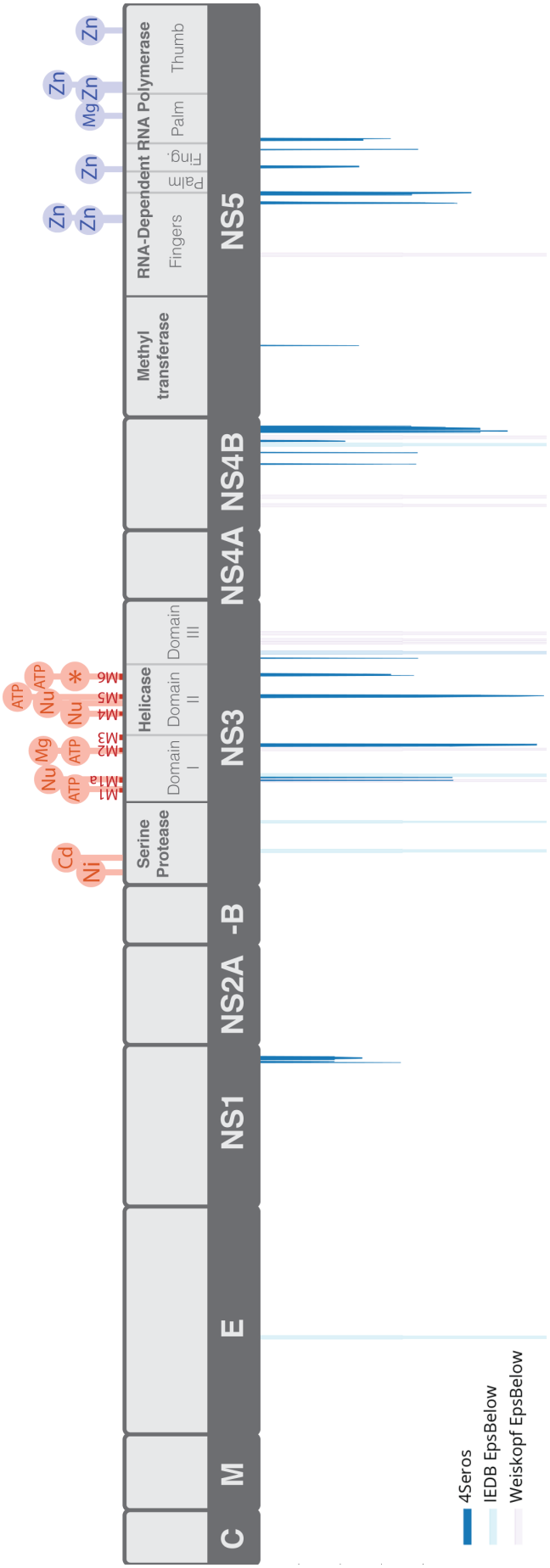
C
M
E
NS1
NS2A
-B
NS2B
NS3
NS4A
NS4B
NS5
Serine Protease
Helicase
Domain I
Domain II
Domain III
Methyl transferase
RNA-Dependent RNA Polymerase
Fingers
Palm
Fing.
Palm
Thumb
Zn
Zn
Zn
Zn
Mg
Zn
Zn
Cd
Ni
ATP
Nu
Mg
ATP
Nu
ATP
Nu
ATP
*
M1
M1a
M2
M3
M4
M5
M6
4Seros
IEDB EpsBelow
Weiskopf EpsBelow

Figure 5-15 I Conserved domains. NS3 and NS5 protein functions and interactions mapped onto the cumulative conservation plot for four serotypes. Domains are indicated by coloured boxes with motifs above. Interactions are indicated by pins. ATP = Adenosinetriphosphate, Nu=RNA, Mg=Magnesium ion, *=region shown to modulate NTPase/helicase activity, Zn = Zinc Ion. Epitopes from Table 5-2 mapped onto the cumulative conservation plot. Information from NCBI CDD prediction or crystal structures[601,603,605].

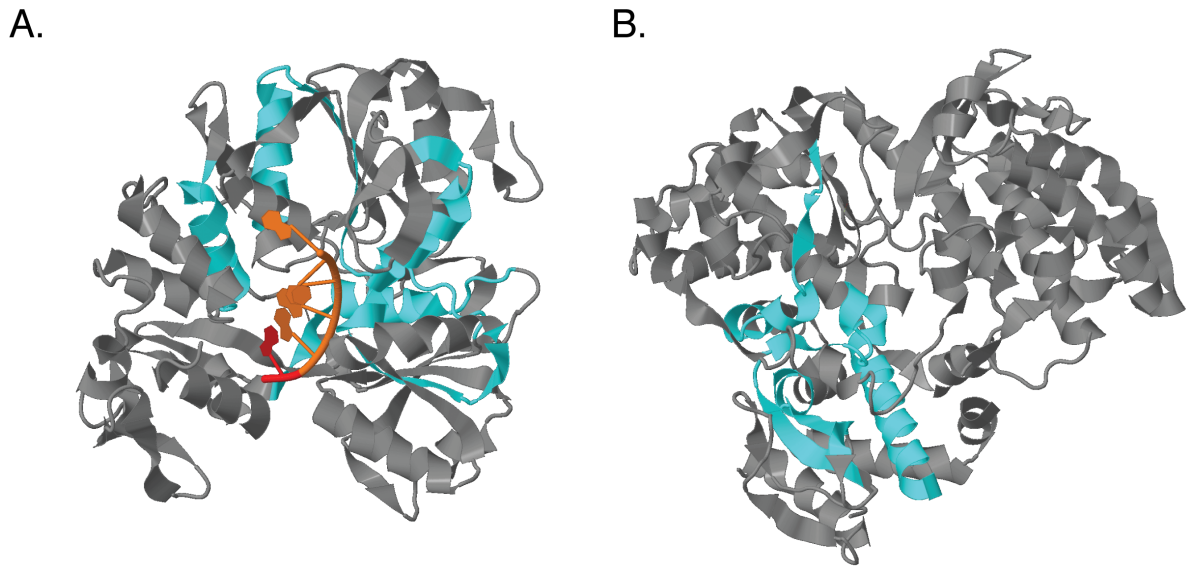

Figure 5-16 I Crystal structures NS3 and NS5. A) Crystal structure of NS3 in association with ADP (PDB: 2JLZ). B) Crystal structure of NS5 (PDB: 2J7U). Inter-serotype fragments conserved in all four serotypes are labelled cyan.

RaptorX protein structure prediction[606] was used to assess the structure of the smart consensus from NS3 onwards. Neither the NS3-NS4A or NS4B-NS4 cleavage sites[474] were present within the smart consensus. However, the signal peptidase cleavage site between NS4A-NS4B[474] was present (AAAIAANEMGLL), suggesting that it could be cleaved *in vivo*. RaptorX predicted three domains, referring to NS3, NS4A&B and NS5 (Figure 5-17a). Domain 1 was predicted to interact with adenosine-diphosphate and uridine-monophosphate and domain 2 was predicted to interact with magnesium, zinc and sulphate ions. Overall the protein structure prediction for NS3 from the smart consensus had a similar structure to full length wildtype NS3 (Figure 5-17b).

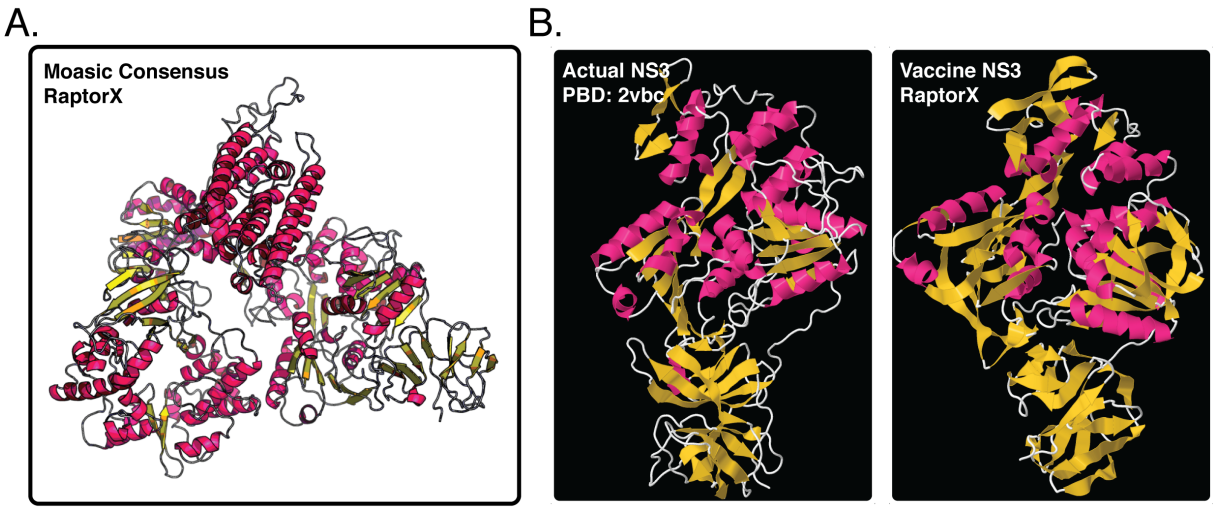

Figure 5-17 l RaptorX prediction. A) Predicted protein structure of the smart vaccine from NS3 onwards. B) Actual NS3 crystal structure (PDB: 2vbc) and RaptorX predicted protein structure of the predicted domain one. B) Actual NS3 crystal structure (PDB: 2vbc) compared to RaptorX predicted protein structure of region one of the smart consensus.

5.2.8 Final Design Approaches

To best assess efficacy, four variants of the dengue vaccine were created (Table 5-6). Due to poor conservation in proteins prior to NS3 all candidates contained only NS3 to NS5. Candidate one consisted the cumulative consensus for regions conserved in all four serotypes only and was 314 aa in length. The aim of this vaccine was to direct the immune response against regions with minimal intra- and inter-serotype variation. This vaccine contained one experimentally characterised epitope and 25 predicted epitopes. To increase the number of epitopes candidate two consisted of the smart consensus based on the mosaic from the cumulative conservation plots conserved in two, three and four serotypes together, producing a 1,507 aa vaccine. This vaccine contained nine experimentally discovered epitopes. To allow pre-clinical assessment of whether any remaining regions conserved in only one serotype could be protective candidate three contained all of candidate two but with regions conserved only in one serotype also included. This produced a 1,712 aa vaccine.

Table 5-6 I Vaccine candidates.

Vaccine	Description	Length (aa)
Candidate 1 DENT8-1	Contains the cumulative conservation consensus from regions conserved in all four serotypes from NS3 onwards. ***With one epitope string***	314
Candidate 2 DENT8-2	Contains the cumulative conservation consensus from regions conserved in four, three and two serotypes from NS3 onwards.	1507
Candidate 3 DENT8-3	Contains the cumulative conservation consensus from regions conserved in four, three and two serotypes plus regions conserved in only one serotype from NS3 onwards.	1712
Candidate 4 DENT8-4	Contains the cumulative conservation consensus from regions conserved in four, three and two serotypes plus regions conserved in only one serotype from NS3 onwards. ***With epitope strings***.	1819

NS3-5 full = 2000bp.

However, these candidates only included the most common weighted epitope variant. There is mixed evidence[112,113,547] as to whether including all epitope variants would be beneficial or detrimental. To investigate this, candidate one and four contained epitope variants strings to include common different serotype variants. Briefly, variants of an already present experimentally defined epitope were strung together in the location of the original epitope. All of the high T-cell responding epitopes (Table 5-2) had multiple variants, for example, epitope 1971 had a total of four variants each with high T-cell response so including all may be beneficial. Another benefit is that many of the variants are restricted to different HLA types allowing greater population coverage. To avoid introducing additional artificial epitopes the consensus fragments were joined directly. These joins were also checked for artificial epitopes using Syfpeithi. The vaccines designs are summarised in Figure 5-18.

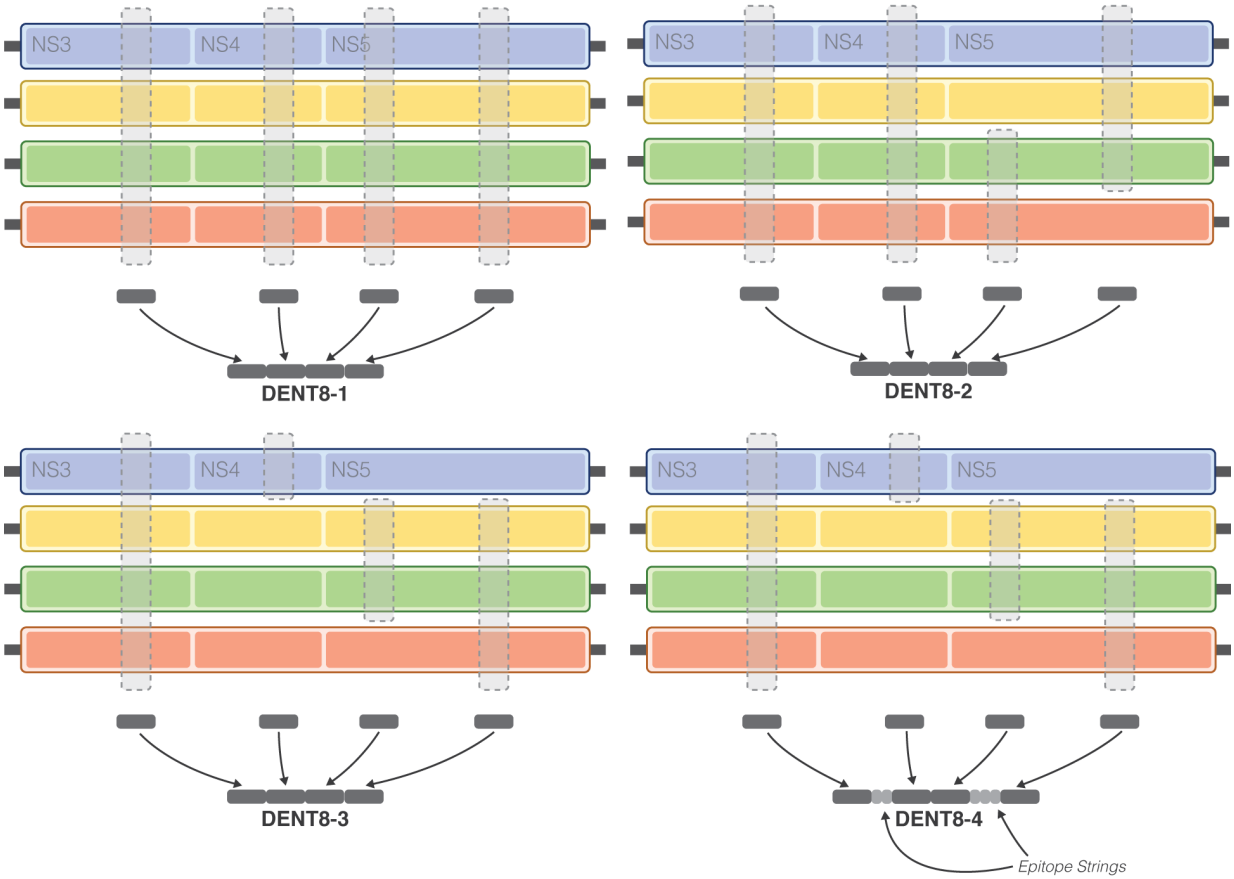

Figure 5-18 I Vaccine candidates design summary. Diagrammatic representation of the four vaccine candidates. Each colour represents the weighed serotype consensus. Grey dotted boxes represent regions conserved across serotypes. Dark grey boxes represent fragments of smart consensus.

The Adenovirus/Modified Virus Ankara (MVA) viral vectored system was chosen as the approach for our vaccines due to its ability to raise robust CD8 T-cell responses (reviewed in reference[607]).

5.2.9 Experimental Efficacy

The immunogenicity of the four vaccine candidates were assessed by Dr Cesar Lopez using chimpanzee adenoviruses and MVA recombinant viruses expressing each of the DENT8 candidates in mice. A vaccine expressing NS3 to NS5 from a wildtype (wt) DENV2 sequence was created as a control. Balb/c mice were vaccinated using an adeno prime/MVA boost regime (four week prime, two week boost) and vaccine specific CD8 responses assessed using peptide pools from either the three non-structural regions of the vaccines or from a wt DENV2 in an *ex vivo* IFNɣ enzyme-linked immunosorbent spot (ELISpot) assay (Figure 5-19a-b). All vaccine candidates elicited robust responses against both the vaccine NS3 and wt NS3. NS4 was the least immunogenic, however the median response against the wt NS4 was 4.0, 3.0, 7.5 and 1.6 times greater than the vaccine peptide pool respectively. NS5 also induced a response 1.8, 1.5, 1.9 and 2.5 times greater in the wt DENV peptide pool respectively

(Figure 5-19a-b). This indicated that the vaccine was able to produce memory CD8 T-cells that respond to a wt DENV2 serotype.

Subsequently, peptides representing either the NS3 or NS5 region from each vaccine were separated into 12 pools to identify the most immunogenic regions of each vaccine candidate (Figure 5-19c-d). Peptide pools 5-6 were the most immunogenic in all vaccine candidates in NS3 (Figure 5-19c). These represented the helicase DI-DII junction and motifs 2, 3 and 4 and both peptide pools overlapped a fragment conserved in all four serotypes (1771-6; Table 5-5). A strong IFNγ response in the vaccine candidate based on regions conserved in all four serotypes (DENT8-1) indicated that the conserved fragments in pools five and six were the main immunogenic regions. Pools four and seven also contained regions conserved across all serotypes and a moderate T-cell response and were located within DI and DIII respectively.

T-cell responses were more diverse between vaccine candidates for the NS5 region (Figure 5-19d). The most conserved vaccines (DENT8-1) induced limited responses within the RdRp however the responses to pools five and nine were likely background as this vaccine candidate did not contain regions conserved in these pools. Addition of epitope strings also had a limited effect as again all the pools with a response were not within the vaccine candidate. This suggests that the most conserved regions in NS5 were poorly immunogenic. The mosaic vaccine candidates also induce poor CD8 responses.

Efficacy studies are currently progressing in mouse and macaque challenge models with preliminary results showing strong cross-serotype protection. The most suitable vaccine candidate will then be enter into Phase I Trials in 2017-18.

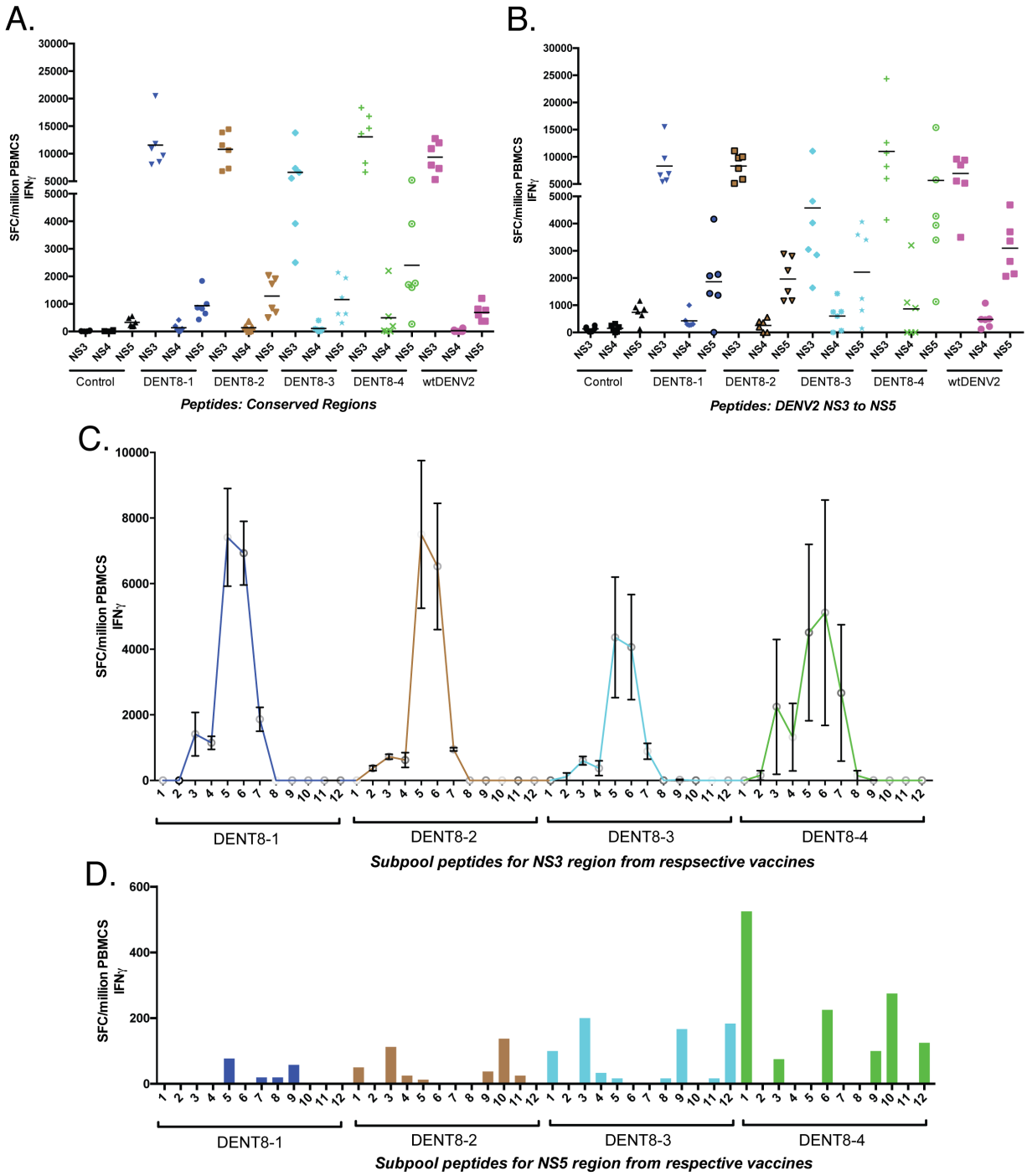

Figure 5-19 | *In vivo* immunogenicity of four dengue vaccine candidates. A) *Ex vivo* IFNɣ ELISpot assay against Balb/c peripheral blood mononuclear cells from mice two weeks after boost with either a vaccine candidate or wt DENV2. T-cells were stimulated using peptide pools from DENT8-4. B) Same as (A), but T-cells were stimulated using peptide pools the wt DENV2 NS3 to NS5. C-D) T-cells from (A) were stimulated using 12 subpools from the DENT8-4 NS3 (C) or NS5 (D). Thanks to Dr Lopez for sharing this data.

5.2.10 Development of Other Vaccines Using The Program.

Upon the success of using the program to design a dengue vaccine the program was subsequently used to design conservation-based vaccines for other mosquito-borne

viral pathogens such as chikungunya. Furthermore, in collaboration with Professor Lucy Dorrell and Gemma Hancock in Oxford to create a human papilloma virus (HPV) anti-oncogenic vaccine and with Dr Daniela Ferreira and Jessica Owugha at the Liverpool School of Tropical Medicine to create a prophylactic *Streptococcus Pneumonia* Vaccine. The HPV and chikungunya vaccines will be entering into clinical trials soon after showing very promising pre-clinical results. Additionally, the HPV vaccine showed effective inhibition of *in vitro* tumour models.

5.3 Discussion

Antibodies have long been implicated in serotype-specific protection against dengue[500]. However, the only licenced dengue vaccine which is designed to elicit this antibody response shows limited cross-serotype protection[104,108,109]. Furthermore, it also appeared to enhance disease severity in some cases[108], likely through eliciting poorly neutralizing antibodies that enhance viral load (ADE). The role of CD8 T-cells in protection however is still not fully understood and has traditionally also been associated with disease enhancement via a phenomenon known as antigenic sin[547,552]. Described as, an ineffective immune response to heterotypic dengue infection by cross-protective CD8 T-cells with low avidity[110]. However, more recently CD8 T-cells have been implicated in protection from severe disease, particularly a polyfunctional response[112,113,548,550].

It is instead starting to be appreciated that cross-protective CD8's may possibly only be detrimental when stimulated under certain conditions, in particular involving epitopes with variants[113]. For example, stimulation by certain epitope variants which induce short TCR interaction inducing a monofunctional CD8 response[113]. The exact reasons for this are unknown, it may be due to sequence characteristics of certain epitope variants and the associated HLA binding properties. Additionally, it has been suggested that ADE may enhance this phenotype by increasing the availability of presented peptides[547,552]. Alternatively, certain HLA alleles have been linked to a monofunctional response[112]. Therefore, a CD8-based hypothesis driven vaccine design avoiding these described situations offers untapped potential and without the worry of ADE during vaccination.

To attempt to achieve this a conservation-based approach was chosen to create four monovalent vaccine candidates aimed at eliciting slightly different CD8 responses based on previous CD8 correlates[112,113,548,550]. In particular using conservation in a monovalent vaccine allows the control of epitopes that are conserved across serotypes and ones with variants. Furthermore, the majority of the DENV genome is under purifying selection[569,582] with some positive selection[561,562,564,570,572,580,581] making it a suitable candidate for a conservation-based vaccine design.

The genetics of dengue serotypes are complex and each serotype is separated into many lineages[560] which are a known determinant of disease severity[564,565,567,568]. Furthermore, although generally geographically distributed[560], lineages show temporal changes in prevalence and a continual turnover[564,565]. Unfortunately, the dynamics and genetic mutations associated with fitness advantages are not understood enough to apply it to vaccine design[560,562,564,565,568-571]. Instead the worldwide publically contributed NCBI protein database was used to obtain the greatest number of lineages possible to enable a vaccine with the greatest possible lineage coverable. This is also important to prevent lineage replacements especially since some lineages are more virulent[564,565,567,568,588].

1257, 893, 660 and 119 human origin full-length sequences were collected for DENV1 to 4 respectively. Sylvatic sequences were excluded due to the rare number of human

infections[608]. The geographic origin of these sequences closely represented the lineage distributions for each serotype[560] (Table 5-7), indicating suitable coverage. However, the limited sequences from Africa (four sequences) and limited countries of origin (Angola, Burkina Faso, Mozambique and Seychelles) meant that all African lineages from DENV1 to 3 were represented by only four sequences and therefore the vaccine may have limited representation of this continent.

Table 5-7 I Dengue genotype distributions.

Genotype:	I	II	III	IV	V
DENV1	*SEA, China, East Africa*	*Thailand*	*Malaysia*	*Australasia*	*Americas, West Africa, (few Asia)*
DENV2	*Asian*	*Cosmopolitan (Australia, Africa, India, Middle east)*	*Americas*	*Thailand, Vietnam and Americas*	*Sylvatic Strain (some human infections)*
DENV3	*Indonesia, Malaysia, Philippines*	*Thailand, Vietnam, Bangladesh*	*Sri Lanka, India, Africa, Samoa*	*Americas*	—
DENV4	*Thailand, Philippines, Sri Lanka, Japan*	*Indonesia, Malaysia, Caribbean, Americas*	*Thailand*	*Sylvatic*	—

The distribution of dengue genotypes worldwide. Using phylogenies from reference[560].

Conservation between serotypes was assessed using a sliding window approach. To overcome the selection bias associated with using public databases, sequences were weighted to promote uniqueness enabling all lineages to be equally represented[591]. Since the majority of lineages are geographically restrained[560] the effectiveness of weighting was confirmed by showing an inverse correlation between the number of sequences per country and the median sequence weighting per country. The country with the greatest sequence number was from Vietnam, representing 68% of total DENV1 sequences, which had the lowest median sequence weight per country. Furthermore, this large number of homogenous sequences caused the DENV1 serotypes to have the lowest median sequence weight of all serotypes. DENV4 however showed the highest indicating that the majority of sequences were distinct from each other. This correlated with an even distribution of sequences across countries.

Structural genes (C, M, E) and the non-structural genes (NS1, NS2A, NS2B) showed limited intra-serotype conservation with 11, 17, 19 and 16% of windows conserved compared to 35, 31, 30 and 34% in NS3 to NS5 genes for DENV1 to 4 respectively. Furthermore, only 20, 29, 32 and 27% of the total windows conserved across the whole

proteome were within the C-NS2B region of the genome for DENV1-4 respectively, which represented 44% of the complete polyprotein length. Additionally, DENV4 showed the lowest overall diversity. NS3 was the most conserved protein with 40, 36, 36 and 36% of windows conserved within the protein.

Inter-serotype conservation was then assessed by measuring regions conserved across serotypes (cumulative conservation), which identified clustered regions within NS1, NS3, NS4B and NS5 conserved in all four serotypes. NS3 and NS5 had the greatest number of windows conserved across all four serotypes. When the scope was widened to include regions conserved in three or two serotypes, significant clustering was still seen around these regions. Furthermore, every protein had at least one window conserved in three serotypes in all proteins. The envelope protein showed the lowest level of inter-serotype conservation. This is not unexpected due to the considerable immune pressure exerted by neutralising antibodies and positive selection which has been identified in E and NS2A[561,562,572,580,581].

The clustering of regions conserved across all serotypes suggested they may be part of a critical functional domain. Interestingly a study identified nine amino acid substitutions associated with a DENV2 lineage replacement which had greater fitness[564]. Two were in NS5 (R410K, T290I) which the program didn't identify as conserved across serotypes or conserved within DENV2, indicating that these mutations either had no fitness advantage or only an advantage in certain geographical locations. These residues were actually in regions with some of the greatest intra-serotype diversity in DENV2. A further observation was that the T290I mutation was present in the majority of DENV1, 2 and 3 serotypes but not DENV4.

As predicted, further investigation of the regions conserved in all serotypes showed correlation with key functional domains in NS3 and NS5. NS3 has multiple functions including, serine protease, helicase, NTPase and RNA triphosphate activity[473-475,480,481]. Five cross-serotype conserved regions were identified within the helicase. The helicase/NTPase consist of three structural domains and six motifs[601]. Three of the regions conserved in all serotypes were predicted to play a critical role in the function of the NTPase and helicase[601]. Conserved fragment 1697-703 (across Motif 1a), which also contains the only characterised epitope conserved across all serotypes, is predicted to interact with NTP phosphodiester backbone using arginine-225[601]. Interestingly conserved fragment 1924-8 (Motif 6) contained arginine-457 and -458 which when mutated inhibits helicase activity and decreases ATPase activity[604]. These residues are theorised to function in linking NTPase activity with helicase activity and are also predicted to interact with ATP[604]. The fragment 1877-82 was also predicated using NCBI CDD[603] to interact with ATP. It has been suggested the domain III is important in the interaction of NS5 with NS3[601], it is therefore possible that the final fragment (1962) is important in this interaction. These suggest important functions for many of these conserved regions would therefore be effective vaccine targets.

NS5 is critical for viral RNA replication via is methyltransferase and RdRp activities[605] and contains one and five fragments conserved in all four serotypes respectively. The methyltransferase mediates +RNA capping by its KDKE catalytic motif. The conserved fragment (2640) within this region contains the aspartate-146 of the KDKE motif (61K, 146D, 180K, 216E)[605]. Many of the mutational analysis done on NS5 RdRp is not within the conserved fragments so their functional relevance is unknown[605]. Finally, NS4B contains four conserved fragments, although the exact function is yet to be determined but it does have a role in RNA replication[488].

Following conservation analysis, four vaccine candidates were designed based on different hypothesises with the aim of eliciting a theorised protective high avidity polyfunctional CD8 T-cell response[112,113,550]. These hypotheses were based on the type of epitopes that should be included within the vaccine; conserved epitopes or epitopes with variants between serotypes. Studies on an NS3 epitope with variants have associated detrimental CD8 T-cell responses in secondary infection with epitopes with a variant in the heterologous dengue serotype infection, which activates pre-existing CD8's against the original epitope which are low avidity, monofunctional with low cytotoxicity[547,552].

However, evidence suggests that a CD8 response to a variant does not predispose to a poor CD8 response but instead characteristics of each variant may determine whether a CD8 response is protective by mediating the amount of TCR signalling that occurs[113]. For example, Juthathip Mongkolsapaya's[547,552] theory that epitope variants interact with poor avidity was proven incorrect and instead due to the amino acid sequence of the epitope which determined the binding avidity[113]. HLA's themselves have also been associated with the type of CD8 response elicited[112] and may even be explained by the same hypothesis as above but due to HLA determining the binding ability of variants.

Therefore, some vaccine candidates were designed to only include epitopes conserved across serotypes (i.e. no variants) by using regions conserved in all four serotypes. The Weiskopf group[112] have actually shown that subsequent infections skew CD8 responses to epitopes conserved between the new and previously seen serotypes and that they are still high avidity and polyfunctional. An alternative method used was to include all the characterised epitope variants together (epitope strings) to attempt to raise CD8's against all variants.

Epitopes were obtained from previous *ex vivo* studies[112] or epitope prediction[598]. A major focus was made on the epitopes from the 2013 study by Weiskopf and colleagues[112] as they comprehensively tested predicted CD8 epitopes across the whole proteome by *ex vivo* ELIspot and contributed the majority of known MHCI epitopes. The top 25 epitopes (some with variants) and six others from the IEDB were automatically compared against the raw DENV sequences which identified 15 epitopes found within a conserved window within at least one serotype. 26 predicted epitopes were found within the fragments conserved in all serotypes. Only one *ex vivo* epitope conserved across all serotypes was identified. However, most of these *ex vivo* epitopes were

identified using limited HLA alleles, therefore epitope prediction software identified eight epitopes conserved across all four serotypes covering 10 HLA alleles. In total the 26 predicted epitopes covered 15 unique HLA epitopes. Only well characterised *ex vivo* epitopes were included within epitope strings however, as they had been shown to give a polyfunctional CD8 response[112] and furthermore introducing predicted epitopes that do not mount a good polyfunctional CD8 response could be detrimental[112,113,548,550]. No correlation was found between T-cell response and whether *ex vivo* epitopes were in a conserved window or the degree of conservation.

Other vaccine candidates also contained regions conserved in three, two and one serotype in a mosaic/smart consensus, with the aim of increasing the number of epitopes available and to allow later pre-clinical studies into the effect of epitope variants using *in vivo* models. It would also allow the identification of any additional highly immunogenic regions that may have been missed by the strict candidates (DENT8-1, -2). Another consideration was the ability of these candidates to elicit an effective response, as structural prediction showed that the mosaic candidate (DENT8-4) folded to create a similar tertiary structure for NS3, NS4 & NS5, and contained a host cleavage site, which may make the vaccine more immunogenic.

All candidates contained NS3, NS4 and NS5 only, due to limited conservation in other proteins and experimentally most CD8 epitopes are shown to be in NS3 to NS5[112]. Furthermore, the few CD4 known epitopes are against structural proteins[542] and this vaccine aimed to avoid antibody responses that may cause ADE. Although NS1 showed inter-serotype conservation it was also avoided as it may associated with pathogenesis[498].

Preliminary immunogenicity was assessed in mice which showed that memory CD8's from vaccinated animals responded effectively to a wild type DENV2 with similar or greater IFNγ responses than against the original vaccine. However, NS4 and NS5 had poor immunogenicity in all vaccine candidates. Only IFNγ response was measured however so it is possible that these T-cell produce other cytokines and have effective cytotoxic response.

Peptide pools against different regions of the vaccines showed that the majority of responses were against the central helicase DI-DII junction (pools 5-6) containing motif 2, 3 and 4 which have predicted ATP and RNA binding properties[601]. These peptide pools contain one fragment conserved in all four serotypes (1771-6). The responses to both pools were highest in the vaccine candidates made from only regions conserved in all four serotypes (DENT8-1) or in regions conserved in four, three or two serotypes. This therefore suggests that the fragment conserved across all serotypes (1771-6) is highly immunogenic. The fragment did not contain any known *ex vivo* epitopes, but did contain five predicted epitopes. Pool four also contained a fragment conserved in all four serotypes (1697-703) and the Weiskopf epitope conserved across serotypes, however it was not associated with a strong T-cell response in any of the vaccine candidates.

This suggests that there are new conserved epitope(s) in dengue NS3 (pools 5-6). Future efficacy studies will determine whether they are protective. DENT8-1 and DENT8-4 also contain epitope variants which did not appear to modify the responses. The responses were similar across all vaccines indicating that the immunogenic regions are the more conserved (i.e. present in the most conserved vaccines). Unfortunately NS5 was poorly immunogenic even though the vaccine candidates based on mosaics (DENT8-3, -4) contained *ex vivo* identified epitopes that had shown high T-cell responses previously[112]. A possible explanation could be due to mouse HLA's. The next stages in this study will be to test against blood from infected populations.

CD8 T-cell responses were recently assessed against the NIH tetravalent attenuated vaccine which contains the structural M and E from DENV1 to 4, plus C and non-structural genes of DENV1, 3 and 4[609]. Similarly, they found limited responses against NS4B measured by IFNγ response. They also found that vaccination with the tetravalent form induced strong NS3 and NS5 responses, however vaccination with one component of the vaccine only (monovalent) elicited a broad response across the proteome. Unlike the DENT8 vaccines, median T-cell responses were greater in NS5 than NS3. The whole NS proteins were used in this vaccine however which may explain the disparity[609].

They also find that 93% of the responses from tetravalent vaccination were against conserved regions[609]. Similarly, in immunised mice the DENT8 vaccines elicit strong responses against conserved regions in NS3. Earlier work from Daniela Weiskopf[112] also showed that responses against secondary infection are directed toward conserved epitopes and were associated with protective responses. In influenza T-cells against conserved epitopes have been associated with protection against secondary infection[610]. Therefore, pre-clinical challenge data will show whether vaccination with the most conserved vaccine (DENT8-1) provides effective protection.

In summary, the development of a conservation-based approach to design a dengue vaccine to specifically elicit CD8 T-cell responses using either conserved or epitopes variants may help to answer the question of CD8-mediated protection. Furthermore, it may help to improve our understanding of any detrimental CD8-mediated effects.

6 Conclusion

6.1 Overview

Both malaria and dengue contribute significant mortality and morbidity[45,103], however current intervention methods are either developing resistance[46-49] or showing limited efficacy[108], highlighting the need for new and highly effective intervention methods. This thesis contributes to the development of new intervention methods against malaria or dengue using three approaches. Firstly, by the development of an improved research tool for the investigation of liver-stage malaria which showed a significant improvement over previous tools. Secondly the improved understanding of *Wolbachia* interactions in the *An. gambiae* host and finally the development of a novel CD8 T-cell based dengue vaccine.

6.2 Conclusions and Future Directions

6.2.1 The Future of Malaria Liver Stage Research

During this thesis the major problems of the *in vitro* method currently used for studying liver-stage malaria was acknowledged, discussed and an appreciation for the impacts on the development on new pre-erythrocytic intervention methods explored. In response, a novel purification method was developed for quickly extracting high numbers of high purity sporozoites which showed a 12 times increase in the number primary hepatocyte infections. The implications for this are a dramatic increase in the amount of material available to study the EEF stage with huge benefits for the identification of new vaccine and drug target.

Although impressive, the protocol is still in its early development and future research can work to improve it including the optimisation of the microfluidic liver-model. In particular, newer FFE machines are now available with greater resolutions and shorter sample transit times. Furthermore, alternative buffer systems and the newer interval zone electrophoresis technique should be investigated to determine if mosquito MASH original sporozoites can be purified aseptic.

6.2.2 The Future of Wolbachia in An. gambiae

During this thesis the interactions of *Wolbachia* with the TOR signalling pathway were investigated to improve our understanding of the *Wolbachia*-host interaction, with the aim of helping to solve the problem of establishing a stable *Wolbachia* infection in the *An. gambiae* mosquito for use as a malaria intervention method. The *w*MelPop strain was found to be associated with elevated TORC1 signalling, which although it had no beneficial effect on *Wolbachia in vitro* may have consequences for infection of the germline *in vivo*. Furthermore, elevated TOR may mediate some of the anti-*Plasmodium* effects in the mosquito host by modulating nutrient availability and lifespan.

The early TOR manipulation results in *An. gambiae* cell lines will enable future work directed at further elucidating the TOR mediated effects in *in vivo* somatic mosquito infections and investigation of whether its manipulation is able to modulate both *Wolbachia's* pathogen inhibitory effect and aid in the establishment of a stable trans-infection of *An. gambiae.*

6.2.3 The Future of Conserve, the Conservation Algorithm

During this thesis a novel conservation-based approach was used to design a CD8 T-cell based dengue vaccine which broke away from the conventions of B-cell based dengue vaccines in an attempt to avoid pathogenic effects and capitalise on recent work showing the possible protective effects of CD8 T-cells[112]. Early pre-clinical efficacy studies in macaques are looking promising and will be followed by phase I studies soon.

The algorithm itself was also used to design a multitude of other conservation-based vaccines, which are also showing promising pre-clinical data. The program is currently being developed into a publically available tool by myself to aid in the development of conservation-based vaccine design know with early application concepts shown in Figure 6-1.

[REDACTED]

Figure 6-1 | Development of the Conserve application.

6.3 Final Remarks

In conclusion, the work here uses a combination of approaches to improve intervention methods targeted against malaria and dengue. Successfully developing a highly infective *in vitro* liver-stage malaria model. Providing initial data on *Wolbachia's* TOR axis manipulations in *An. gambiae*. And developing both a tool for designing conservation-based vaccines and a novel dengue vaccine soon to enter phase I trials.

7 Bibliography

1. Rutledge CR. Mosquitoes (Diptera: Culcidae). In: Capinera JL, editor. Encylopedia of Entomology. 2nd ed. Florida: Kluwer Academic Publishers; 2008. pp. 2476–83.

2. Reiter P. Climate change and mosquito-borne disease. Environmental Health Perspectives. National Institute of Environmental Health Science; 2001 Mar;109 Suppl 1(Suppl 1):141–61.

3. Hansen IA, Attardo GM, Roy SG, Raikhel AS. Target of rapamycin-dependent activation of S6 kinase is a central step in the transduction of nutritional signals during egg development in a mosquito. J Biol Chem. 2005 May 27;280(21):20565–72.

4. Attardo GM, Hansen IA, Raikhel AS. Nutritional regulation of vitellogenesis in mosquitoes: Implications for anautogeny. Insect Biochemistry and Molecular Biology. 2005 Jul;35(7):661–75.

5. Tolle MA. Mosquito-borne Diseases. Current Problems in Pediatric and Adolescent Health Care. 2009 Apr;39(4):97–140.

6. Cowman AF, Healer J, Marapana D, Marsh K. Malaria: Biology and Disease. Cell. 2016 Oct;167(3):610–24.

7. Simmons CP, Farrar JJ, Van Vinh Chau N, Wills B. Dengue. N Engl J Med. 2012 Apr 12;366(15):1423–32.

8. Campion EW, Weaver SC, Lecuit M. Chikungunya Virus and the Global Spread of a Mosquito-Borne Disease. N Engl J Med. 2015 Mar 26;372(13):1231–9.

9. Mackenzie JS, Gubler DJ, Petersen LR. Emerging flaviviruses: the spread and resurgence of Japanese encephalitis, West Nile and dengue viruses. Nat Med. 2004 Dec;10(12 Suppl):S98–109.

10. Paily KP, Hoti SL, Das PK. A review of the complexity of biology of lymphatic filarial parasites. Journal of Parasitic Diseases: Official Organ of the Indian Society for Parasitology. 2nd ed. Springer; 2009 Dec 1;33(1-2):3–12.

11. Titus RG, Ribeiro JMC. The role of vector saliva in transmission of arthropod-borne disease. Parasitology Today. 1990 May;6(5):157–60.

12. Ikegami T, Makino S. The Pathogenesis of Rift Valley Fever. Viruses. 2011 Dec;3(12):493–519.

13. Baden LR, Petersen LR, Jamieson DJ, Powers AM, Honein MA. Zika Virus. N Engl J Med. 2016 Apr 21;374(16):1552–63.

14. Khasnis AA, Nettleman MD. Global Warming and Infectious Disease. Archives of Medical Research. 2005 Nov;36(6):689–96.

15. White GB. Anopheles gambiae complex and disease transmission in Africa. Trans R Soc Trop Med Hyg. 1974 Jan;68(4):278–98.

16. Pates H, Curtis C. Mosquito Behavior and Vector Control. Annu Rev Entomol. 2005 Jan;50(1):53–70.

17. Ferguson HM, Read AF. Why is the effect of malaria parasites on mosquito survival still unresolved? Trends Parasitol. 2002 Jun;18(6):256–61.

18. Dawes EJ, Churcher TS, Zhuang S, Sinden RE, Basáñez M-G. Anopheles mortality is both age- and Plasmodium -density dependent: implications for malaria transmission. Malar J. BioMed Central; 2009 Oct 12;8(1):228.

19. Yamana TK, Eltahir EAB. Incorporating the effects of humidity in a mechanistic model of Anopheles gambiae mosquito population dynamics in the Sahel region of Africa. Parasit Vectors. BioMed Central; 2013 Aug 9;6(1):235.

20. Crans WJ. A classification system for mosquito life cycles: life cycle types for mosquitoes of the northeastern United States. J Vector Ecol. 2004 Jun;29(1):1–10.

21. Fradin MS. Mosquitoes and Mosquito Repellents: A Clinician's Guide. Ann Intern Med. American College of Physicians; 1998 Jun 1;128(11):931–40.

22. Jawara M, Pinder M, Drakeley CJ, Nwakanma DC, Jallow E, Bogh C, et al. Dry season ecology of Anopheles gambiae complex mosquitoes in The Gambia. Malar J. BioMed Central; 2008 Aug 18;7(1):156.

23. Bayoh MN, Lindsay SW. Effect of temperature on the development of the aquatic stages of Anopheles gambiae sensu stricto (Diptera: Culicidae). Bull Entomol Res. 2003 Oct;93(5):375–81.

24. Beck-Johnson LM, Nelson WA, Paaijmans KP, Read AF, Thomas MB, Bjørnstad ON. The Effect of Temperature on Anopheles Mosquito Population Dynamics and the Potential for Malaria Transmission. PLoS ONE. 2013 Nov 14;8(11):e79276.

25. Rohani A, Wong YC, Zamre I, Lee HL, Zurainee MN. The effect of extrinsic incubation temperature on development of dengue serotype 2 and 4 viruses in Aedes aegypti (L.). Southeast Asian J Trop Med Public Health. 2009 Sep;40(5):942–50.

26. Patz JA, Reisen WK. Immunology, climate change and vector-borne diseases. Trends in Immunology. 2001 Apr;22(4):171–2.

27. Kovats RS, Bouma MJ, Hajat S, Worrall E, Haines A. El Niño and health. The Lancet. 2003 Nov 1;362(9394):1481–9.

28. Mabaso MLH, Kleinschmidt I, Sharp B, Smith T. El Niño Southern Oscillation (ENSO) and annual malaria incidence in Southern Africa. Trans R Soc Trop Med Hyg. 2007 Apr;101(4):326–30.

29. Cai W, Borlace S, Lengaigne M, van Rensch P, Collins M, Vecchi G, et al. Increasing frequency of extreme El Niño events due to greenhouse warming. Nature Climate change. 2014 Jan 19;4(2):111–6.

30. Reiter P. From Shakespeare to Defoe: malaria in England in the Little Ice Age. Emerging Infect Dis. Centers for Disease Control and Prevention; 2000 Feb;6(1):1–11.

31. Walker KR, Joy TK, Ellers-Kirk C, Ramberg FB. Human and Environmental Factors Affecting Aedes aegypti Distribution in an Arid Urban Environment. Journal of the American Mosquito Control Association. 2011 Jun;27(2):135–41.

32. Dalla Pozza GL, Romi R, Severini C. Source and spread of Aedes albopictus in the Veneto region of Italy. Journal of the American Mosquito Control Association. 1994 Dec;10(4):589–92.

33. Schaffner F, Karch S. First report of Aedes albopictus (Skuse, 1984) in metropolitan France. C R Acad Sci III, Sci Vie. 2000 Apr;323(4):373–5.

34. Vazeille M, Jeannin C, Martin E, Schaffner F, Failloux A-B. Chikungunya: A risk for Mediterranean countries? Acta Tropica. 2008 Feb;105(2):200–2.

35. Russell TL, Govella NJ, Azizi S, Drakeley CJ, Kachur SP, Killeen GF. Increased proportions of outdoor feeding among residual malaria vector populations following increased use of insecticide-treated nets in rural Tanzania. Malar J. BioMed Central; 2011 Apr 9;10(1):80.

36. Reddy MR, Overgaard HJ, Abaga S, Reddy VP, Caccone A, Kiszewski AE, et al. Outdoor host seeking behaviour of Anopheles gambiae mosquitoes following initiation of malaria vector control on Bioko Island, Equatorial Guinea. Malar J. BioMed Central; 2011 Jul 7;10(1):184.

37. Koella JC, Sørensen FL, Anderson RA. The malaria parasite, Plasmodium falciparum, increases the frequency of multiple feeding of its mosquito vector, Anopheles gambiae. Proceedings of the Royal Society of London B: Biological Sciences. 1998 May 7;265(1398):763–8.

38. Wekesa JW, Copeland RS, Mwangi RW. Effect of Plasmodium falciparum on blood feeding behavior of naturally infected Anopheles mosquitoes in western Kenya. Am J Trop Med Hyg. 1992 Oct;47(4):484–8.

39. Anderson RA, Koella JC, Hurd H. The effect of Plasmodium yoelii nigeriensis infection on the feeding persistence of Anopheles stephensi Liston throughout the sporogonic cycle. Proceedings of the Royal Society B: Biological Sciences. 1999 Sep 7;266(1430):1729–33.

40. Lacroix R, Mukabana WR, Gouagna LC, Koella JC. Malaria Infection Increases Attractiveness of Humans to Mosquitoes. PLoS Biol. 2005 Aug 9;3(9):e298.

41. Mack SR, Samuels S, Vanderberg JP. Hemolymph of Anopheles stephensi from uninfected and Plasmodium berghei-infected mosquitoes. 2. Free amino acids. The Journal of Parasitology. 1979 Feb;65(1):130–6.

42. Hurd H, Hogg JC, Renshaw M. Interactions between bloodfeeding, fecundity and infection in mosquitoes. Parasitology Today. 1995 Nov;11(11):411–6.

43. Dimopoulos G, Seeley D, Wolf A, Kafatos FC. Malaria infection of the mosquito Anopheles gambiae activates immune-responsive genes during critical transition stages of the parasite life cycle. EMBO J. 1998 Nov 2;17(21):6115–23.

44. White NJ, Pukrittayakamee S, Hien TT, Faiz MA, Mokuolu OA, Dondorp AM. Malaria. The Lancet. 2014 Feb 22;383(9918):723–35.

45. WHO. World Malaria Report 2016 [Internet]. WHO; 2016. 1 p. Available from: http://www.who.int/malaria/publications/world-malaria-report-2016/report/en/

46. Feachem RGA, Phillips AA, Targett GA, Snow RW. Call to action: priorities for malaria elimination. Lancet. 2010 Nov 6;376(9752):1517–21.

47. Ranson H, Lissenden N. Insecticide Resistance in African Anopheles Mosquitoes: A Worsening Situation that Needs Urgent Action to Maintain Malaria Control. Trends Parasitol. 2016 Mar;32(3):187–96.

48. Ashley EA, Dhorda M, Fairhurst RM, Amaratunga C, Lim P, Suon S, et al. Spread of artemisinin resistance in Plasmodium falciparum malaria. N Engl J Med. 2014 Jul 31;371(5):411–23.

49. Dondorp AM, Nosten F, Yi P, Das D, Phyo AP, Tarning J, et al. Artemisinin Resistance in Plasmodium falciparum Malaria. N Engl J Med. 2009 Jul 30;361(5):455–67.

50. WHO. WHO | World Malaria Report 2015. WHO [Internet]. World Health Organization; 2015 Dec. Available from:

http://www.who.int/malaria/publications/world-malaria-report-2015/report/en/

51. Bhatt S, Gething PW, Brady OJ, Messina JP, Farlow AW, Moyes CL, et al. The global distribution and burden of dengue. Nature. 2013 Apr 7;496(7446):504–7.

52. Petersen LR, Powers AM. Chikungunya: epidemiology. F1000Res. 2016;5.

53. Weaver SC, Forrester NL. Chikungunya: Evolutionary history and recent epidemic spread. Antiviral Research. 2015 Aug;120:32–9.

54. Gibbons RV, Kalanarooj S, Jarman RG, Nisalak A, Vaughn DW, Endy TP, et al. Analysis of repeat hospital admissions for dengue to estimate the frequency of third or fourth dengue infections resulting in admissions and dengue hemorrhagic fever, and serotype sequences. Am J Trop Med Hyg. 2007 Nov;77(5):910–3.

55. Burke DS, Nisalak A, Johnson DE, Scott RM. A prospective study of dengue infections in Bangkok. Am J Trop Med Hyg. 1988 Jan;38(1):172–80.

56. Halstead SB. Observations related to pathogensis of dengue hemorrhagic fever. VI. Hypotheses and discussion. Yale J Biol Med. 1970 Apr;42(5):350–62.

57. Lengeler C. Insecticide-treated bed nets and curtains for preventing malaria. Cochrane Database Syst Rev. 2004;(2):CD000363.

58. Bhatt S, Weiss DJ, Cameron E, Bisanzio D, Mappin B, Dalrymple U, et al. The effect of malaria control on Plasmodium falciparum in Africa between 2000 and 2015. Nature. 2015 Sep 16;526(7572):207–11.

59. Hemingway J, Hawkes NJ, McCarroll L, Ranson H. The molecular basis of insecticide resistance in mosquitoes. Insect Biochemistry and Molecular Biology. 2004 Jul;34(7):653–65.

60. Githeko AK, Adungo NI, Karanja DM, Hawley WA, Vulule JM, Seroney IK, et al. Some Observations on the Biting Behavior of Anopheles gambiae s.s, Anopheles arabiensis, and Anopheles funestus and Their Implications for Malaria Control. Exp Parasitol. 1996 Apr;82(3):306–15.

61. Corbel V, Akogbeto M, Damien GB, Djenontin A, Chandre F, Rogier C, et al. Combination of malaria vector control interventions in pyrethroid resistance area in Benin: a cluster randomised controlled trial. Lancet Infect Dis. 2012 Aug;12(8):617–26.

62. Trape J-F, Tall A, Diagne N, Ndiath O, Ly AB, Faye J, et al. Malaria morbidity and pyrethroid resistance after the introduction of insecticide-treated bednets and artemisinin-based combination therapies: a longitudinal study. Lancet Infect Dis. 2011 Dec;11(12):925–32.

63. Hemingway J, Ranson H. Insecticide Resistance in Insect Vectors of Human Disease. Annu Rev Entomol. 2000 Jan;45(1):371–91.

64. Mnzava AP, Knox TB, Temu EA, Trett A, Fornadel C, Hemingway J, et al. Implementation of the global plan for insecticide resistance management in malaria vectors: progress, challenges and the way forward. Malar J. BioMed Central; 2015 Apr 23;14(1):173.

65. WHO. WHO | Global plan for insecticide resistance management in malaria vectors. WHO, editor. WHO [Internet]. World Health Organization; 2012;:132. Available from: http://www.who.int/malaria/publications/atoz/gpirm/en/

66. Kamtchum-Tatuene J, Makepeace BL, Benjamin L, Baylis M, Solomon T. The potential role of Wolbachia in controlling the transmission of emerging human arboviral infections. Current Opinion in Infectious Diseases. 2017 Feb 1;30(1):108.

67. Zug R, Hammerstein P. Bad guys turned nice? A critical assessment of Wolbachia mutualisms in arthropod hosts. Biological Reviews. 2015 Feb 1;90(1):89–111.

68. Zug R, Hammerstein P. Still a Host of Hosts for Wolbachia: Analysis of Recent Data Suggests That 40% of Terrestrial Arthropod Species Are Infected. Cordaux R, editor. PLoS ONE. Public Library of Science; 2012 Jun 7;7(6):e38544.

69. Hilgenboecker K, Hammerstein P, Schlattmann P, Telschow A, Werren JH. How many species are infected with Wolbachia?-A statistical analysis of current data. FEMS Microbiol Lett. 2008 Apr;281(2):215–20.

70. Moreira LA, Iturbe-Ormaetxe I, Jeffery JA, Lu G, Pyke AT, Hedges LM, et al. A Wolbachia Symbiont in Aedes aegypti Limits Infection with Dengue, Chikungunya, and Plasmodium. Cell. 2009 Dec 24;139(7):1268–78.

71. Dutra HLC, Rocha MN, Dias FBS, Mansur SB, Caragata EP, Moreira LA. Wolbachia Blocks Currently Circulating Zika Virus Isolates in Brazilian Aedes aegypti Mosquitoes. Cell Host Microbe. 2016 Jun;19(6):771–4.

72. Kambris Z, Blagborough AM, Pinto SB, Blagrove MSC, Godfray HCJ, Sinden RE, et al. Wolbachia Stimulates Immune Gene Expression and Inhibits Plasmodium Development in Anopheles gambiae. Vernick KD, editor. PLoS Pathog. 2010 Oct 7;6(10):e1001143.

73. Hughes GL, Koga R, Xue P, Fukatsu T, Rasgon JL. Wolbachia Infections Are Virulent and Inhibit the Human Malaria Parasite Plasmodium Falciparum in Anopheles Gambiae. Schneider DS, editor. PLoS Pathog. 2011 May 19;7(5):e1002043.

74. Walker T, Johnson PH, Moreira LA, Iturbe-Ormaetxe I, Frentiu FD, McMeniman CJ, et al. The wMel Wolbachia strain blocks dengue and invades caged Aedes aegypti populations. Nature. 2011 Aug 24;476(7361):450–3.

75. McMeniman CJ, Lane RV, Cass BN, Fong AWC, Sidhu M, Wang Y-F, et al. Stable Introduction of a Life-Shortening Wolbachia Infection into the Mosquito Aedes aegypti. Science. 2009 Jan 2;323(5910):141–4.

76. Yeap HL, Mee P, Walker T, Weeks AR, O'Neill S, Johnson P, et al. Dynamics of the "Popcorn" Wolbachia Infection in Outbred Aedes aegypti Informs Prospects for Mosquito Vector Control. Genetics. 2011 Feb 1;187(2):583–95.

77. Frentiu FD, Zakir T, Walker T, Popovici J, Pyke AT, van den Hurk A, et al. Limited Dengue Virus Replication in Field-Collected Aedes aegypti Mosquitoes Infected with Wolbachia. Turell MJ, editor. PLoS Negl Trop Dis. 2014 Feb 20;8(2):e2688.

78. Jeffries CL, Walker T. Wolbachia Biocontrol Strategies for Arboviral Diseases and the Potential Influence of Resident Wolbachia Strains in Mosquitoes. Curr Trop Med Rep. 2016 Feb 2;3(1):20–5.

79. Bian G, Joshi D, Dong Y, Lu P, Zhou G, Pan X, et al. Wolbachia Invades Anopheles stephensi Populations and Induces Refractoriness to Plasmodium Infection. Science. 2013 May 9;340(6133):748–51.

80. Alphey L. Genetic Control of Mosquitoes. Annual Reviews; 2014 Jan 7;59(1):205–24.

81. Alphey L, Benedict M, Bellini R, Clark GG, Dame DA, Service MW, et al. Sterile-insect methods for control of mosquito-borne diseases: an analysis. Vector Borne Zoonotic Dis. 2010 Apr;10(3):295–311.

82. Benedict MQ, Robinson AS. The first releases of transgenic mosquitoes: an argument for the sterile insect technique. Trends Parasitol. 2003 Aug;19(8):349–55.

83. Thailayil J, Magnusson K, Godfray HCJ, Crisanti A, Catteruccia F. Spermless males elicit large-scale female responses to mating in the malaria mosquito Anopheles gambiae. Proceedings of the National Academy of Sciences. 2011 Aug 16;108(33):13677–81.

84. Wang S, Jacobs-Lorena M. Genetic approaches to interfere with malaria transmission by vector mosquitoes. Trends in Biotechnology. 2013 Mar;31(3):185–93.

85. Franz AWE, Sanchez-Vargas I, Adelman ZN, Blair CD, Beaty BJ, James AA, et

al. Engineering RNA interference-based resistance to dengue virus type 2 in genetically modified Aedes aegypti. Proc Natl Acad Sci USA. 2006 Mar 14;103(11):4198–203.

86. Lambrechts L, Koella JC, Boëte C. Can transgenic mosquitoes afford the fitness cost? Trends Parasitol. 2008 Jan;24(1):4–7.

87. Marrelli MT, Moreira CK, Kelly D, Alphey L, Jacobs-Lorena M. Mosquito transgenesis: what is the fitness cost? Trends Parasitol. 2006 May;22(5):197–202.

88. Harris AF, Nimmo D, McKemey AR, Kelly N, Scaife S, Donnelly CA, et al. Field performance of engineered male mosquitoes. Nat Biotechnol. 2011 Oct 30;29(11):1034–7.

89. Harris AF, McKemey AR, Nimmo D, Curtis Z, Black I, Morgan SA, et al. Successful suppression of a field mosquito population by sustained release of engineered male mosquitoes. Nat Biotechnol. 2012 Sep 10;30(9):828–30.

90. Carvalho DO, McKemey AR, Garziera L, Lacroix R, Donnelly CA, Alphey L, et al. Suppression of a Field Population of Aedes aegypti in Brazil by Sustained Release of Transgenic Male Mosquitoes. PLoS Negl Trop Dis. 2015 Jul 2;9(7):e0003864.

91. Gorman K, Young J, Pineda L, Márquez R, Sosa N, Bernal D, et al. Short-term suppression of Aedes aegypti using genetic control does not facilitate Aedes albopictus. Pest Management Science. 3rd ed. John Wiley & Sons, Ltd; 2016 Mar 1;72(3):618–28.

92. Nabel GJ. Designing Tomorrow's Vaccines. N Engl J Med. 2013 Feb 7;368(6):551–60.

93. Gosling R, Seidlein von L. The Future of the RTS,S/AS01 Malaria Vaccine: An Alternative Development Plan. PLoS Med. 2016 Apr 12;13(4):e1001994.

94. European Medicines Agency. First malaria vaccine receives positive scientific opinion from EMA. ema.europa.eu. London; 2015.

95. Theander TG, Lusingu J. Efficacy and safety of RTS, S/AS01 malaria vaccine with or without a booster dose in infants and children in Africa. Lancet. 2015 April 23;386(9988):31-45.

96. WHO. Meeting of the Strategic Advisory Group of Experts on immunization, October 2015 – conclusions and recommendations. 2015. pp. 681–99.

97. Ockenhouse CF, Regules J, Tosh D, Cowden J, Kathcart A, Cummings J, et al. Ad35.CS.01 - RTS,S/AS01 Heterologous Prime Boost Vaccine Efficacy against

Sporozoite Challenge in Healthy Malaria-Naïve Adults. PLoS ONE. 2015 Jul 6;10(7):e0131571.

98. Regules JA, Cicatelli SB, Bennett JW, Paolino KM, Twomey PS, Moon JE, et al. Fractional Third and Fourth Dose of RTS,S/AS01 Malaria Candidate Vaccine: A Phase 2a Controlled Human Malaria Parasite Infection and Immunogenicity Study. J Inject Dis. 2016 Sep 1;214(5):762–71.

99. Epstein JE, Paolino KM, Richie TL, Sedegah M, Singer A, Ruben AJ, et al. Protection against Plasmodium falciparum malaria by PfSPZ Vaccine. JCI Insight. 2017 Jan 12;2(1).

100. Sissoko MS, Healy SA, Katile A, Omaswa F, Zaidi I, Gabriel EE, et al. Safety and efficacy of PfSPZ Vaccine against Plasmodium falciparum via direct venous inoculation in healthy malaria-exposed adults in Mali: a randomised, double-blind phase 1 trial. Lancet Infect Dis. 2017 Feb 15;17(5):498-509.

101. Greenwood B. Progress with the PfSPZ Vaccine for malaria. Lancet Infect Dis. 2017 Feb;S1473-3099(17):30105-6

102. WHO. Malaria Vaccine Rainbow Tables [Internet]. [cited 2017 Mar 25]. Available from: http://www.who.int/immunization/research/development/Rainbow_tables/en/

103. Guzman MG, Harris E. Dengue. The Lancet. 2015 Jan;385(9966):453–65.

104. Pang T, Mak TK, Gubler DJ. Prevention and control of dengue—the light at the end of the tunnel. Lancet Infect Dis. 2017 Mar;17(3):e79–e87.

105. Halstead SB, Russell PK. Protective and immunological behavior of chimeric yellow fever dengue vaccine. Vaccine. 2016 Mar;34(14):1643–7.

106. Capeding MR, Tran NH, Hadinegoro SRS, Ismail HIHM, Chotpitayasunondh T, Chua MN, et al. Clinical efficacy and safety of a novel tetravalent dengue vaccine in healthy children in Asia: a phase 3, randomised, observer-masked, placebo-controlled trial. The Lancet. 2014 Oct;384(9951):1358–65.

107. Villar L, Dayan GH, Arredondo-García JL, Rivera DM, Cunha R, Deseda C, et al. Efficacy of a Tetravalent Dengue Vaccine in Children in Latin America. N Engl J Med. 2015 Jan 8;372(2):113–23.

108. Hadinegoro SR, Arredondo-García JL, Capeding MR, Deseda C, Chotpitayasunondh T, Dietze R, et al. Efficacy and Long-Term Safety of a Dengue Vaccine in Regions of Endemic Disease. N Engl J Med. 2015 Sep 24;373(13):1195–206.

109. Sabchareon A, Wallace D, Sirivichayakul C, Limkittikul K, Chanthavanich P,

Suvannadabba S, et al. Protective efficacy of the recombinant, live-attenuated, CYD tetravalent dengue vaccine in Thai schoolchildren: a randomised, controlled phase 2b trial. The Lancet. 2012 Nov 3;380(9853):1559–67.

110. Weiskopf D, Sette A. T-Cell Immunity to Infection with Dengue Virus in Humans. Frontiers in Immunology. 2014 Mar 7;5(Pt 1):571.

111. Rothman AL. Immunity to dengue virus: a tale of original antigenic sin and tropical cytokine storms. Nat Rev Immunol. 2011 Jul 15;11(8):532–43.

112. Weiskopf D, Angelo MA, de Azeredo EL, Sidney J, Greenbaum JA, Fernando AN, et al. Comprehensive analysis of dengue virus-specific responses supports an HLA-linked protective role for CD8+ T cells. Proceedings of the National Academy of Sciences. 2013 May 28;110(22):E2046–53.

113. Friberg H, Burns L, Woda M, Kalayanarooj S, Endy TP, Stephens HAF, et al. Memory CD8+ T cells from naturally acquired primary dengue virus infection are highly cross-reactive. Immunol Cell Biol. 2011 Jan;89(1):122–9.

114. Akahata W, Yang Z-Y, Andersen H, Sun S, Holdaway HA, Kong W-P, et al. A virus-like particle vaccine for epidemic Chikungunya virus protects nonhuman primates against infection. Nat Med. 2010 Jan 28;16(3):334–8.

115. Smalley C, Erasmus JH, Chesson CB, Beasley DWC. Status of research and development of vaccines for chikungunya. Vaccine. 2016 Jun;34(26):2976–81.

116. Abdelnabi R, Neyts J, Delang L. Towards antivirals against chikungunya virus. Antiviral Research. 2015 Sep;121:59–68.

117. Lescar J, Luo D, Xu T, Sampath A, Lim SP, Canard B, et al. Towards the design of antiviral inhibitors against flaviviruses: the case for the multifunctional NS3 protein from Dengue virus as a target. Antiviral Research. 2008 Nov;80(2):94–101.

118. Noble CG, Chen Y-L, Dong H, Gu F, Lim SP, Schul W, et al. Strategies for development of dengue virus inhibitors. Antiviral Research. 2010 Mar;85(3):450–62.

119. Cheung YY, Chen KC, Chen H, Seng EK, Chu JJH. Antiviral activity of lanatoside C against dengue virus infection. Antiviral Research. 2014 Nov;111:93–9.

120. Lani R, Hassandarvish P, Chiam CW, Moghaddam E, Chu JJH, Rausalu K, et al. Antiviral activity of silymarin against chikungunya virus. Sci Rep. 2015 Jun 16;5(1):11421.

121. Noedl H, Se Y, Schaecher K, Smith BL, Socheat D, Fukuda MM. Evidence of

Artemisinin-Resistant Malaria in Western Cambodia. N Engl J Med. 2008 Dec 11;359(24):2619–20.

122. Amaratunga C, Sreng S, Suon S, Phelps ES, Stepniewska K, Lim P, et al. Artemisinin-resistant Plasmodium falciparum in Pursat province, western Cambodia: a parasite clearance rate study. Lancet Infect Dis. 2012 Nov;12(11):851–8.

123. Phyo AP, Nkhoma S, Stepniewska K, Ashley EA, Nair S, McGready R, et al. Emergence of artemisinin-resistant malaria on the western border of Thailand: a longitudinal study. The Lancet. 2012 May;379(9830):1960–6.

124. Huang F, Tang L, Yang H, Zhou S, Sun X, Liu H. Therapeutic efficacy of artesunate in the treatment of uncomplicated Plasmodium falciparum malaria and anti-malarial, drug-resistance marker polymorphisms in populations near the China-Myanmar border. Malar J. 2012 Aug 16;11(1):278.

125. Kyaw MP, Nyunt MH, Chit K, Aye MM, Aye KH, Aye MM, et al. Reduced Susceptibility of Plasmodium falciparum to Artesunate in Southern Myanmar. Borrmann S, editor. PLoS ONE. 2013 Mar 8;8(3):e57689.

126. Ariey F, Witkowski B, Amaratunga C, Beghain J, Langlois A-C, Khim N, et al. A molecular marker of artemisinin-resistant Plasmodium falciparum malaria. Nature. 2014 Jan 2;505(7481):50–5.

127. O'Neill PM, Amewu RK, Charman SA, Sabbani S, Gnädig NF, Straimer J, et al. A tetraoxane-based antimalarial drug candidate that overcomes PfK13-C580Y dependent artemisinin resistance. Nature Communications. 2017 May 24;8:ncomms15159.

128. Kato N, Comer E, Sakata-Kato T, Sharma A, Sharma M, Maetani M, et al. Diversity-oriented synthesis yields novel multistage antimalarial inhibitors. Nature. 2016 Oct 20;538(7625):344–9.

129. Yuan J, Cheng KC-C, Johnson RL, Huang R, Pattaradilokrat S, Liu A, et al. Chemical Genomic Profiling for Antimalarial Therapies, Response Signatures, and Molecular Targets. Science. 2011 Aug 5;333(6043):724–9.

130. Chong CR, Chen X, Shi L, Liu JO, Sullivan DJ. A clinical drug library screen identifies astemizole as an antimalarial agent. Nature Chemical Biology. 2006 Aug 1;2(8):415–6.

131. Weisman JL, Liou AP, Shelat AA, Cohen FE, Kiplin Guy R, DeRisi JL. Searching for new antimalarial therapeutics amongst known drugs. Chemical Biology & Drug Design. 2006 Jun;67(6):409–16.

132. Rottmann M, McNamara C, Yeung BKS, Lee MCS, Bin Zou, Russell B, et al. Spiroindolones, a Potent Compound Class for the Treatment of Malaria. Science. 2010 Sep 3;329(5996):1175–80.

133. Hovlid ML, Winzeler EA. Phenotypic Screens in Antimalarial Drug Discovery. Trends Parasitol. 2016 Sep 1;32(9):697–707.

134. Swinney DC. Phenotypic vs. target-based drug discovery for first-in-class medicines. Clin Pharmacol Ther. 2013 Apr;93(4):299–301.

135. Plouffe D, Brinker A, McNamara C, Henson K, Kato N, Kuhen K, et al. In silicoactivity profiling reveals the mechanism of action of antimalarials discovered in a high-throughput screen. Proc Natl Acad Sci USA. 2008 Jun 25;105(26):9059–64.

136. Meister S, Plouffe DM, Kuhen KL, Bonamy GMC, Wu T, Barnes SW, et al. Imaging of Plasmodium Liver Stages to Drive Next-Generation Antimalarial Drug Discovery. Science. 2011 Dec 9;334(6061):1372–7.

137. Vos MW, Stone WJR, Koolen KM, van Gemert G-J, Ben van Schaijk, Leroy D, et al. A semi-automated luminescence based standard membrane feeding assay identifies novel small molecules that inhibit transmission of malaria parasites by mosquitoes. Sci Rep. 2015 Dec 21;5(1):srep18704.

138. Kariu T, Ishino T, Yano K, Chinzei Y, Yuda M. CelTOS, a novel malarial protein that mediates transmission to mosquito and vertebrate hosts. Molecular Microbiology. 2006 Jan 20;59(5):1369–79.

139. Ishino T, Yano K, Chinzei Y, Yuda M. Cell-Passage Activity Is Required for the Malarial Parasite to Cross the Liver Sinusoidal Cell Layer. Gary Ward, editor. PLoS Biol. 2004 Jan 20;2(1):e4.

140. Ishino T, Chinzei Y, Yuda M. Two proteins with 6-cys motifs are required for malarial parasites to commit to infection of the hepatocyte. Molecular Microbiology. 2005 Sep 5;58(5):1264–75.

141. Salman AM, Montoya-Díaz E, West H, Lall A, Atcheson E, Lopez-Camacho C, et al. Rational development of a protective P. vivax< vaccine evaluated with transgenic rodent parasite challenge models. Sci Rep. 2017 Apr 18;7:srep46482.

142. Kaiser K, Camargo N, Kappe SHI. Transformation of Sporozoites into Early Exoerythrocytic Malaria Parasites Does Not Require Host Cells. The Journal of Experimental Medicine. 2003 Apr 21;197(8):1045–50.

143. House BL, Hollingdale MR, Sacci JB Jr., Richie TL. Functional immunoassays

using an in-vitro malaria liver-stage infection model: where do we go from here? Trends Parasitol. 2009 Nov;25(11):525–33.

144. Sattabongkot J, Yimamnuaychoke N, Leelaudomlipi S, Rasameesoraj M, Jenwithisuk R, Coleman RE, et al. Establishment of a human hepatocyte line that supports in vitro development of the exo-erythrocytic stages of the malaria parasites Plasmodium falciparum and P. vivax. Am J Trop Med Hyg. 2006 May;74(5):708–15.

145. Pfaffl MW. A new mathematical model for relative quantification in real-time RT–PCR. Nucleic Acids Research. 2001 May 1;29(9):e45–193.

146. Konet DS, Anderson J, Piper J, Akkina R, Suchman E, Carlson J. Short-hairpin RNA expressed from polymerase III promoters mediates RNA interference in mosquito cells. Insect Molecular Biology. 2007 Apr 1;16(2):199–206.

147. Barth JMI, Szabad J, Hafen E, Köhler K. Autophagy in Drosophila ovaries is induced by starvation and is required for oogenesis. Cell Death Differ. 2010 Dec 10;18(6):915–24.

148. Müller HM, Dimopoulos G, Blass C, Kafatos FC. A hemocyte-like cell line established from the malaria vector Anopheles gambiae expresses six prophenoloxidase genes. J Biol Chem. 1999 Apr 23;274(17):11727–35.

149. Pinto SB, Mariconti M, Bazzocchi C, Bandi C, Sinkins SP. Wolbachia surface protein induces innate immune responses in mosquito cells. BMC Microbiol. 2012;12(Suppl 1):S11.

150. Ingber DE. Fibronectin controls capillary endothelial cell growth by modulating cell shape. Proc Natl Acad Sci USA. 1990 May;87(9):3579–83.

151. Kostadinova R, Boess F, Applegate D, Suter L, Weiser T, Singer T, et al. A long-term three dimensional liver co-culture system for improved prediction of clinically relevant drug-induced hepatotoxicity. Toxicology and Applied Pharmacology. 2013 Apr 1;268(1):1–16.

152. Smedsrød B, Pertoft H. Preparation of pure hepatocytes and reticuloendothelial cells in high yield from a single rat liver by means of Percoll centrifugation and selective adherence. Journal of Leukocyte Biology. 1985 Aug;38(2):213–30.

153. Lin J-W, Annoura T, Sajid M, Chevalley-Maurel S, Ramesar J, Klop O, et al. A novel “gene insertion/marker out” (GIMO) method for transgene expression and gene complementation in rodent malaria parasites. Kappe S, editor. PLoS ONE. 2011;6(12):e29289.

154. Miyake Y, Karanis P, Uga S. Cryopreservation of protozoan parasites.

Cryobiology. 2004 Feb;48(1):1–7.

155. Laboratory TJ. Sperm Cryopreservation Protocol [Internet]. 2017 [cited 2017 Apr 12]. Available from: https://www.jax.org/~/media/jaxweb/files/jax-mice-and-services/sperm-cryo-protocol.pdf?la=en

156. Kennedy M, Fishbaugher ME, Vaughan AM, Patrapuvich R, Boonhok R, Yimamnuaychok N, et al. A rapid and scalable density gradient purification method for Plasmodium sporozoites. Malar J. 2012 Dec 17;11(1):421.

157. Hegge S, Kudryashev M, Smith A, Frischknecht F. Automated classification of Plasmodium sporozoite movement patterns reveals a shift towards productive motility during salivary gland infection. Biotechnology Journal. 2009 Jun 1;4(6):903–13.

158. Lee KS, Ram RJ. Plastic–PDMS bonding for high pressure hydrolytically stable active microfluidics. Lab Chip. 2009 Jun 7;9(11):1618–24.

159. Tang L, Lee NY. A facile route for irreversible bonding of plastic-PDMS hybrid microdevices at room temperature. Lab Chip. 2010 May 5;10(10):1274–80.

160. Severs NJ. Freeze-fracture electron microscopy. 2007;2(3):547–76.

161. Phadwal K, Alegre-Abarrategui J, Watson AS, Pike L, Anbalagan S, Hammond EM, et al. A novel method for autophagy detection in primary cells: impaired levels of macroautophagy in immunosenescent T cells. Autophagy. 2012 Apr;8(4):677–89.

162. Plotly. Plotly Graphs [Internet]. Available from: https://plot.ly.

163. Team RDC. R: A language and environment for statistical computing. R Foundation for Statistical Computing [Internet]. Vienna, Austria. Available from: http://www.R-project.org

164. Tukey JW. Exploratory Data Analysis. 1st ed. Pearson; 1977.

165. Razali NM, Wah YB. Power comparisons of shapiro-wilk, kolmogorov-smirnov, lilliefors and anderson-darling tests. Journal of statistical modeling and analytics. 2011;2(1):21-33.

166. Amino R, Thiberge S, Martin B, Celli S, Shorte S, Frischknecht F, et al. Quantitative imaging of Plasmodium transmission from mosquito to mammal. Nat Med. 2006 Feb 1;12(2):220–4.

167. Ménard R, Tavares J, Cockburn I, Markus M, Zavala F, Amino R. Looking under the skin: the first steps in malarial infection and immunity. Nature Reviews Microbiology. 2013 Oct 1;11(10):701–12.

168. Vanderberg JP. Plasmodium berghei: quantitation of sporozoites injected by mosquitoes feeding on a rodent host. Exp Parasitol. 1977 Jun;42(1):169–81.

169. Coppi A, Natarajan R, Pradel G, Bennett BL, James ER, Roggero MA, et al. The malaria circumsporozoite protein has two functional domains, each with distinct roles as sporozoites journey from mosquito to mammalian host. The Journal of Experimental Medicine. 2011 Feb 14;208(2):341–56.

170. HAWKING F. Pre-erythrocytic Stage in Mammalian Malaria Parasites. Nature. 1948 Jan 31;161(4083):175–5.

171. Hollingdale MR, Leland P, Schwartz AL. In vitro cultivation of the exoerythrocytic stage of Plasmodium berghei in a hepatoma cell line. Am J Trop Med Hyg. 1983 Jul;32(4):682–4.

172. March S, Ng S, Velmurugan S, Galstian A, Shan J, Logan DJ, et al. A Microscale Human Liver Platform that Supports the Hepatic Stages of Plasmodium falciparum and vivax. Cell Host Microbe. 2013 Jul;14(1):104–15.

173. Bhanot P, Schauer K, Coppens I, Nussenzweig V. A Surface Phospholipase Is Involved in the Migration of Plasmodium Sporozoites through Cells. J Biol Chem. 2005 Feb 18;280(8):6752–60.

174. Risco-Castillo V, Topçu S, Marinach C, Manzoni G, Bigorgne AE, Briquet S, et al. Malaria Sporozoites Traverse Host Cells within Transient Vacuoles. Cell Host Microbe. 2015 Nov;18(5):593–603.

175. Moreira CK, Templeton TJ, Lavazec C, Hayward RE, Hobbs CV, Kroeze H, et al. The Plasmodium TRAP/MIC2 family member, TRAP-Like Protein (TLP), is involved in tissue traversal by sporozoites. Cell Microbiol. 2008 Jul 1;10(7):1505–16.

176. Sigler CI, Leland P, Hollingdale MR. In vitro infectivity of irradiated Plasmodium berghei sporozoites to cultured hepatoma cells. Am J Trop Med Hyg. 1984 Jul;33(4):544–7.

177. Nüssler A, Follezou JY, Miltgen F, Mazier D. Effect of irradiation on Plasmodium sporozoites depends on the species of hepatocyte infected. Trop Med Parasitol. 1989 Dec;40(4):468–9.

178. Hoffman SL, Billingsley PF, James E, Richman A, Loyevsky M, Li T, et al. Development of a metabolically active, non-replicating sporozoite vaccine to prevent Plasmodium falciparum malaria. Human Vaccines. 2010 Jan 1;6(1):97–106.

179. Hoffman SL, Doolan DL. Malaria vaccines–targeting infected hepatocytes -

Nature Medicine. Nat Med. 2000 Nov 1;6(11):1218–9.

180. Hoffman SL, Goh LML, Luke TC, Schneider I, Le TP, Doolan DL, et al. Protection of Humans against Malaria by Immunization with Radiation-Attenuated Plasmodium falciparum Sporozoites. J Infect Dis. 2002 Apr 15;185(8):1155–64.

181. Carlton JM, Angiuoli SV, Suh BB, Kooij TW, Pertea M, Silva JC, et al. Genome sequence and comparative analysis of the model rodent malaria parasite Plasmodium yoelii. Nature. 2002 Oct 3;419(6906):512–9.

182. Florens L, Washburn MP, Raine JD, Anthony RM, Grainger M, Haynes JD, et al. A proteomic view of the Plasmodium falciparum life cycle. Nature. 2002 Oct 3;419(6906):520–6.

183. Lasonder E, Janse CJ, van Gemert G-J, Mair GR, Vermunt AMW, Douradinha BG, et al. Proteomic Profiling of Plasmodium Sporozoite Maturation Identifies New Proteins Essential for Parasite Development and Infectivity. Goldberg DE, editor. PLoS Pathog. 2008 Oct 31;4(10):e1000195.

184. Sato Y, Montagna GN, Matuschewski K. Plasmodium berghei sporozoites acquire virulence and immunogenicity during mosquito hemocoel transit. Infect Immun. 2014 Mar;82(3):1164–72.

185. Hollingdale MR, Nardin EH, Tharavanij S, Schwartz AL, Nussenzweig RS. Inhibition of entry of Plasmodium falciparum and P. vivax sporozoites into cultured cells; an in vitro assay of protective antibodies. The Journal of Immunology. 1984 Feb;132(2):909–13.

186. Mazier D, Beaudoin RL, Mellouk S, Druilhe P, Texier B, Trosper J, et al. Complete development of hepatic stages of Plasmodium falciparum in vitro. Science. 1985 Jan 25;227(4685):440–2.

187. Siau A, Silvie O, Franetich J-F, Yalaoui S, Marinach C, Hannoun L, et al. Temperature shift and host cell contact up-regulate sporozoite expression of Plasmodium falciparum genes involved in hepatocyte infection. PLoS Pathog. 2008 Aug 8;4(8):e1000121.

188. Zou X, House BL, Zyzak MD, Richie TL, Gerbasi VR. Towards an optimized inhibition of liver stage development assay (ILSDA) for Plasmodium falciparum. Malar J. 2013;12(1):394.

189. Beier JC, Davis JR, Vaughan JA, Noden BH, Beier MS. Quantitation of Plasmodium falciparum sporozoites transmitted in vitro by experimentally infected Anopheles gambiae and Anopheles stephensi. Am J Trop Med Hyg. 1991 May;44(5):564–70.

190. Wen-yue X, Xing-xiang W, Jie Q, Jian-hua D, Fu-sheng H. Plasmodium yoelii: Influence of immune modulators on the development of the liver stage. Exp Parasitol. 2010 Oct;126(2):254–8.

191. Tavares J, Formaglio P, Thiberge S, Mordelet E, Van Rooijen N, Medvinsky A, et al. Role of host cell traversal by the malaria sporozoite during liver infection. The Journal of Experimental Medicine. 2013 May 6;210(5):905–15.

192. Coppi A, Tewari R, Bishop JR, Bennett BL, Lawrence R, Esko JD, et al. Heparan sulfate proteoglycans provide a signal to Plasmodium sporozoites to stop migrating and productively invade host cells. Cell Host Microbe. 2007 Nov;2(5):316–27.

193. Pradel G, Garapaty S, Frevert U. Proteoglycans mediate malaria sporozoite targeting to the liver. Molecular Microbiology. 2002 Aug 1;45(3):637–51.

194. Cha S-J, Kim M-S, Pandey A, Jacobs-Lorena M. Identification of GAPDH on the surface of Plasmodium sporozoites as a new candidate for targeting malaria liver invasion. The Journal of Experimental Medicine. 2016 Aug 16;213(10):jem.20160059–2112.

195. Talman AM, Lacroix C, Marques SR, Blagborough AM, Carzaniga R, Ménard R, et al. PbGEST mediates malaria transmission to both mosquito and vertebrate host. Molecular Microbiology. 2011 Oct 1;82(2):462–74.

196. Mota MM, Pradel G, Vanderberg JP, Hafalla JCR, Frevert U, NUSSENZWEIG RS, et al. Migration of Plasmodium Sporozoites Through Cells Before Infection. Science. 2001 Jan 5;291(5501):141–4.

197. Frevert U, Engelmann S, Zougbédé S, Stange J, Ng B, Matuschewski K, et al. Intravital Observation of Plasmodium berghei Sporozoite Infection of the Liver. PLoS Biol. 2005 May 24;3(6):e192.

198. Amino R, Giovannini D, Thiberge S, Gueirard P, Boisson B, Dubremetz J-F, et al. Host Cell Traversal Is Important for Progression of the Malaria Parasite through the Dermis to the Liver. Cell Host Microbe. 2008 Feb;3(2):88–96.

199. Rodrigues CD, Hannus M, Prudêncio M, Martin C, Gonçalves LA, Portugal S, et al. Host Scavenger Receptor SR-BI Plays a Dual Role in the Establishment of Malaria Parasite Liver Infection. Cell Host Microbe. 2008 Sep;4(3):271–82.

200. Silvie O, Rubinstein E, Franetich J-F, Prenant M, Belnoue E, Rénia L, et al. Hepatocyte CD81 is required for Plasmodium falciparum and Plasmodium yoelii sporozoite infectivity. Nat Med. 2002 Dec 16;9(1):93–6.

201. Manzoni G, Marinach C, Topçu S, Briquet S, Grand M, Tolle M, et al.

Plasmodium P36 determines host cell receptor usage during sporozoite invasion. eLife Sciences. 2017 May 16;6:e25903.

202. Matuschewski K. Plasmodium sporozoite invasion into insect and mammalian cells is directed by the same dual binding system. EMBO J. 2002 Apr 1;21(7):1597–606.

203. Silvie O, Franetich JF, Charrin S, Mueller MS, Siau A, Bodescot M, et al. A Role for Apical Membrane Antigen 1 during Invasion of Hepatocytes by Plasmodium falciparum Sporozoites. J Biol Chem. 2004 Feb 27;279(10):9490–6.

204. Sinnis P, Coppi A. A long and winding road: The Plasmodium sporozoite's journey in the mammalian host. Parasitology International. 2007 Sep;56(3):171–8.

205. Kaushansky A, Ye AS, Austin LS, Mikolajczak SA, Vaughan AM, Camargo N, et al. Suppression of host p53 is critical for Plasmodium liver-stage infection. Cell Reports. 2013 Mar;3(3):630–7.

206. Sturm A, Graewe S, Franke-Fayard B, Retzlaff S, Bolte S, Roppenser B, et al. Alteration of the Parasite Plasma Membrane and the Parasitophorous Vacuole Membrane during Exo-Erythrocytic Development of Malaria Parasites. Protist. 2009 Feb;160(1):51–63.

207. Schmidt-Christensen A, Sturm A, Horstmann S, Heussler VT. Expression and processing of Plasmodium berghei SERA3 during liver stages. Cell Microbiol. 2008 Aug;10(8):1723–34.

208. van de Sand C, Horstmann S, Schmidt A, Sturm A, Bolte S, Krueger A, et al. The liver stage of Plasmodium berghei inhibits host cell apoptosis. Molecular Microbiology. 2005 Sep 22;58(3):731–42.

209. Rennenberg A, Lehmann C, Heitmann A, Witt T, Hansen G, Nagarajan K, et al. Exoerythrocytic Plasmodium Parasites Secrete a Cysteine Protease Inhibitor Involved in Sporozoite Invasion and Capable of Blocking Cell Death of Host Hepatocytes. PLoS Pathog. 2010 Mar 26;6(3):e1000825.

210. Graewe S, Rankin KE, Lehmann C, Deschermeier C, Hecht L, Froehlke U, et al. Hostile Takeover by Plasmodium: Reorganization of Parasite and Host Cell Membranes during Liver Stage Egress. PLoS Pathog. 2011 Sep 1;7(9):e1002224.

211. Sturm A, Amino R, van de Sand C, Regen T, Retzlaff S, Rennenberg A, et al. Manipulation of Host Hepatocytes by the Malaria Parasite for Delivery into Liver Sinusoids. Science. 2006 Sep 1;313(5791):1287–90.

212. Baer K, Klotz C, Kappe SHI, Schnieder T, Frevert U. Release of Hepatic Plasmodium yoelii Merozoites into the Pulmonary Microvasculature. PLoS Pathog. 2007;3(11):e171.

213. Weiss GE, Gilson PR, Taechalertpaisarn T, Tham W-H, de Jong NWM, Harvey KL, et al. Revealing the Sequence and Resulting Cellular Morphology of Receptor-Ligand Interactions during Plasmodium falciparum Invasion of Erythrocytes. PLoS Pathog. 2015 Feb 27;11(2):e1004670.

214. Cowman AF, Crabb BS. Invasion of Red Blood Cells by Malaria Parasites. Cell. 2006 Feb;124(4):755–66.

215. Koch M, Baum J. The mechanics of malaria parasite invasion of the human erythrocyte - towards a reassessment of the host cell contribution. Cell Microbiol. 2016 Jan 11;18(3):319–29.

216. Lin CS, Uboldi AD, Epp C, Bujard H, Tsuboi T, Czabotar PE, et al. Multiple Plasmodium falciparum Merozoite Surface Protein 1 Complexes Mediate Merozoite Binding to Human Erythrocytes. Journal of Biological Chemistry. 2016 Apr 1;291(14):7703–15.

217. Tham W-H, Healer J, Cowman AF. Erythrocyte and reticulocyte binding-like proteins of Plasmodium falciparum. Trends Parasitol. 2012 Jan;28(1):23–30.

218. Besteiro S, Dubremetz J-F, Lebrun M. The moving junction of apicomplexan parasites: a key structure for invasion. Cell Microbiol. 2011 Jun 1;13(6):797–805.

219. Mantel P-Y, Hoang AN, Goldowitz I, Potashnikova D, Hamza B, Vorobjev I, et al. Malaria-Infected Erythrocyte-Derived Microvesicles Mediate Cellular Communication within the Parasite Population and with the Host Immune System. Cell Host Microbe. 2013 May;13(5):521–34.

220. Regev-Rudzki N, Wilson DW, Carvalho TG, Sisquella X, Coleman BM, Rug M, et al. Cell-Cell Communication between Malaria-Infected Red Blood Cells via Exosome-like Vesicles. Cell. 2013 May;153(5):1120–33.

221. Joice R, Nilsson SK, Montgomery J, Dankwa S, Egan E, Morahan B, et al. Plasmodium falciparum transmission stages accumulate in the human bone marrow. Science Translational Medicine. 2014 Jul 9;6(244):244re5–244re5.

222. Aly ASI, Vaughan AM, Kappe SHI. Malaria Parasite Development in the Mosquito and Infection of the Mammalian Host. Annu Rev Microbiol. 2009 Oct;63(1):195–221.

223. de Koning-Ward TF, Dixon MWA, Tilley L, Gilson PR. Plasmodium species:

master renovators of their host cells. Nature Reviews Microbiology. 2016 Jul 4;14(8):494–507.

224. Corradetti A, Verolini F, Sebastiani A, Proietti AM, Amati L. Fluorescent antibody testing with sporozoites of plasmodia. Bulletin of the World Health Organization. World Health Organization; 1964;30(5):747–50.

225. Ozaki LS, Gwadz RW, Godson GN. Simple Centrifugation Method for Rapid Separation of Sporozoites from Mosquitoes. The Journal of Parasitology. 1984 Oct;70(5):831.

226. Bosworth AB, Schneider I, Freier JE. Mass Isolation of Anopheles stephensi Salivary Glands Infected with Malarial Sporozoites. The Journal of Parasitology. 1975 Aug;61(4):769.

227. Touray MG, Warburg A, Laughinghouse A, Krettli AU, Miller LH. Developmentally regulated infectivity of malaria sporozoites for mosquito salivary glands and the vertebrate host. The Journal of Experimental Medicine. 1992 Jun 1;175(6):1607–12.

228. Krettli A, Chen Dh, Nussenzweig RS. Immunogenicity and Infectivity of Sporozoites of Mammalian Malaria Isolated by Density-Gradient Centrifugation. Journal of Eukaryotic Microbiology. 1973 Nov 1;20(5):662–5.

229. Beaudoin RL, Strome CPA, Mitchell F, Tubergen TA. Plasmodium berghei: Immunization of mice against the ANKA strain using the unaltered sporozoite as an antigen. Exp Parasitol. 1977 Jun;42(1):1–5.

230. Pacheco ND, Strome CPA, Mitchell F, Bawden MP, Beaudoin RL. Rapid, Large-Scale Isolation of Plasmodium berghei Sporozoites from Infected Mosquitoes. The Journal of Parasitology. 1979 Jun;65(3):414.

231. Wood DE, Smrkovski LL, McConnell E, Pacheco ND, Bawden MP. The use of membrane screen filters in the isolation of Plasmodium berghei sporozoites from mosquitos. Bulletin of the World Health Organization. 1979;57 Suppl 1(Suppl):69–74.

232. Schulman S, Oppenheim JD, Vanderberg JP. Plasmodium berghei and Plasmodium knowlesi: Serum binding to sporozoites. Exp Parasitol. 1980 Jun;49(3):420–9.

233. Heidrich H-G, Danforth HD, Leef JL, Beaudoin RL. Free-Flow Electrophoretic Separation of Plasmodium berghei Sporozoites. The Journal of Parasitology. 1983 Apr;69(2):360.

234. Mack SR, Vanderberg JP, Nawrot R. Column separation of Plasmodium berghei

sporozoites. The Journal of Parasitology. 1978 Feb;64(1):166–8.

235. Moser G, Brohn FH, Danforth HD, Nussenzweig RS. Sporozoites of Rodent and Simian Malaria, Purified by Anion Exchangers, Retain their Immunogenicity and Infectivity. Journal of Eukaryotic Microbiology. 1978 Feb 1;25(1):119–24.

236. Hegge S, Kudryashev M, Barniol L, Frischknecht F. Key factors regulating Plasmodium berghei sporozoite survival and transformation revealed by an automated visual assay. FASEB J. 2010 Dec;24(12):5003–12.

237. Lupton EJ, Roth A, Patrapuvich R, Maher SP, Singh N, Sattabongkot J, et al. Enhancing longevity of Plasmodium vivax and P. falciparum sporozoites after dissection from mosquito salivary glands. Parasitology International. 2015 Apr;64(2):211–8.

238. Montagna GN, Buscaglia CA, Munter S, Goosmann C, Frischknecht F, Brinkmann V, et al. Critical Role for Heat Shock Protein 20 (HSP20) in Migration of Malarial Sporozoites. J Biol Chem. 2012 Jan 20;287(4):2410–22.

239. Sinnis P, La Vega De P, Coppi A, Krzych U, Mota MM. Quantification of Sporozoite Invasion, Migration, and Development by Microscopy and Flow Cytometry. Methods in molecular biology (Clifton, NJ). Totowa, NJ: NIH Public Access; 2013;923(Chapter 27):385–400.

240. Hollingdale MR, Leland P, Leef JL, Schwartz AL. Entry of Plasmodium berghei sporozoites into cultured cells, and their transformation into trophozoites. Am J Trop Med Hyg. 1983 Jul;32(4):685–90.

241. Hollingdale MR, Leef JL, McCullough M, Beaudoin RL. In vitro cultivation of the exoerythrocytic stage of Plasmodium berghei from sporozoites. Science. 1981 Aug 28;213(4511):1021–2.

242. Calvo-Calle JM, Moreno A, Eling WM, Nardin EH. In vitro development of infectious liver stages of P. yoelii and P. berghei malaria in human cell lines. Exp Parasitol. 1994 Nov;79(3):362–73.

243. Long GW, Leath S, Schuman R, Hollingdale MR, Ballou WR, Sim BKL, et al. Cultivation of the exoerythrocytic stage of Plasmodium berghei in primary cultures of mouse hepatocytes and continuous mouse cell lines. In Vitro Cell Dev Biol. 1989 Sep;25(9):857–62.

244. Soldatow VY, LeCluyse EL, Griffith LG, Rusyn I. In vitro models for liver toxicity testing. Toxicol Res. 2013;2(1):23–39.

245. Maher SP, Crouse RB, Conway AJ, Bannister EC, Achyuta AKH, Clark AY, et al. Microphysical space of a liver sinusoid device enables simplified long-term

maintenance of chimeric mouse-expanded human hepatocytes. Biomed Microdevices. 5 ed. 2014 Jun 7;16(5):727–36.

246. Epshteyn AA, Maher S, Taylor AJ, Holton AB, Borenstein JT, Cuiffi JD. Membrane-integrated microfluidic device for high-resolution live cell imaging. Biomicrofluidics. 2011 Dec;5(4):046501.

247. Toh Y-C, Lim TC, Tai D, Xiao G, van Noort D, Yu H. A microfluidic 3D hepatocyte chip for drug toxicity testing. Lab Chip. 2009 Jul 21;9(14):2026–35.

248. Lee PJ, Hung PJ, Lee LP. An artificial liver sinusoid with a microfluidic endothelial-like barrier for primary hepatocyte culture. Biotechnol Bioeng. 2007;97(5):1340–6.

249. Kane BJ, Zinner MJ, Yarmush ML, Toner M. Liver-specific functional studies in a microfluidic array of primary mammalian hepatocytes. Anal Chem. 2006 Jul;78(13):4291–8.

250. Choi HJ, Choi D. Successful mouse hepatocyte culture with sandwich collagen gel formation. J Korean Surg Soc. 2013 Apr;84(4):202–8.

251. Hegde M, Jindal R, Bhushan A, Bale SS, McCarty WJ, Golberg I, et al. Dynamic interplay of flow and collagen stabilizes primary hepatocytes culture in a microfluidic platform. Lab Chip. 2014 May 19;14(12):2033–9.

252. Khetani SR, Bhatia SN. Microscale culture of human liver cells for drug development. Nat Biotechnol. 2007 Nov 18;26(1):120–6.

253. Nakatsuka H. Shear stress induces hepatocyte PAI-1 gene expression through cooperative Sp1/Ets-1 activation of transcription. AJP: Gastrointestinal and Liver Physiology. 2006 Mar 24;291(1):G26–G34.

254. Tilles AW, Baskaran H, Roy P, Yarmush ML, Toner M. Effects of oxygenation and flow on the viability and function of rat hepatocytes cocultured in a microchannel flat-plate bioreactor. Biotechnol Bioeng. 2001 Jun 5;73(5):379–89.

255. Shah V, Haddad FG, Garcia-Cardena G, Frangos JA, Mennone A, Groszmann RJ, et al. Liver sinusoidal endothelial cells are responsible for nitric oxide modulation of resistance in the hepatic sinusoids. J Clin Invest. 1997 Dec 1;100(11):2923–30.

256. Braet F, Shleper M, Paizi M, Brodsky S, Kopeiko N, Resnick N, et al. Liver sinusoidal endothelial cell modulation upon resection and shear stress in vitro. Comp Hepatol. 2004;3(1):7.

257. Epstein JE, Tewari K, Lyke KE, Sim BKL, Billingsley PF, Laurens MB, et al. Live

Attenuated Malaria Vaccine Designed to Protect Through Hepatic CD8+ T Cell Immunity. Science. 2011 Oct 28;334(6055):475–80.

258. Shekalaghe S, Rutaihwa M, Billingsley PF, Chemba M, Daubenberger CA, James ER, et al. Controlled human malaria infection of Tanzanians by intradermal injection of aseptic, purified, cryopreserved Plasmodium falciparum sporozoites. Am J Trop Med Hyg. 2014 Sep;91(3):471–80.

259. Sheehy SH, Spencer AJ, Douglas AD, Sim BKL, Longley RJ, Edwards NJ, et al. Optimising Controlled Human Malaria Infection Studies Using Cryopreserved P. falciparum Parasites Administered by Needle and Syringe. Ellis RD, editor. PLoS ONE. 2013 Jun 18;8(6):e65960.

260. FFE Service GmbH. FFE Service Website [Internet]. Munich; [cited 2017]. Available from: http://www.ffeservice.com

261. Hannig K, Heidrich H-G. Free-Flow Electrophoresis: An Important Preparative and Analytical Technique for Biology, Biochemistry and Diagnostics. 1st ed. Darmstadt: Git Verlag; 1990.

262. Winn WC, Koneman EW. Koneman's Color Atlas and Textbook of Diagnostic Microbiology. 7 ed. Lippincott Williams & Wilkins; 2016.

263. Hubálek Z. Protectants used in the cryopreservation of microorganisms. Cryobiology. 2003 Jun;46(3):205–29.

264. Diamond LS. Cryopreservation and Storage of Parasitic Protozoa in Liquid Nitrogen. Journal of Eukaryotic Microbiology. 1995 Sep 1;42(5):585–90.

265. Booth KS, James ER, Popiel I. Cryopreservation of an Attenuated Vaccine Strain of the Protozoan ParasiteToxoplasma gondii. Cryobiology. 1996 Jun;33(3):330–7.

266. Blanch E, Tomás C, Hernández M, Roca J, Martínez EA, Vázquez JM, et al. Egg Yolk and Glycerol Requirements for Freezing Boar Spermatozoa Treated with Methyl β-Cyclodextrin or Cholesterol-loaded Cyclodextrin. J Reprod Dev. 2014;60(2):143–9.

267. Vaccines TMCGO. A Research Agenda for Malaria Eradication: Vaccines. PLoS Med. 2011 Jan 25;8(1):e1000398.

268. Drugs TMCGO. A Research Agenda for Malaria Eradication: Drugs. PLoS Med. 2011 Jan 25;8(1):e1000402.

269. Yoshida N, Nussenzweig RS, Potocnjak P, Nussenzweig V, Aikawa M. Hybridoma produces protective antibodies directed against the sporozoite stage of malaria parasite. Science. 1980 Jan 4;207(4426):71–3.

270. Ferguson DJP, Balaban AE, Patzewitz E-M, Wall RJ, Hopp CS, Poulin B, et al. The Repeat Region of the Circumsporozoite Protein is Critical for Sporozoite Formation and Maturation in Plasmodium. Silvie O, editor. PLoS ONE. 2014 Dec 1;9(12):e113923.

271. Coppi A, Pinzon-Ortiz C, Hutter C, Sinnis P. The Plasmodium circumsporozoite protein is proteolytically processed during cell invasion. The Journal of Experimental Medicine. 2005 Jan 3;201(1):27–33.

272. Vanderberg JP. Development of Infectivity by the Plasmodium berghei Sporozoite. The Journal of Parasitology. 1975 Feb;61(1):43.

273. Fairley B. Sidelights on malaria in man obtained by subinoculation experiments. Transactions of the Royal Society of Tropical Medicine and Hygiene. May 1947;40(5):612-676.

274. Yamauchi LM, Coppi A, Snounou G, Sinnis P. Plasmodium sporozoites trickle out of the injection site. Cell Microbiol. 2007 May 1;9(5):1215–22.

275. Billman ZP, Seilie AM, Murphy SC. Purification of Plasmodium Sporozoites Enhances Parasite-Specific CD8+ T Cell Responses. Adams JH, editor. Infect Immun. 2016 Aug 1;84(8):2233–42.

276. Singh N, Barnes SJ, Kennedy S, Adams JH. Experimental evaluation of cryopreservative solutions to maintain in vitro and in vivo infectivity of P. berghei sporozoites. PLoS ONE. 2017 May 22;12(5):e0177304.

277. Werren JH, Baldo L, Clark ME. Wolbachia: master manipulators of invertebrate biology. Nature Reviews. 2008 Oct;6(10):741–51.

278. Xi Z. Wolbachia Establishment and Invasion in an Aedes aegypti Laboratory Population. Science. 2005 Oct 14;310(5746):326–8.

279. Koehncke A, Telschow A, Werren JH, Hammerstein P. Life and Death of an Influential Passenger: Wolbachia and the Evolution of CI-Modifiers by Their Hosts. Ausubel FM, editor. PLoS ONE. 2009 Feb 11;4(2):e4425.

280. Hosokawa T, Koga R, Kikuchi Y, Meng XY, Fukatsu T. Wolbachia as a bacteriocyte-associated nutritional mutualist. Proc Natl Acad Sci USA. 2010 Jan 12;107(2):769–74.

281. Fenton A, Johnson KN, Brownlie JC, Hurst GDD. Solving the Wolbachia Paradox: Modeling the Tripartite Interaction between Host, Wolbachia, and a Natural Enemy. The American Naturalist. 2011 Sep;178(3):333–42.

282. Jones EO, White A, Boots M. Interference and the persistence of vertically transmitted parasites. Journal of Theoretical Biology. 2007 May;246(1):10–7.

283. Lively CM, Keith Clay, Wade MJ, Fuqua C. Competitive co-existence of vertically and horizontally transmitted parasites. Evol Ecol Res. 2005;7(8):1183–90.

284. Hughes GL, Vega-Rodriguez J, Xue P, Rasgon JL. Wolbachia Strain wAlbB Enhances Infection by the Rodent Malaria Parasite Plasmodium berghei in Anopheles gambiae Mosquitoes. Applied and Environmental Microbiology. 2012 Feb 14;78(5):1491–5.

285. Moreira LA, Iturbe-Ormaetxe I, Jeffery JA, Lu G, Pyke AT, Hedges LM, et al. A Wolbachia Symbiont in Aedes aegypti Limits Infection with Dengue, Chikungunya, and Plasmodium. Cell. 2009 Dec;139(7):1268–78.

286. Hughes GL, Ren X, Ramirez JL, Sakamoto JM, Bailey JA, Jedlicka AE, et al. Wolbachia Infections in Anopheles gambiae Cells: Transcriptomic Characterization of a Novel Host-Symbiont Interaction. PLoS Pathog. 2011 Feb 17;7(2):e1001296.

287. Min KT, Benzer S. Wolbachia, normally a symbiont of Drosophila, can be virulent, causing degeneration and early death. Proc Natl Acad Sci USA. 1997 Sep 30;94(20):10792–6.

288. Briegel H. Fecundity, Metabolism, and Body Size in Anopheles (Diptera: Culicidae), Vectors of Malaria. Journal of Medical Entomology. 1990 Sep 1;27(5):839–50.

289. Arsic D, Guerin PM. Nutrient content of diet affects the signaling activity of the insulin/target of rapamycin/p70 S6 kinase pathway in the African malaria mosquito Anopheles gambiae. Journal of Insect Physiology. 2008 Aug;54(8):1226–35.

290. Brandon MC, Pennington JE, Isoe J, Zamora J, Schillinger A-S, Miesfeld RL. TOR signaling is required for amino acid stimulation of early trypsin protein synthesis in the midgut of Aedes aegypti mosquitoes. Insect Biochemistry and Molecular Biology. 2008 Oct;38(10):916–22.

291. Hughes GL, Pike AD, Xue P, Rasgon JL. Invasion of Wolbachia into Anopheles and Other Insect Germlines in an Ex vivo Organ Culture System. PLoS ONE. 2012 Apr 30;7(4):e36277.

292. Kapahi P, Zid BM, Harper T, Koslover D, Sapin V, Benzer S. Regulation of Lifespan in Drosophila by Modulation of Genes in the TOR Signaling Pathway. Current Biology. 2004 May;14(10):885–90.

293. Weichhart T, Hengstschläger M, Linke M. Regulation of innate immune cell function by mTOR. Nat Rev Immunol. 2015 Sep 25;15(10):599–614.

294. Soulard A, Cohen A, Hall MN. TOR signaling in invertebrates. Current Opinion in Cell Biology. 2009 Dec;21(6):825–36.

295. Wullschleger S, Loewith R, Hall MN. TOR Signaling in Growth and Metabolism. Cell. 2006 Feb;124(3):471–84.

296. Nidai Ozes O, Mayo LD, Gustin JA, Pfeffer SR, Pfeffer LM, Donner DB. NF-[kappa]B activation by tumour necrosis factor requires the Akt serine-threonine kinase. Nature. 1999 Sep 2;401(6748):82–5.

297. Crespo JL, Hall MN. Elucidating TOR signaling and rapamycin action: lessons from Saccharomyces cerevisiae. Microbiol Mol Biol Rev. 2002 Dec;66(4):579–91.

298. Heitman J, Movva NR, Hall MN. Targets for cell cycle arrest by the immunosuppressant rapamycin in yeast. Science. 1991 Aug 23;253(5022):905–9.

299. Loewith R, Jacinto E, Wullschleger S, Lorberg A, Crespo JL, Bonenfant D, et al. Two TOR Complexes, Only One of which Is Rapamycin Sensitive, Have Distinct Roles in Cell Growth Control. Molecular Cell. 2002 Sep;10(3):457–68.

300. Feldman ME, Apsel B, Uotila A, Loewith R, Knight ZA, Ruggero D, et al. Active-Site Inhibitors of mTOR Target Rapamycin-Resistant Outputs of mTORC1 and mTORC2. PLoS Biol. 2009 Feb 1;7(2):e1000038.

301. Sarbassov DD, Ali SM, Sengupta S, Sheen J-H, Hsu PP, Bagley AF, et al. Prolonged Rapamycin Treatment Inhibits mTORC2 Assembly and Akt/PKB. Molecular Cell. 2006 Apr;22(2):159–68.

302. Facchinetti V, Ouyang W, Wei H, Soto N, Lazorchak A, Gould C, et al. The mammalian target of rapamycin complex 2 controls folding and stability of Akt and protein kinase C. EMBO J. 2008 Jul 23;27(14):1932–43.

303. D Sarbassov Dos, Guertin DA, Ali SM, Sabatini DM. Phosphorylation and Regulation of Akt/PKB by the Rictor-mTOR Complex. Science. 2005 Feb 18;307(5712):1098–101.

304. Alessi DR, Andjelkovic M, Caudwell B, Cron P, Morrice N, Cohen P, et al. Mechanism of activation of protein kinase B by insulin and IGF-1. EMBO J. 1996 Dec 2;15(23):6541–51.

305. Manning BD, Cantley LC. AKT/PKB Signaling: Navigating Downstream. Cell. 2007 Jun;129(7):1261–74.

306. Shimobayashi M, Hall MN. Making new contacts: the mTOR network in metabolism and signalling crosstalk. Nature Reviews Molecular Cell Biology.

2014 Mar 1;15(3):155–62.

307. Hall MN. TOR and paradigm change: cell growth is controlled. Mol Biol Cell. 2016 Sep 15;27(18):2804–6.

308. Dobrenel T, Caldana C, Hanson J, Robaglia C, Vincentz M, Veit B, et al. TOR Signaling and Nutrient Sensing. Annu Rev Plant Biol. 2016 Apr 29;67(1):261–85.

309. Hansen IA, Attardo GM, Park J-H, Peng Q, Raikhel AS. Target of rapamycin-mediated amino acid signaling in mosquito anautogeny. Proc Natl Acad Sci USA. 2004 Jul 20;101(29):10626–31.

310. Sancak Y, Thoreen CC, Peterson TR, Lindquist RA, Kang SA, Spooner E, et al. PRAS40 Is an Insulin-Regulated Inhibitor of the mTORC1 Protein Kinase. Molecular Cell. 2007 Mar;25(6):903–15.

311. Riehle MA, Brown MR. Molecular analysis of the serine/threonine kinase Akt and its expression in the mosquito Aedes aegypti. Insect Molecular Biology. 2003 Jun 1;12(3):225–32.

312. Oh WJ, Wu CC, Kim SJ, Facchinetti V, Julien LA, Finlan M, et al. mTORC2 can associate with ribosomes to promote cotranslational phosphorylation and stability of nascent Akt polypeptide. EMBO J. 2010 Dec 1;29(23):3939–51.

313. Fernandez R, Tabarini D, Azpiazu N, Frasch M, Schlessinger J. The Drosophila insulin receptor homolog: a gene essential for embryonic development encodes two receptor isoforms with different signaling potential. EMBO J. 1995 Jul 17;14(14):3373–84.

314. Chen C, Jack J, Garofalo RS. The Drosophila insulin receptor is required for normal growth. Endocrinology.; 1996 Mar 1;137(3):846–56.

315. Riehle MA, Garczynski SF, Crim JW, Hill CA, Brown MR. Neuropeptides and Peptide Hormones in Anopheles gambiae. Science. 2002 Oct 4;298(5591):172–5.

316. Potter CJ, Huang H, Xu T. Drosophila Tsc1 Functions with Tsc2 to Antagonize Insulin Signaling in Regulating Cell Growth, Cell Proliferation, and Organ Size. Cell. 2001 May;105(3):357–68.

317. Dong J, Pan D. Tsc2 is not a critical target of Akt during normal Drosophila development. Genes Dev. 2004 Oct 15;18(20):2479–84.

318. Long X, Lin Y, Ortiz-Vega S, Yonezawa K, Avruch J. Rheb Binds and Regulates the mTOR Kinase. Current Biology. 2005 Apr;15(8):702–13.

319. D Sarbassov Dos, Ali SM, Kim D-H, Guertin DA, Latek RR, Erdjument-Bromage H, et al. Rictor, a Novel Binding Partner of mTOR, Defines a Rapamycin-Insensitive and Raptor-Independent Pathway that Regulates the Cytoskeleton. Current Biology. 2004 Jul;14(14):1296–302.

320. Jacinto E, Facchinetti V, Liu D, Soto N, Wei S, Jung SY, et al. SIN1/MIP1 Maintains rictor-mTOR Complex Integrity and Regulates Akt Phosphorylation and Substrate Specificity. Cell. 2006 Oct;127(1):125–37.

321. Lee G, Chung J. Discrete functions of rictor and raptor in cell growth regulation in Drosophila. Biochemical and Biophysical Research Communications. 2007 Jun;357(4):1154–9.

322. Inoki K, Zhu T, Guan K-L. TSC2 Mediates Cellular Energy Response to Control Cell Growth and Survival. Cell. 2003 Nov;115(5):577–90.

323. Hahn-Windgassen A, Nogueira V, Chen C-C, Skeen JE, Sonenberg N, Hay N. Akt activates the mammalian target of rapamycin by regulating cellular ATP level and AMPK activity. J Biol Chem. 2005 Sep 16;280(37):32081–9.

324. Edinger AL, Thompson CB. Akt maintains cell size and survival by increasing mTOR-dependent nutrient uptake. Mol Biol Cell. 2002 Jul;13(7):2276–88.

325. Taguchi A, White MF. Insulin-Like Signaling, Nutrient Homeostasis, and Life Span. Annu Rev Physiol. 2008 Mar;70(1):191–212.

326. Guertin DA, Stevens DM, Thoreen CC, Burds AA, Kalaany NY, Moffat J, et al. Ablation in Mice of the mTORC Components raptor, rictor, or mLST8 Reveals that mTORC2 Is Required for Signaling to Akt-FOXO and PKCα, but Not S6K1. Developmental Cell. 2006 Dec;11(6):859–71.

327. Teleman AA, Chen Y-W, Cohen SM. Drosophila Melted Modulates FOXO and TOR Activity. Developmental Cell. 2005 Aug;9(2):271–81.

328. Lee JH, Budanov AV, Park EJ, Birse R, Kim TE, Perkins GA, et al. Sestrin as a Feedback Inhibitor of TOR That Prevents Age-Related Pathologies. Science. 2010 Mar 5;327(5970):1223–8.

329. Hay N. Interplay between FOXO, TOR, and Akt. Biochim Biophys Acta. 2011 Nov;1813(11):1965–70.

330. Feng Z, Zhang H, Levine AJ, Jin S. The coordinate regulation of the p53 and mTOR pathways in cells. Proc Natl Acad Sci USA. 2005 Jun 7;102(23):8204–9.

331. Stambolic V, MacPherson D, Sas D, Lin Y, Snow B, Jang Y, et al. Regulation of PTEN Transcription by p53. Molecular Cell. 2001 Aug;8(2):317–25.

332. Greer EL, Oskoui PR, Banko MR, Maniar JM, Gygi MP, Gygi SP, et al. The Energy Sensor AMP-activated Protein Kinase Directly Regulates the Mammalian FOXO3 Transcription Factor. J Biol Chem. 2007 Aug 3;282(41):30107–19.

333. Greer EL, Dowlatshahi D, Banko MR, Villen J, Hoang K, Blanchard D, et al. An AMPK-FOXO Pathway Mediates Longevity Induced by a Novel Method of Dietary Restriction in C. elegans. Current Biology. 2007 Oct;17(19):1646–56.

334. Ma L, Chen Z, Erdjument-Bromage H, Tempst P, Pandolfi PP. Phosphorylation and Functional Inactivation of TSC2 by Erk. Cell. 2005 Apr 22;121(2):179–93.

335. Findlay GM, Yan L, Procter J, Mieulet V, Lamb RF. A MAP4 kinase related to Ste20is a nutrient-sensitive regulator of mTOR signalling. Biochemical Journal. 2007 Apr 1;403(1):13–20.

336. Chapuis N, Tamburini J, Green AS, Willems L, Bardet V, Park S, et al. Perspectives on inhibiting mTOR as a future treatment strategy for hematological malignancies. Leukemia. 2010 Aug 12;24(10):1686–99.

337. Gao X, Zhang Y, Arrazola P, Hino O, Kobayashi T, Yeung RS, et al. Tsc tumour suppressor proteins antagonize amino-acid–TOR signalling. Nat Cell Biol. 2002 Aug 12;4(9):699–704.

338. Saucedo LJ, Gao X, Chiarelli DA, Li L, Pan D, Edgar BA. Rheb promotes cell growth as a component of the insulin/TOR signalling network. Nat Cell Biol. 2003 May 27;5(6):566–71.

339. Garami A, Zwartkruis FJT, Nobukuni T, Joaquin M, Roccio M, Stocker H, et al. Insulin activation of Rheb, a mediator of mTOR/S6K/4E-BP signaling, is inhibited by TSC1 and 2. Molecular Cell. 2003 Jun;11(6):1457–66.

340. Anthony JC, Lang CH, Crozier SJ, Anthony TG, MacLean DA, Kimball SR, et al. Contribution of insulin to the translational control of protein synthesis in skeletal muscle by leucine. American Journal of Physiology - Endocrinology and Metabolism. 2002 May 1;282(5):E1092–101.

341. Byfield MP, Murray JT, Backer JM. hVps34 is a nutrient-regulated lipid kinase required for activation of p70 S6 kinase. J Biol Chem. 2005 Sep 23;280(38):33076–82.

342. Nobukuni T, Joaquin M, Roccio M, Dann SG, Kim SY, Gulati P, et al. Amino acids mediate mTOR/raptor signaling through activation of class 3 phosphatidylinositol 3OH-kinase. Proc Natl Acad Sci USA. 2005 Oct 4;102(40):14238–43.

343. Juhaz G. The class III PI(3)K Vps34 promotes autophagy and endocytosis but not TOR signaling in Drosophila. [Internet]. Vol. 181, The Journal of Cell Biology. 2008 May 18;181(4):655–66.

344. Kim E, Goraksha-Hicks P, Li L, Neufeld TP, Guan K-L. Regulation of TORC1 by Rag GTPases in nutrient response. Nat Cell Biol. 2008 Jul 6;10(8):935–45.

345. Sancak Y, Peterson TR, Shaul YD, Lindquist RA, Thoreen CC, Bar-Peled L, et al. The Rag GTPases Bind Raptor and Mediate Amino Acid Signaling to mTORC1. Science. 2008 Jun 13;320(5882):1496–501.

346. Peyrollier K, Hajduch E, Blair AS, Hyde R, Hundal HS. l-Leucine availability regulates phosphatidylinositol 3-kinase, p70 S6 kinase and glycogen synthase kinase-3 activity in L6 muscle cells: evidence for the involvement of the mammalian target of rapamycin (mTOR) pathway in the l-leucine-induced up-regulation of System A amino acid transport. Biochemical Journal. 2000 Sep 1;350(2):361–8.

347. Roos S, Kanai Y, Prasad PD, Powell TL, Jansson T. Regulation of placental amino acid transporter activity by mammalian target of rapamycin. American Journal of Physiology - Cell Physiology. 2009 Jan 1;296(1):C142–50.

348. Jacinto E, Loewith R, Schmidt A, Lin S, Rüegg MA, Hall A, et al. Mammalian TOR complex 2 controls the actin cytoskeleton and is rapamycin insensitive. Nat Cell Biol. 2004 Nov 1;6(11):1122–8.

349. Ridley AJ. [33] Growth factor-induced actin reorganization in Swiss 3T3 cells. In: Small GTPases and Their Regulators Part B: Rho Family. Elsevier; 1995. pp. 306–13. (Methods in Enzymology; vol. 256).

350. Xia Y, Wen HY, Young ME, Guthrie PH, Taegtmeyer H, Kellems RE. Mammalian target of rapamycin and protein kinase A signaling mediate the cardiac transcriptional response to glutamine. J Biol Chem. 2003 Apr 11;278(15):13143–50.

351. García-Martínez JM, Alessi DR. mTOR complex 2 (mTORC2) controls hydrophobic motif phosphorylation and activation of serum- and glucocorticoid-induced protein kinase 1 (SGK1). Biochemical Journal. 2008 Dec 15;416(3):375–85.

352. Jones KT, Greer ER, Pearce D, Ashrafi K. Rictor/TORC2 Regulates Caenorhabditis elegans Fat Storage, Body Size, and Development through sgk-1. Hunter T, editor. PLoS Biol. 2009 Mar 3;7(3):e1000060.

353. Soukas AA, Kane EA, Carr CE, Melo JA, Ruvkun G. Rictor/TORC2 regulates fat metabolism, feeding, growth, and life span in Caenorhabditis elegans. Genes

Dev. 2009 Feb 15;23(4):496–511.

354. Miron M, Sonenberg N. Regulation of Translation via TOR Signaling: Insights from Drosophila melanogaster. J Nutr. 2001 Nov 1;131(11):2988S–2993S.

355. Miron M, Verdú J, Lachance PED, Birnbaum MJ, Lasko PF, Sonenberg N. The translational inhibitor 4E-BP is an effector of PI(3)K/Akt signalling and cell growth in : Drosophila. Nat Cell Biol. 2001 May 17;3(6):596–601.

356. Pende M, Um SH, Mieulet V, Sticker M, Goss VL, Mestan J, et al. S6K1(-/-)/S6K2(-/-) mice exhibit perinatal lethality and rapamycin-sensitive 5'-terminal oligopyrimidine mRNA translation and reveal a mitogen-activated protein kinase-dependent S6 kinase pathway. Mol Cell Biol. 2004 Apr;24(8):3112–24.

357. Ruvinsky I. Ribosomal protein S6 phosphorylation is a determinant of cell size and glucose homeostasis. Genes Dev. 2005 Sep 15;19(18):2199–211.

358. Thoreen CC, Chantranupong L, Keys HR, Wang T, Gray NS, Sabatini DM. A unifying model for mTORC1-mediated regulation of mRNA translation. Nature. 2012 May 2;485(7396):109–13.

359. Chauvin C, Koka V, Nouschi A, Mieulet V, Hoareau-Aveilla C, Dreazen A, et al. Ribosomal protein S6 kinase activity controls the ribosome biogenesis transcriptional program. Oncogene. 2013 Jan 14;33(4):474–83.

360. Mieulet V, Roceri M, Espeillac C, Sotiropoulos A, Ohanna M, Oorschot V, et al. S6 kinase inactivation impairs growth and translational target phosphorylation in muscle cells maintaining proper regulation of protein turnover. American Journal of Physiology - Cell Physiology. 2007 Apr 11;293(2):C712–22.

361. Gingras A-C, Raught B, Sonenberg N. eIF4 initiation factors: effectors of mRNA recruitment to ribosomes and regulators of translation. Annu Rev Biochem. 1999 Jun;68(1):913–63.

362. Hsieh AC, Liu Y, Edlind MP, Ingolia NT, Janes MR, Sher A, et al. The translational landscape of mTOR signalling steers cancer initiation and metastasis. Nature. 2012 Feb 22;485(7396):55–61.

363. Harrington LS, Findlay GM, Gray A, Tolkacheva T, Wigfield S, Rebholz H, et al. The TSC1-2 tumor suppressor controls insulin-PI3K signaling via regulation of IRS proteins. The Journal of Cell Biology. 2004 Jul 19;166(2):213–23.

364. Shah OJ, Wang Z, Hunter T. Inappropriate Activation of the TSC/Rheb/mTOR/S6K Cassette Induces IRS1/2 Depletion, Insulin Resistance, and Cell Survival Deficiencies. Current Biology. 2004 Sep;14(18):1650–6.

365. Um SH, Frigerio F, Watanabe M, Picard F, Joaquin M, Sticker M, et al. Absence

of S6K1 protects against age- and diet-induced obesity while enhancing insulin sensitivity. Nature. 2004 Aug 11;431(7005):200–5.

366. Tremblay F, Jacques H, Marette A. Modulation of insulin action by dietary proteins and amino acids: role of the mammalian target of rapamycin nutrient sensing pathway. Curr Opin Clin Nutr Metab Care. 2005 Jul;8(4):457–62.

367. Manning BD. Balancing Akt with S6K: implications for both metabolic diseases and tumorigenesis. The Journal of Cell Biology. 2004 Nov 8;167(3):399–403.

368. Demontis F, Perrimon N. Integration of Insulin receptor/Foxo signaling and dMyc activity during muscle growth regulates body size in Drosophila. Development. 2009 Feb 20;136(6):983–93.

369. Teleman AA, Hietakangas V, Sayadian AC, Cohen SM. Nutritional Control of Protein Biosynthetic Capacity by Insulin via Myc in Drosophila. Cell Metabolism. 2008 Jan;7(1):21–32.

370. Read RD, Cavenee WK, Furnari FB, Thomas JB. A Drosophila Model for EGFR-Ras and PI3K-Dependent Human Glioma. PLoS Genet. 2009 Feb 13;5(2):e1000374.

371. Peng T, Golub TR, Sabatini DM. The immunosuppressant rapamycin mimics a starvation-like signal distinct from amino acid and glucose deprivation. Mol Cell Biol. American Society for Microbiology; 2002 Aug;22(15):5575–84.

372. Düvel K, Yecies JL, Menon S, Raman P, Lipovsky AI, Souza AL, et al. Activation of a Metabolic Gene Regulatory Network Downstream of mTOR Complex 1. Molecular Cell. 2010 Jul;39(2):171–83.

373. Hagiwara A, Cornu M, Cybulski N, Polak P, Betz C, Trapani F, et al. Hepatic mTORC2 Activates Glycolysis and Lipogenesis through Akt, Glucokinase, and SREBP1c. Cell Metabolism. 2012 May;15(5):725–38.

374. Gstaiger M, Luke B, Hess D, Oakeley EJ, Wirbelauer C, Blondel M, et al. Control of Nutrient-Sensitive Transcription Programs by the Unconventional Prefoldin URI. Science. 2003 Nov 14;302(5648):1208–12.

375. Fingar DC. Mammalian cell size is controlled by mTOR and its downstream targets S6K1 and 4EBP1/eIF4E. Genes Dev. 2002 Jun 15;16(12):1472–87.

376. Barbet NC, Schneider U, Helliwell SB, Stansfield I, Tuite MF, Hall MN. TOR controls translation initiation and early G1 progression in yeast. Mol Biol Cell. 1996 Jan 1;7(1):25–42.

377. Fingar DC, Richardson CJ, Tee AR, Cheatham L, Tsou C, Blenis J. mTOR Controls Cell Cycle Progression through Its Cell Growth Effectors S6K1 and 4E-

BP1/Eukaryotic Translation Initiation Factor 4E. Mol Cell Biol. 2003 Dec 12;24(1):200–16.

378. Leevers SJ. Growth control: Invertebrate insulin surprises! Current Biology. 2001 Mar;11(6):R209–12.

379. Carter AJ. TOR of the cell cycle: Are there important implications for diabetics in the era of the drug-eluting stent? Catheterization and Cardiovascular Interventions. 2004 Feb 1;61(2):233–6.

380. Moreno-Torres M, Jaquenoud M, De Virgilio C. TORC1 controls G1–S cell cycle transition in yeast via Mpk1 and the greatwall kinase pathway. Nature Communications. 2015 Sep 10;6:8256.

381. Zhou BP, Liao Y, Xia W, Spohn B, Lee M-H, Hung M-C. Cytoplasmic localization of p21Cip1/WAF1 by Akt-induced phosphorylation in HER-2/neu-overexpressing cells. Nat Cell Biol. 2001 Feb 5;3(3):245–52.

382. Rossig L, Jadidi AS, Urbich C, Badorff C, Zeiher AM, Dimmeler S. Akt-Dependent Phosphorylation of p21Cip1 Regulates PCNA Binding and Proliferation of Endothelial Cells. Mol Cell Biol. 2001 Aug 15;21(16):5644–57.

383. Malagoli D, Abdalla FC, Cao Y, Feng Q, Fujisaki K, Gregorc A, et al. Autophagy and its physiological relevance in arthropods: current knowledge and perspectives. Autophagy. 2010 Jul;6(5):575–88.

384. Bryant B, Raikhel AS. Programmed Autophagy in the Fat Body of Aedes aegypti Is Required to Maintain Egg Maturation Cycles. PLoS ONE. 2011 Nov 17;6(11):e25502.

385. Yorimitsu T, Klionsky DJ. Autophagy: molecular machinery for self-eating. Cell Death Differ. 2005 Nov;12 Suppl 2:1542–52.

386. Meléndez A, Neufeld TP. The cell biology of autophagy in metazoans: a developing story. Development. 2008 Aug;135(14):2347–60.

387. Levine B, Mizushima N, Virgin HW. Autophagy in immunity and inflammation. Nature. 2011 Jan 20;469(7330):323–35.

388. Deretic V, Saitoh T, Akira S. Autophagy in infection, inflammation and immunity. Nat Rev Immunol. 2013 Oct;13(10):722–37.

389. Owen KA, Casanova JE. Salmonella Manipulates Autophagy to “Serve and Protect.” Cell Host Microbe. 2015 Nov 11;18(5):517–9.

390. Krokowski S, Mostowy S. Interactions between Shigella flexneri and the Autophagy Machinery. Front Cell Infect Microbiol. 2016 Feb 10;6(219):448.

391. Mesquita FS, Thomas M, Sachse M, Santos AJM, Figueira R, Holden DW. The Salmonella Deubiquitinase SseL Inhibits Selective Autophagy of Cytosolic Aggregates. PLoS Pathog. 2012 Jun 14;8(6):e1002743.

392. Kreibich S, Emmenlauer M, Fredlund J, Rämö P, Münz C, Dehio C, et al. Autophagy Proteins Promote Repair of Endosomal Membranes Damaged by the Salmonella Type Three Secretion System 1. Cell Host Microbe. 2015 Nov;18(5):527–37.

393. Baxt LA, Goldberg MB. Host and Bacterial Proteins That Repress Recruitment of LC3 to Shigella Early during Infection. Chakravortty D, editor. PLoS ONE. 2014 Apr 10;9(4):e94653.

394. Rancès E, Voronin D, Tran-Van V, Mavingui P. Genetic and functional characterization of the type IV secretion system in Wolbachia. J Bacteriol. 2008 Jul;190(14):5020–30.

395. Travassos LH, Carneiro LAM, Ramjeet M, Hussey S, Kim Y-G, Magalhães JG, et al. Nod1 and Nod2 direct autophagy by recruiting ATG16L1 to the plasma membrane at the site of bacterial entry. Nat Immunol. 2009;11(1):55–62.

396. Hayashi-Nishino M, Fujita N, Noda T, Yamaguchi A, Yoshimori T, Yamamoto A. A subdomain of the endoplasmic reticulum forms a cradle for autophagosome formation. Nat Cell Biol. 2009 Dec;11(12):1433–7.

397. Klionsky DJ. Autophagy: from phenomenology to molecular understanding in less than a decade. Nature Reviews Molecular Cell Biology. 2007 Nov;8(11):931–7.

398. Virgin HW, Levine B. Autophagy genes in immunity. Nat Immunol. 2009 May;10(5):461–70.

399. Deretic V, Levine B. Autophagy, immunity, and microbial adaptations. Cell Host Microbe. 2009 Jun 18;5(6):527–49.

400. Sumpter R, Levine B. Autophagy and innate immunity: triggering, targeting and tuning. Semin Cell Dev Biol. 2010 Sep;21(7):699–711.

401. Yang Z, Klionsky DJ. Eaten alive: a history of macroautophagy. Nat Cell Biol. 2010 Sep 1;12(9):814–22.

402. Liu B, Cheng Y, Liu Q, Bao J-K, Yang J-M. Autophagic pathways as new targets for cancer drug development. Acta Pharmacologica Sinica. 2010 Aug 9;31(9):1154–64.

403. Ma XM, Blenis J. Molecular mechanisms of mTOR-mediated translational control. Nature Reviews Molecular Cell Biology. 2009 Apr 2;10(5):307–18.

404. Noriega FG, Colonna AE, A Wells M. Increase in the size of the amino acid pool is sufficient to activate translation of early trypsin mRNA in Aedes aegypti midgut. Insect Biochemistry and Molecular Biology. 1999 Mar;29(3):243–7.

405. Brown MR, Clark KD, Gulia M, Zhao Z, Garczynski SF, Crim JW, et al. An insulin-like peptide regulates egg maturation and metabolism in the mosquito Aedes aegypti. Proceedings of the National Academy of Sciences. 2008 Apr 15;105(15):5716–21.

406. Wen Z, Gulia M, Clark KD, Dhara A, Crim JW, Strand MR, et al. Two insulin-like peptide family members from the mosquito Aedes aegypti exhibit differential biological and receptor binding activities. Molecular and Cellular Endocrinology. 2010 Oct;328(1-2):47–55.

407. Gulia-Nuss M, Robertson AE, Brown MR, Strand MR. Insulin-Like Peptides and the Target of Rapamycin Pathway Coordinately Regulate Blood Digestion and Egg Maturation in the Mosquito Aedes aegypti. Hansen IA, editor. PLoS ONE. 2011 May 27;6(5):e20401.

408. Riehle MA, Brown MR. Insulin receptor expression during development and a reproductive cycle in the ovary of the mosquito Aedes aegypti. Cell Tissue Res. 2002 Jun 1;308(3):409–20.

409. Graf R, Neuenschwander S, Brown MR, Ackermann U. Insulin-mediated secretion of ecdysteroids from mosquito ovaries and molecular cloning of the insulin receptor homologue from ovaries of bloodfed Aedes aegypti. Insect Molecular Biology. 1997 May 1;6(2):151–63.

410. Martín D, Wang S-F, Raikhel AS. The vitellogenin gene of the mosquito Aedes aegypti is a direct target of ecdysteroid receptor. Molecular and Cellular Endocrinology. 2001 Feb;173(1-2):75–86.

411. Hansen IA, Attardo GM, Park JH, Peng Q, Raikhel AS. Target of rapamycin-mediated amino acid signaling in mosquito anautogeny. Proc Natl Acad Sci USA. 2004 Jul 20;101(29):10626–31.

412. Park J-H, Attardo GM, Hansen IA, Raikhel AS. GATA factor translation is the final downstream step in the amino acid/target-of-rapamycin-mediated vitellogenin gene expression in the anautogenous mosquito Aedes aegypti. J Biol Chem. 2006 Apr 21;281(16):11167–76.

413. Tatar M, Kopelman A, Epstein D, Tu MP, Yin CM, Garofalo RS. A Mutant Drosophila Insulin Receptor Homolog That Extends Life-Span and Impairs Neuroendocrine Function. Science. 2001 Apr 6;292(5514):107–10.

414. Riehle MA, Fan Y, Cao C, Brown MR. Molecular characterization of insulin-like

peptides in the yellow fever mosquito, Aedes aegypti: Expression, cellular localization, and phylogeny. Peptides. 2006 Nov;27(11):2547–60.

415. Wu Q, Zhang Y, Xu J, Shen P. Regulation of hunger-driven behaviors by neural ribosomal S6 kinase in Drosophila. Proc Natl Acad Sci USA. 2005 Sep 13;102(37):13289–94.

416. Beier MS, Pumpuni CB, Beier JC, Davis JR. Effects of Para-Aminobenzoic Acid, Insulin, and Gentamicin on Plasmodium falciparum Development in Anopheline Mosquitoes (Diptera: Culicidae). Journal of Medical Entomology. 1994 Jul 1;31(4):561–5.

417. Hopwood JA, Ahmed AM, Polwart A, Williams GT, Hurd H. Malaria-induced apoptosis in mosquito ovaries: a mechanism to control vector egg production. Journal of Experimental Biology. 2001 Aug;204(Pt 16):2773–80.

418. Fulton D, Gratton JP, McCabe TJ, Fontana J, Fujio Y, Walsh K, et al. Regulation of endothelium-derived nitric oxide production by the protein kinase Akt. Nature. 1999 Jun 10;399(6736):597–601.

419. Bian G, Xu Y, Lu P, Xie Y, Xi Z. The Endosymbiotic Bacterium Wolbachia Induces Resistance to Dengue Virus in Aedes aegypti. Schneider DS, editor. PLoS Pathog. 2010 Apr 1;6(4):e1000833.

420. Thoreen CC, Kang SA, Chang JW, Liu Q, Zhang J, Gao Y, et al. An ATP-competitive mammalian target of rapamycin inhibitor reveals rapamycin-resistant functions of mTORC1. J Biol Chem. 2009 Mar 20;284(12):8023–32.

421. Benjamin D, Colombi M, Moroni C, Hall MN. Rapamycin passes the torch: a new generation of mTOR inhibitors. Nat Rev Drug Discov. 2011 Oct 31;10(11):868–80.

422. Yang H, Rudge DG, Koos JD, Vaidialingam B, Yang HJ, Pavletich NP. mTOR kinase structure, mechanism and regulation. Nature. 2013 May 9;497(7448):217–23.

423. Jacinto E, Hall MN. TOR signalling in bugs, brain and brawn. Nature Reviews Molecular Cell Biology. 2003 Feb;4(2):117–26.

424. Lamming DW, Ye L, Katajisto P, Goncalves MD, Saitoh M, Stevens DM, et al. Rapamycin-Induced Insulin Resistance Is Mediated by mTORC2 Loss and Uncoupled from Longevity. Science. 2012 Mar 30;335(6076):1638–43.

425. Hoang B, Frost P, Shi Y, Belanger E, Benavides A, Pezeshkpour G, et al. Targeting TORC2 in multiple myeloma with a new mTOR kinase inhibitor. Blood. 2010 Nov 25;116(22):4560–8.

426. Voronin D, Cook DAN, Steven A, Taylor MJ. Autophagy regulates Wolbachia populations across diverse symbiotic associations. PNAS. 2012 Jun 19;109(25):E1638–46.

427. Klionsky DJ, Abdalla FC, Abeliovich H, Abraham RT, Acevedo-Arozena A, Adeli K, et al. Guidelines for the use and interpretation of assays for monitoring autophagy. Vol. 8, Autophagy. 2012. pp. 445–544.

428. Oh Y, Bi E. Septin structure and function in yeast and beyond. Trends in Cell Biology. 2011 Mar 1;21(3):141–8.

429. Mostowy S, Bonazzi M, Hamon MA, Tham TN, Mallet A, Lelek M, et al. Entrapment of Intracytosolic Bacteria by Septin Cage-like Structures. Cell Host Microbe. 2010 Nov;8(5):433–44.

430. Wu YT, Tan HL, Shui G, Bauvy C, Huang Q, Wenk MR, et al. Dual role of 3-methyladenine in modulation of autophagy via different patterns of inhibition on class I and III phosphoinositide 3-kinase. J Biol Chem. 2010 Mar 26;285(14):10850–61.

431. Rancès E, Ye YH, Woolfit M, McGraw EA, O'Neill S. The Relative Importance of Innate Immune Priming in Wolbachia-Mediated Dengue Interference. PLoS Pathog. 2012 Feb 23;8(2):e1002548.

432. Osborne SE, Iturbe-Ormaetxe I, Brownlie JC, O'Neill S, Johnson KN. Antiviral protection and the importance of Wolbachia density and tissue tropism in Drosophila simulans. Applied and Environmental Microbiology. 2012 Oct;78(19):6922–9.

433. Osborne SE, Leong YS, O'Neill S, Johnson KN. Variation in Antiviral Protection Mediated by Different Wolbachia Strains in Drosophila simulans. Schneider DS, editor. PLoS Pathog. 2009 Nov 13;5(11):e1000656.

434. Lu P, Bian G, Pan X, Xi Z. Wolbachia Induces Density-Dependent Inhibition to Dengue Virus in Mosquito Cells. PLoS Negl Trop Dis. 2012 Jul 24;6(7):e1754.

435. Frentiu FD, Robinson J, Young PR, McGraw EA, O'Neill S. Wolbachia-Mediated Resistance to Dengue Virus Infection and Death at the Cellular Level. Coffey LL, editor. PLoS ONE. 2010 Oct 15;5(10):e13398.

436. Shackelford RE, Kaufmann WK, Paules RS. Oxidative stress and cell cycle checkpoint function. Free Radic Biol Med. 2000 May 1;28(9):1387–404.

437. Le Clec'h W, Braquart-Varnier C, Raimond M, Ferdy J-B, Bouchon D, Sicard M. High Virulence of Wolbachia after Host Switching: When Autophagy Hurts. PLoS Pathog. 2012 Aug 2;8(8):e1002844.

438. Henault J, Martinez J, Riggs JM, Tian J, Mehta P, Clarke L, et al. Noncanonical Autophagy Is Required for Type I Interferon Secretion in Response to DNA-Immune Complexes. Immunity. 2012 Dec;37(6):986–97.

439. Martinez J, Almendinger J, Oberst A, Ness R, Dillon CP, Fitzgerald P, et al. Microtubule-associated protein 1 light chain 3 alpha (LC3)-associated phagocytosis is required for the efficient clearance of dead cells. Proc Natl Acad Sci USA. 2011 Oct 18;108(42):17396–401.

440. Mathieu J. Interactions between Autophagy and Bacterial Toxins: Targets for Therapy? Toxins. 2015 Aug 4;7(8):2918–58.

441. Lerena MC, Colombo MI. Mycobacterium marinum induces a marked LC3 recruitment to its containing phagosome that depends on a functional ESX-1 secretion system. Cell Microbiol. 2011 Jun;13(6):814–35.

442. Lai S-C, Devenish RJ. LC3-Associated Phagocytosis (LAP): Connections with Host Autophagy. Cells. 2012 Dec;1(4):396–408.

443. Sirajuddin M, Farkasovsky M, Hauer F, Kühlmann D, Macara IG, Weyand M, et al. Structural insight into filament formation by mammalian septins. Nature. 2007 Jul 18;449(7160):311–5.

444. Kinoshita M. The septins. Genome Biol. 2003;4(11):236.

445. Mostowy S, Shenoy AR. The cytoskeleton in cell-autonomous immunity: structural determinants of host defence. Nat Rev Immunol. 2015 Aug 21;15(9):559–73.

446. Mostowy S, Sancho-Shimizu V, Hamon MA, Simeone R, Brosch R, Johansen T, et al. p62 and NDP52 proteins target intracytosolic Shigella and Listeria to different autophagy pathways. Journal of Biological Chemistry. 2011 Jul 29;286(30):26987–95.

447. Pichon S, Bouchon D, Cordaux R, Chen L, Garrett RA, Grève P. Conservation of the Type IV Secretion System throughout Wolbachia evolution. Biochemical and Biophysical Research Communications. 2009 Aug;385(4):557–62.

448. Cascales E, Christie PJ. The versatile bacterial type IV secretion systems. Nature Reviews Microbiology. 2003 Nov 1;1(2):137–49.

449. Selbach M, Moese S, Hauck CR, Meyer TF, Backert S. Src Is the Kinase of the Helicobacter pyloriCagA Protein in Vitroand in Vivo. J Biol Chem. 2002 Feb 22;277(9):6775–8.

450. Rennoll-Bankert KE, Rahman MS, Gillespie JJ, Guillotte ML, Kaur SJ, Lehman SS, et al. Which Way In? The RalF Arf-GEF Orchestrates Rickettsia Host Cell

Invasion. PLoS Pathog. 2015 Aug 20;11(8):e1005115.

451. Landmann F, Voronin D, Sullivan W, Taylor MJ. Anti-filarial Activity of Antibiotic Therapy Is Due to Extensive Apoptosis after Wolbachia Depletion from Filarial Nematodes. PLoS Pathog. 2011 Nov 3;7(11):e1002351.

452. Zheng Y, Wang J-L, Liu C, Wang C-P, Walker T, Wang Y-F. Differentially expressed profiles in the larval testes of Wolbachia infected and uninfected Drosophila. BMC Genomics. 2011 Dec 6;12(1):595.

453. Ikeya T, Broughton S, Alic N, Grandison R, Partridge L. The endosymbiont Wolbachia increases insulin/IGF-like signalling in Drosophila. Proceedings of the Royal Society of London: Biological Sciences. 2009 Nov 7;276(1674):3799–807.

454. Greer EL, Brunet A. FOXO transcription factors in ageing and cancer. Acta Physiol. 2008 Jan;192(1):19–28.

455. Serbus LR, White PM, Silva JP, Rabe A, Teixeira L, Albertson R, et al. The Impact of Host Diet on Wolbachia Titer in Drosophila. PLoS Pathog. 2015 Mar 31;11(3):e1004777.

456. Turley AP, Moreira LA, O'Neill S, McGraw EA. Wolbachia Infection Reduces Blood-Feeding Success in the Dengue Fever Mosquito, Aedes aegypti. PLoS Negl Trop Dis. 2009 Sep 15;3(9):e516.

457. Moreira LA, Saig E, Turley AP, Ribeiro JMC, O'Neill S, McGraw EA. Human Probing Behavior of Aedes aegypti when Infected with a Life-Shortening Strain of Wolbachia. PLoS Negl Trop Dis. 2009 Dec 15;3(12):e568.

458. Pannebakker BA, Loppin B, Elemans CPH, Humblot L, Vavre F. Parasitic inhibition of cell death facilitates symbiosis. Proc Natl Acad Sci USA. 2007 Jan 2;104(1):213–5.

459. Fast EM, Toomey ME, Panaram K, Desjardins D, Kolaczyk ED, Frydman HM. Wolbachia Enhance Drosophila Stem Cell Proliferation and Target the Germline Stem Cell Niche. Science. 2011 Nov 17;334(6058):990–2.

460. Childs LM, Cai FY, Kakani EG, Mitchell SN, Paton D, Gabrieli P, et al. Disrupting Mosquito Reproduction and Parasite Development for Malaria Control. PLoS Pathog. 2016 Dec 15;12(12):e1006060.

461. Brownlie JC, Cass BN, Riegler M, Witsenburg JJ, Iturbe-Ormaetxe I, McGraw EA, et al. Evidence for Metabolic Provisioning by a Common Invertebrate Endosymbiont, Wolbachia pipientis, during Periods of Nutritional Stress. PLoS Pathog. 2009 Apr 3;5(4):e1000368.

462. Unckless RL, Jaenike J. Maintenance of a male-killing Wolbachia in Drosophila innubila by male-killing dependent and male-killing independent mechanisms. Evolution. 2012 Mar;66(3):678–89.

463. Diamond MS, Pierson TC. Molecular Insight into Dengue Virus Pathogenesis and Its Implications for Disease Control. Cell. 2015 Jul 30;162(3):488–92.

464. Briant L, Desprès P, Choumet V, Missé D. Role of skin immune cells on the host susceptibility to mosquito-borne viruses. Virology. 2014 Sep;464-465:26–32.

465. Wichit S, Ferraris P, Choumet V, Missé D. The effects of mosquito saliva on dengue virus infectivity in humans. Current Opinion in Virology. 2016 Dec;21:139–45.

466. Mukhopadhyay S, Kuhn RJ, Rossmann MG. A structural perspective of the flavivirus life cycle. Nature Reviews Microbiology. 2005 Jan;3(1):13–22.

467. Cruz-Oliveira C, Freire JM, Conceição TM, Higa LM, Castanho MARB, Da Poian AT. Receptors and routes of dengue virus entry into the host cells. FEMS Microbiol Rev. 2015 Mar;39(2):155–70.

468. Screaton G, Mongkolsapaya J, Yacoub S, Roberts C. New insights into the immunopathology and control of dengue virus infection. Nat Rev Immunol. 2015 Nov 25;15(12):745–59.

469. Unckless RL, Jaenike J. Structure of dengue virus: implications for flavivirus organization, maturation, and fusion. Evolution. 2011 Nov 11;66(3):678–89.

470. Allison SL, Schalich J, Stiasny K, Mandl CW, Heinz FX. Mutational Evidence for an Internal Fusion Peptide in Flavivirus Envelope Protein E. J Virol. 2001 May 1;75(9):4268–75.

471. Srikiatkhachorn A, Yoon I-K. Immune correlates for dengue vaccine development. Expert Review of Vaccines. 2016 Jan 4;15(4):455–65.

472. Rodenhuis-Zybert IA, Wilschut J, Smit JM. Dengue virus life cycle: viral and host factors modulating infectivity. Cell Mol Life Sci. 2010 Aug;67(16):2773–86.

473. Chanprapaph S, Saparpakorn P, Sangma C, Niyomrattanakit P, Hannongbua S, Angsuthanasombat C, et al. Competitive inhibition of the dengue virus NS3 serine protease by synthetic peptides representing polyprotein cleavage sites. Biochemical and Biophysical Research Communications. 2005 May;330(4):1237–46.

474. Chambers TJ, Hahn CS, Galler R, Rice CM. Flavivirus Genome Organization, Expression, and Replication. Annu Rev Microbiol. 1990 Oct;44(1):649–88.

475. Falgout B, Pethel M, Zhang YM, Lai CJ. Both nonstructural proteins NS2B and NS3 are required for the proteolytic processing of dengue virus nonstructural proteins. J Virol. 1991 May;65(5):2467–75.

476. Yusof R, Clum S, Wetzel M, Murthy HM, Padmanabhan R. Purified NS2B/NS3 serine protease of dengue virus type 2 exhibits cofactor NS2B dependence for cleavage of substrates with dibasic amino acids in vitro. J Biol Chem. 2000 Apr 7;275(14):9963–9.

477. Noble CG, Seh CC, Chao AT, Shi PY. Ligand-Bound Structures of the Dengue Virus Protease Reveal the Active Conformation. J Virol. 2011 Dec 9;86(1):438–46.

478. Clyde K, Kyle JL, Harris E. Recent advances in deciphering viral and host determinants of dengue virus replication and pathogenesis. J Virol. 2006 Nov 10;80(23):11418–31.

479. Malet H, Massé N, Selisko B, Romette J-L, Alvarez K, Guillemot JC, et al. The flavivirus polymerase as a target for drug discovery. Antiviral Research. 2008 Oct;80(1):23–35.

480. Selisko B, Wang C, Harris E, Canard B. Regulation of Flavivirus RNA synthesis and replication. Current Opinion in Virology. 2014 Dec;9:74–83.

481. Luo D, Xu T, Hunke C, Grüber G, Vasudevan SG, Lescar J. Crystal structure of the NS3 protease-helicase from dengue virus. J Virol. 2008 Jan;82(1):173–83.

482. Li L, Lok SM, Yu I-M, Zhang Y, Kuhn RJ, Chen J, et al. The Flavivirus Precursor Membrane-Envelope Protein Complex: Structure and Maturation. Science. 2008 Mar 28;319(5871):1830–4.

483. Yu I-M, Zhang W, Holdaway HA, Li L, Kostyuchenko VA, Chipman PR, et al. Structure of the immature dengue virus at low pH primes proteolytic maturation. Science. 2008 Mar 28;319(5871):1834–7.

484. Junjhon J, Lausumpao M, Supasa S, Noisakran S, Songjaeng A, Saraithong P, et al. Differential Modulation of prM Cleavage, Extracellular Particle Distribution, and Virus Infectivity by Conserved Residues at Nonfurin Consensus Positions of the Dengue Virus pr-M Junction. J Virol. 2008 Oct 16;82(21):10776–91.

485. Miller S, Kastner S, Krijnse-Locker J, Bühler S, Bartenschlager R. The non-structural protein 4A of dengue virus is an integral membrane protein inducing membrane alterations in a 2K-regulated manner. J Biol Chem. 2007 Mar 23;282(12):8873–82.

486. Boon den JA, Diaz A, Ahlquist P. Cytoplasmic viral replication complexes. Cell

Host Microbe. 2010 Jul 22;8(1):77–85.

487. Pietro Scaturro, Cortese M, Chatel-Chaix L, Fischl W, Bartenschlager R. Dengue Virus Non-structural Protein 1 Modulates Infectious Particle Production via Interaction with the Structural Proteins. PLoS Pathog. 2015 Nov 12;11(11):e1005277.

488. Xie X, Gayen S, Kang C, Yuan Z, Shi P-Y. Membrane topology and function of dengue virus NS2A protein. J Virol. American Society for Microbiology; 2013 Apr;87(8):4609–22.

489. Riedel S. Edward Jenner and the history of smallpox and vaccination. Proceedings (Baylor University Medical Center). Baylor Health Care System; 2005 Jan 1;18(1):21–689.

490. Dudas RA, Karron RA. Respiratory syncytial virus vaccines. Clinical Microbiology Reviews. 1998 Jul;11(3):430–9.

491. Kim HW, Canchola JG, Brandt CD, Pyles G, Chanock RM, Jensen K, et al. Respiratory syncytial virus disease in infants despite prior administration of antigenic inactivated vaccine. Am J Epidemiol. 1969 Apr;89(4):422–34.

492. Halstead SB. Dengue Antibody-Dependent Enhancement: Knowns and Unknowns. Microbiology Spectrum. 2014 Dec 10;2(6).

493. Sabin AB. Research on dengue during World War II. Am J Trop Med Hyg. 1952 Jan;1(1):30–50.

494. Montoya M, Gresh L, Mercado JC, Williams KL, Vargas MJ, Gutierrez G, et al. Symptomatic Versus Inapparent Outcome in Repeat Dengue Virus Infections Is Influenced by the Time Interval between Infections and Study Year. PLoS Negl Trop Dis. 2013 Aug 8;7(8):e2357.

495. Anderson KB, Gibbons RV, Cummings DAT, Nisalak A, Green S, Libraty DH, et al. A Shorter Time Interval Between First and Second Dengue Infections Is Associated With Protection From Clinical Illness in a School-based Cohort in Thailand. J Infect Dis. 2014 Jan 7;209(3):360–8.

496. Salje H, Lessler J, Endy TP, Curriero FC, Gibbons RV, Nisalak A, et al. Revealing the microscale spatial signature of dengue transmission and immunity in an urban population. PNAS. 2012 Jun 12;109(24):9535–8.

497. Reich NG, Shrestha S, King AA, Rohani P, Lessler J, Kalayanarooj S, et al. Interactions between serotypes of dengue highlight epidemiological impact of cross-immunity. Journal of The Royal Society Interface. 2013 Sep 6;10(86):20130414–4.

498. Vaughn DW, Green S, Kalayanarooj S, Innis BL, Nimmannitya S, Suntayakorn S, et al. Dengue viremia titer, antibody response pattern, and virus serotype correlate with disease severity. J Infect Dis. 2000 Jan;181(1):2–9.

499. Libraty DH, Endy TP, Houng HSH, Green S, Kalayanarooj S, Suntayakorn S, et al. Differing influences of virus burden and immune activation on disease severity in secondary dengue-3 virus infections. J Infect Dis. 2002 May 1;185(9):1213–21.

500. Kliks SC, Nimmanitya S, Nisalak A, Burke DS. Evidence that maternal dengue antibodies are important in the development of dengue hemorrhagic fever in infants. Am J Trop Med Hyg. 1988 Mar;38(2):411–9.

501. Halstead SB, O'Rourke EJ, Allison AC. Dengue viruses and mononuclear phagocytes. II. Identity of blood and tissue leukocytes supporting in vitro infection. The Journal of Experimental Medicine. 1977 Jul 1;146(1):218–29.

502. Guzman MG, Vazquez S. The Complexity of Antibody-Dependent Enhancement of Dengue Virus Infection. Viruses. 2010 Dec;2(12):2649–62.

503. Dejnirattisai W, Jumnainsong A, Onsirisakul N, Fitton P, Vasanawathana S, Limpitikul W, et al. Cross-reacting antibodies enhance dengue virus infection in humans. Science. 2010 May 7;328(5979):745–8.

504. Beltramello M, Williams KL, Simmons CP, Macagno A, Simonelli L, Quyen NTH, et al. The Human Immune Response to Dengue Virus Is Dominated by Highly Cross-Reactive Antibodies Endowed with Neutralizing and Enhancing Activity. Cell Host Microbe. 2010 Sep;8(3):271–83.

505. Halstead SB. In vivo enhancement of dengue virus infection in rhesus monkeys by passively transferred antibody. J Infect Dis. 1979 Oct;140(4):527–33.

506. Goncalvez AP, Engle RE, St Claire M, Purcell RH, Lai C-J. Monoclonal antibody-mediated enhancement of dengue virus infection in vitro and in vivo and strategies for prevention. PNAS. 2007 May 29;104(22):9422–7.

507. Dung NTP, Duyen HTL, Thuy NTV, Ngoc TV, Chau NVV, Hien TT, et al. Timing of CD8+ T cell responses in relation to commencement of capillary leakage in children with dengue. The Journal of Immunology. 2010 Jun 15;184(12):7281–7.

508. Flipse J, Diosa-Toro MA, Hoornweg TE, van de Pol DPI, Urcuqui-Inchima S, Smit JM. Antibody-Dependent Enhancement of Dengue Virus Infection in Primary Human Macrophages; Balancing Higher Fusion against Antiviral Responses. Sci Rep. 2016 Jul 6;6(1):465.

509. Modhiran N, Kalayanarooj S, Ubol S. Subversion of Innate Defenses by the Interplay between DENV and Pre-Existing Enhancing Antibodies: TLRs Signaling Collapse. PLoS Negl Trop Dis. 2010 Dec 21;4(12):e924.

510. Chareonsirisuthigul T, Kalayanarooj S, Ubol S. Dengue virus (DENV) antibody-dependent enhancement of infection upregulates the production of anti-inflammatory cytokines, but suppresses anti-DENV free radical and pro-inflammatory cytokine production, in THP-1 cells. Journal of General Virology. 2007 Feb 1;88(2):365–75.

511. Ubol S, Phuklia W, Kalayanarooj S, Modhiran N. Mechanisms of Immune Evasion Induced by a Complex of Dengue Virus and Preexisting Enhancing Antibodies. J Infect Dis. 2010 Mar 15;201(6):923–35.

512. Kou Z, Lim JYH, Beltramello M, Quinn M, Chen H, Liu S-N, et al. Human antibodies against dengue enhance dengue viral infectivity without suppressing type I interferon secretion in primary human monocytes. Virology. 2011 Feb;410(1):240–7.

513. Boonnak K, Dambach KM, Donofrio GC, Tassaneetrithep B, Marovich MA. Cell Type Specificity and Host Genetic Polymorphisms Influence Antibody-Dependent Enhancement of Dengue Virus Infection. J Virol. 2011 Jan 20;85(4):1671–83.

514. Modhiran N, Watterson D, Muller DA, Panetta AK, Sester DP, Liu L, et al. Dengue virus NS1 protein activates cells via Toll-like receptor 4 and disrupts endothelial cell monolayer integrity. Science Translational Medicine. 2015 Sep 9;7(304):304ra142–2.

515. Beatty PR, Puerta-Guardo H, Killingbeck SS, Glasner DR, Hopkins K, Harris E. Dengue virus NS1 triggers endothelial permeability and vascular leak that is prevented by NS1 vaccination. Science Translational Medicine. 2015 Sep 9;7(304):304ra141–1.

516. Ng JKW, Zhang SL, Tan HC, Yan B, Gomez JMM, Tan WY, et al. First Experimental In Vivo Model of Enhanced Dengue Disease Severity through Maternally Acquired Heterotypic Dengue Antibodies. PLoS Pathog. 2014 Apr 3;10(4):e1004031.

517. Hober D, Poli L, Roblin B, Gestas P, Chungue E, Granic G, et al. Serum levels of tumor necrosis factor-alpha (TNF-alpha), interleukin-6 (IL-6), and interleukin-1 beta (IL-1 beta) in dengue-infected patients. Am J Trop Med Hyg. 1993 Mar;48(3):324–31.

518. Green S, Vaughn DW, Kalayanarooj S, Nimmannitya S, Suntayakorn S, Nisalak A, et al. Early Immune Activation in Acute Dengue Illness Is Related to

Development of Plasma Leakage and Disease Severity. J Infect Dis. 1999 Apr;179(4):755–62.

519. Lok S-M, Kostyuchenko V, Nybakken GE, Holdaway HA, Battisti AJ, Sukupolvi-Petty S, et al. Binding of a neutralizing antibody to dengue virus alters the arrangement of surface glycoproteins. Nat Struct Mol Biol. 2008 Feb 10;15(3):312–7.

520. Pierson TC, Diamond MS. Molecular mechanisms of antibody-mediated neutralisation of flavivirus infection. Expert Rev Mol Med. 2008;10:e12.

521. Halstead SB. Neutralization and antibody-dependent enhancement of dengue viruses. Adv Virus Res. 2003;60:421–67.

522. Halstead SB, Venkateshan CN, Gentry MK, Larsen LK. Heterogeneity of infection enhancement of dengue 2 strains by monoclonal antibodies. The Journal of Immunology. 1984 Mar;132(3):1529–32.

523. Tsai W-Y, Durbin A, Tsai J-J, Hsieh S-C, Whitehead S, Wang W-K. Complexity of Neutralizing Antibodies against Multiple Dengue Virus Serotypes after Heterotypic Immunization and Secondary Infection Revealed by In-Depth Analysis of Cross-Reactive Antibodies. J Virol. 2015 Jun 18;89(14):7348–62.

524. Kliks SC, Nisalak A, Brandt WE, Wahl L, Burke DS. Antibody-dependent enhancement of dengue virus growth in human monocytes as a risk factor for dengue hemorrhagic fever. Am J Trop Med Hyg. 1989 Apr;40(4):444–51.

525. Rodenhuis-Zybert IA, van der Schaar HM, da Silva Voorham JM, van der Ende-Metselaar H, Lei H-Y, Wilschut J, et al. Immature Dengue Virus: A Veiled Pathogen? Gale M, editor. PLoS Pathog. 2010 Jan 8;6(1):e1000718.

526. Rodenhuis-Zybert IA, Moesker B, da Silva Voorham JM, van der Ende-Metselaar H, Diamond MS, Wilschut J, et al. A fusion-loop antibody enhances the infectious properties of immature flavivirus particles. J Virol. 2011 Nov;85(22):11800–8.

527. Lai CY, Tsai WY, Lin SR, Kao CL, Hu HP, King CC, et al. Antibodies to Envelope Glycoprotein of Dengue Virus during the Natural Course of Infection Are Predominantly Cross-Reactive and Recognize Epitopes Containing Highly Conserved Residues at the Fusion Loop of Domain II. J Virol. 2008 Jun 10;82(13):6631–43.

528. de Alwis R, Smith SA, Olivarez NP, Messer WB, Huynh JP, Wahala WMPB, et al. Identification of human neutralizing antibodies that bind to complex epitopes on dengue virions. Proc Natl Acad Sci USA. 2012 May 8;109(19):7439–44.

529. Teoh EP, Kukkaro P, Teo EW, Lim APC, Tan TT, Yip A, et al. The Structural Basis for Serotype-Specific Neutralization of Dengue Virus by a Human Antibody. Science Translational Medicine. 2012 Jun 20;4(139):139ra83–3.

530. Fibriansah G, Tan JL, Smith SA, de Alwis R, Ng T-S, Kostyuchenko VA, et al. A highly potent human antibody neutralizes dengue virus serotype 3 by binding across three surface proteins. Nature Communications. 2015 Feb 20;6:6341.

531. Rouvinski A, Guardado-Calvo P, Barba-Spaeth G, Duquerroy S, Vaney M-C, Kikuti CM, et al. Recognition determinants of broadly neutralizing human antibodies against dengue viruses. Nature. 2015 Jan 12;520(7545):109–13.

532. Dejnirattisai W, Wongwiwat W, Supasa S, Zhang X, Dai X, Rouvinsky A, et al. A new class of highly potent, broadly neutralizing antibodies isolated from viremic patients infected with dengue virus. Nat Immunol. 2014 Dec 15;16(2):170–7.

533. Churdboonchart V, Bhamarapravati N, Peampramprecha S, Sirinavin S. Antibodies against dengue viral proteins in primary and secondary dengue hemorrhagic fever. Am J Trop Med Hyg. 1991 May;44(5):481–93.

534. Valdés K, Alvarez M, Pupo M, Vázquez S, Rodríguez R, Guzmán MG. Human Dengue antibodies against structural and nonstructural proteins. Clinical and Diagnostic Laboratory Immunology. 2000 Sep;7(5):856–7.

535. Avirutnan P, Punyadee N, Noisakran S, Komoltri C, Thiemmeca S, Auethavornanan K, et al. Vascular Leakage in Severe Dengue Virus Infections: A Potential Role for the Nonstructural Viral Protein NS1 and Complement. J Infect Dis. 2006 Apr 15;193(8):1078–88.

536. Vazeille M, Gaborit P, Mousson L, Girod R, Failloux A-B. Competitive advantage of a dengue 4 virus when co-infecting the mosquito Aedes aegypti with a dengue 1 virus. BMC Infectious Diseases. 2016 Jul 8;16(1):318.

537. Sabchareon A, Lang J, Chanthavanich P, Yoksan S, Forrat R, Attanath P, et al. Safety and immunogenicity of tetravalent live-attenuated dengue vaccines in Thai adult volunteers: role of serotype concentration, ratio, and multiple doses. Am J Trop Med Hyg. 2002 Mar;66(3):264–72.

538. Sabchareon A, Wallace D, Sirivichayakul C, Limkittikul K, Chanthavanich P, Suvannadabba S, et al. Protective efficacy of the recombinant, live-attenuated, CYD tetravalent dengue vaccine in Thai schoolchildren: a randomised, controlled phase 2b trial. The Lancet. 2012 Nov;380(9853):1559–67.

539. Simmons CP, Dong T, Chau NV, Dung NTP, Chau TNB, Thao LTT, et al. Early T-cell responses to dengue virus epitopes in Vietnamese adults with secondary

dengue virus infections. J Virol. 2005 May;79(9):5665–75.

540. Duangchinda T, Dejnirattisai W, Vasanawathana S, Limpitikul W, Tangthawornchaikul N, Malasit P, et al. Immunodominant T-cell responses to dengue virus NS3 are associated with DHF. Proc Natl Acad Sci USA. 2010 Sep 28;107(39):16922–7.

541. Weiskopf D, Yauch LE, Angelo MA, John DV, Greenbaum JA, Sidney J, et al. Insights into HLA-Restricted T Cell Responses in a Novel Mouse Model of Dengue Virus Infection Point toward New Implications for Vaccine Design. The Journal of Immunology. 2011 Oct 3;187(8):4268–79.

542. Rivino L, Kumaran EAP, Jovanovic V, Nadua K, Teo EW, Pang SW, et al. Differential Targeting of Viral Components by CD4+ versus CD8+ T Lymphocytes in Dengue Virus Infection. J Virol. 2013 Feb 11;87(5):2693–706.

543. Vita R, Overton JA, Greenbaum JA, Ponomarenko J, Clark JD, Cantrell JR, et al. The immune epitope database (IEDB) 3.0. Nucleic Acids Research. 2015 Jan 15;43(D1):D405–12.

544. Murphy K, Travers P, Walport M. Janeway's Immunobiology. 7 ed. Goatly B, editor. New York: Garland Science; 2008.

545. Remakus S, Sigal LJ. Memory CD8+ T Cell Protection. In: Crossroads Between Innate and Adaptive Immunity IV. New York, NY: Springer New York; 2013. pp. 77–86. (Advances in Experimental Medicine and Biology; vol. 785).

546. Sant AJ, McMichael A. Revealing the role of CD4(+) T cells in viral immunity. The Journal of Experimental Medicine. 2012 Jul 30;209(8):1391–5.

547. Mongkolsapaya J, Dejnirattisai W, Xu X-N, Vasanawathana S, Tangthawornchaikul N, Chairunsri A, et al. Original antigenic sin and apoptosis in the pathogenesis of dengue hemorrhagic fever. Nat Med. 2003 Jul;9(7):921–7.

548. Friberg H, Bashyam H, Toyosaki-Maeda T, Potts JA, Greenough T, Kalayanarooj S, et al. Cross-Reactivity and Expansion of Dengue-Specific T cells During Acute Primary and Secondary Infections in Humans. Sci Rep. 2011 Aug 1;1(1):2.

549. Zellweger RM, Miller R, Eddy WE, White LJ, Johnston RE, Shresta S. Role of Humoral versus Cellular Responses Induced by a Protective Dengue Vaccine Candidate. PLoS Pathog. 2013 Oct 31;9(10):e1003723.

550. Hatch S, Endy TP, Thomas S, Mathew A, Potts J, Pazoles P, et al. Intracellular Cytokine Production by Dengue Virus-specific T cells Correlates with Subclinical

Secondary Infection. J Infect Dis. 2011 Mar 31;203(9):1282–91.

551. Yauch LE, Zellweger RM, Kotturi MF, Qutubuddin A, Sidney J, Peters B, et al. A Protective Role for Dengue Virus-Specific CD8+ T Cells. The Journal of Immunology. American Association of Immunologists; 2009 Apr 15;182(8):4865–73.

552. Mongkolsapaya J, Duangchinda T, Dejnirattisai W, Vasanawathana S, Avirutnan P, Jairungsri A, et al. T Cell Responses in Dengue Hemorrhagic Fever: Are Cross-Reactive T Cells Suboptimal? The Journal of Immunology. 2006 Mar 15;176(6):3821–9.

553. Mathew A, Rothman AL. Understanding the contribution of cellular immunity to dengue disease pathogenesis. Immunol Rev. 2008 Oct;225(1):300–13.

554. Kurane I, Rothman AL, Livingston PG, Green S, Gagnon SJ, Janus J, et al. Immunopathologic mechanisms of dengue hemorrhagic fever and dengue shock syndrome. Arch Virol Suppl. 1994;9:59–64.

555. Mangada MM, Endy TP, Nisalak A, Chunsuttiwat S, Vaughn DW, Libraty DH, et al. Dengue-specific T cell responses in peripheral blood mononuclear cells obtained prior to secondary dengue virus infections in Thai schoolchildren. J Infect Dis. 2002 Jun 15;185(12):1697–703.

556. Green S, Pichyangkul S, Vaughn DW, Kalayanarooj S, Nimmannitya S, Nisalak A, et al. Early CD69 Expression on Peripheral Blood Lymphocytes from Children with Dengue Hemorrhagic Fever. J Infect Dis. 1999 Nov;180(5):1429–35.

557. Almeida JR, Sauce D, Price DA, Papagno L, Shin SY, Moris A, et al. Antigen sensitivity is a major determinant of CD8+ T-cell polyfunctionality and HIV-suppressive activity. Blood. 2009 Jun 18;113(25):6351–60.

558. Park SH, Shin EC, Capone S, Caggiari L, Re VD, Nicosia A, et al. Successful Vaccination Induces Multifunctional Memory T-Cell Precursors Associated With Early Control of Hepatitis C Virus. Gastroenterology. 2012 Oct;143(4):1048–1060.e4.

559. Yachi PP, Ampudia J, Zal T, Gascoigne NRJ. Altered Peptide Ligands Induce Delayed CD8-T Cell Receptor Interaction—a Role for CD8 in Distinguishing Antigen Quality. Immunity. 2006 Aug;25(2):203–11.

560. Weaver SC, Vasilakis N. Molecular evolution of dengue viruses: Contributions of phylogenetics to understanding the history and epidemiology of the preeminent arboviral disease. Infection, Genetics and Evolution. 2009 Jul;9(4):523–40.

561. Twiddy SS, Farrar JJ, Vinh Chau N, Wills B, Gould EA, Gritsun T, et al. Phylogenetic relationships and differential selection pressures among genotypes of dengue-2 virus. Virology. 2002 Jun 20;298(1):63–72.

562. Zhang C, Mammen MP, Chinnawirotpisan P, Klungthong C, Rodpradit P, Monkongdee P, et al. Clade Replacements in Dengue Virus Serotypes 1 and 3 Are Associated with Changing Serotype Prevalence. J Virol. 2005 Nov 23;79(24):15123–30.

563. A-Nuegoonpipat A, Berlioz-Arthaud A, Chow V, Endy T, Lowry K, Mai LQ, et al. Sustained transmission of dengue virus type 1 in the Pacific due to repeated introductions of different Asian strains. Virology. 2004 Nov;329(2):505–12.

564. OhAinle M, Balmaseda A, Macalalad AR, Tellez Y, Zody MC, Saborío S, et al. Dynamics of Dengue Disease Severity Determined by the Interplay Between Viral Genetics and Serotype-Specific Immunity. Science Translational Medicine. 2011 Dec 21;3(114):114ra128–8.

565. Lambrechts L, Fansiri T, Pongsiri A, Thaisomboonsuk B, Klungthong C, Richardson JH, et al. Dengue-1 Virus Clade Replacement in Thailand Associated with Enhanced Mosquito Transmission. J Virol. 2012 Jan 12;86(3):1853–61.

566. Wittke V, Robb TE, Thu HM, Nisalak A, Nimmannitya S, Kalayanrooj S, et al. Extinction and Rapid Emergence of Strains of Dengue 3 Virus during an Interepidemic Period. Virology. 2002 Sep;301(1):148–56.

567. Rico-Hesse R. Dengue Virus Virulence and Transmission Determinants. In: Dengue Virus. Berlin, Heidelberg: Springer Berlin Heidelberg; 2009. pp. 45–55. (Current Topics in Microbiology and Immunology; vol. 338).

568. Hang VTT, Holmes EC, Veasna D, Quy NT, Hien TT, Quail M, et al. Emergence of the Asian 1 Genotype of Dengue Virus Serotype 2 in Viet Nam: In Vivo Fitness Advantage and Lineage Replacement in South-East Asia. Rico-Hesse R, editor. PLoS Negl Trop Dis. 2010 Jul 20;4(7):e757.

569. Costa RL, Voloch CM, Schrago CG. Comparative evolutionary epidemiology of dengue virus serotypes. Infection, Genetics and Evolution. 2012 Mar;12(2):309–14.

570. King C-C, Chao D-Y, Chien L-J, Chang G-J, Ling T-H, Wu Y-C, et al. Comparative analysis of full genomic sequences among different genotypes of dengue virus type 3. Virol J. 2008;5(1):63.

571. Adams B, Holmes EC, Zhang C, Mammen MP, Nimmannitya S, Kalayanarooj S, et al. Cross-protective immunity can account for the alternating epidemic

pattern of dengue virus serotypes circulating in Bangkok. Proc Natl Acad Sci USA. 2006 Sep 19;103(38):14234–9.

572. Holmes EC, Twiddy SS, Woelk CH. Phylogenetic evidence for adaptive evolution of dengue viruses in nature. Journal of General Virology. 2002 Jul 1;83(7):1679–89.

573. Wearing HJ, Rohani P. Ecological and immunological determinants of dengue epidemics. Proc Natl Acad Sci USA. 2006 Aug 1;103(31):11802–7.

574. Adams B, Boots M. Modelling the relationship between antibody-dependent enhancement and immunological distance with application to dengue. Journal of Theoretical Biology. 2006 Sep;242(2):337–46.

575. Recker M, Blyuss KB, Simmons CP, Hien TT, Wills B, Farrar J, et al. Immunological serotype interactions and their effect on the epidemiological pattern of dengue. Proceedings of the Royal Society of London: Biological Sciences. 2009 Jul 22;276(1667):2541–8.

576. Cologna R, Armstrong PM, Rico-Hesse R. Selection for Virulent Dengue Viruses Occurs in Humans and Mosquitoes. J Virol. 2004 Dec 20;79(2):853–9.

577. Armstrong PM, Rico-Hesse R. Efficiency of dengue serotype 2 virus strains to infect and disseminate in Aedes aegypti. Am J Trop Med Hyg. 2003 May;68(5):539–44.

578. Armstrong PM, Rico-Hesse R. Differential susceptibility of Aedes aegypti to infection by the American and Southeast Asian genotypes of dengue type 2 virus. Vector-Borne and Zoonotic Diseases. 2001 Jun;1(2):159–68.

579. Libraty DH, Young PR, Pickering D, Endy TP, Kalayanarooj S, Green S, et al. High Circulating Levels of the Dengue Virus Nonstructural Protein NS1 Early in Dengue Illness Correlate with the Development of Dengue Hemorrhagic Fever. J Infect Dis. 2002 Oct 15;186(8):1165–8.

580. Bennett SN. Selection-Driven Evolution of Emergent Dengue Virus. Molecular Biology and Evolution. 2003 Jun 27;20(10):1650–8.

581. Vasilakis N, Holmes EC, Fokam EB, Faye O, Diallo M, Sall AA, et al. Evolutionary Processes among Sylvatic Dengue Type 2 Viruses. J Virol. 2007 Aug 14;81(17):9591–5.

582. Holmes EC. Patterns of intra- and interhost nonsynonymous variation reveal strong purifying selection in dengue virus. J Virol. 2003 Oct;77(20):11296–8.

583. Holmes EC, Twiddy SS. The origin, emergence and evolutionary genetics of dengue virus. Infect Genet Evol. 2003 May;3(1):19–28.

584. Foster JE, Bennett SN, Carrington CVF, Vaughan H, McMillan WO. Phylogeography and molecular evolution of dengue 2 in the Caribbean basin, 1981–2000. Virology. 2004 Jun;324(1):48–59.

585. Thu HM, Lowry KS, Myint TT, Shwe TN, Han AM, Khin KK, et al. Myanmar dengue outbreak associated with displacement of serotypes 2, 3, and 4 by dengue 1. Faculty of Science and Technology. 2004.

586. Sittisombut N, Sistayanarain A, Cardosa MJ. Possible occurrence of a genetic bottleneck in dengue serotype 2 viruses between the 1980 and 1987 epidemic seasons in Bangkok Thailand. Am J Tropical. 1997;57(1).

587. Halstead SB. Dengue virus-mosquito interactions. Annu Rev Entomol. 2008;53(1):273–91.

588. Morrison AC, Minnick SL, Rocha C, Forshey BM, Stoddard ST, Getis A, et al. Epidemiology of Dengue Virus in Iquitos, Peru 1999 to 2005: Interepidemic and Epidemic Patterns of Transmission. PLoS Negl Trop Dis. 2010 May 4;4(5):e670.

589. Cummings DAT, Schwartz IB, Billings L, Shaw LB, Burke DS. Dynamic effects of antibody-dependent enhancement on the fitness of viruses. Proc Natl Acad Sci USA. 2005 Oct 18;102(42):15259–64.

590. Nagao Y, Koelle K. Decreases in dengue transmission may act to increase the incidence of dengue hemorrhagic fever. PNAS. 2008 Feb 12;105(6):2238–43.

591. Henikoff S, Henikoff JG. Position-based sequence weights. J Mol Biol. 1994 Nov 4;243(4):574–8.

592. Thompson JD, Higgins DG, Gibson TJ. Improved sensitivity of profile searches through the use of sequence weights and gap excision. Comput Appl Biosci. 1994 Feb;10(1):19–29.

593. Lüthy R, Xenarios I, Bucher P. Improving the sensitivity of the sequence profile method. Protein Sci. 1994 Jan;3(1):139–46.

594. Felsenstein J. Phylogenies and the comparative method. The American Naturalist. 1985;125(1):1–15.

595. Altschul SF, Carroll RJ, Lipman DJ. Weights for data related by a tree. J Mol Biol. 1989 Jun 20;207(4):647–53.

596. Vingron M, Sibbald PR. Weighting in sequence space: a comparison of methods in terms of generalized sequences. PNAS. 1993 Oct 1;90(19):8777–81.

597. Sievers F, Wilm A, Dineen D, Gibson TJ, Karplus K, Li W, et al. Fast, scalable generation of high-quality protein multiple sequence alignments using Clustal

Omega. Molecular Systems Biology. 2011 Jan 1;7(1):539–9.

598. Rammensee H, Bachmann J, Emmerich NP, Bachor OA, Stevanović S. SYFPEITHI: database for MHC ligands and peptide motifs. Immunogenetics. 1999 Nov;50(3-4):213–9.

599. Luo D, Xu T, Watson RP, Becker DS, Sampath A, Jahnke W, et al. Insights into RNA unwinding and ATP hydrolysis by the flavivirus NS3 protein. EMBO J. 2008 Dec 3;27(23):3209–19.

600. Yap TL, Xu T, Chen Y-L, Malet H, Egloff M-P, Canard B, et al. Crystal structure of the dengue virus RNA-dependent RNA polymerase catalytic domain at 1.85-angstrom resolution. J Virol.; 2007 May;81(9):4753–65.

601. Xu T, Sampath A, Chao A, Wen D, Nanao M, Chene P, et al. Structure of the Dengue virus helicase/nucleoside triphosphatase catalytic domain at a resolution of 2.4 A. J Virol. 2005 Aug;79(16):10278–88.

602. Caruthers JM, McKay DB. Helicase structure and mechanism. Current Opinion in Structural Biology. 2002 Feb;12(1):123–33.

603. Marchler-Bauer A, Bo Y, Han L, He J, Lanczycki CJ, Lu S, et al. CDD/SPARCLE: functional classification of proteins via subfamily domain architectures. Nucleic Acids Research. 2017 Jan 3;45(D1):D200–3.

604. Matusan AE, Pryor MJ, Davidson AD, Wright PJ. Mutagenesis of the Dengue Virus Type 2 NS3 Protein within and outside Helicase Motifs: Effects on Enzyme Activity and Virus Replication. J Virol. 2001 Oct 15;75(20):9633–43.

605. Klema VJ, Ye M, Hindupur A, Teramoto T, Gottipati K, Padmanabhan R, et al. Dengue Virus Nonstructural Protein 5 (NS5) Assembles into a Dimer with a Unique Methyltransferase and Polymerase Interface. PLoS Pathog. 2016 Feb 19;12(2):e1005451.

606. Källberg M, Wang H, Wang S, Peng J, Wang Z, Lu H, et al. Template-based protein structure modeling using the RaptorX web server. Nature. 2012 Aug 1;7(8):1511–22.

607. Rollier CS, Reyes-Sandoval A, Cottingham MG, Ewer K, Hill AV. Viral vectors as vaccine platforms: deployment in sight. Current Opinion in Immunology. 2011 Jun;23(3):377–82.

608. Franco L, Palacios G, Martinez JA, Vázquez A, Savji N, De Ory F, et al. First Report of Sylvatic DENV-2-Associated Dengue Hemorrhagic Fever in West Africa. PLoS Negl Trop Dis. 2011 Aug 2;5(8):e1251.

609. Weiskopf D, Angelo MA, Bangs DJ, Sidney J, Paul S, Peters B, et al. The

Human CD8+ T Cell Responses Induced by a Live Attenuated Tetravalent Dengue Vaccine Are Directed against Highly Conserved Epitopes. Diamond MS, editor. J Virol. 2015 Jan 1;89(1):120–8.

610. Gras S, Kedzierski L, Valkenburg SA, Laurie K, Liu YC, Denholm JT, et al. Cross-reactive CD8 +T-cell immunity between the pandemic H1N1-2009 and H1N1-1918 influenza A viruses. PNAS. 2010 Jul 13;107(28):12599–604.

611. University of California, Los Angeles Centre for Iron Disorders. Primary Hepatocyte Isolation Protocol [Internet]. [cited 2016 Apr 12]. Available from: http://iron.med.ucla.edu/protocol-primary-hepatocyte-isolation.html

612. Ateş M, Pınarlı FA, Kaplanoğlu GT, Tiryaki M, Mercan S. A Modified Method for Isolation of Rat Hepatocyte: Saving Time Increases Viability. Niche. 2012;1(1):8–11.

613. Shulman M, Nahmias Y. Long-term culture and coculture of primary rat and human hepatocytes. Malaria. Totowa, NJ: Humana Press; 2012 Sep 16;945(Chapter 17):287–302.

614. Bhatia SN, Ingber DE. Microfluidic organs-on-chips. Nat Biotechnol. 2014 Aug 5;32(8):760–72.

8 Appendix

8.1.1 Table of Failed Antibodies (Mostly Drosophila Specific)

Failed Antibody	Supplier	Catalogue Number
Anti-WIPI2	Sigma	SAB42000400
Anti-DnaK	Abcam	Ab69617
Anti-S6Kp	Cell Signalling	9206s
Anti-Peanut (Septin)	Developmental Studies Hybridoma Bank (DSHB)	4C9H4
Anti-AKT	Cell Signalling	9272s
Anti-Phospho AKT	Cell Signalling	4060s
Anti-drosophila FOXO	Abcam	Ab195977
Anti-Drosophila Sestrin	From[328]	N/A
Anti-Phospho JNK	Cell Signalling	9251s
Anti-JNK	SAB	21241
Anti dFoxO	Cosmo Bio	CAC-THU-A-DFOXO

Table 8-1 I Table of failed antibodies against mosquitoes. List of the antibodies tested in 4a3b cells that failed by western blot assessment. Generally, antibodies targeted against insect proteins were tested.

8.1.2 Development of an Amaxa Protocol for 4a3b Cells

4a3b cells were electroporated using a Nucleofector II (Lonza) with 1µg pIEX-*ag*SESN plasmid using five different Amaxa protocols with the Nucleofector V kit and morphology assessed as a correlate of viability. Protocol T001 provided greatest viability (Figure 8-1). Greater than 1µg DNA significantly reduced viability in all protocols (data not shown).

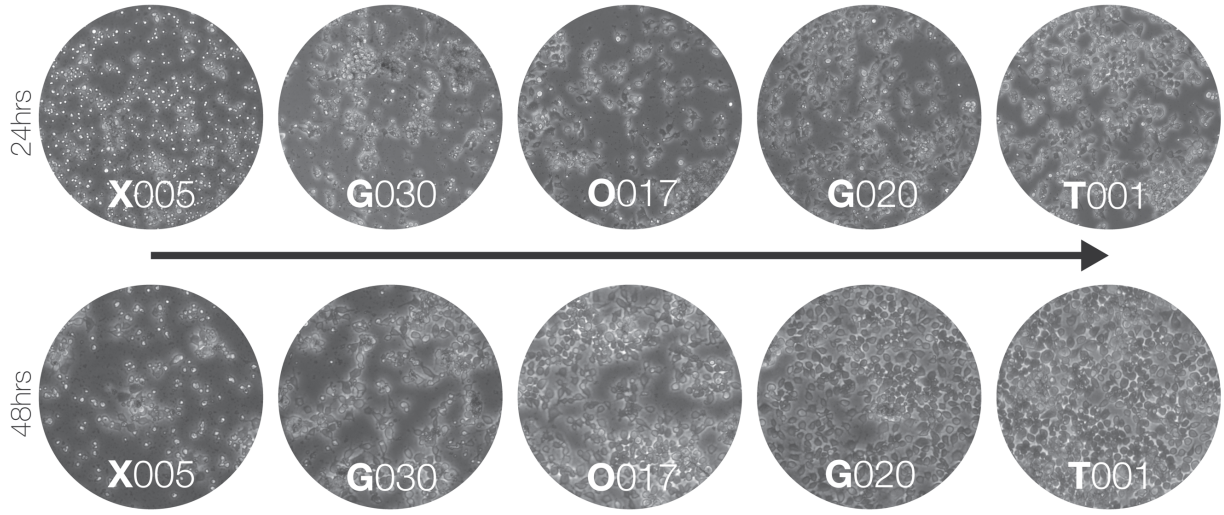

Figure 8-1 I Development of a 4a3b Amaxa protocol. Brightfield images of 4a3b cells 24 and 48 hr after electroporation with 1µg pIEX-*ag*SESN.

8.1.3 Primary Hepatocyte Extraction Protocol

A protocol for extraction of rat primary hepatocytes using was developed using previous literature[151,152]. Rats were chosen instead of mice due to the greater achievable cell yield and the associated difficulty with the smaller anatomy of mice. Anaesthetised rats were cannulated using the hepatic portal vein, and the vena cava cut while the liver was perfused using a wash buffer which was later exchanged for a collagenase buffer to dissociate the cells. Following this, parenchymal (PC) and non-parenchymal cells (NPC) were purified using percoll-based density centrifugation. To purify PC's four percoll protocols were tested[151,611-613], some were modified slightly due to the available equipment (Figure 8-2a). Protocol 2[151] modified to a 100 xg spin provided the best purification (assessed by morphology) and 100% viability (assessed by trypan blue) thus was chosen for the extraction. After protocol optimisation the yields per liver were improved from a minimum of $1x10^6$cells/liver to $50x10^6$cells/liver (Figure 8-2b). Over the first 20 hr post plating primary hepatocytes took on a mature morphological appearance (Figure 8-2c). NPC's were purified using a two layer percoll centrifugation[152] (Figure 8-2d-e).

Extraction of primary hepatocytes requires considerable skill and time. Therefore, cryopreservation of primary rat hepatocytes was investigated using BAMBANKER freezing media. Viability upon thawing assessed by trypan blue showed a 29% drop in viability (Figure 8-2f), indicating further optimisations would be needed if this was to be used.

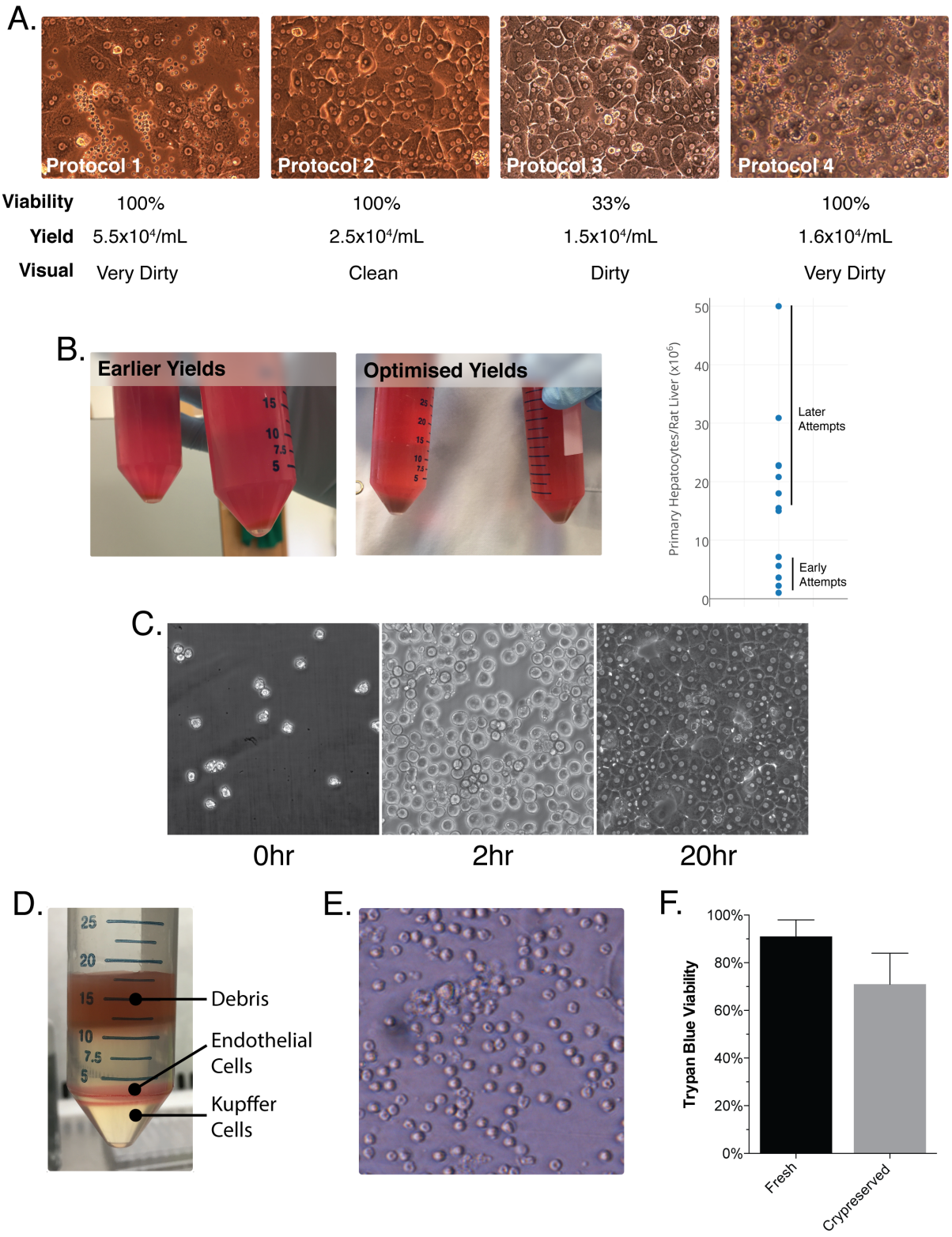

Figure 8-2 I Primary hepatocyte extraction. A) Brightfield images of primary hepatocytes extracted using four different percoll methods 24 hr after plating. Yields, viability and visual purity were noted. B) Left; photographs of purified primary hepatocyte pellets from earlier and later procedures. Right; primary hepatocyte yields from earlier and later purifications. C) Brightfield images of primary hepatocytes 0, 2 and 20 hr after plating. D) Two-layer percoll purification of NPC's post-centrifugation. E) Combined Kupffer cell and endothelial enriched percoll layers 24 hr after plating. F) Mean primary hepatocyte viability assessed by trypan blue after fresh purification and thawing from Bambanker cryopreservation.

1. Anaesthetise rat and open the body cavity. Using a 21G cannula pierce the hepatic portal vein and seal with tissue adhesive.
2. Attach the cannula to the peristaltic pump and start to perfuse the liver with hepatocyte wash buffer (37^{o}C) at ~10mL/min
3. Subsequently cut the vena cava below the liver allowing blood to escape. Subsequently increase the perfusion to 40mL/min and periodical block and unblock the vena cava with forceps allowing the liver the increase in size each time
4. Once blood has been successfully removed from the liver replace the perfusate with liver digestion media (37^{o}C) and continue the process for 5-8 min.
5. Remove the liver and place in ice-cold complete DMEM. Subsequently break open the liver capsule and gently homogenise the tissue.
6. Pass the homogenate through 100µM cell strainers and was cells twice by centrifugation (50xg, 3 min, 4^{o}c).
    a. Keep the supernatant if you wish to collect NPC's
7. Purify PC's by resuspending in 19mL cold DMEM and adding 20mL Sterile isotonic Percoll (SIP) and centrifuging (100xg, 10 min, 4^{o}C).
    a. The purify NPC's layer 10mL onto a 2 layer Percoll gradient (15mL 1.066g/mL Percoll, 20mL 1.037g/mL Percoll) and centrifuge (800xg, 15 min, 4^{o}C). The bottom layer contains Kupffer cells and the band between both layers contains endothelial cells.
8. Wash the pellet three times in cold DMEM and finally re-suspend in 37^{o}C DMEM for plating
9. After 2 hr replace with serum-free hepatocyte growth medium (Promocell)

8.1.4 Microfluidic Liver Model

The liver model contained two layers (Figure 8-3a-b). The bottom layer contained contain primary hepatocytes (PC) and the upper layer on a polycarbonate membrane with 10µM pores the NPC's cells (including endothelial cells). Media under flow was run through the upper chamber with sporozoites added to this media flow. This model contains many features shown to promote maturity, including media flow[251] and growth in 200µM channels[245,248]. The sinusoid endothelial cells and hepatocytes experience considerably different shear stresses of 10-15 dynes*s/cm^2 and 0.01-0.33 dynes*s/cm^2 respectively[253-256]. Therefore, media was pumped through the upper chamber only.

The model was created by designing flow chambers in AutoCAD (Figure 8-3c) and brass moulds created using photolithographgy[614] which were used to create polydimethylsiloxane (PDMS) casts for the lower and upper portion. Each constituent

part was bonded using plasma treatment. Bonding the polycarbonate membrane to PDMS required surface modification for silane bonding following plasma treatment[158,159]. The constructed model was attached to an Ibidi pump system (Ibidi) to maintain media flow in the upper chamber (Figure 8-3d).

[Redacted]

Figure 8-3 I Development of a microfluidic liver model. A) Exploded cross-sectional view of the microfluidic liver model. B) Cross sectional view of the microfluidic liver model as it would be set up. C) AutoCAD 2D drawings of developed microfluidic channels patterns. D) Left to right; PDMS models in brass moulds, PDMS upper sections, microfluidic model.

8.1.5 Free-Flow Electrophoresis Protocol

[Redacted]